AECL EACL

CA9700694

AECL-11494-5, COG-95-552-5

The Disposal of Canada's Nuclear Fuel Waste: A Study of Postclosure Safety of In-Room Emplacement of Used CANDU Fuel in Copper Containers in Permeable Plutonic Rock Volume 5: Radiological Assessment

Le stockage permanent des déchets de combustible nucléaire du Canada : Étude de la sûreté post-fermeture de la mise en place en chambre du combustible CANDU irradié renfermé dans des conteneurs en cuivre enfouis dans la roche plutonique perméable Volume 5 : Évaluation radiologique

B.W. Goodwin, T.H. Andres, W.C. Hajas, D.M. LeNeveu, T.W. Melnyk, J.G. Szekely, A.G. Wikjord, D.C. Donahue, S.B. Keeling, C.I. Kitson, S.E. Oliver, K. Witzke, L. Wojciechowski

June 1996 juin

AECL EACL

THE DISPOSAL OF CANADA'S NUCLEAR FUEL WASTE: A STUDY OF POSTCLOSURE SAFETY OF IN-ROOM EMPLACEMENT OF USED CANDU FUEL IN COPPER CONTAINERS IN PERMEABLE PLUTONIC ROCK VOLUME 5: RADIOLOGICAL ASSESSMENT

by

B.W. Goodwin, T.H. Andres, W.C. Hajas, D.M. LeNeveu,
T.W. Melnyk, J.G. Szekely, A.G. Wikjord, D.C. Donahue, S.B. Keeling,
C.I. Kitson, S.E. Oliver, K. Witzke and L. Wojciechowski

Atomic Energy of Canada Limited
Whiteshell Laboratories
Pinawa, Manitoba R0E 1L0
1996

AECL-11494-5
COG-95-552-5

THE DISPOSAL OF CANADA'S NUCLEAR FUEL WASTE: A STUDY OF POSTCLOSURE SAFETY OF IN-ROOM EMPLACEMENT OF USED CANDU FUEL IN COPPER CONTAINERS IN PERMEABLE PLUTONIC ROCK VOLUME 5: RADIOLOGICAL ASSESSMENT

by

B.W. Goodwin, T.H. Andres, W.C. Hajas, D.M. LeNeveu,
T.W. Melnyk, J.G. Szekely, A.G. Wikjord, D.C. Donahue, S.B. Keeling,
C.I. Kitson, S.E. Oliver, K. Witzke and L. Wojciechowski

ABSTRACT

The concept for disposal of Canada's nuclear fuel waste involves isolating the waste in long-lived containers placed in a sealed vault at a depth of 500 to 1000 m in plutonic rock of the Canadian Shield. The concept permits a choice of methods, materials, sites and designs. The engineered system would be designed for the geological conditions of the disposal site.

The technical feasibility of the disposal concept, and its impact on the environment and human health, have been presented in an Environmental Impact Statement (EIS) (AECL 1994a,b), supported by nine primary references (Davis et al. 1993; Davison et al. 1994a,b; Goodwin et al. 1994; Greber et al. 1994; Grondin et al. 1994; Johnson et al. 1994a,b; Simmons and Baumgartner 1994). One of these primary references (Goodwin et al. 1994) presents the postclosure assessment, a case study that integrates relevant information from engineering design studies, field investigations, laboratory studies, expert judgment and detailed mathematical analyses to evaluate the long-term system performance in terms of safety criteria, guidelines and standards.

In the EIS case study, we examined a hypothetical implementation that conforms to the overall characteristics of the concept, and uses specific site and design choices to ensure that the information and data underlying the assessment are consistent and justified. We assumed that corrosion-resistant containers were constructed from Grade-2 titanium, that the containers were placed in boreholes drilled into the floors of the disposal rooms, and that the vault was located in a domain of low-permeability sparsely fractured plutonic rock.

In this report, we evaluate the long-term safety of a second hypothetical implementation of the concept that has several notable differences in site and design features compared to the EIS case study. We assume that the containers are constructed from copper, that they are placed within the disposal rooms, and that the vault is located in a more permeable rock domain.

In this study, we consider the groundwater transport scenario and the radionuclides expected to be the most important contributors to dose and radiological risk. We use a prototype systems assessment code, comprising the SYVAC3 executive (the third generation of the SYstems Variability Analysis Code) and models representing the vault, geosphere and biosphere. We have not dealt with other, less likely scenarios, other radionuclides, chemically toxic elements, and some aspects of software quality assurance.

The present study provides evidence that the second hypothetical implementation of the disposal concept would meet the radiological risk criterion established by the Atomic Energy Control Board by about an order of magnitude. The study illustrates the flexibility for designing engineered barriers to accommodate a permeable host-rock condition in which advection is the dominant contaminant transport process.

Atomic Energy of Canada Limited
Whiteshell Laboratories
Pinawa, Manitoba R0E 1L0
1996

AECL-11494-5
COG-95-552-5

LE STOCKAGE PERMANENT DES DÉCHETS DE COMBUSTIBLE NUCLÉAIRE DU CANADA : ÉTUDE DE LA SÛRETÉ POST-FERMETURE DE LA MISE EN PLACE EN CHAMBRE DU COMBUSTIBLE CANDU IRRADIÉ RENFERMÉ DANS DES CONTENEURS EN CUIVRE ENFOUIS DANS LA ROCHE PLUTONIQUE PERMÉABLE VOLUME 5 : ÉVALUATION RADIOLOGIQUE

par

B. W. Goodwin, T. H. Andres, W. C. Hajas, D. M. LeNeveu,
T. W. Melnyk, J. G. Szekely, A. G. Wikjord, D. C. Donahue, S. B. Keeling,
C.I. Kitson, S. E. Oliver, K. Witzke et L. Wojciechowski

RÉSUMÉ

Le concept de stockage permanent des déchets de combustible nucléaire du Canada prévoit l'isolement des déchets dans des conteneurs de longue durée de vie placés dans une installation de stockage à une profondeur de 500 à 1 000 m, dans la roche plutonique du Bouclier canadien. Ce concept permet une large gamme de méthodes, de matériaux, de sites et de modèles. Le système ouvragé serait conçu en fonction du site de stockage permanent retenu.

La faisabilité technique de ce concept et ses incidences sur l'environnement et la santé humaine sont présentées dans l'Étude d'impact sur l'environnement (EIE) (EACL 1994a,b), appuyée par neuf rapports de référence (Davis et coll. 1993; Davison et coll. 1994a,b; Goodwin et coll. 1994; Greber et coll. 1994; Grondin et coll. 1994; Johnson et coll. 1994a,b; Simmons et Baumgartner 1994). Un des rapports (Goodwin et coll. 1994) présente l'évaluation de post-fermeture, une étude de cas qui intègre des informations tirées d'études techniques, de recherches sur le terrain, d'analyses en laboratoire, d'opinions de spécialistes et d'analyses mathématiques détaillées pour évaluer les performances à long terme du système de stockage permanent par rapport aux critères de sûreté, aux lignes directrices et aux normes.

Dans l'étude de cas de l'EIE, nous avons analysé une réalisation hypothétique qui est conforme aux caractéristiques globales du concept et qui utilise un site et un modèle précis afin d'assurer que les informations et les données utilisées pour l'évaluation sont uniformes et pertinentes. Nous avons supposé que les conteneurs résistants à la corrosion étaient en titane de nuance 2, qu'ils avaient été placés dans des trous forés dans les chambres de l'installation de stockage et que cette dernière se trouvait dans la roche plutonique faiblement fracturée et de faible perméabilité.

Dans le présent rapport, nous évaluons la sûreté à long terme d'une deuxième réalisation hypothétique du concept qui présente plusieurs différences significatives sur le plan des caractéristiques du site et du modèle par rapport à l'étude de cas de l'EIE. Nous avons supposé que les conteneurs étaient en cuivre, qu'ils

avaient été placés dans les chambres à l'intérieur de l'installation de stockage et que cette dernière était située dans la roche de plus grande perméabilité.

Pour cette étude, nous avons supposé que le scénario de migration des eaux souterraines et les radionucléides étaient les facteurs les plus importants dans les risques liés à la dose et aux effets radiologiques. Nous avons utilisé un programme d'évaluation prototype comprenant le SYVAC3 (*System Variability Analysis Code*), troisième génération du programme de calcul pour l'analyse de la variabilité des systèmes, et des modèles représentant l'installation, la géosphère et la biosphère. Nous n'avons pas examiné d'autres scénarios moins vraisemblables ni d'autres radionucléides, éléments chimiques toxiques ou aspects d'assurance qualité du logiciel.

La présente étude démontre que la deuxième réalisation hypothétique du concept de stockage permanent satisferait d'environ un ordre de grandeur supplémentaire aux critères établis par la Commission de contrôle de l'énergie atomique en matière de risque radiologique. L'étude démontre la souplesse de la conception des barrières ouvragées dans une situation où la roche d'accueil est perméable et pour laquelle l'advection est le principal processus de transport des contaminants.

Énergie atomique du Canada limitée
Laboratoires de Whiteshell
Pinawa (Manitoba) R0E 1L0
1996

AECL-11494-5
COG-95-552-5

CONTENTS

LIST OF TABLES

LIST OF FIGURES

PREFACE

The concept for disposal of Canada's nuclear fuel waste involves isolating the waste in corrosion-resistant containers emplaced and sealed within a vault at a depth of 500 to 1000 m in plutonic rock of the Canadian Shield. The technical feasibility and social aspects of the concept, and its impact on the environment and human health, are presented in an Environmental Impact Statement (EIS) (AECL 1994a), a summary of the EIS (AECL 1994b) and a set of nine primary references (Davis et al. 1993; Davison et al. 1994a,b; Goodwin et al. 1994a; Greber et al. 1994; Grondin et al. 1994; Johnson et al. 1994a,b; Simmons and Baumgartner 1994).

The disposal concept permits a choice of methods, materials, site locations and designs (AECL 1994a,b; Johnson et al. 1994a; Simmons and Baumgartner 1994). This preface puts into perspective the following three studies which illustrate the long-term safety of different implementations of the concept:

- the postclosure assessment case study of a reference disposal system presented in the EIS (AECL 1994a,b; Goodwin et al. 1994a);

- a study to illustrate how to identify a favourable vault location that would ensure long groundwater travel times from the vault to the accessible environment (Stevenson et al. 1995, 1996; Ophori et al. 1995, 1996); and

- the present study that illustrates (i) the flexibility for designing engineered barriers to accommodate a permeable host-rock condition in which advection is the rate-determining contaminant transport process (Baumgartner et al. 1996), and (ii) the flexibility of the modelling methodology to simulate the long-term performance of different design options and site characteristics (this report, Johnson et al. 1996, Stanchell et al. 1996, Wikjord et al. 1996, Zach et al. 1996).

THE POSTCLOSURE ASSESSMENT CASE STUDY PRESENTED IN THE EIS

The EIS (AECL 1994a,b) and four of the primary references (Davis et al. 1993, Davison et al. 1994b, Goodwin et al. 1994a and Johnson et al. 1994b) describe a case study of the long-term (i.e., postclosure) performance of a hypothetical implementation of the concept, referred to as the *reference disposal system*.

The reference system illustrates what a disposal system, including the vault, geosphere and biosphere, might be like. Although it is hypothetical, it is based on information derived from extensive laboratory, field and engineering investigations. Many of the assumptions made about the long-term performance of the reference system are conservative; that is, they would tend to overestimate adverse effects. The technology specified is either available or judged to be readily achievable. The reference disposal system includes one possible choice among the options for such things as the waste form, the disposal container, the buffer and backfill, the shaft seals and bulkheads, the location and depth of the vault, and the orientation and layout of the vault with respect to the geological features of the site. The components and designs chosen for the engineered barriers and the site conditions represented in the reference system are not being recommended, but rather, they illustrate a technically feasible way of implementing the disposal concept. In an actual implementation of the concept, the engineered system would be adapted to the lithostructural, hydrogeological, geochemical, geothermal, geomechanical, and geomicrobiological conditions of the host rock formation, and the expected evolution of those conditions over thousands of years.

The *reference vault* (Johnson et al. 1994b) of the EIS postclosure assessment case study includes used-fuel bundles from CANDU® reactors, encapsulated in thin-walled Grade-2 titanium alloy containers packed with particulate for mechanical support, emplaced in boreholes in the floor of rooms, and surrounded by a sand-bentonite mixture. The rooms are filled with a lower backfill of crushed granite and lake clay and an upper backfill of sand and bentonite, and the entrances are sealed with concrete bulkheads. The plan area and the design capacity of the vault were initially set at 4.0 km^2 and 10.1 million fuel bundles (191 000 Mg U) respectively. The fuel inventory is roughly equivalent to the waste that would accrue in 100 a at the current production rates in Canada. The plan area was subsequently reduced to 3.2 km^2 and the inventory to 8.5 million bundles (162 000 Mg U), as a result of design constraints to ensure a large margin of safety in the case study. The borehole-emplacement geometry was modelled as layered planar elements (slabs) representing the waste form, buffer, backfill and host rock.

The *reference geosphere* (Davison et al. 1994b) consists of the host rock formation, its groundwater flow system, the materials used to seal the shafts and exploration boreholes, and a water well. The geological characteristics of the reference geosphere are derived from data from AECL's Whiteshell Research Area (WRA), located near Lac du Bonnet, Manitoba. This area includes a substantive portion of the Lac du Bonnet Batholith, a large granitic rock body several kilometres deep with an exposed surface measuring over 60 km long and 20 km across at its widest part. The granitic body was intruded over 2.5 billion years ago into the rocks existing at the time. The batholith, the surrounding rocks, and the interfaces between them have been the subject of field investigations for more than 15 a. Most of the information about the rock mass, such as the location and orientation of fractures and fracture zones, is based on field studies of the WRA, including detailed investigations that were conducted to locate and construct an Underground Research Laboratory (URL) to a depth of 440 m. For geological structures outside the areas where detailed borehole information was available, inferences have been made on the basis of nearby boreholes; geological mapping; and satellite, airborne and ground-based geophysical surveys. The hypothetical vault for the reference system was located at a depth of 500 m within the rock mass investigated at the URL to ensure that the maximum amount of available subsurface data was used to construct the geosphere model.

In the postclosure assessment of the reference system, we assumed that a large, low-dipping, fracture zone — designated LD1 — was located close to the vault horizon. Although field evidence from the URL revealed that this fracture zone did not extend beyond a depth of about 400 m, we conservatively assumed that it continued to much greater depths and connected with other vertical fracture zones. In this situation, LD1 became a pathway for rapid groundwater flow from the depth of the hypothetical vault to the accessible environment. We constrained all waste disposal rooms to be located beneath LD1 (i.e., to the footwall side of the fracture) and imposed a waste exclusion distance of 50 m within the low-permeability, sparsely fractured rock domain between this fracture zone and the nearest waste disposal room of the vault. To accommodate the waste exclusion distance, we chose to restrict the waste capacity of the vault relative to the capacity specified in a conceptual engineering study (Simmons and Baumgartner 1994). These design constraints, together with the hydrogeological properties of the rock beneath LD1, ensured that (i) contaminants passed through the backfill, a large reservoir which reacts strongly with most of the contaminants, and (ii) diffusion was the dominant transport process from the waste disposal rooms through the lower rock domain to the fracture zone.

The *reference biosphere* (Davis et al. 1993) consists of the surface and near-surface environment, including the water, soil, air, people, and other organisms, as encountered on the Canadian Shield as a whole. However, the parts of the biosphere that interface with the geosphere are specific to the WRA. In all other respects, the biosphere is assumed to be typical of the Canadian Shield, consisting of rocky outcrops; bottom lands with pockets of soil, bogs, and lakes; and uplands with meadows, bush, and

---

CANDU® is a registered trademark of Atomic Energy of Canada Limited (AECL).

forests. No major changes in the topography of the region are likely to occur during the 10 000 a following closure of a disposal facility. Changes in climate, surface water flow patterns, soils, and vegetation types are expected to be within the range of variation currently observed across the Shield; such variations are included in the distributions of values of model parameters specified for the EIS case study.

The long-term safety analyses of this system of engineered and geological barriers indicated that the maximum estimated mean dose rate to an individual in the critical group during the first 10 000 a is about 100 million times smaller than dose rate from natural background radiation. The corresponding risk is about a million times smaller than the radiological risk criterion specified by the Atomic Energy Control Board in Regulatory Document R-104 (AECB 1987).

A STUDY TO IDENTIFY A FAVOURABLE VAULT LOCATION

In an actual implementation, it would be advantageous to locate the disposal vault in a hydraulically favourable setting within the large-scale groundwater flow system of a siting area. Recently, we completed a separate study to illustrate how such a location could be found within the WRA. The conceptual hydrogeological model of the WRA was revised using information from a program of regional geologic mapping, geophysical surveys and borehole drilling and testing (Stevenson et al. 1995, 1996). Large-scale groundwater flow modelling was then performed using a three-dimensional, finite-element hydrogeological code; and groundwater travel times, flow pathways and discharge locations were determined with a particle tracking code (Ophori et al. 1995, 1996).

This study has indicated that diffusion is the rate-determining transport process and diffusive transport times greater than 10^5 a could likely be achieved by selecting a vault location at 750 m depth about 5 km northeast of the URL. Advective travel times are about two orders of magnitude longer than the diffusive transport time. Since the groundwater flow and particle-tracking analyses indicated that such a favourable location would likely ensure a margin of safety even greater than that calculated for the EIS case study, a full systems analysis was not carried out. Instead, we directed our efforts to the present study in which we evaluate the long-term effects of a hypothetical geological setting with a permeable host-rock condition.

THE PRESENT STUDY

A wide range of design options is possible within the general definition of the disposal concept (AECL 1994a,b; Johnson et al. 1994a; Simmons and Baumgartner 1994). In the present study, we illustrate the potential of designing the engineered barriers and the vault to increase the robustness of the long-term safety case, or to compensate for hydrogeological conditions that could result in a less effective geosphere barrier than the one we specified for the EIS case study. In addition, we illustrate the flexibility of the modelling approach to integrate new features, processes and data representing different design options and site characteristics into a full systems assessment. To achieve these ends, we have undertaken an analysis of the feasibility and safety of emplacing long-lasting copper containers within vault rooms (as opposed to deposition in boreholes in the floor of rooms) in a hypothetical volume of permeable plutonic rock where advective travel times from the vault to the biosphere are very short relative to those in the EIS case study. Although we have not encountered such conditions at disposal-vault depths in our investigations at various research areas on the Shield, performance assessments done for the Swedish and Finnish nuclear waste disposal programs have considered these conditions in the crystalline rocks of the Fennoscandian Shield. We are not suggesting that such rock conditions might constitute favourable, desirable, or even acceptable conditions for an eventual disposal site on the Canadian Shield. Rather, the study is intended to illustrate the effectiveness of the in-room emplacement method and copper containers in inhibiting the release of contaminants from the vault.

The vault model for the present study simulates dissolution of used CANDU fuel in a geochemical environment, which evolves from an initial oxidative condition, caused by residual air and radiolysis, to an eventual steady-state anoxic condition. The model simulating the performance of copper containers is based on pinhole manufacturing defects and indefinite lifetime (i.e., no corrosion-induced failures). The in-room emplacement geometry is modelled as a line source representing the waste form, point sources representing pinholes in the defected containers randomly located in the vault, and concentric cylinders representing the buffer, backfill and excavation disturbed zone.

The geosphere model for the present study is more speculative than the one used for the EIS case study because it does not represent conditions we have encountered at any of our geologic research areas. We assume that the vault depth, the geometry of the geosphere model, and the arrangement of major fracture zones and rock mass domains surrounding the disposal vault are identical to those of the EIS case study. However, we assume much higher permeability and lower porosity conditions in the rock domain adjacent to the vault than the conditions observed at the URL and used in the EIS case study. As a result, the lower rock domain is not a diffusion-dominated barrier and the low-dipping fracture zone, LD1, is not the dominant advection pathway to the surface. The effects of geothermal gradient, vault heat and a water supply well on the groundwater flow field have been simulated and the implications on the long-term redox conditions in the vault have been assessed. The groundwater travel times from the disposal vault to the surface are up to 10 000 times shorter in this present geosphere model than in the model used for the EIS case study.

For this study, there is no advantage to constraining the location of the disposal rooms relative to LD1 as was done in the EIS case study. Thus the waste disposal rooms are located both below and above LD1 (i.e., on both the footwall and hangingwall sides of the fracture). The 50-m waste exclusion distance is retained but is relatively insignificant because advection is the dominant transport process in the permeable lower rock domain. Thermal restrictions and shielding requirements of the in-room emplacement option result in a reduction in the density of waste containers of roughly 50% relative to the borehole emplacement option of the EIS case study.

The biosphere model for the present study includes a number of changes, notably inclusion of additional radionuclides with shorter half-lives, inhalation pathways for animals, the most recent internal dose conversion factors of the International Commission on Radiological Protection (ICRP 1991a, b), geosphere dose limits for non-human biota, and updated values of model input parameters. Moreover, the part of the model representing the biosphere/geosphere interface was improved to account more fully for terrestrial discharge of radionuclides.

COMPARISON OF THE EIS CASE STUDY AND THE PRESENT STUDY

The key features of the EIS postclosure assessment case study and the present study are summarized as follows:

	EIS CASE STUDY	PRESENT STUDY
DESIGN CONSIDERATIONS		
Emplacement option	borehole	in-room
Vault area/depth	3.2 km^2/500 m	3.4 km^2/500 m
Fuel inventory: number of bundles	8.5 million	4.3 million
mass of uranium	162 000 Mg	82 000 Mg
Fuel Burnup	685 GJ/kg U	720 GJ/kg U
Fuel Cooling time	10 a	10 a
Number of bundles per container	72	72
Number of waste containers	118 700	60 100
Room locations	footwall of LD1	footwall and hangingwall of LD1

	EIS CASE STUDY	PRESENT STUDY
VAULT MODEL		
Vault model geometry	layered slabs	nested cylinders
Fuel dissolution model	thermodynamic	kinetic
Container shell material	Grade-2 Ti	high purity Cu
Container corrosion mechanisms	localized crevice and delayed hydride cracking	general corrosion and pitting
Fraction of containers failed instantly	10^{-3} to 10^{-4} (complete failure)	10^{-3} to 10^{-4} (pinhole failure)
Fraction of containers failed by 10^4 a	1.0	10^{-3} to 10^{-4}
Effective buffer thickness	0.25 m	1.48 m
Effective backfill thickness	1.4 m	0.76 m
Excavation disturbed zone	evaluated outside system model	evaluated explicitly within system model
GEOSPHERE MODEL		
Conceptual model of fracture zones and rock domains	URL area of WRA	URL area of WRA*
Permeability of rock domain surrounding vault	10^{-19} m^2	10^{-17} m^2
Effective transport porosity of rock domain surrounding vault	3×10^{-3}	10^{-3} to 10^{-5}
Minimum contaminant transport times from vault to biosphere	tens of thousands of years	tens of years
Rate-determining transport process	diffusion	advection
Maximum well depth	200 m	100 m
BIOSPHERE MODEL	BIOTRAC1 - typical of the Canadian Shield	BIOTRAC2 - modifications to improve the model and update the parameters
SYSTEMS ANALYSIS		
Computer Code	third generation code (SYVAC3-CC3-ML3)	prototype (PR4) of fourth generation code (SYVAC3-CC4)
Maximum estimated dose rate to a member of critical group up to 10^4 a	about 10^{-11} Sv/a	about 10^{-6} Sv/a
Time at which estimated dose rate reaches peak	> 10^5 a	about 10^4 a
Key radionuclides contributing to estimated dose rate up to 10^4 a	^{129}I ^{36}Cl ^{14}C	^{129}I, ^{36}Cl ^{14}C, ^{79}Se ^{90}Sr, ^{90}Y, ^{99}Tc
Principal safety feature	low permeability rock domain surrounding vault	long-lasting containers

* The conceptual model used for this present study does not represent a combination of conditions that we have encountered at any of our geologic research areas on the Shield. It has the same geometric arrangement of fracture zones and rock domains as was used in the EIS case study; however, the permeability of the rock domain surrounding the vault has been assumed to be 10^{-17} m^2. This permeability is 100 times greater than the value specified for the EIS case study, which was based on actual measurements within the lower rock zone at the URL.

The EIS case study, the study to identify a favourable vault location, and the present study illustrate the flexibility of AECL's disposal concept in taking advantage of the retention, delay, dispersion, dilution and radioactive decay of contaminants in a system of natural barriers provided by the geosphere and the hydrosphere and of engineered barriers such as the waste form, container, buffer and backfill. In an actual implementation, the engineered system would be designed for the geological conditions encountered at the host site.

HIERARCHY AND SCOPE OF DOCUMENTS FOR THE PRESENT STUDY

This study, presented in five main volumes and a number of supporting documents, is organized as follows:

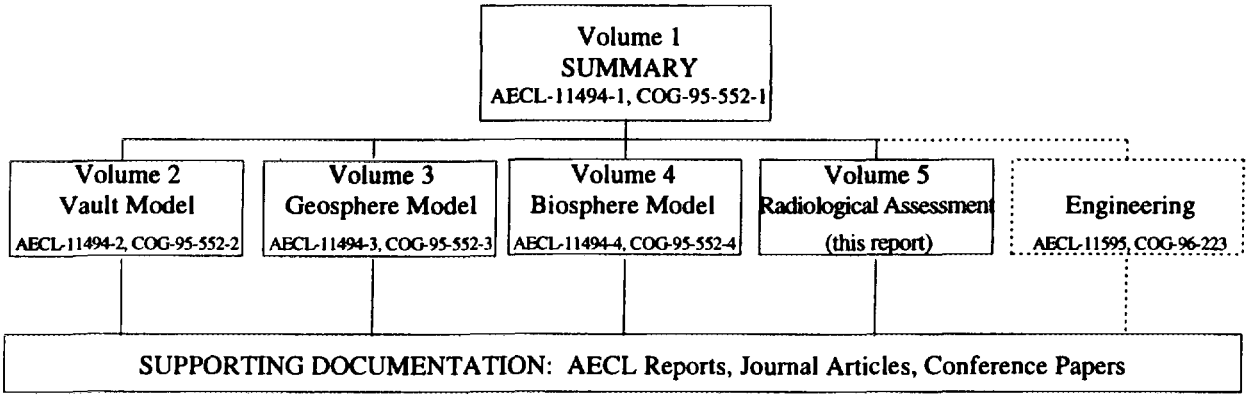

Volume 1, Summary (Wikjord et al. 1996), provides an overview of this study and summarizes the design considerations and safety of in-room emplacement of CANDU used-fuel in long-lasting copper containers in permeable plutonic rock.

Volume 2, Vault Model (Johnson et al. 1996), describes and justifies the assumptions, model and data used to analyze the long-term behaviour of the engineered system (the near-field), including the waste form (used CANDU fuel), container shell (deoxidized, low-phosphorous copper), buffer (precompacted bentonite clay and silica sand), backfill (glacial lake clay and crushed rock), and excavation disturbed zone.

Volume 3, Geosphere Model (Stanchell et al. 1996), describes and justifies the assumptions, model and data used to analyze the transport of contaminants through permeable plutonic rock of the Canadian Shield, including the effects of a pumping well. The geological characteristics assumed in this study are not based on an integrated data set for any particular field research area.

Volume 4, Biosphere Model (Zach et al. 1996), describes and justifies the assumptions, model and data used to analyze the movement of contaminants through the near-surface and surface environments and to estimate radiological impacts on humans and other biota.

Volume 5, Radiological Assessment (this report), provides an estimate of long-term radiological effects of the hypothetical disposal system on human health and the natural environment, including an analysis of how uncertainties of the assumed site and design features affect system performance.

A separate engineering study (Baumgartner et al. 1996), shown by the dotted lines, is closely linked to this 5-volume series. It describes the conceptual design, technical feasibility, thermal and mechanical analyses, and project lifecycle for implementing an engineered system based on the in-room emplacement of copper containers. It is applicable to a broader range of geosphere conditions than assumed in the present study.

1. INTRODUCTION

1.1 BACKGROUND

In 1978, Atomic Energy of Canada Limited (AECL) and Ontario Hydro were assigned responsibility, by the Governments of Canada and Ontario, for the Canadian Nuclear Fuel Waste Management Program. This research program was established to evaluate the feasibility and safety of the concept of deep underground disposal of nuclear fuel waste in intrusive igneous rock of the Canadian Shield (Joint Statement 1978, 1981).

AECL has submitted an Environmental Impact Statement (EIS) (AECL 1994a,b) of the disposal concept to a federal Environmental Assessment and Review Panel (EARP 1992) for public and regulatory review. The proposed disposal concept is based on deep geological disposal of nuclear fuel waste in which

- the waste form is either used CANDU® fuel or the solidified high-level waste from reprocessing;
- the waste form is sealed in a container designed to last at least 500 a and possibly much longer;
- the containers of waste are emplaced in rooms in a disposal vault or in boreholes drilled from the rooms;
- the disposal rooms are nominally 500 to 1000 m below the surface;
- the geological medium is plutonic rock of the Canadian Shield;
- each container of waste is surrounded by a buffer;
- each room is sealed with backfill and other vault seals; and
- all tunnels, shafts and exploration boreholes are ultimately sealed in such a way that long-term safety would not depend on institutional controls (AECL 1994a,b).

The disposal concept permits a choice of methods, materials, site locations and designs. If the concept were accepted for implementation, a disposal facility would be designed specifically for a selected disposal site.

The EIS is supported by 9 primary references (Davis et al. 1993; Davison et al. 1994a,b; Goodwin et al. 1994a; Greber et al. 1994; Grondin et al. 1994; Johnson et al. 1994a,b; Simmons and Baumgartner 1994). One of these (Goodwin et al. 1994a) describes a long-term environmental and safety assessment, or postclosure assessment. The postclosure assessment described in the EIS evaluated one particular hypothetical implementation of the concept, in which we assumed several specific site and design choices so that the assessment study would be firmly supported by a set of engineering and scientific research information (AECL 1994a, Goodwin et al. 1994a). For example, we assumed in the EIS study (part (a) of Figure 1) that

- the corrosion-resistant containers were constructed from Grade-2 titanium alloy;
- the containers were placed in boreholes drilled into the floors of the disposal rooms;

CANDU® is a registered trademark of Atomic Energy of Canada Limited (AECL).

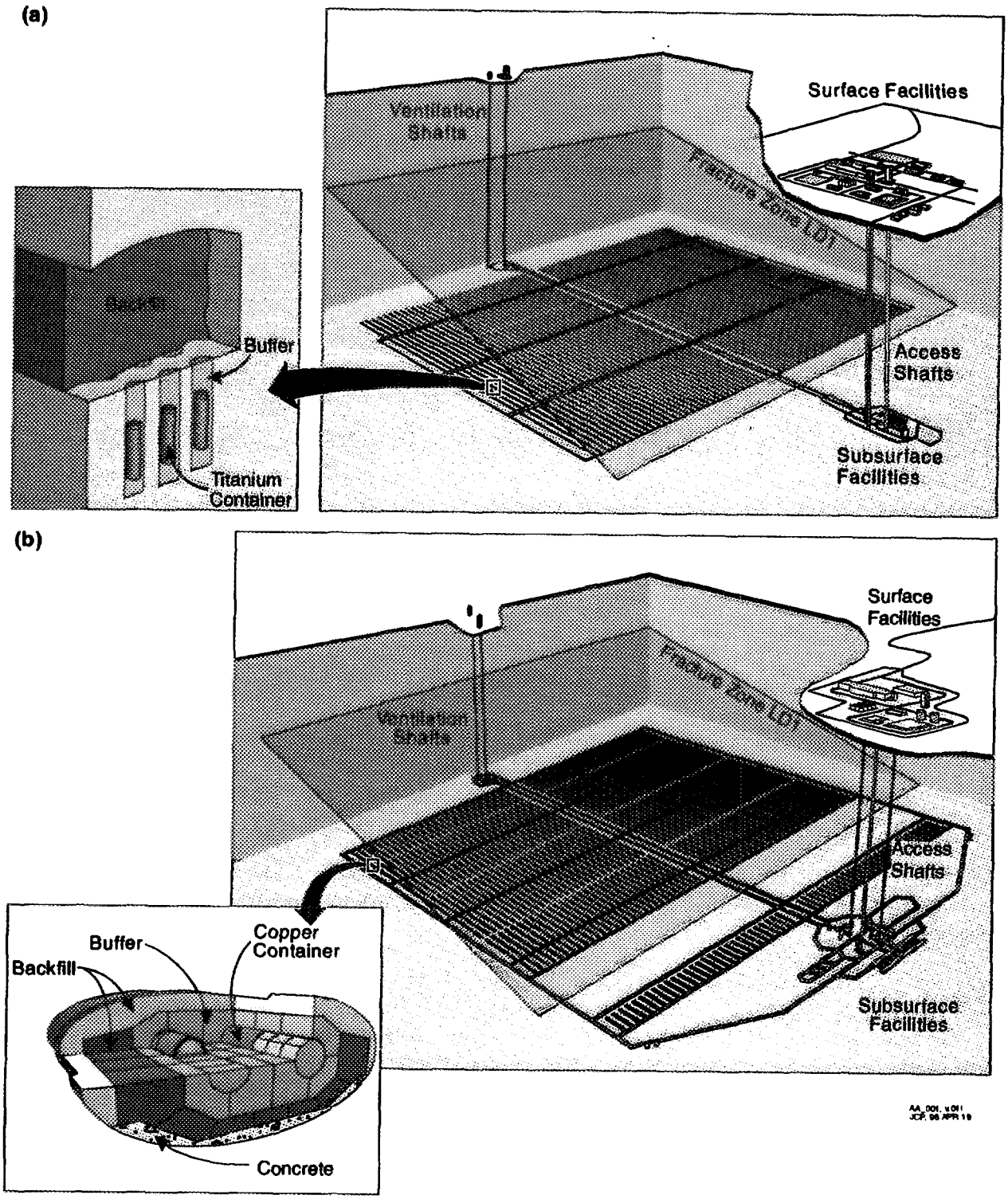

FIGURE 1: Illustration of Two Hypothetical Disposal Systems for the Disposal of Canada's Nuclear Fuel Waste. Part (a) depicts the disposal system that was evaluated in the EIS (AECL 1994a, Goodwin et al. 1994a): the vault is located at a depth of 500 m in low-permeability sparsely fractured rock, the disposal rooms lie below a nearby fracture zone, and Grade-2 titanium alloy containers are emplaced in boreholes drilled into the floors of the disposal rooms (shown in the inset). Part (b) portrays the disposal system evaluated in this report: the vault is at a depth of 500 m in a permeable host rock, the disposal rooms lie above and below the fracture zone, and copper containers are emplaced within the rooms. These illustrations are not drawn to scale and some features have been exaggerated.

- the vault was located in a domain of low-permeability, sparsely fractured plutonic rock (with properties based on hydrologic and geologic studies at the Underground Research Laboratory within the Whiteshell Research Area); and

- the disposal vault was located beneath a nearby fracture zone.

This report presents a postclosure assessment of a second hypothetical implementation of the disposal concept. There are significant differences between the system specified for this study and the system specified for the EIS case study. In particular, we assume in this study that (part (b) of Figure 1)

- the corrosion-resistant containers are constructed from high-purity copper,

- the containers are placed within the confines of the disposal rooms,

- the vault is located in a domain of permeable plutonic rock, and

- the disposal vault has disposal rooms above and below a nearby fracture zone.

Some of these choices were made to deal with specific criticisms of the EIS and to emphasize that the concept includes flexible alternatives. In general, this second hypothetical implementation uses more robust engineered barriers and assumes a much less effective geosphere barrier compared with the disposal system evaluated in the EIS case study. The main objective of this report is to determine if these engineered barriers can compensate for a geosphere that is less effective in terms of long-term performance and safety.

1.2 SCOPE OF THIS POSTCLOSURE ASSESSMENT

This report presents a postclosure assessment - a long-term environmental and safety assessment that starts from the time a disposal facility is closed and extends thousands of years into the future. We follow the methodology described by Goodwin et al. (1994a) and apply it in this report to a second hypothetical implementation of the concept for disposal of Canada's nuclear fuel waste.

This study is qualified to be a "scoping" or preliminary assessment with the following limitations.

- Only variations on the groundwater transport scenario are examined. The groundwater transport scenario describes the long-term behaviour of the disposal system where contaminants escape from a disposal vault dissolved in groundwater. It is considered to be the most likely way in which people and the environment would be affected. The variations considered in this report are similar to those studied in the EIS case study (called the SYVAC scenarios in Goodwin et al. (1994a)). Many modifications to the scenario were made to accommodate the differences between the two disposal systems. In addition, some restrictions are placed on the allowable variations (for example, the unlikely occurrence of a well deeper than 100 m is not included). A full postclosure assessment would evaluate other, less likely scenarios.

- Only the radionuclides expected to be the most important contributors to dose and risk are considered. We have used the results of a radionuclide screening study to identify an abbreviated list of radionuclides that are expected to be the most significant contributors to total dose for times up to 10^5 a after closure. A full postclosure assessment would analyze a more exhaustive list of radionuclides.

- The analysis provides quantitative estimates of radiation dose rate for times up to 10^4 a for comparison with the AECB radiological risk criterion (AECB 1987). (We present quantitative results for longer time periods, up to ten million years, for mathematical completeness, but the models used to generate them are not considered reliable for such lengthy periods.) A full postclosure assessment would also include qualitative arguments covering longer time frames and would include an evaluation of potential toxicity impacts from chemical elements in the nuclear fuel waste.

- The quantitative estimates of impact use prototype computer code. Our software development procedures allow the creation of preliminary (or prototype) code to examine the accuracy and computational efficiency of new mathematical algorithms and to perform scoping studies. Although this prototype code was subject to many elements of software quality assurance, a full postclosure assessment would utilize computer code that complies with a more comprehensive set of quality assurance standards.

Thus this study deals with the central issues that make it different from the EIS case study. However, it is not as comprehensive as the EIS case study. Further analyses are required to evaluate less likely scenarios such as scenarios involving deep wells and inadvertent human intrusion; to evaluate other radionuclides and chemically toxic elements, and to evaluate potential impacts over time scales longer than 10^4 a after closure.

1.3 ORGANIZATION OF THIS REPORT

In the previous sections, we outlined the connections of this study with the EIS case study. In the remainder of this report, we document a scoping postclosure assessment of a second hypothetical implementation of the concept for disposal of Canada's nuclear fuel waste. We assume that this second implementation involves more robust engineered barriers and a more permeable host rock.

We summarize in Section 2 the method used to estimate postclosure impacts of the deep underground disposal of Canada's nuclear fuel waste. More details are provided by Goodwin et al. (1994a).

The application of this method to the disposal system specified for this study is described in the remaining sections. Section 3 outlines the characteristics of the disposal system that are relevant to a long-term study. Section 4 describes a scenario analysis that identifies the features, events and processes that require evaluation. Section 5 discusses the system model used in the quantitative estimation of postclosure radiological impacts.

We discuss the results of our analysis in Section 6. Our estimates of impacts use an approach known as systems variability analysis or probabilistic systems analysis. This approach has been developed to include the effects of parameter uncertainty and uses a large set of simulations in which parameter values are randomly sampled from associated probability distributions. We also discuss in Section 6 the results of a probabilistic sensitivity analysis, aimed at identifying influential radionuclides, parameters and processes, and quantifying their effects. In the Appendix, we provide data on 32 randomly sampled simulations to show the variations that are possible within this probabilistic framework. We also provide a more detailed analysis of four selected simulations, including extreme simulations that yield very large and very small estimates of dose rate.

The overall results are summarized in Section 7, where we show that the estimated impacts comply with the radiological risk criterion prescribed by the Atomic Energy Control Board (AECB) in regulatory document R-104 (AECB 1987).

2. THE POSTCLOSURE ASSESSMENT METHODOLOGY

Figure 2 illustrates the methodology used in the postclosure assessment for the EIS case study (Goodwin et al. 1994a) which is followed in the present study. There are six main steps and connections with other elements of the Canadian Nuclear Fuel Waste Management Program.

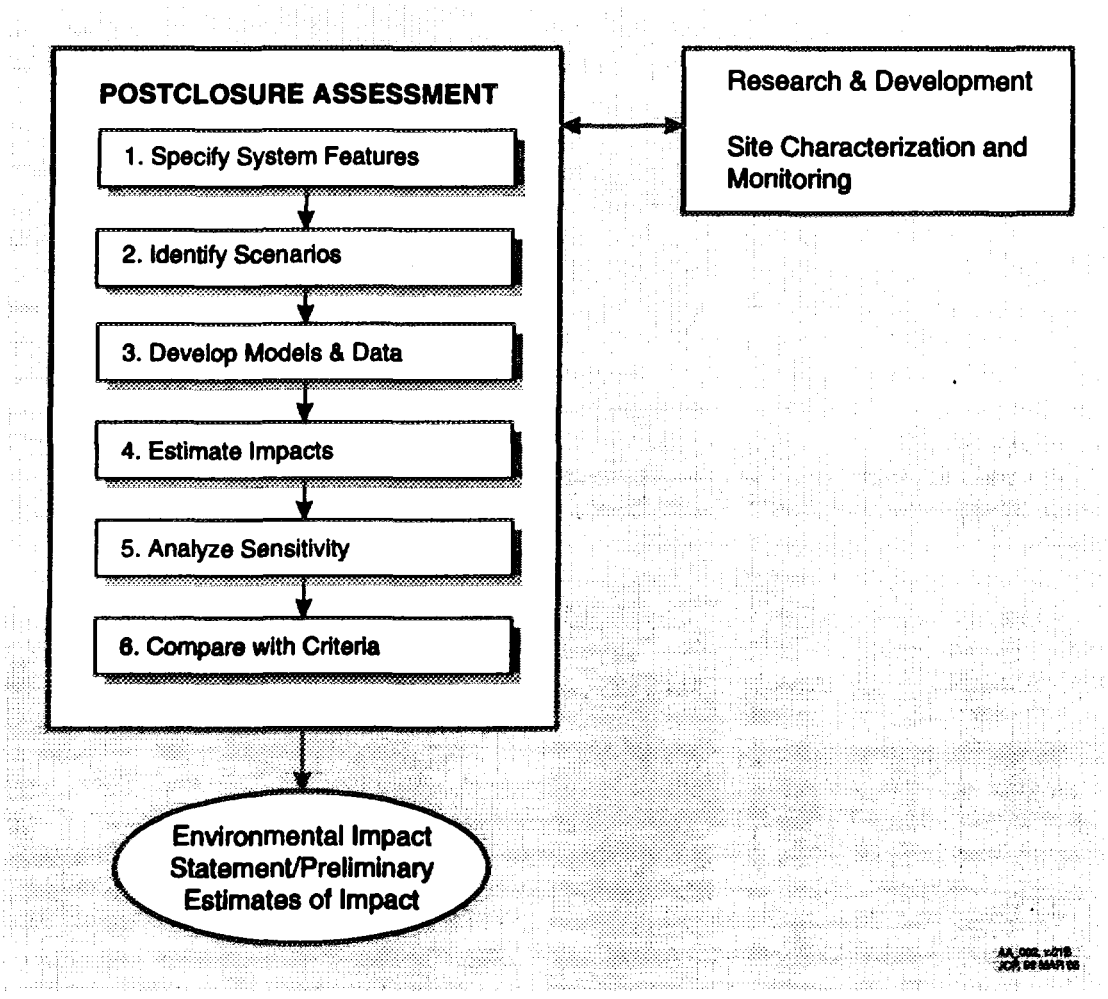

FIGURE 2: Main Steps in the Postclosure Assessment Methodology. In the first step, we specify the characteristics of the disposal system; we then identify all scenarios that require quantitative evaluation. In steps 3 and 4, we develop the models and data required to simulate the long-term behaviour of the disposal system and then use the models and data to estimate potential impacts. We apply sensitivity analysis in step 5 to identify influential factors that could affect safety and performance. In the last step, estimated impacts are compared with regulatory criteria, standards and guidelines. Results may be documented in an environmental impact statement for a formal postclosure assessment or used to provide preliminary information that may be used to guide changes to the design of the disposal system and the models and data used to describe the system. There is a strong interplay between the postclosure assessment and programs for research and development and for site characterization and monitoring.

The outcome from the scoping assessment described herein is not fully comprehensive, but it can, nonetheless, be used to evaluate safety by, for example, estimating risk for comparison with the radiological risk criterion. This information would be used in decision-making processes aimed at determining the potential technical suitability of the hypothetical disposal system, if a design change would be beneficial, and if there is a need to refine the models and data used in the analysis.

It has been our experience that the steps in the postclosure assessment methodology are not completed linearly. Frequently there is extensive feedback wherein results from one step may require revisions to preceding steps (Goodwin et al. 1994a). In fact, this entire report is part of a larger feedback loop because it responds to issues that arose from the review of the EIS case study. We anticipate that the results of this scoping assessment would be used to refine some of the details that would be incorporated in subsequent studies.

The purpose and outcome of the six steps in Figure 2 are discussed briefly below. Their applications in the present study are described in Sections 3 to 7.

1. *Specify System Features.* The Canadian Nuclear Fuel Waste Management Program is a conceptual study and, therefore, the postclosure assessment must deal with a concept as opposed to an actual disposal facility at a particular site. However, our research indicates that studies of a generic design and generic location are of limited value because the long-term performance of a disposal system is strongly dependent on its detailed characteristics. To resolve this issue, we evaluate the performance of hypothetical implementations that assume a particular design and site location but that are consistent with the concept. Thus in the first step of the methodology, we describe (in Section 3) the hypothetical implementation that is being studied, including the assumed design features and the assumed facility location.

2. *Identify Scenarios.* The postclosure assessment deals with very long time frames, and we use a systematic procedure to identify factors (e.g., features, events and processes) that could have a significant effect on the future performance of the disposal system. We then decide how these factors should be taken into account in the postclosure assessment. Our analysis (documented in Section 4) draws from closely related work performed for the EIS case study (Goodwin et al. 1994a,b).

3. *Develop Models and Data for Simulating the System.* The disposal system is designed to protect humans and the environment for tens of thousands of years after closure. Over these long time scales, quantitative assessments of long-term performance are based on a simulation approach, using mathematical models to infer the long-term behaviour of a disposal system and to estimate its potential effects. The development of a system model and the specification of its associated data are made by qualified experts in a wide range of scientific and engineering disciplines. These data may be uncertain because, for example, they pertain to very long time scales; thus our assessment approach allows for the use of probability distributions to define the range and weighting of feasible values. Where it is not possible (or not necessary) to develop realistic models and data, we make conservative assumptions that would lead to overestimates of impact. We present (in Section 5) an overview of the mathematical models; more details, including the underlying scientific and engineering analysis, are provided by Johnson et al. (1996) for the vault model, by Stanchell et al. (1996) for the geosphere model, and by Zach et al. (1996) for the biosphere model.

4. *Estimate Impacts Using Mathematical Simulations.* We use the models and data to simulate the expected long-term behaviour of contaminants (radiotoxic and chemically toxic materials) in the nuclear fuel waste and to provide quantitative estimates of potential effects of the disposal system on humans and the environment. Our analysis (described in Section 6) is focussed on variations of the groundwater

transport scenario and the radionuclides that are expected to be the most important contributors to dose. The simulations are performed using a computer code called PR4 (the prototype of SYVAC3-CC4, an acronym for SYstems Variability Analysis Code, Generation 3 with the 4th generation of the system model describing the concept for disposal of Canada's nuclear fuel waste). Systems variability analysis, also known as probabilistic systems analysis, provides a comprehensive and systematic method to deal with parameter uncertainties in the estimation of impacts (Goodwin et al. 1994a).

5. *Analyze the Sensitivity of System Performance.* The goal of sensitivity analysis is to obtain a simpler understanding of the disposal system by identifying features of the system model that control estimated impacts. For example, we are interested in identifying parameters, radionuclides and pathways that have a strong influence on estimated dose rates to humans. Results from sensitivity analysis (summarized in Section 6.3) could also be used in studies aimed at improving and optimizing the overall performance. We use a technique called iterated fractional factorial design (IFFD) (Andres 1995) to identify influential parameters and to examine their effects; IFFD works efficiently with complex models having large numbers of candidate parameters.

6. *Compare Estimated Impacts with Regulatory Requirements.* The last step in Figure 2 compares estimated impacts with regulatory criteria, standards and guidelines. For our scoping study, the main impact of interest is the annual effective dose equivalent (called *dose rate* throughout this document) to a member of the critical group. The corresponding criterion is expressed as a radiological risk limit, which is associated with a dose rate limit of 5×10^{-5} Sv/a (AECB 1987). We show curves of dose rate and the (conditional) risk associated with the groundwater transport scenario. We also discuss estimated dose rates to representative nonhuman biota. Our comparisons (in Section 7) use the estimated dose rates from the probabilistic analysis to take into account the strong influence of parameter uncertainty.

In applying the postclosure assessment methodology to the present study, we have made some adjustments to respond to comments by reviewers of the EIS case study. These adjustments include the following (and more details are provided in the remainder of this report):

- Modelling the roles of the engineered barriers and the host rock (Section 5). In the EIS case study, our analysis showed that the geosphere was one of the most effective barriers to transport of contaminants from the disposal vault to the surface environment. Reviewers of the EIS expressed concern that an adequate volume of host rock may not exist. We also assumed in the EIS case study that all of the Grade-2 titanium alloy containers failed within several thousands of years and that they were ineffective as barriers starting from the instant of failure. In this study, we have assumed properties for the geosphere that make it a much less effective barrier. We have also assumed the use of a more durable copper-shell container, and our model allows that a failed container can still be an effective barrier by restricting contaminant releases to diffusion through small pinhole-sized defects.

- Documenting more scenarios (Section 6.4). Reviewers expressed concerns that the combined results presented in the EIS case study concealed scenarios where mean doses might exceed regulatory limits, such as scenarios where the critical group obtains its water from a water-supply well. We believe that the most efficient and most accurate approach for estimating mean dose rates is to combine scenarios together (where feasible) by building simulation models that handle a wide variety of conditions. We can then investigate selected scenarios by extracting appropriate simulations from our database. We examine in this report several specific scenarios to demonstrate that this type of analysis is possible and to show their associated dose rates.

- Showing more detailed simulation results (Section 6.2, Appendix). Reviewers of the EIS expressed a desire for more information on simulations that have extreme dose rates. We present

percentile bands that show the ranges of results for high- and low-dose simulations from a large set of randomly sampled simulations. We further examine a representative set of 32 randomly sampled simulations and list their input data for influential parameters and their estimated dose rates, and then we describe in detail the two highest-dose simulations and a low-dose simulation.

- Showing results over a longer time frame (Section 6, Appendix). Reviewers of the EIS expressed concern that dose rates were still rising at 10^5 a (the end-time of simulations in the EIS postclosure analysis) and that very high dose rates might occur at longer times. In this report, we plot results to 10 million years, even though the system model and data provides a less acceptable representation of the disposal system at these long times. We present the results primarily for mathematical completeness, and also to demonstrate that dose rates (in this study) have gone through a maximum near 10^4 a.

3. DESCRIPTION OF THE DISPOSAL SYSTEM

Figure 1a illustrates the hypothetical disposal system evaluated in the EIS (AECL 1994a, Goodwin et al. 1994a) and Figure 1b the hypothetical implementation evaluated in this report. Both of these systems are consistent with the proposed concept for disposal of Canada's nuclear fuel waste. As noted earlier, they differ mainly in the following specific choices.

- The container materials. This report examines the effect of containers fabricated from copper that would provide a much longer period of protection (Johnson et al. 1996).

- The design of the disposal vault. This report examines a vault design that would more readily accommodate a host rock that is highly stressed (Baumgartner et al. 1996) and that uses in-room emplacement so that the containers are surrounded by buffer and backfill.

- The location of the vault. We assume the general geological setting for the vault is the same as in the EIS case study; however, we assume the host rock is up to 100 times more permeable and thus groundwater velocities are significantly larger. (Stanchell et al. 1996).

These two disposal systems do not encompass the full range of choices that are permitted within the concept (AECL 1994a). For example, one feature in the proposed concept is a nominal vault depth of 500 to 1000 m, whereas the two hypothetical systems assume identical depths of 500 m.

Table 1 and the following text summarize some of the major similarities and differences between the two hypothetical disposal systems. More detailed descriptions of the system studied in this report, and the reasons for the differences, are provided in reports by Baumgartner et al. (1996) on engineering design, by Johnson et al. (1996) on the disposal vault, by Stanchell et al. (1996) on the geosphere, and by Zach et al. (1996) on the biosphere.

TABLE 1

COMPARISON OF DISPOSAL SYSTEMS
ASSESSED IN THE EIS CASE STUDY AND IN THIS REPORT*

Feature	DISPOSAL SYSTEM EIS Case Study	 Evaluated in this Report
Nuclear fuel waste		
type	Used-fuel bundles from CANDU reactors	Used-fuel bundles from CANDU reactors
burnup	685 GJ/kg U	720 GJ/kg U
number of bundles	8.5×10^6	4.3×10^6
total mass	1.62×10^8 kg U	8.2×10^7 kg U
Container		
material	Grade-2 titanium alloy	High-purity copper
failure mechanisms	Fabrication defects, crevice corrosion, delayed hydride cracking	Fabrication defects
fraction failed in 10^4 a	1.0	about 0.0002
dimensions	2.2 m long, 0.63 m diameter, 6.35 mm thick	1.2 m long, 0.86 m diameter, 25.4 mm thick
internal support	Ceramic (or other material) basket and glass beads	Stainless steel tubes and silica sand or glass beads
maximum temperature	94°C at 30 a	75°C at 15 a
number of containers	118 680	60 088
fuel bundles per container	72	72
Emplacement Method	Boreholes drilled into the floors of the vault, surrounded by buffer	Within the disposal rooms surrounded by buffer and and backfill
Buffer		
material	Bentonite clay and silica sand (50:50)	Bentonite clay and silica sand (50:50)
volume per container	4.9 m^3	9.4 m^3
dry density (minimum)	1.67 Mg/m^3	1.67 Mg/m^3
Backfill		
material	Lower backfill: glacial lake clay, crushed rock (25:75); upper backfill: bentonite and silica sand (50:50)	Dense backfill: glacial lake clay, bentonite and crushed granite (25:5:70); light backfill: bentonite and crushed granite (50:50)
volume per container	Lower: 15 m^3 Upper: 8 m^3	Dense backfill: 6.3 m^3 Light backfill: 5.5 m^3

* Unless otherwise stated, data are typical values.

continued ....\

TABLE 1 (continued)

Feature	DISPOSAL SYSTEM EIS Case Study	 Evaluated in this Report
dry density (minimum)	Lower: 2.1 Mg/m^3 Upper: 1.4 Mg/m^3	Dense: 2.1 Mg/m^3 Light: >1.2 Mg/m^3
Excavation damaged zone		
thickness	(not explicitly evaluated in	1.4 m
porosity	the postclosure assessment - would have no significant effect in this disposal system)	10^{-5} to $5x10^{-4}$ (value used cannot be smaller than that for rock layer 3)
axial permeability		10^{-17} to $6.7x10^{-13}m^2$
Vault design and layout		
depth	500 m	500 m
location	below fracture zone LD1	above and below LD1
minimum distance to LD1		
horizontal	150 m	150 m
perpendicular	50 m	50 m
dimensions	1900 x 1625 m	1900 x 1625 m (below LD1) and 1900 x 153 m (above LD1)
plan area	3.2 km^2	3.4 km^2
number of disposal rooms	448 (384 are 234 m long and 64 are 139 m long)	464 (348 are 230 m long and 116 are 110 m long)
Properties of the lower rock zone surrounding the disposal vault (layer 3)		
thickness	200 m	180 m
porosity	3×10^{-3}	10^{-5} to 10^{-3}
permeability	1×10^{-19} m^2	1×10^{-17} m^2
groundwater velocity (typical)	6×10^{-6} m/a	0.4 m/a
example retardation factors (median)	Am: 32000, C: 1.0, Cs: 2400, I: 1.0, Pu: 1100, Se: 110, Sn: 700, Sr: 120, Tc: 2.6, U: 24	Am: 2700, C: 1.0, Cs: 2300, I: 1.0, Pu: 760, Se: 85, Sn: 1900, Sr: 3.7, Tc: 2.0, U: 16
Properties of fracture zone LD1		
thickness	20 m	20 m
porosity	0.10	0.01 to 0.10
permeability	1×10^{-13} m^2	1×10^{-13} m^2
groundwater velocity (typical)	1.3 m/a	5.0 m/a
example retardation factors (median)	Am: 10000, C: 11, Cs: 880, I: 1.0, Pu: 2300, Se: 90, Sn: 5700, Sr: 20, Tc: 45, U: 920	Am: 3600, C: 12, Cs: 430, I: 1.0, Pu: 150, Se: 62, Sn: 6000, Sr: 5.0, Tc: 9.0, U: 220

continued ....\

TABLE 1 (concluded)

Feature	DISPOSAL SYSTEM EIS Case Study	DISPOSAL SYSTEM Evaluated in this Report
Properties of the intermediate zone of rock (layer 2)		
thickness	150 m	190 m
porosity	4×10^{-3}	10^{-5} to 10^{-3}
permeability	5×10^{-17} m^2	2×10^{-17} m^2
groundwater velocity (typical)	4×10^{-3} m/a	0.6 m/a
example retardation factors (median)	Am: 32000, C: 1.0, Cs: 2300, I: 1.0, Pu: 1100, Se: 130, Sn: 700, Sr: 120, Tc: 2.6, U: 24	Am: 2700, C: 1.0, Cs: 2300, I: 1.0, Pu: 760, Se: 85, Sn: 1900, Sr: 3.7, Tc: 2, U: 16
Properties of the upper zone of rock (layer 1)		
thickness	150 m	106 m
porosity	5×10^{-3}	10^{-5} to 10^{-3}
permeability	5×10^{-15} m^2	5×10^{-15} m^2
groundwater velocity (typical)	1.5 m/a	90 m/a
example retardation factors (median)	Am: 3900, C: 100, Cs: 63, I: 1.0, Pu: 1300, Se: 120, Sn: 360, Sr: 7.4, Tc: 12, U: 3200	Am: 1900, C: 68, Cs: 40, I: 1.0, Pu: 850, Se: 130, Sn: 8300, Sr: 5.0, Tc: 9, U: 290
Characteristics of the Biosphere		
general properties	typical of the Canadian Shield	typical of the Canadian Shield
critical group	rural, self-sufficient community	rural, self-sufficient community
well depth	up to 200 m	up to 100 m

Nuclear Fuel Waste

We assume that the nuclear fuel waste placed in the vault consists entirely of used-fuel bundles from CANDU nuclear power reactors. The used-fuel bundles comprise irradiated UO_2 fuel pellets enclosed in Zircaloy fuel sheaths that hold the fuel while it is in the reactor. Figure 3 shows a typical CANDU fuel bundle. A bundle from the CANDU reactor at Ontario Hydro's Bruce Nuclear Generating Station has a total mass of about 24 kg, including 19 kg of uranium. After release from the reactor, approximately 98.5% of the initial uranium remains unchanged. About 1.5% has been transformed during the nuclear fission process into stable and radioactive fission products and activation products. We examine in this report the radioactive isotopes (radionuclides) that are of most concern because they may have large contributions to the total dose rate (Section 5.5).

We assume in this report that the disposal vault holds about 4.3 million bundles, about half the number evaluated in the EIS case study. This smaller number of bundles arises because we have assumed the

dimensions of the vault are approximately the same in both studies, but the in-room emplacement option requires a smaller waste-loading density to meet the desired temperature and radiological shielding limits (Baumgartner et al. 1996)

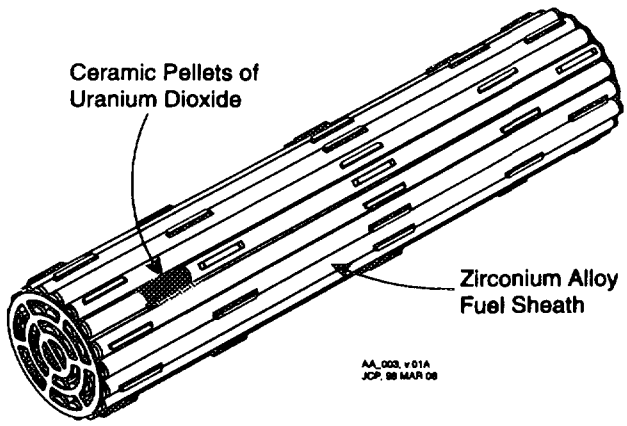

FIGURE 3: A Typical CANDU Fuel Bundle. Uranium dioxide is formed into ceramic pellets designed to withstand the conditions found inside a nuclear reactor. The pellets are sealed inside tubes, called fuel sheaths, constructed from a zirconium alloy. Fuel sheaths are then welded together to form a fuel bundle.

Container

The used-fuel bundles are placed in corrosion-resistant containers constructed with a 25.4 mm (minimum) external shell of high-purity (deoxidized low-phosphorous) copper. Figure 4 illustrates the general design in which each container holds 72 used-fuel bundles. One key element of the design is the method of internal mechanical support that would withstand the large external pressures. Two options are currently undergoing engineering analysis (Johnson et al. 1996). The option illustrated in Figure 4, and evaluated herein, uses steel tubes with a packed particulate such as silica sand or glass beads filling the void space around the fuel bundles; the second option uses an internal steel shell. For both designs, potential corrosion mechanisms affecting the copper shell in the environment of the vault are expected to be so slow that no corrosion-induced failures would occur within 10^6 a (Shoesmith et al. 1995).

Emplacement Method

Baumgartner et al. (1995, 1996) describe engineering details for the disposal vault considered in the present study that includes the spacing between adjacent pairs of containers in the disposal rooms (about 2.2 m centre to centre across the width of a vault room and 2.7 m centre to centre along the length of a room) and the spacing between disposal rooms (30 m centre to centre). An important factor used to establish these spacings is the heat produced by the radioactive decay of the nuclear fuel waste. Heat production is greatest at early times, causing temperatures to rise in the disposal vault and in the surrounding rock. The maximum temperature in the disposal vault would occur soon after closure and decrease to ambient conditions after more than 10^5 a. The maximum temperature on the surface of the containers is about 75°C, occurring about 15 a after closure (Wai and Tsai 1995). This value is lower than the specified design limit of 90°C because of an additional consideration of radiological shielding during emplacement (Baumgartner et al. 1996).

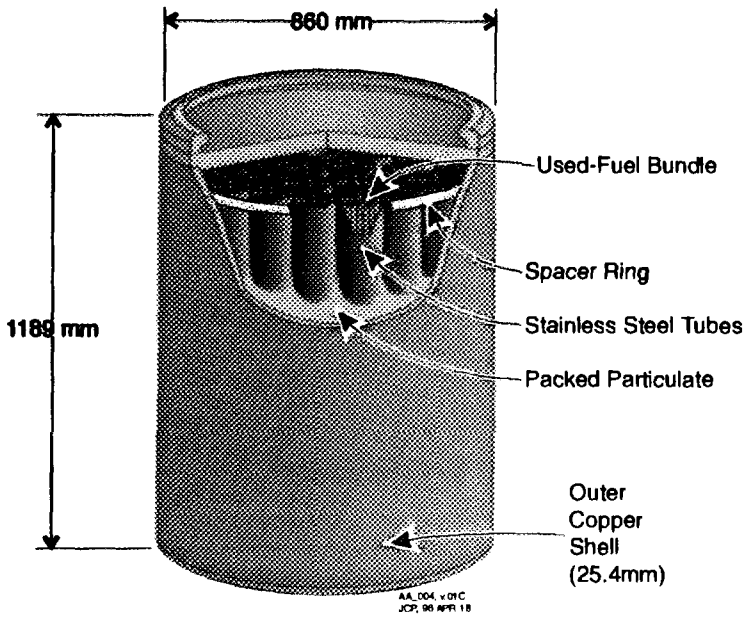

FIGURE 4: Copper Shell Container Assumed for This Assessment. The container is designed to hold 72 used-fuel bundles. The outer shell consists of deoxidized low-phosphorous copper with a minimum thickness of 25.4 mm. Internal mechanical support, designed to resist external hydrostatic and lithostatic pressures, is provided by steel tubes and a packed particulate such as silica sand or glass beads.

Figure 5 shows the in-room emplacement method for the containers (Baumgartner et al. 1995, 1996). For the vault considered in this report, the disposal rooms are elliptical in cross section to accommodate potentially high *in-situ* stress fields in the surrounding rock. The containers are oriented two abreast across the width of the room and are completely surrounded by buffer, which consists of a highly compacted mixture of bentonite clay and silica sand. The main functions of the buffer are to restrict water flow around the container, to swell when wetted and thereby seal any openings between the container and host rock, and to sorb and retain contaminants that would be released if a container fails. The buffer is surrounded by dense and light backfill. The dense backfill consists of a mixture of glacial lake clay, bentonite and crushed granite, and the light backfill is bentonite and crushed granite. The functions of the backfill are similar to that of the buffer. The backfill has a relatively large porosity that slows groundwater movement and it also sorbs and retains contaminants, thereby delaying releases from the disposal vault. The disposal rooms contain high-performance concrete liners on the floor that are used during the operation phase and concrete bulkheads at the entrances that seal the rooms and protect the integrity of the sealing materials (Baumgartner et al. 1995, 1996).

Figure 5 also portrays a feature called the excavation damaged zone (also called the excavation disturbed zone) (EDZ). We assume that all rooms and tunnels are surrounded by a thin layer of rock that has been affected by mining and stress-induced damage. The properties of the rock in the EDZ are somewhat different from the properties of the unaffected host rock. For example, we assume that the EDZ is more highly fractured than the host rock and thus its porosity is larger. The EDZ was not specifically modelled in the postclosure assessment of the EIS case study because a detailed analysis indicated it would have no significant effects for a vault located in low-permeability sparsely fractured rock (Davison et al. 1994b). In the present study, however, the EDZ is expected to be influential because we assume a much larger permeability for the host rock (and because only a few containers fail at random locations in the vault).

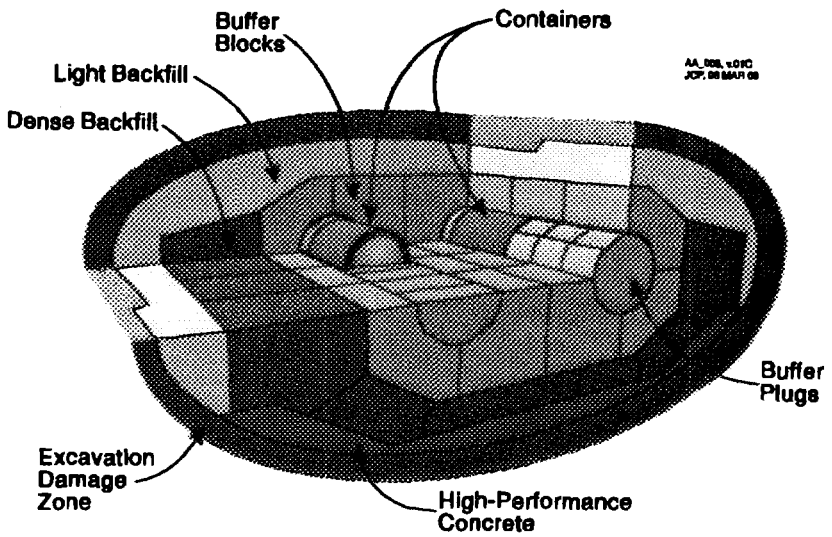

FIGURE 5: Disposal Room Showing the In-Room Emplacement of Containers. The high-purity copper containers are isolated from the surrounding rock by layers of buffer and backfill.

Vault Design and Layout

Figure 6 illustrates the vault design layout considered in this report. The vault is partitioned into two parts to provide isolation from a fracture zone (called fracture zone LD1) that is assumed to pass through the plane of the disposal vault. The vault is oriented so that the long axis of the disposal rooms is perpendicular to the intersection of LD1 with the plane of the disposal vault. The disposal rooms are separated from LD1 by about 150 m in a horizontal direction. However, because we assume LD1 is a planar structure that dips at an angle of about 18^{o} from the horizontal, the shortest separation distance is only about 50 m. The orientations of LD1 and the disposal vault are more clearly seen in the figures that follow.

There are a total of 464 (8 rows of 58) disposal rooms shown in Figure 6. Of these, 348 are about 230 m long and each holds 152 containers. Two rows of rooms, those closest to LD1, are only about 110 m long and each holds 62 containers. Since there are 72 used-fuel bundles per container, and about 19 kg U per fuel bundle, we assess in this study a total of 60 088 containers and 8.2×10^{7} kg U in the disposal vault.

In addition to the disposal rooms, the disposal vault has openings in the host rock for access and ventilation shafts, tunnels and subsurface facilities (Figure 6). We assume in this postclosure assessment that these features would have been completely sealed and that they would have no influence on groundwater flow or on the potential release and movement of contaminants.

Properties of the Geosphere

We have assumed the geometry of the geosphere for the present study is the same as that in the EIS case study, but with two major exceptions noted below. An important feature of this geosphere, shown in Figure 7, is fracture zone LD1, a low-dipping structure that outcrops on the surface. We assume that LD1 passes from ground surface through the plane of the vault to a depth of about 1 km where it meets a vertical fracture zone, and that this vertical fracture zone connects to an upland area. This hydraulic

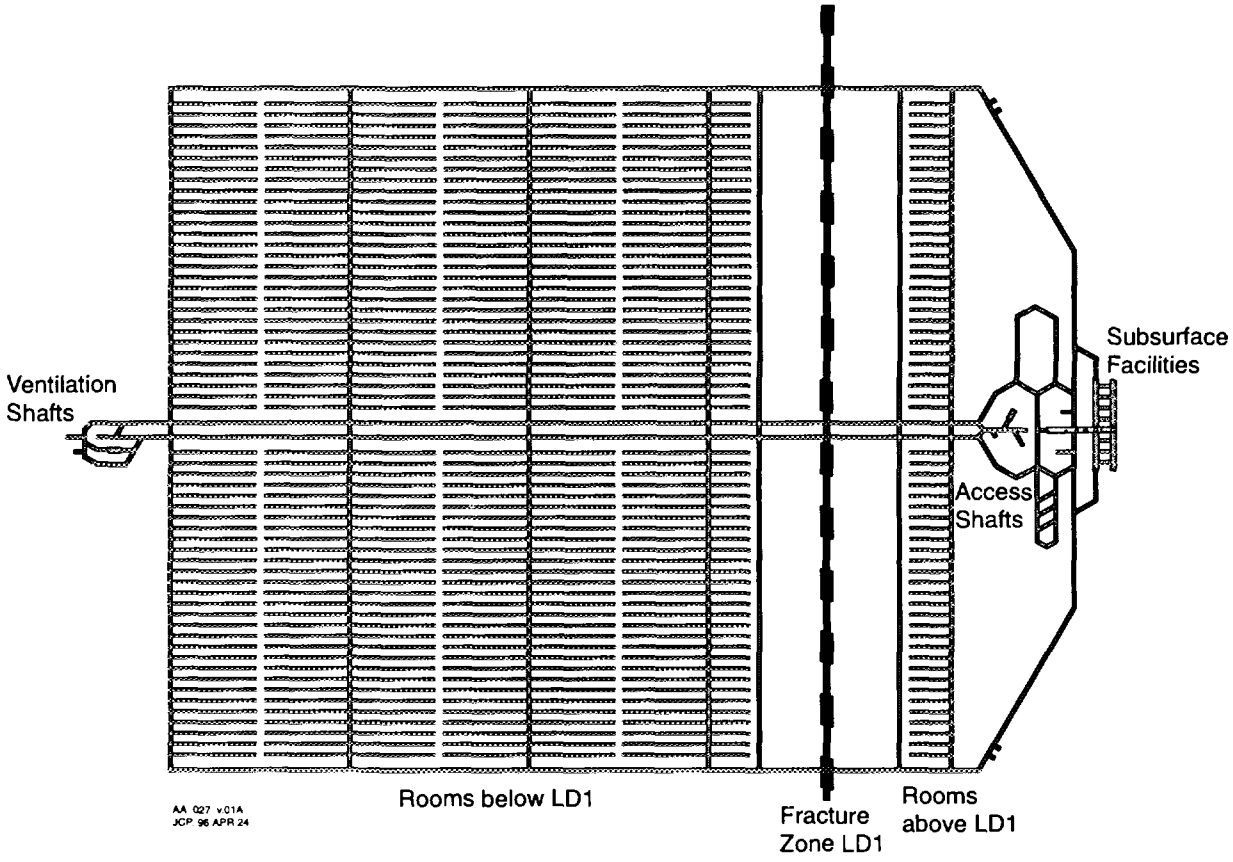

FIGURE 6: Vault Design Layout Considered in This Assessment. The disposal vault is divided into two parts, separated by the planar fracture zone LD1 (other figures show LD1 dips at an angle of about 18° from the horizontal). The vault is oriented with the long axes of the disposal rooms perpendicular to the intersection of the vault plane with LD1. The larger part of the vault, about 1900 m x 1625 m, lies beneath LD1, and the smaller part, about 1900 m x 153 m, lies above LD1.

arrangement causes relatively large groundwater flows up LD1 from disposal vault depths. Current information from studies of the Whiteshell Research Area indicates that LD1 does not extend beyond about 400 m depth (Davison et al. 1994b).

We assume that the geosphere contains other features that are characteristic of a disposal system located in the Canadian Shield, such as more permeable, fractured rock near the surface and less permeable rock below. However, the geological and hydrogeological details used in the geosphere model (Section 5.3) are based on those of a particular hypothetical site, to ensure that the data used in the assessment are self-consistent to the extent possible. Figure 7 shows three different layers of rock, each of which has different hydrogeological properties. The upper two layers are relatively thin and represent the uppermost portion of more permeable rock and the less permeable rock immediately below. The vault is located in the third layer. Figure 7 shows several low-dipping fractures and vertical fracture zones; because of their high permeability, these features control the overall direction and volume of groundwater flow in the rock at the site. We have assumed that LD1 extends as shown, and that there is about 50 metres of intact rock in layer 3 between the plane of the LD1 and the nearest disposal room.

The geologic structure, and the associated geological and hydrological data, are largely similar to that used in the EIS (Davison et al. 1994b), although there have been some changes, to the retardation factors for instance, to reflect new field and laboratory results. There are, however, two major exceptions that have a very large effect on groundwater velocities in the geosphere for this study.

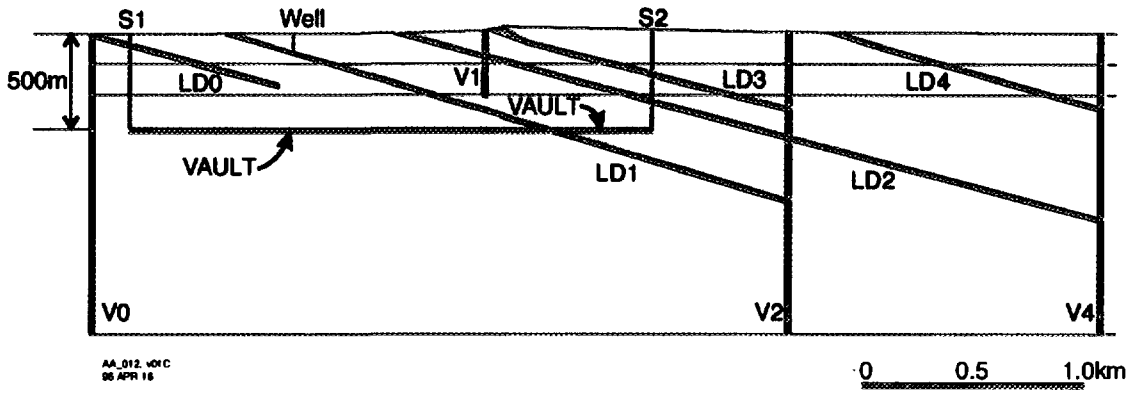

FIGURE 7: Vertical Cross Section In the Vicinity of the Disposal Vault. This cross section through the hypothetical vault shows low-dipping fracture zones (labelled LD0 to LD4) and vertical fracture zones (V0 to V4) (Davison et al. 1994b, Stanchell et al. 1996). S1 and S2 represent the shafts leading to the disposal vault. We assume that LD1 cuts through the plane of the vault such that most of the disposal rooms are beneath LD1 (compare with Figure 6). In this report, we assume that the permeabilities are similar for rock layers 2 and 3. In the assessment of the disposal system described in the EIS, we assumed the permeability of layer 3 was about 1% of the permeability of layer 2.

1. The first exception concerns the permeability of the rock immediately surrounding the vault, rock layer 3 in Figure 7. In the EIS case study, this domain was assigned a low permeability of 1×10^{-19} m^2, based on information from field studies at the Whiteshell Research Area (Davison et al. 1994b). For the assessment discussed herein, we have assumed that the rock in layer 3 has a 100-fold larger permeability (1×10^{-17} m^2) (Stanchell et al. 1996). This assumption is not based on field observations at the Whiteshell Research Area. Rather, it reflects a hypothetical situation which we introduced so that we could better demonstrate how well long-lived containers and in-room emplacement could compensate for a geosphere that is less effective as a barrier than the geosphere used in the EIS case study.

2. The second exception involves the effective transport porosity of the rock, notably rock layer 3. In the EIS case study, we assumed this low-permeability sparsely fractured rock had a total porosity (and effective transport porosity) equal to 0.003, and used a groundwater velocity scaling factor to account for the net uncertainty in hydrological flow properties (Davison et al. 1994b). For the present assessment, we assume that this rock layer contains a network of permeable fractures and that contaminant transport takes place within these fractures (and not within the intact rock). Thus the effective transport porosity is equal to the fracture porosity. This fracture porosity is uncertain, and values have been assumed that range from 10^{-5} to 10^{-3} to reflect different possible conceptualizations of the effects of the fracturing (Stanchell et al. 1996). We assume a similar, wide range of effective transport porosities for rock layers 1 and 2 and for the fracture zones (see Table 1 and Stanchell et al. 1996). In the geosphere model (described in Section 5.3), the range of values for the effective transport porosity of the rock domains

has a strong influence on the calculated variability of contaminant transport through the geosphere.

The smaller values assumed for effective transport porosity, plus the larger values assumed for permeability, result in much larger groundwater velocities in the present study compared with the EIS case study. In particular, in rock that surrounds the disposal vault, calculated groundwater velocities are up to 5 orders of magnitude larger in this study than for the EIS case study. For instance, Stanchell et al. (1996) show that, for the disposal system assessed herein, groundwater transit times from the disposal vault to the surface can be less than 100 a. The corresponding groundwater transit times in the EIS case study were much longer, of the order of 10^5 a or more (Davison et al. 1994b).

The net effect of these assumptions is a significant reduction in the effectiveness in the present study of the geosphere as a barrier to contaminant transport. Goodwin et al. (1994a) have shown that the lower rock zone described in the EIS is a very effective barrier because contaminant transport in the rock immediately surrounding the location of the disposal vault was dominated by slow diffusion in pore water. In the geosphere studied herein, however, groundwater velocities are sufficiently large in the region of rock immediately surrounding the disposal vault that contaminant transport is dominated by advection in which particulate or dissolved contaminants from the vault would be swept along with the moving groundwater.

Characteristics of the Biosphere

We assume that the disposal systems evaluated in this study and in the EIS case study are at the same sites. Thus the biosphere component in the study described herein is identical to the biosphere associated with the EIS case study. That is, we assume that the local biosphere has characteristics typical of the Canadian Shield, with physical elements that include a lake and the mixed sediment on the lake bottom, a well that may supply domestic and irrigation water, the soils in nearby cultivated and natural areas that supply food, fuel and building materials and that serve as the habitat for native wildlife and plants, and the atmosphere above the lake and fields and inside buildings (Davis et al. 1993).

An important element of the biosphere is the characteristics of the people who would be affected by the disposal facility. We use the concept of a critical group, consistent with AECB criteria that require estimates of radiological impacts to a hypothetical "*group of people that is assumed to be located at a time and place where the risks are likely to be the greatest, irrespective of national boundaries* (AECB 1987)". We have defined the behaviour of the critical group such that its members would be exposed to the greatest risk. Thus we assume, as in the EIS case study, that a succession of individuals spend their entire lives in an area where they would be exposed to discharging groundwater potentially contaminated by the disposal vault and that they obtain all their food, water, fuel and building materials from this area. This lifestyle is consistent with, but more self-sufficient than, current habits. We also estimate radiation dose to representative nonhuman biota that are assumed to inhabit the discharge area.

4. RESULTS OF SCENARIO ANALYSIS

Scenario analysis deals with the specific disposal system described in Section 3 and has two main objectives in a postclosure assessment:

- identify and describe all the possible factors that could affect the long-term performance of the disposal system, and

- construct a set of scenarios that require further evaluation using combinations of these factors.

A scenario is defined to be "*a set of factors ... that could affect the performance of the disposal facility to immobilize and isolate nuclear fuel waste* (Goodwin et al. 1994a)." Factors may be classified as features, events or processes as an aid in identifying a comprehensive list. A feature is a characteristic of a component of the disposal system, such as the material used to construct the containers, fractures in the rock that pass near the disposal vault and a garden used by the critical group that may be exposed to contaminated groundwater. An event is an incident, generally of short duration, that could affect the system, such as a nearby earthquake, a failure in the containers caused by fabrication defects and the drilling of exploration boreholes that intersect the contents of the vault. A process is a natural phenomenon occurring in the disposal system, such as the dissolution of the nuclear fuel waste in groundwater, the movement of groundwater in the geosphere caused by head and thermal gradients, and the transfer of contaminants in the soil rooting zone to the edible parts of a plant.

The postclosure assessment documented in the EIS followed a systematic six-step procedure for scenario analysis (Goodwin et al. 1994a,b). For the scoping assessment described herein, we employed an abbreviated form of the procedure for two reasons.

1. We could draw extensively from the scenario analysis of the disposal system considered in the EIS because it is very similar to the disposal system considered in this report. Factors that were important or unimportant in the EIS study would likely have a similar significance in this study. Thus we are able to focus more on differences between the two disposal systems that might affect long-term performance.

2. This scoping assessment is aimed at a quantitative evaluation of the groundwater transport scenario, the scenario that describes the most likely way in which people and the environment would be affected by the disposal vault Thus we do not need to identify and characterize all possible less likely scenarios.

Figure 8 summarizes the scenario analysis procedure and the results of its application. The first three steps in the procedure, the identification, classification and screening of factors, were largely completed at a formal meeting involving more than 30 participants with expertise in areas that include applied mathematics and statistics, biology, chemistry, civil engineering, computer science, electrochemistry, environmental assessment, geochemistry, hydrogeology, mechanical engineering, meteorology, mining engineering, nuclear physics, sociology, structural geology and systems analysis. Before the meeting, participants were provided with the text of the scenario analysis report (Goodwin et al. 1994b), a list of all factors identified in the scenario analysis of the disposal system evaluated in the EIS case study (including all factors that had been eliminated), an outline of the differences between the disposal system evaluated in the EIS and the disposal system evaluated herein, and a provisional list of additional factors that could pertain to the present study. The main objectives of the meeting were to identify factors that could affect the performance of the disposal system evaluated in this report, to discuss their potential importance, and to recommend their overall treatment in the postclosure assessment. All participants were asked to review and approve the summary record and conclusions of the meeting. (We note that identification of factors was not restricted to this single meeting. It is an ongoing process, and new factors are typically postulated and evaluated throughout the postclosure assessment).

Approximately 90 factors were identified and discussed. Not surprisingly, most could be recast as variants of one or more of the factors previously identified in the EIS case study. For example, a common factor is "Inventory"; this factor was discussed because the reduced performance of the geosphere in the present study could lead to a larger list of radionuclides that could be significant contributors to total dose. Table 2 lists representative examples of factors that were discussed, with

preference for factors that pertain to the vault design and location of the disposal system evaluated herein.

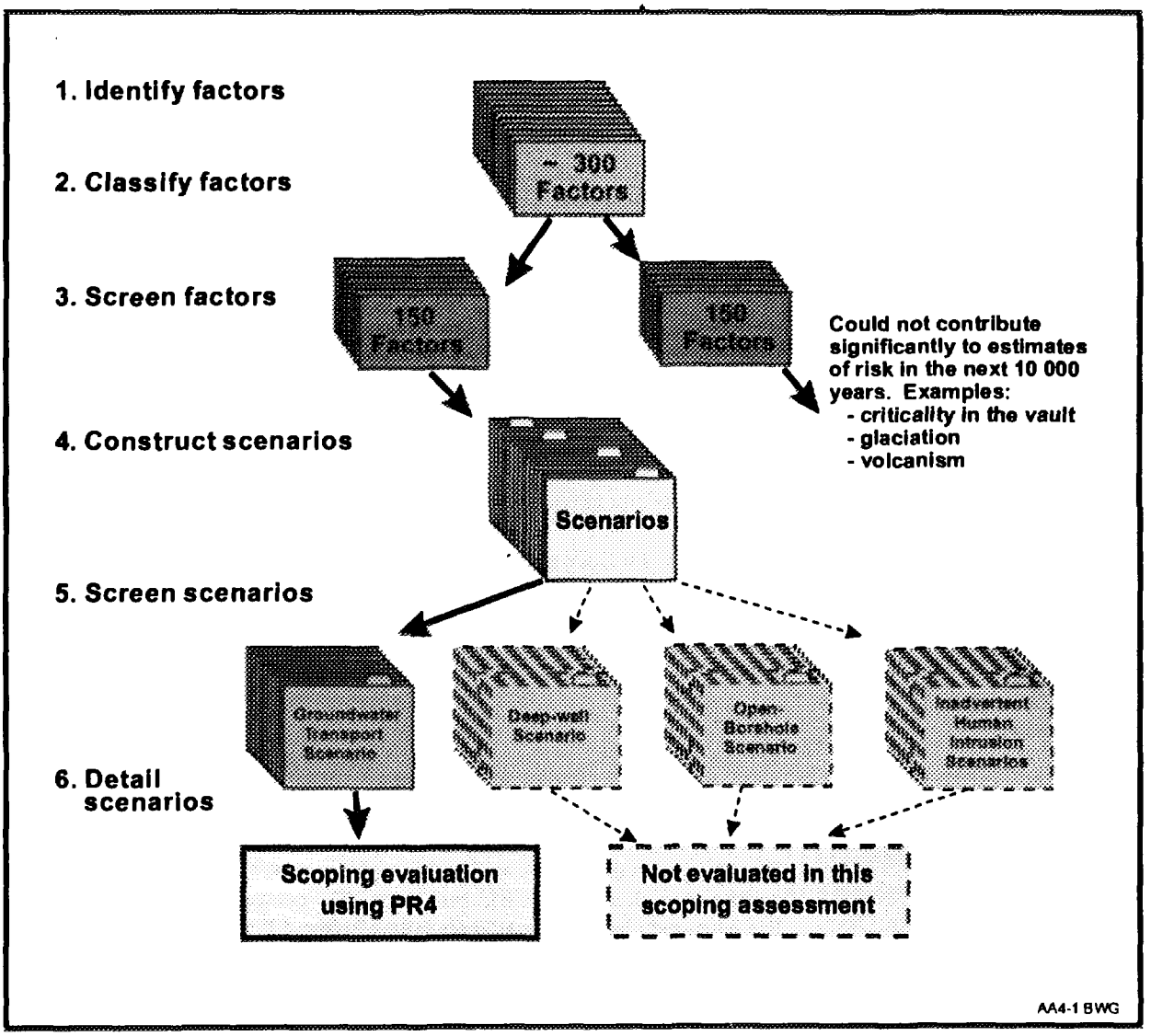

FIGURE 8: Summary of the Scenario Analysis Procedure. This figure illustrates the results of the six-step procedure used to identify factors and to define scenarios that require quantitative evaluation for time scales up to 10^4 a. In steps 1 and 2, a few new factors were added to approximately 300 that were carried forward from the scenario analysis of the disposal system evaluated in the EIS. About half of these factors passed the screening in step 3 and are used to construct scenarios in step 4. For this scoping study, we were interested in defining only the groundwater transport scenario that describes the most likely way in which people and the environment could be affected by contaminants escaping from the disposal vault. Three other tentative scenarios are also shown; all are much less likely.

TABLE 2

SAMPLE FACTORS PERTAINING TO THE PERFORMANCE OF THE DISPOSAL SYSTEM EVALUATED IN THIS REPORT

Factors[a]	Comment[b]
Backfill characteristics, Buffer characteristics	Compared with the vault considered in the EIS case study, the vault considered herein contains more buffer and less backfill. In addition, because only a few containers are expected to fail (at random locations in the vault), it may be necessary to use a multi-dimensional description of contaminant transport through the buffer and backfill. Recommended treatment: include (for quantitative evaluation to 10^4a) in the groundwater transport scenario.
Backfill evolution, Buffer evolution	The large groundwater flows in the rock surrounding the vault could promote the geochemical alteration of the buffer and backfill. Recommended treatment: exclude further evaluation; would not occur to any appreciable extent in the expected environment of the vault (see Johnson et al. 1994b, 1996).
Chemical toxicity of copper	The large quantity of copper used in the construction of the containers may give rise to chemical toxicity impacts. Recommended treatment: include in the groundwater transport scenario. (This scoping study, however, does not consider chemical toxicity impacts.)
Concrete	The vault will include more concrete than the vault in the EIS case study, and its potential effect on the chemical environment of the vault should be evaluated. Recommended treatment: exclude further evaluation; effects are expected to be unimportant (see Johnson et al. 1996).
Containers - partial corrosion	For copper containers, it may be overly conservative to assume that a fabrication-defected container offers no resistance to contaminant release. It may be worthwhile to include the effects of pinhole-sized defects. Recommended treatment: include in the groundwater transport scenario.
Container failure (mechanical processes), Glaciation	These related factors arose because of expected differences in the performance of the copper containers evaluated in this report and the Grade-2 titanium alloy containers evaluated in the EIS case study. The conservative model used in the EIS case study led to all containers failing before 10^4 a, whereas most of the copper containers are expected to remain intact for longer periods of time. The onset of glaciation would increase the external pressures (ice loading and hydrostatic heads) and could lead to mechanical failure. This process has been shown to be insignificant for the container design option in which mechanical support is provided by an internal steel shell because this design will withstand glacial loading. However, studies of the significance of glacial loading are not yet complete for the design option in which mechanical support is provided by packed particulate. For both design options, quantitative estimates of impact are not required because glaciation is expected to occur after 10^4 a. For the packed-particulate option, there may be a need for qualitative analysis over longer time scales. Recommended treatment: for an assessment that evaluates the packed particulate option, exclude further evaluation or, depending on results from studies-in-progress, include with qualitative evaluations for times beyond 10^4a (see Johnson et al. 1996). For an assessment involving the steel-shell design option, the recommended treatment is exclude further evaluation (see Johnson et al. 1996).

continued ....\

TABLE 2 (continued)

Factors	Comments
Container failure from internal corrosion	One of the two container design options uses an internal steel shell to provide support against external pressures. For this option, containers that fail early because of fabrication defects in the copper shell might experience an increase in the size of the defect, caused by the pressures exerted by the larger-volume magnetite that results from the corrosion of steel by groundwater. In turn, the larger defect size could significantly enhance the rate of transport of contaminants out of the defect-failed container. This process is thought to be unlikely over 10^4 a because of the slow transport of material in and out of the container through pinhole-sized defects, and because the dense buffer would resist internally generated pressures. Recommended treatment: exclude further evaluation for the packed-particulate design option (the option evaluated in this report); include in a quantitative assessment involving the steel-shell design option. Johnson et al. (1996) provides more discussion and describes a preliminary analysis of consequences for the steel-shell option.
Container failure by sulfide and microbial-induced corrosion of copper	These may be significant processes affecting the copper containers considered in this report. Recommended treatment: include in the groundwater transport scenario if required. (Johnson et al. (1996) conclude these processes are not important over the time frames of interest.)
Excavation damaged zone (EDZ)	The effect of the EDZ may be important in the current study because of the larger permeability of the host rock. Recommended treatment: include in the groundwater transport scenario.
Formation of gases, Transport in gases or of gases	This factor was eliminated from quantitative evaluation in the postclosure assessment of the disposal system evaluated in the EIS case study after consideration of the rates of production of hydrogen and the minimum time needed before a gas phase could form (Johnson et al. 1996b). This factor is also excluded in the present study for similar reasons and because small quantities of iron would be exposed since only a small percentage of the copper shell containers would fail. Recommended treatment: exclude further evaluation (see Johnson et al. 1994b, 1996).
Inconsistencies in data	Some of the properties of the geosphere evaluated in this report are assumed to differ from what is observed; in particular, the permeability of the rock surrounding the disposal vault is assumed to be much larger than is actually measured. This may lead to serious inconsistencies in the data and thus to systematic errors in estimates of performance, although not to the actual performance. For example, larger permeabilities imply larger groundwater flows that could affect groundwater composition (including dissolved oxygen and electrochemical potential) and temperature rises in the rock, and there could be considerations which influence the vault design and vault sealing. All such implications should be studied and any secondary assumptions should be documented. Recommended treatment: eliminate this as a specific factor but regard it as a general qualification that is attached to other more specific factors.

continued....

TABLE 2 (concluded)

Factors	Comments
Inventory	The assessment should deal with all radionuclides that could have significant contributions to the total dose rate. A repeat of the screening study documented by Goodwin and Mehta (1994) is required to take into account the reduced performance of the geosphere. Recommended treatment: include in the groundwater transport scenario.
Microbes, Microorganisms	These factors can likely be eliminated for reasons similar to those cited for the disposal system evaluated in the EIS case study (Johnson et al 1994a) (microbial-induced corrosion of copper containers is treated as a separate factor). However, the design and location of the disposal system evaluated herein, with different groundwater flows, nutrient levels and radiation fields, may be significant and potential effects should be re-evaluated. Recommended treatment: exclude further evaluation (see Johnson et al. 1996).
Reflooding, Short-term transient processes	The resaturation of the disposal vault and other transient effects can likely be eliminated. However, the arguments supporting this conclusion should be reviewed and possibly revised, taking into consideration the different vault design and location evaluated in the present study. Recommended treatment: exclude further evaluation (see Johnson et al. 1994b, 1996).
Wells, Wells (high-demand)	The larger permeabilities assumed in this report for the geosphere will significantly influence the ability of wells to supply water. Moreover, the wells may have good hydraulic connections to the rest of the geosphere, so that drawdowns from the well could have wide-ranging influences on hydraulic heads in the surrounding rock. Recommended treatment: include in the groundwater transport scenario.

[a] Most of these factors, or similar variants, were identified and discussed in the scenario analysis of the disposal system evaluated in the EIS case study (Goodwin et al. 1994b). Additions for this study include Chemical toxicity of copper, Container failure from internal corrosion, Container failure by sulfide and microbial-induced corrosion of copper, and Inconsistencies in data.

[b] One of three types of recommended treatments apply for each factor:

- include in the groundwater transport scenario over the 10^4-year time frame for which quantitative estimates of impact are required by the AECB (1987);
- include with evaluations using qualitative arguments over longer periods of time, but exclude from the groundwater transport scenario because the factor would have no significant influence over the 10^4-year time frame; and
- exclude further evaluation in the postclosure assessment because the factor would have no significant influence over any time frame, but document arguments that support this recommendation. For the sample factors that are excluded in this table, supporting arguments are discussed in Johnson et al. (1996).

The last three steps in the procedure for scenario analysis involve the construction, screening and detailed description of scenarios (including estimating their probabilities of occurrence) (Goodwin et al. 1994b). The comments in Table 2 indicate the recommendations of the participants on whether or not the factor should be included in the groundwater transport scenario.

One general conclusion of the analysis was that the groundwater transport scenario is, for the most part, similar for the disposal system evaluated herein and for the disposal system evaluated in the EIS. (The equivalent to the groundwater transport scenario is called the SYVAC scenarios in Goodwin et al. (1994a) because quantitative analyses used the probabilistic system assessment computer code, SYVAC3-CC3.) In the groundwater transport scenario, the primary pathway leading to impacts involves groundwater-mediated processes. Groundwater enters the vault and passes through the backfill and buffer and reaches the surface of the containers. The groundwater eventually penetrates the failed containers and dissolves contaminants (radionuclides and chemically toxic elements) from the nuclear fuel waste. Radiolysis may alter the groundwater composition and affect its ability to dissolve and transport the waste. The contaminants then move in groundwater, by diffusion and advection, through the vault buffer, backfill and the excavation damaged zone surrounding the vault, traverse the geosphere with preferential transport in microfractures and fracture zones, and enter the biosphere at discharge zones generally located in topographical lows and at sites of water-supply wells. Once in the biosphere, contaminants could affect members of the critical group through contamination of their food, water and air. Other environmental impacts may also occur, such as radiation doses to nonhuman biota. For this scoping assessment, we conservatively assume a value of unity for the probability of occurrence of the groundwater transport scenario.

One important difference between the groundwater transport scenario for the disposal system evaluated herein and for the disposal system evaluated in the EIS pertains to the characteristics of the well. The postclosure assessment of the EIS case study included water-supply wells that could be as deep as 200 m (Davison et al. 1994b, Goodwin et al. 1994a). For the disposal system evaluated in this report, however, the maximum well depth is restricted to 100 m because of simplifications that were required in the development of the geosphere model for this scoping assessment (see Section 5.3). In a full postclosure assessment, we would also need to evaluate the "deep-well" scenario. (On the other hand, future revisions to the geosphere model could encompass the full range of well depths. Thus the deep-well scenario would be subsumed within the groundwater transport scenario and remove the need for separate evaluations.) The deep-well scenario is relatively unlikely; based on the probability distribution assigned to well depth in the EIS case study (Davison et al. 1994b), the probability of occurrence of deeper wells, between 100 and 200 m depth, is about 9%.

No other scenarios were explicitly identified for this scoping assessment. However, based on the scenario analysis of the disposal system considered in the EIS, at least two other possibilities exist: the open-borehole scenario and the inadvertent human intrusion scenarios. They would be expected to have the following characteristics.

- The open-borehole scenario would contain the same factors as those in the groundwater transport scenario, plus an "open borehole" factor. This factor would account for the possibility that a deep borehole remains open at the time of closure and is located such that it provides a significant pathway for contaminant transport from the vault to the surface environment. An analysis of this scenario in the EIS case study concluded that "*three redundant quality assurance procedures would provide a high degree of confidence that no boreholes would remain open at the time of vault closure that could have a significant effect on the performance or safety of the reference disposal system* (Goodwin et al. 1994a). The objectives of the three quality assurance procedures are to (1) ensure that all boreholes are properly sealed, (2) avoid the drilling of deep boreholes near disposal rooms, and (3) confirm by means of geophysical surveys that there are no open

boreholes near disposal rooms. These procedures are expected to be equally effective for the disposal system evaluated in this report.

- The inadvertent human intrusion scenarios describe a disruption of the disposal system caused by drilling, mining or blasting activities that are carried out in the vicinity of the disposal vault by an intruder who is unaware of the presence of the disposal vault and its potential hazards. An analysis of inadvertent human intrusion in the EIS case study concluded that its probability of occurrence is less than 5×10^{-6} for all times up to 10^4 a (Goodwin et al. 1994a). A similar probability of occurrence is expected for the disposal system evaluated in this report.

5. DESCRIPTION OF THE SYSTEM MODEL

5.1 INTRODUCTION

The quantitative evaluation of long-term performance uses a mathematical model of the disposal system to infer long-term behaviour and to estimate potential effects. The model represents the disposal system described in Section 3 and includes the factors outlined in Section 4 for the groundwater transport scenario.

The disposal system model consists of three linked models that represent the vault, the geosphere and the biosphere. There are many similarities between the models used in the EIS case study and in the present study. However, there are also significant differences, notably for the vault model and for parameter values describing properties of the geosphere near the vault. Sections 5.2 to 5.4 below describe briefly the models and key parameters used in this study. More information is available in reports by Johnson et al. (1996) on the vault model, by Stanchell et al. (1996) on the geosphere model, and by Zach et al. (1996) on the biosphere model.

Section 5.5 discusses the selection of radionuclides for this scoping assessment.

5.2 DESCRIPTION OF THE VAULT MODEL

Figure 6 illustrates some features of the vault design. The vault is located 500 m below the surface and there are access shafts connecting the surface to the vault level, surface and subsurface facilities, and a total of 464 disposal rooms (Baumgartner et al. 1995, 1996). We assume in this postclosure assessment that the surface facilities have been removed, that shafts and boreholes leading to the vault have been thoroughly sealed, and that all disposal rooms, tunnels and subsurface facilities have been backfilled. Moreover, we assume that resaturation of the vault is complete at the time of closure and that steady-state groundwater flow conditions have been attained.

The plan area of the disposal vault in the present study occupies about 3.4 km^2, and the surrounding rock exhibits significant variations in its hydrogeological properties, notably groundwater velocities. To account for these variations, we divide the vault into sectors and estimate contaminant releases from each sector. Each sector serves as a source to a contaminant transport pathway through the geosphere (see Section 5.3).

The number of sectors, and their sizes and locations, are chosen so that the properties of the rock surrounding each sector, especially groundwater velocities, are relatively uniform. Another consideration is the lengths of the disposal rooms: each sector is defined such that it consists of equal-length rooms. For the present study, we have divided the vault into 24 sectors, shown in Figure 9

(Stanchell et al. 1996, Johnson et al. 1996). Sectors 1 through 18 have identical room lengths and sectors 19 to 24 are considerably shorter (sectors 19 to 21 are slightly shorter than sectors 22 to 24). These sectors provide a detailed resolution of releases from different parts of the disposal vault into the surrounding geosphere and reflect the expected spatial variability in rock properties near the disposal vault.

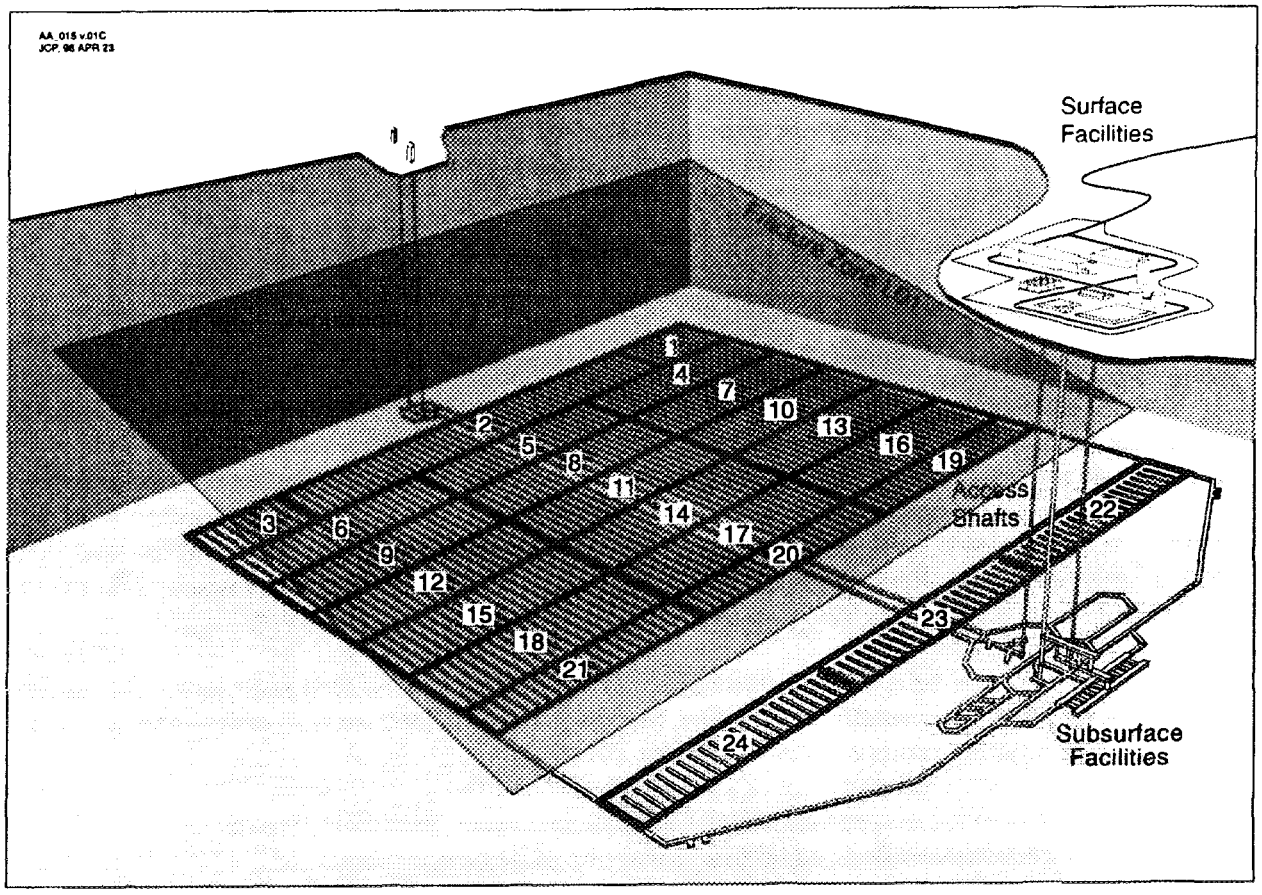

FIGURE 9: Location of the 24 Vault Sectors. Vault sectors are chosen such that the properties of the rock surrounding each sector are relatively uniform. Estimates of contaminant release from each sector serve as a source term to a contaminant pathway through the geosphere.

The vault model estimates the release of contaminants from each vault sector. It simulates the following processes:

- failure of the copper containers;
- release of contaminants from the UO_2 fuel and Zircaloy fuel sheaths to the interior of a failed container;
- precipitation of contaminants inside a failed container if solubility limits are exceeded;

- transport by diffusion of dissolved contaminants through a small defect (pinhole) in the failed container to enter the surrounding buffer; and

- transport by diffusion and advection of contaminants through the buffer, backfill and excavation damaged zone into the surrounding host rock.

In contrast to the one-dimensional vault model used in EIS case study (Johnson et al. 1994b), this vault model uses multi-dimensional equations to model a cylindrical room with concentric layers of buffer, backfill and an excavation damaged zone, having a point source (the pinhole in a failed container) along the central axis (Johnson et al. 1996). Releases of contaminants are integrated over the entire surface of the outermost cylinder, to provide an input to the network of flowpaths in the geosphere that start at each of the 24 vault sectors.

Failure of the Copper Containers

In this scoping study, we assume that the only failure mechanism for the copper containers involves undetected fabrication defects. These defects are envisioned to be small, pinhole-sized openings in the outer copper shell that permit the ingress of groundwater and the subsequent escape of contaminants, starting immediately after closure of the vault. We assume the size of the openings are time-independent. (This last assumption is consistent with the container design option that is assessed in this report and that uses packed particulate to provide internal mechanical support. Another design option involving an internal steel shell to provide structural support is expected to have the same failure mechanism, but the size of the defect may be enlarged by internal swelling pressures caused by corrosion of the steel shell. The likelihood of this effect is expected to be small and its consequences are discussed by Johnson et al. (1996) in the report describing the vault model.)

Three parameters are used to estimate the number of failed containers in each vault sector: the probability of fabrication defects that would cause failure, the total number of containers in each sector, and a sector-dependent binomial probability variate (LeNeveu 1994).

- Within the entire vault, about 1 in 5000 containers are expected to fail because of fabrication defects, equal to a probability of fabrication defects of 2×10^{-4}. This value is uncertain and thus the parameter is represented by a lognormal probability distribution with a range of probabilities of 10^{-4} to 10^{-3} (Johnson et al. 1994b, 1996).

- The vault has a total of 60 088 containers placed uniformly in the disposal rooms. The number in a vault sector is proportional to its plan area; there are 1368 containers in sectors 1 and 3; 6080 in sector 2; 3040 in sectors 4, 6, 7, 9, 10, 12, 13, 15, 16 and 18; 2736 in 5, 8, 11, 14 and 17; 1240 in sectors 19, 21, 22 and 24; and 1116 in sectors 20 and 23 (compare with Figure 9).

We make the further assumption that each container has an equal and independent probability of failure from fabrication defects, and sample (for each sector) a binomial probability variate from a uniform distribution to estimate the number that have failed in each sector (LeNeveu 1994). Our use of these parameters means that failed containers occur at random locations in the vault. In a randomly sampled simulation, all the failed containers might be found in one sector, or distributed amongst the 24 sectors. With the probability of fabrication defects equal to 2×10^{-4}, the entire vault would have about 12 defect-failed containers (with a standard deviation of about 3.5). With the probability of fabrication defects equal to its specified upper limit of 10^{-3} failures, the vault would have a total of about 60 defect-failed containers (with a standard deviation of about 7.7).

The net release rate of a contaminant from a vault sector is equal to the product of the number of failed containers in that sector and the calculated release rate from one failed container for that sector. Calculation of the latter quantity is described in the following subsections.

Releases from the Used-Fuel and Zircaloy in a Failed Container

We assume that a failed container fills with groundwater immediately upon closure of the disposal vault. We then estimate releases of contaminants to the water inside the container from the UO_2 fuel and from the Zircaloy fuel sheaths. We model two release mechanisms: congruent and instant release for the irradiated UO_2 fuel and congruent release for the Zircaloy matrix.

Congruent release refers to the release of contaminants that are uniformly immobilized in the host matrix (UO_2 fuel or Zircaloy sheaths). We assume a contaminant is released as the matrix dissolves, at a rate that is proportional to the contaminant's fractional abundance within the matrix and the rate of dissolution of the matrix (Johnson et al. 1996).

- The contaminant's fractional abundance is given by its initial inventory, which is modified as a function of time to account for radioactive decay and (for the UO_2 matrix) to discount the instant-release inventory described below.

- The rate of dissolution of the UO_2 fuel matrix is based on a chemical kinetic (corrosion) model that is strongly dependent on the extent of radiolysis occurring at the fuel surface. At early times, radiolysis of water from α-, β-, and γ-radiation causes relatively rapid dissolution rates (calculated using rate data at a conservatively assumed temperature of 100° C). After about 10^3 a, radiation fields would be acutely attenuated, but we assume that a minimum rate of dissolution persists to the time limit of the simulations. For UO_2, the congruent-release mechanism is modelled using parameters that determine the relative magnitudes and durations of α-, β-, and γ-radiation (Johnson et al. 1996), and the effects of subsequent radiolysis on UO_2 dissolution rates.

- The rate of dissolution of the Zircaloy matrix is determined by two factors: the solubility of zirconium and the rate at which zirconium is removed from the container (by diffusion through the defect in the container). For the Zircaloy matrix, the congruent-release mechanism is modelled using a solubility parameter for zirconium and by parameters (discussed below) that describe mass transport from a failed container.

Instant release refers to release of contaminants that are not immobilized in the UO_2 matrix. The "instant-release" fraction is the fraction of the inventory of some contaminants that is located in the gaps and at the grain boundaries of the fuel pellets (the remaining inventory is bound in the UO_2 matrix and is released congruently), and that we assume is released to the interior of the failed container at the time of closure of the disposal vault. In this scoping study, we assume a fraction of the inventory of the following radionuclides undergo instant release: ^{14}C, ^{36}Cl, ^{135}Cs, ^{137}Cs, ^{129}I, ^{126}Sn, ^{79}Se, ^{90}Sr and ^{99}Tc (Johnson et al. 1996).

Most of the parameters used in calculating releases from the waste matrices are described using probability distributions to account for uncertainty. Different values are sampled for each vault sector in a single simulation.

Precipitation in a Failed Container

Some contaminants released from the UO_2 and Zircaloy matrices to the interior of the container are relatively insoluble and would precipitate. In this scoping study, we use two different approaches to specify solubility limits (Johnson et al. 1996).

1. For most chemical elements, we specify a conservative solubility limit. Chemical elements such as carbon, chlorine, cesium and iodine are assigned very high solubility limits and would not precipitate in any simulation; others such as palladium and selenium are more insoluble and are would likely precipitate in some simulations. Zirconium is expected to precipitate in every simulation because its solubility limit is relatively small and because there is a large mass of zirconium in the Zircaloy matrix. The solubility limits for these elements are defined using probability distributions to account for uncertainty.

2. For five elements (neptunium, technetium, plutonium, thorium and uranium), solubility limits are calculated using thermodynamic relationships and a groundwater composition that is representative of the disposal vault (Johnson et al. 1994b). For these elements, uncertainty is factored in through the probability distributions describing groundwater composition.

If there are several isotopes for a chemical element, an effective solubility for each isotope is estimated from its relative abundance. Concentrations and isotope ratios may change in time because of radioactive decay. The precipitation model also calculates the accumulated mass of any precipitate.

If the concentration of a contaminant is greater than its effective solubility limit, we assume a constant-concentration source term in modelling transport from the failed container; otherwise we assume the source term is equal to the sum of congruent and instant releases from the used fuel and Zircaloy. Both types of source terms can apply at different modelling times. For instance, the concentration of a contaminant might slowly build up to its solubility limit, maintain that limit until the precipitate is completely dissolved, and thereafter decrease to smaller values; we would then have a congruent-release plus instant-release source term at early times and again at long times, with a constant-concentration source term at intermediate times.

Many of the parameters used to describe precipitation in the container are described using probability distributions to account for uncertainty, and different values are sampled for each vault sector in a single simulation.

Transport from a Failed Container

We assume that contaminants released to the interior of a failed container diffuse into the surrounding buffer through small, pinhole-sized defects. These small defects provide a long-term transport resistance by restricting and delaying the movement of radionuclides out of the container (SKB 1992, LeNeveu 1996).

The vault model provides two different mathematical solutions to this process, depending on the characteristics of the source term. Contaminants that have precipitated inside the container are modelled using a constant-concentration source term; other contaminants are modelled using source term based on the sum of the congruent and instant releases (LeNeveu 1996; LeNeveu and Kolár 1996, Johnson et al. 1996). Key parameters used for these solutions include the contaminant diffusion coefficients (within the pinhole and within the surrounding buffer), the radius and length of the pinhole and the internal

volume and void porosity of the container. We assume the radius of the pinhole is equivalent to the size of the arbitrarily shaped defect. The result of these calculations is the time-dependent rate of release of contaminants into the surrounding buffer.

Many of the parameters used in calculating transport from a failed container are described using probability distributions to account for uncertainty. Different values are sampled for each vault sector in a single simulation.

Transport Through the Buffer, Backfill and Excavation Damaged Zone

For mathematical modelling purposes, the complex three-dimensional geometry of the vault is simplified as illustrated in Figure 10. Thus the containers, buffer, backfill and the excavation damaged zone (EDZ) are represented as nested cylinders, with adjustments to the radii so as to conserve the volumes of the buffer, backfill and EDZ (for a single disposal room and on a per-container basis). The surrounding rock is also treated as an outer cylinder with an infinite radius. We assume the discharge from a failed container is represented as a point source located on the central axis of the cylinders.

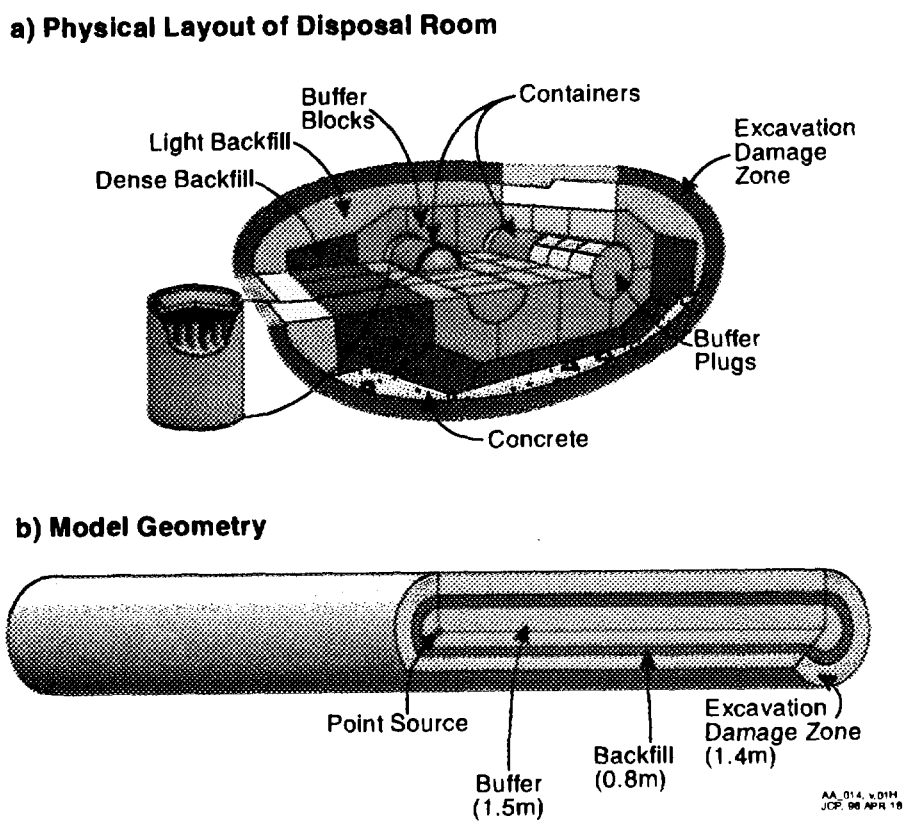

FIGURE 10: Illustration of the Simplified Vault Geometry. Part (a) of this figure is a three-dimensional view of a disposal room, and part (b) shows the geometry that has been assumed for the mathematical simulations. The buffer, backfill and excavation damaged zone are represented as nested cylinders, and the defect point in a failed container is represented as a point source on the central axis of the cylinders.

This simplification permits the use of a semi-analytical solution, based on the boundary integral method, of contaminant transport through the buffer, backfill and EDZ into the surrounding rock (LeNeveu and Kolár 1996, Kolár and LeNeveu 1995, Kolár et al. 1994). The adequacy of this two-dimensional mathematical solution has been demonstrated by comparisons with a three-dimensional finite element model (LeNeveu and Kolár 1996, Johnson et al. 1996).

Releases from all failed containers within all disposal rooms in a single vault sector are added together. The main result from this component of the vault model is the time-dependent flow of contaminants out of a vault sector into the adjoining rock. This is a net flow: it corresponds to the integrated flow out of the entire surface of the outer cylinder that represents the EDZ. Intermediate results can provide the net flow out of the cylinders representing the buffer and the backfill.

Permeabilities in the buffer are very small and we assume that contaminants move only by diffusive transport through the buffer. However, groundwater velocities could be significant in the backfill, EDZ and surrounding rock; in these media we assume uniform radial and axial flows within a sector and include advection, dispersion and diffusion in calculations of contaminant movement.

The important parameters used to describe contaminant transport through the buffer, backfill and EDZ include diffusion coefficients, capacity factors, layer thicknesses, groundwater velocities and dispersivities in the three media. Other important parameters include diffusion coefficients, groundwater velocities and dispersivities in the surrounding rock. Most of these parameters are described using probability distributions to account for uncertainty. Parameters that vary from one sector to the next (such as groundwater velocities in the backfill, EDZ and surrounding rock) are sampled for each vault sector in a single simulation.

Linkages to the Geosphere Model

The vault model describes the effects of the engineered barriers, whereas the geosphere model describes the effects of the rock mass surrounding the vault and extending to the surface environment. Linkages between the two models provide an integrated description of interactions between the two models, so that the combined models provide a consistent representation of the vault within its host rock.

The main result from the vault model is the time-dependent rate of flow of contaminants out of each vault sector into the surrounding geosphere. As noted in the preceding discussion on contaminant transport through the buffer, backfill and EDZ, the vault model treats the surrounding rock as the outermost cylinder. The properties of this rock correspond to the properties of the lower rock zone within which the vault is located. In particular, the geosphere model provides information on the direction and magnitude of groundwater flow in the rock immediately surrounding each vault sector. The geosphere model also provides information on groundwater velocities through the backfill and EDZ for each vault sector. In this way, we ensure that the estimated flow of contaminants from a vault sector is consistent with the properties of the adjoining rock in the geosphere.

5.3 DESCRIPTION OF THE GEOSPHERE MODEL

The geosphere model simulates the transport of contaminants in groundwater within the geosphere. We assume that contaminants that have been released from the vault pass through different domains of rock, fracture zones and vertical joints, overburden and deep lake sediment, to discharge in the biosphere at topographic lows and at a water-supply well drilled into the geosphere. A central feature of the geosphere model is its network of pathways that describe the directions of groundwater flow within the geosphere. We simulate the transport of contaminants through this network (Melnyk 1995).

As noted previously, the vault and geosphere models are integrated to ensure estimated releases of contaminants from the vault are consistent with the properties of the surrounding geosphere. The geosphere and biosphere models are also integrated to ensure consistency in estimated discharges into the biosphere.

Groundwater Flow within the Geosphere

A complete description of groundwater flow in a region of the geosphere typically requires that the region be large enough to act as a self-contained hydrogeological unit. We have assumed for this study, as in the EIS case study, that the simulation of groundwater flow and contaminant transport is confined to the geosphere region represented in Figure 7.

Detailed studies using MOTIF provide an analysis of groundwater flows in this model region (Stanchell et al. 1996). These studies predict groundwater flow patterns for the original, unperturbed geosphere and for a geosphere that contains a hypothetical disposal vault located at a depth of 500 m. The analyses also include the effects on groundwater flow of geothermal gradients and decay heat produced by the vault. Additional modelling shows the potential effects of water-supply wells that draw different volumes of water from fracture zone LD1. The MOTIF code does not consider the relatively thin layers of overburden and lake sediment that overlie the bedrock. The discussion on geosphere-biosphere linkages shows how these layers are taken into consideration as part of the GEONET network.

We use the detailed information from MOTIF to construct a simpler groundwater flow network in the geosphere model. The corresponding code for the geosphere model, GEONET, simulates groundwater flows in the region around the hypothetical vault through a network of segments in the geosphere. These GEONET segments are selected to (i) represent individual parts of the modelled geosphere that have distinct chemical and physical properties, and (ii) duplicate the pattern of flow fields, and the overall pattern of groundwater movement, that is predicted by the detailed studies with MOTIF.

Segments connect to other segments at nodes and may diverge or converge. A sequence of segments and nodes defines a potential pathway that starts at the disposal vault and terminates at the surface environment. Figure 11 illustrates the network of 100 segments used by GEONET to represent the geosphere studied in this report. There are 24 segments that originate at the 24 vault sectors (Figure 9) and nine segments that lead to discharges in the biosphere. Nineteen segments (part (d) of the figure) are used to describe the groundwater flow pattern in LD1.

An important set of parameters used to describe groundwater flow in GEONET is the set that describes the network itself, defining the locations of the nodes and which segments are connected together at the nodes. Properties of the geosphere assigned to nodes are their Cartesian coordinates, temperatures and hydraulic heads; we assume these parameters do not change from one simulation to the next (except for the hydraulic heads which are affected by rate of water withdrawal from the well). Properties of the geosphere assigned to segments are porosity, tortuosity, dispersivity, permeability, salinity of the groundwater, and the types and amounts of minerals affecting sorption of contaminants; we assume these parameters are variable and their possible values are specified by probability distributions (except for permeabilities which we assume are invariant for each different rock zone). All properties are chosen to be consistent with results from MOTIF.

Segment and node properties are used to calculate the major transport parameters for each segment: the groundwater velocity, dispersion coefficient, path length, and contaminant retardation factors. Specific groundwater discharge (Darcy velocity) for each segment is determined from hydraulic heads and temperatures at the inlet and outlet nodes of the segment and from the permeability of the segment. Linear groundwater velocity is then determined using an effective transport porosity that ranges between

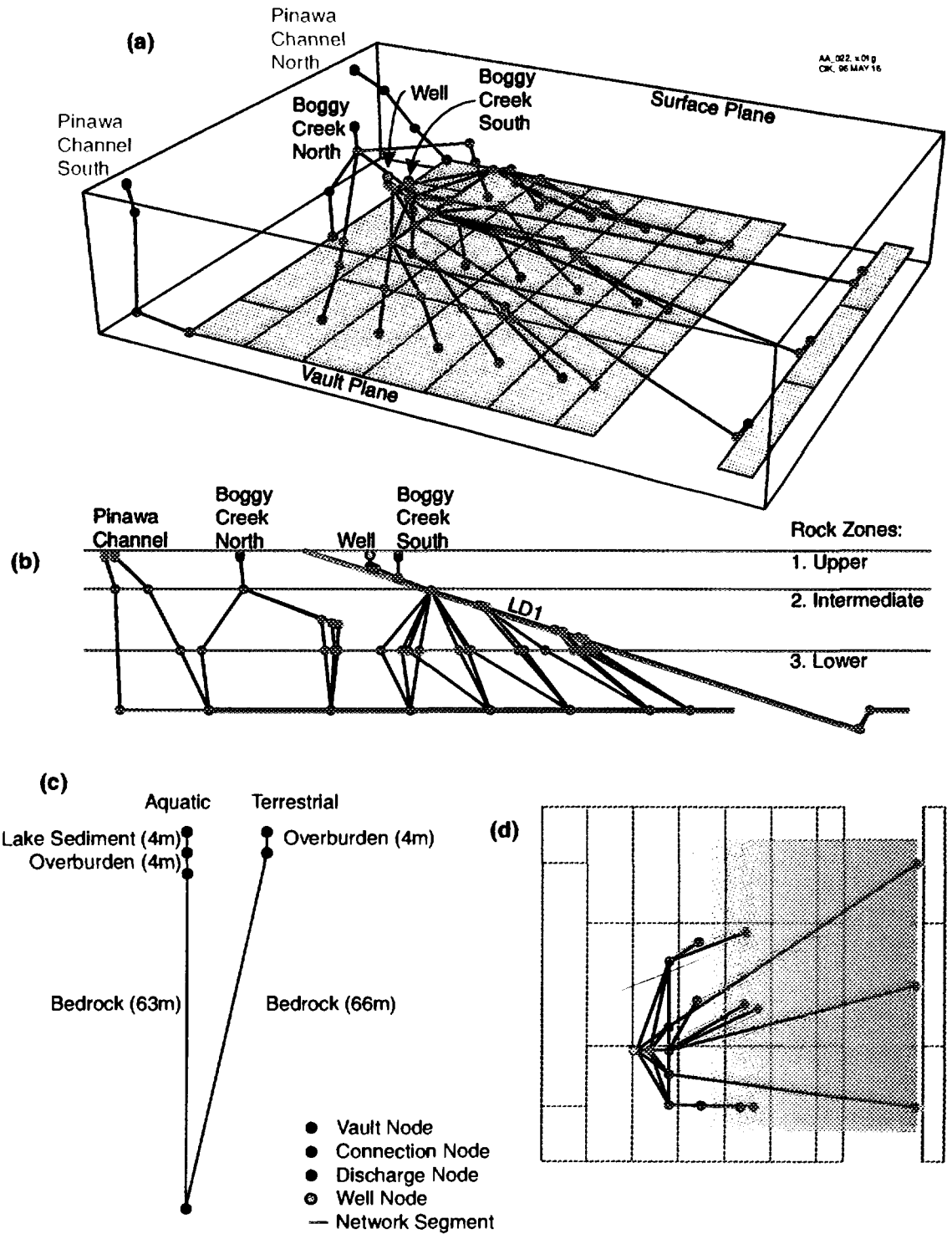

FIGURE 11: Views of the Network of Segments Representing the Modelled Geosphere. Part (a) is a three-dimensional view, and part (b) is a vertical projection. Part (c) is an enlarged cross section near the Boggy Creek South discharge zone, showing the aquatic discharge pathway includes segments for overburden and lake sediment while the terrestrial pathway has only a segment for overburden. Part (d) is a plan view of fracture zone LD1 and illustrates the 19 segments used to represent this feature. The well depth assumed in these views is 33 m.

10^{-5} and 10^{-3} for the layer of rock immediately surrounding the hypothetical vault (rock layer 3 in Figure 7) and for the two rock layers above (layers 1 and 2 in Figure 7). The range of values for these effective transport porosities is responsible for most of the variability in calculated groundwater velocities in the geosphere model.

Figure 12 shows the 9 discharge zones in the biosphere.

- Four discharges are to aquatic bodies located in topographic lows: Boggy Creek North, Boggy Creek South, Pinawa Channel North and Pinawa Channel South; we assume these water bodies are equivalent to a lake in the biosphere model. Part (c) of Figure 11 shows the aquatic discharge pathway includes segments representing overburden and lake sediment.

- For each of these aquatic discharges there is an associated adjacent terrestrial discharge. We assume that a fraction (randomly sampled between 1% to 10%) of the contaminant flows to the aquatic discharges is diverted to the terrestrial discharges. Part (c) of Figure 11 shows the terrestrial pathway includes a segment representing the overburden.

- There may also exist a ninth discharge to a water-supply well used by the critical group as their source of domestic water. In simulations where a well is present, it may be one of the more important discharge points of contaminants from the vault.

The biosphere model specifies whether the critical group uses a lake or a well as their source of water (and whether they also use well water for irrigation purposes). Based on current-day usage of wells on the Canadian Shield, there is about a 50% probability that the critical group would rely on a water-supply well (Davis et al. 1993). To model the associated uncertainty, we use a "switch parameter" (Goodwin et al. 1994a) in the system model; this parameter is characterized by a probability function in which there is a probability of 0.5 that a well will be present in any randomly sampled simulation.

When a well is present, we first sample its depth from a probability distribution that describes current well depths in the vicinity of the WRA. In this scoping assessment, we restrict the maximum well depth to 100 m (measured from ground surface); we exclude deeper wells because they could have large perturbations on groundwater flow patterns at depth, which would invalidate the network of segments described above.

An "overburden" well is relatively shallow and does not reach the underlying bedrock. We assume that contaminant concentrations in the groundwater captured by an overburden well are the same as contaminant concentrations in the lake water. A "bedrock" well is deep enough to reach the bedrock, and we assume it is located such that

- it just reaches fracture zone LD1, and thereby short-circuits as much of the bedrock as possible; and

- it intercepts the centre (based on studies using MOTIF) of the contaminant plume that is moving up LD1.

The well illustrated in Figures 11 and 12 is a bedrock well. Because of the assumptions we use to site bedrock wells, the well in the figures would lie within the current confines of Boggy Creek. This situation could occur in the future if, for example, parts of Boggy Creek become infilled with sediment.

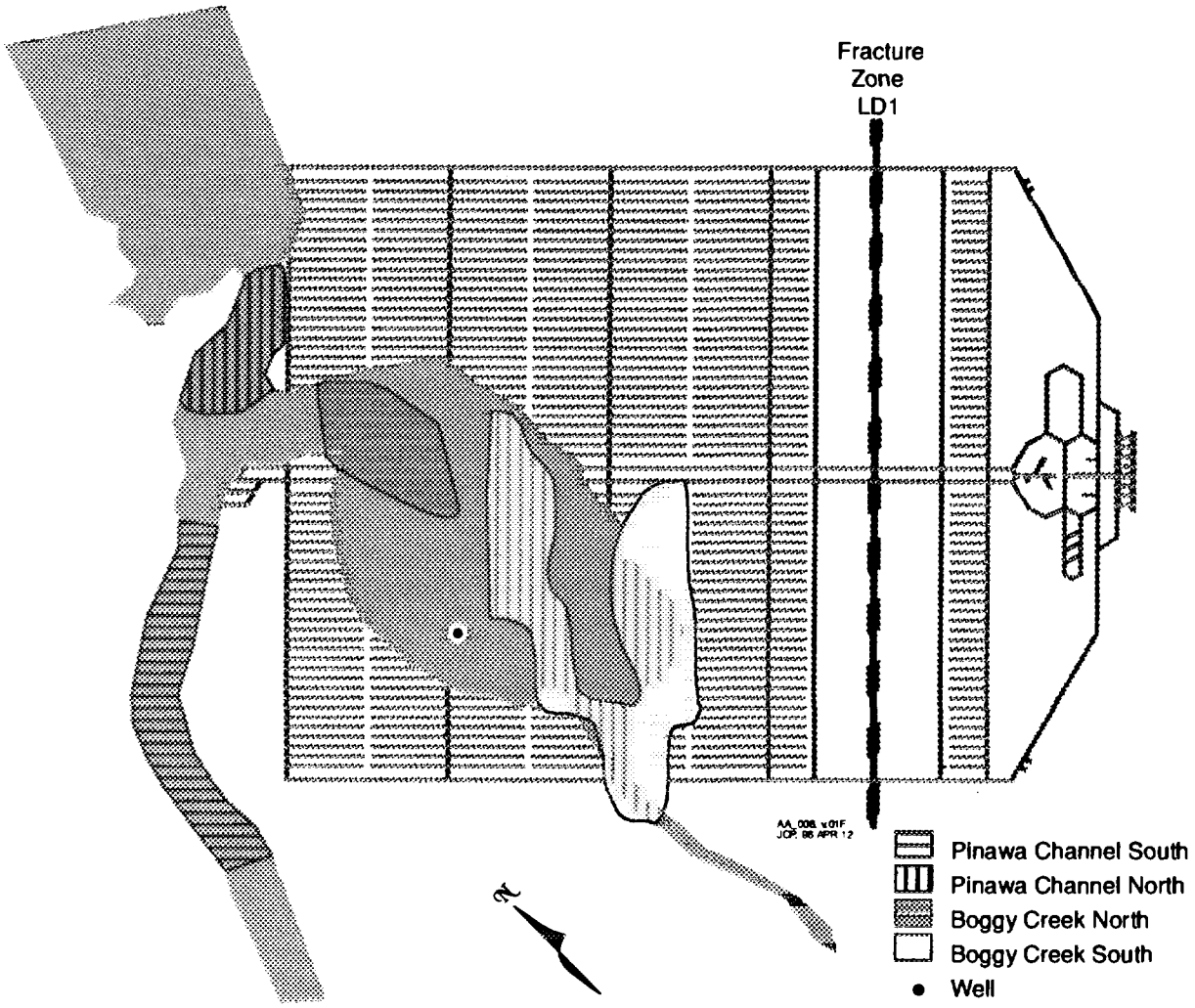

FIGURE 12: Plan View Illustrating the Location of the Discharge Zones. Four discharges are to water bodies at topographic lows and four are to adjacent terrestrial locations. Discharges may also occur to the well (when it is present), which would capture some of the flow moving toward Boggy Creek South. In this figure, we assume the depth of the well is 33 m, deep enough to intercept fracture zone LD1. The conservative method used to site the well (see text) means it would lie within the current confines of Boggy Creek.

Wells that extend into the bedrock, and that are associated with large rates of water withdrawal, can perturb groundwater flow velocities. These effects are taken into account through modifications to the hydraulic heads for all affected nodes (especially nodes lying in or near fracture zone LD1), based on empirical equations developed from simulations using MOTIF (Stanchell et al. 1996).

Contaminant Transport through the Geosphere

We model contaminant movement through the geosphere with the assumption that contaminants move through the segments shown in Figure 11, leading from the vault to the surface environment.

As noted earlier, we assume in this scoping assessment that the permeability of rock in layer 3 (surrounding the disposal vault) is 1×10^{-17} m^2, 100 times larger than the value used in the geosphere model for the EIS case study. With these large permeabilities, and with the prescribed values for effective transport porosity, groundwater velocities in most GEONET segments are sufficiently large that contaminant transport by advection (i.e., in moving groundwater) is much more important than contaminant transport by diffusion. The only exceptions are in the segments representing overburden and lake sediment, where both diffusive transport and advective transport are important.

For each segment, contaminant movement is simulated mathematically using partial differential equations that describe contaminant transport by moving groundwater, dispersion and diffusion (Heinrich and Andres 1985). The equations also describe the increase and loss of contaminants caused by radioactive decay and delays in contaminant movement due to sorption. For the 24 segments adjoining the vault, the source boundary condition is the time-dependent release rates of contaminants computed by the vault model. For all other segments, it is the time-dependent rate of arrival of contaminants from connected segments located closer to the vault. The outlet boundary condition is such that contaminant transport within a segment is not affected by differences in properties between the current segment and any following segments or by the discharge zones in the biosphere.

Contaminant movement will be slowed by sorption on minerals that may be present in a segment. We simulate sorption through the use of a retardation factor, which is equivalent to the ratio of the groundwater velocity to the contaminant transport velocity. Its minimum value is unity, which would mean that the contaminant moves at the same velocity as the groundwater. A value greater than unity means that the migration velocity of the contaminant is slower than that of the groundwater; that is, the movement of the contaminant is retarded relative the movement of the groundwater. We calculate the retardation factor for each contaminant using (Ticknor and Vandergraaf 1996, Vandergraaf et al. 1992)

- the sorptive properties for different chemical elements on different minerals, including the influence of different groundwater compositions;
- the properties of a segment that describe the types and amounts of minerals that are present and the composition of the groundwater found in that segment; and
- a term that describes the associated range of uncertainty in the sorption, including an uncertainty contribution caused by the effects of contaminant concentration.

Linkages to the Biosphere Model

The geosphere model describes the rate of release of contaminants to 4 aquatic and 4 terrestrial discharge zones and to a well (if it is present) in the biosphere. The biosphere model uses these results to simulate contaminant movement through the surface environment and to estimate impacts. Linkages connecting the models provide a consistent representation of interactions that occur between the modelled geosphere and the modelled biosphere.

The principal connection between the geosphere and biosphere models is at the discharge zones and the well. We assume that (see part (c) of Figure 11)

- pathways leading to the aquatic discharge zones include segments representing a layer of overburden and a layer of sediment, located between the last segments in the bedrock and the surface environment; and

- pathways leading to the associated terrestrial discharge zones include a segment representing a layer of overburden.

The layers of overburden and sediment are too small to be represented in the detailed modelling using MOTIF, but they are an important part of the flow pathways for groundwater and contaminants. We simulate their effects by adding extra segments to the GEONET network (part (c) of Figure 11) and define their properties to be consistent with field data and with results from MOTIF. For example, for the segments representing the overburden and lake sediment

- we calculate retardation factors in the same way as for other segments, using field data on the types and amounts of minerals found in overburden and lake sediment; and

- we assume that the groundwater flow is vertically upwards and that its magnitude is consistent with the values determined by MOTIF for adjacent segments in the bedrock.

For simulations that include a well, we ensure that the well-water demands set in the biosphere model are consistent with the supply capacity that is determined in the geosphere model.

- The provisional well demand, or annual volume of water desired from the well, is calculated in the biosphere model. It depends on factors such as the size of the critical group and whether or not they use well water to irrigate their garden.

- The flow capacity of the well is calculated in the geosphere model, taking into consideration factors such as the depth and location of the well and the physical properties of the rock zones from which the water is drawn.

If the provisional well demand exceeds the capacity of the well to supply water, then we reduce the demand by assuming the critical group augments their requirements with water drawn from the lake. The adjusted well demand is then used in the geosphere model to calculate the effects of the rates of water withdrawal on the hydraulic heads of all affected GEONET segments. For large demands, the well may capture water from the surface in addition to deep groundwater; we assume that the captured surface water is contaminated to the same degree as the lake water.

Other related parameters calculated in the geosphere model for use in the biosphere model are the areal extents and groundwater discharge rates associated with the discharges zones. Parts (a) and (b) of Figure 11 show that the discharge zones at Boggy Creek South and the well are fed by common segments. Discharges to Boggy Creek South would be affected by the well, especially when the (adjusted) well demand is high. This effect is simulated in the geosphere model: the presence of a well decreases both the area of, and groundwater flows to, the discharge zones at Boggy Creek South.

5.4 DESCRIPTION OF THE BIOSPHERE MODEL

The biosphere model used in this report is similar to that used in the EIS case study (Davis et al. 1993), and we briefly outline here its main features. Zach et al (1996) provide more detailed information, including enhancements to the model and justification of the assumptions and data.

We assume that contaminants (radionuclides and chemically toxic elements) that have been released from the vault and that have travelled through the geosphere are discharged into the local biosphere at the 9 discharge zones shown in Figure 12. The discharges are to topographic lows, with 4 terrestrial and 4 aquatic components, and to a water-supply well. In the biosphere model, we assume that Boggy Creek North and South, and Pinawa Channel North and South, are represented by a lake. The size of this lake, and other properties such as its watershed area, vary from one simulation to the next to take into account uncertainty in time. For example, 10^3 a from now the lake could be bigger or smaller, but to be conservative we assume that there is always a nearby water body to receive contaminant discharges at these 4 topographical lows.

Figure 13 shows the conceptual landscape of the modelled biosphere, which includes a lake and lake sediment, a water-supply well, the atmosphere outside and inside buildings, and the soils in cultivated and natural fields that supply food, fuel and building materials and that serve as the habitat for native plants and wildlife.

The biosphere model simulates the movement of contaminants from the discharge zones through the surface and near-surface environment and estimates their concentrations in water, soil and air. Figure 14 shows the underlying structure of the biosphere model. The model consists of 6 submodels: one representing the geosphere-biosphere interface and 5 representing the surface water, soil, atmosphere, and human and nonhuman food-chain compartments (Zach et al. 1996).

- The interface submodel estimates contaminant concentrations arriving at the discharge zones;

- The surface water submodel estimates contaminant concentrations in nearby lake and lake sediments;

- The soil submodel estimates contaminant concentrations in the soil of a garden, forage field, woodlot and peat bog used by the critical group;

- The atmosphere submodel estimates contaminant concentrations in the air (indoor and outdoor) surrounding the critical group;

- The human food-chain and dose submodel estimates contaminant concentrations in plants and animals consumed by the critical group, and internal and external radiation exposures to members of the critical group; and

- The nonhuman food-chain and dose submodel estimates internal and external radiation exposures to representative nonhuman biota.

Figure 14 shows that flows from the geosphere enter the surface water and soil compartments of the modelled biosphere (Zach et al. 1996, Davis et al. 1993). We actually assume duplication of mass: whatever enters the soil compartment is also assumed to be in the surface water compartment. This simplifies modelling by implicitly accounting for runoff to the lake. Once in the surface water or soil, contaminants move into the atmosphere and food-chain compartments. The noble gases are treated somewhat differently: we assume that they discharge directly from the geosphere to the atmosphere compartment. Contaminants that have entered the modelled biosphere are lost only by radioactive decay and by down-stream flow of water (flushing) from the lake.

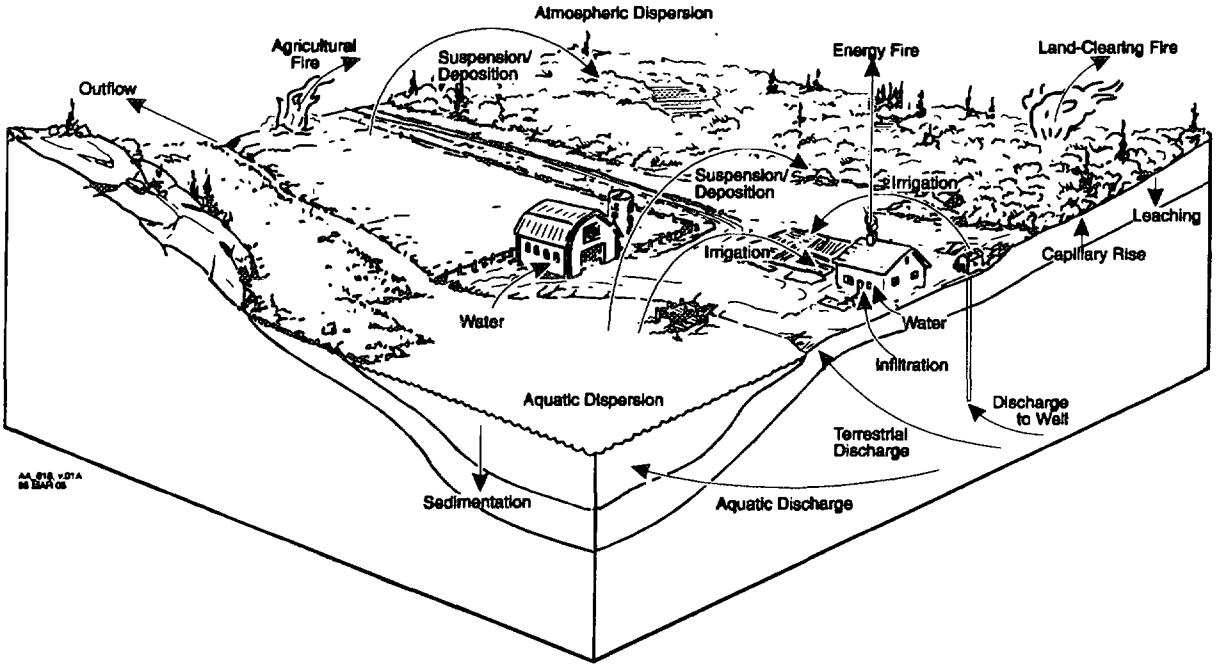

FIGURE 13: Conceptual Landscape of the Modelled Biosphere. Discharges from the disposal vault are to a well and to zones that underlie the lake and adjacent terrestrial areas. The biosphere model simulates transport of radionuclides and chemically toxic elements in a lake and lake sediment; soils in a garden, forage field, woodlot and peat bog; and in the atmosphere above the lake and fields and in the buildings used by the critical group. We assume that members of the critical group spend their entire lives in the modelled biosphere.

The Interface Submodel

The geosphere/biosphere interface submodel completes the linkage between the site-specific geosphere and the generic biosphere model. Some details of the linkage are described in Section 5.3.

The main purpose of the interface submodel is to calculate contaminant concentrations reaching the biosphere, using estimates from the geosphere model of release rates of contaminants and groundwater at the 9 discharge zones. The calculation is straightforward for most contaminants. However, one complication arises for progeny radionuclides that are modelled using the secular equilibrium approximation in the geosphere model. The releases of these radionuclides are calculated from the releases of their precurors plus a term that takes into account the relative mobilities of the precursor and progeny within the last geosphere segment (Szekely et al. 1994).

The Surface Water Submodel

We model the lake as a well-mixed, constant-volume water body fed by runoff from the watershed (Zach et al. 1996, Davis et al. 1993, Bird et al. 1992). Mixed sediment is continuously being deposited to the lake bottom, removing contaminants from the lake water above. Contaminants from the lake and lake sediment water may affect the critical group:

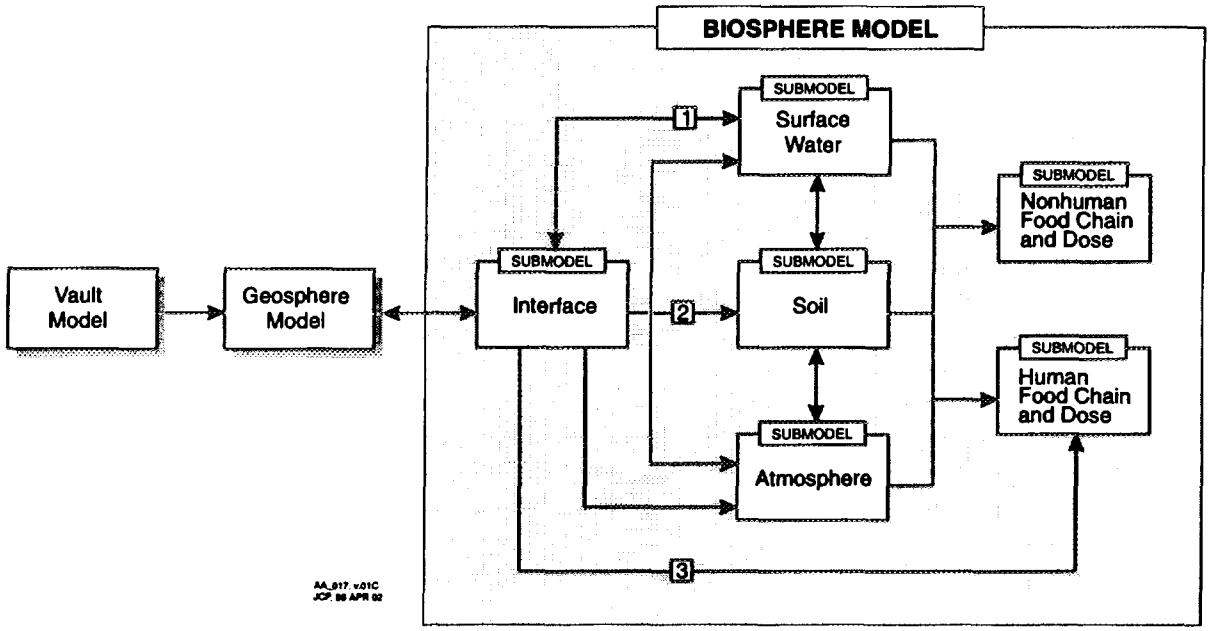

FIGURE 14: Simplified Structure of the Biosphere Model. The geosphere model provides estimates of contaminant release rates that are used by the geosphere/biosphere interface submodel. The interface submodel estimates concentrations reaching (1) the surface water submodel and (2) the soil submodel; releases may also enter the biosphere (3) from the well and (for the noble gases) from discharges directly from the geosphere into the atmosphere. The surface water, soil, atmosphere and the two food-chain and dose submodels describe the transport of contaminants between and within different compartments of the biosphere. The food-chain and dose submodels also estimate radiation dose to members of the critical group and to nonhuman biota.

- directly through the use of lake water to supply household water and irrigation water required by the critical group,

- indirectly through suspension of contaminated particulates and degassing of volatile contaminants to the atmosphere, and

- indirectly through the use of lake sediment as arable land.

The surface water submodel estimates contaminant concentrations in the lake water and lake sediment. It uses parameters such as the rate of flushing of the lake (a function of the size of the lake and its watershed and the annual meteoric precipitation), the rates of suspension of particulates and degassing of volatile contaminants, and the rate of removal of contaminants to the mixed sediment (Zach et al. 1996, Davis et al. 1993, Bird et al. 1992). Feasible values for these parameters are specified using probability distributions.

The Soil Submodel

We simulate contaminant movement in the soil of a garden, a forage field used by domestic and wild plants and animals, and a woodlot and peat bog supplying wood for construction and fuel for heating (Zach et al. 1996, Davis et al. 1993, Sheppard 1992). We use a conservative siting strategy to locate these soil compartments, taking into account their areas (determined largely by the number of people making up the critical group) and the areal extents of the discharge zones (computed in the geosphere model). In order of priority, we site the peat bog first, the garden second, and then the forage field and woodlot, on the discharge zones that have the highest contaminant concentrations. Peat bogs have a probability of occurrence of about 0.14 and, therefore, the garden is usually sited on the terrestrial discharge zone (or zones) with the highest contaminant concentrations (Zach et al. 1996, Davis et al. 1993, Sheppard 1992). In a randomly sampled simulation, any of the discharge zones can exhibit the highest degree of contamination.

The soil submodel estimates contaminant concentrations in the soil of the garden, forage field, woodlot and peat bog. It uses parameters (and associated probability distributions) such as soil type, soil depth, areas of the four fields, effective meteoric precipitation, volume of irrigation water, and the extent of sorption of contaminants on the soil solids. There are four possible soil types: sand, loam, clay and organic. Fresh lake sediment may also be used as soil with a probability of about 0.01 (Davis et al. 1993).

The Atmosphere Submodel

Contaminants reach the atmosphere by suspension of particulates, by degassing of volatile contaminants from the lake and the soil compartments, by direct releases (for the noble gases only) from the geosphere and by release in smoke from burning contaminated vegetation and fuel (wood and peat). Contaminants enter indoor air by infiltration of outside air; by releases from domestic water, such as showers and humidifiers; and by infiltration from the underlying soil (for radon gas).

The atmosphere submodel calculates contaminant concentrations in the outdoor and indoor air used by the critical group, and the deposition rates of contaminants to underlying surfaces (Zach et al. 1996, Davis et al. 1993, Amiro 1992a). Important parameters in the atmosphere model describe the rates at which contaminated particulates and volatile contaminants enter air from soils and the lake, the frequency of fires, contaminant emission rates from fires, and the dispersion of contaminants in the atmosphere (Zach et al. 1996, Davis et al. 1993). Feasible values for these parameters are defined using probability distributions.

The Human Food-Chain and Dose Submodel

The human food-chain and dose submodel uses estimated concentrations of contaminants in lake water, well water, soils in the fields, indoor and outdoor air, and the deposition rates from air and irrigation, to estimate the degree of contamination of plants and animals (Zach et al. 1996, Davis et al. 1993, Zach and Sheppard 1992). It then estimates the dose rate to a member of the critical group caused by internal exposure (ingestion and inhalation) and external exposure.

We assume that the critical group is a self-sufficient rural community that obtains all its air, water and food from the vicinity of groundwater discharges from the hypothetical vault (Zach et al. 1966, Davis et al. 1993). Table 3 lists the 26 possible exposure pathways that are considered. Compared with the EIS case study, there are several added pathways involving inhalation by terrestrial animals that affect estimates of dose rate to the critical group.

TABLE 3

EXPOSURE PATHWAYS TO HUMANS CONSIDERED IN THE BIOSPHERE MODEL

	Pathway	Comment
	Uptake from Soil	
1.	Soil/plant/meat/human	Used to estimate dose rate to a member of the critical group from the ingestion of plants and animal products that have been contaminated by uptake from soil.
2.	Soil/plant/milk/human	
3.	Soil/plant/bird/human	
4.	Soil/plant/human	
	Atmospheric Deposition	
5.	Air/plant/meat/human	Used to estimate dose rate to a member of the critical group from the ingestion of plants and animal products that have been contaminated by deposition on plant leaves.
6.	Air/plant/milk/human	
7.	Air/plant/bird/human	
8.	Air/plant/human	
	Animal Air Inhalation	
9.	Air/meat/human	Used to estimate dose rate to a member of the critical group from the ingestion of animal products that have been contaminated by the air that the animals inhale.
10.	Air/milk/human	
11.	Air/bird/human	
	Ingestion of Water	
12.	Water/meat/human	Used to estimate dose rate to a member of the critical group from the direct ingestion of drinking water, and from the ingestion of animal products that have been contaminated by drinking water and by irrigation water.
13.	Water/milk/human	
14.	Water/bird/human	
15.	Water/human	
	Ingestion of Soil	
16.	Soil/meat/human	Used to estimate dose rate to a member of the critical group from the ingestion of contaminated soil; includes direct ingestion of contaminated soil(#19) and ingestion of animal products from animals that have ingested contaminated soil (#16-18).
17.	Soil/milk/human	
18.	Soil/bird/human	
19.	Soil/human	
	Other Internal Routes	
20.	Fish/human	Used to estimate dose rate to the critical group from the ingestion of fish in a lake contaminated with radionuclides and from the inhalation of air contaminated with radionuclides.
21.	Inhalation	
	External Routes	
22.	Air	Used to estimate external dose rate to the critical group from immersion in contaminated air and water, exposure to contaminated ground (groundshine), and exposure to buildings constructed of wood and inorganic materials.
23.	Water	
24.	Ground	
25.	Wood	
26.	Inorganic	

Internal exposures to the critical group involve ingestion and inhalation (pathways 1 through 21 in Table 3). We calculate radiation doses to the critical group using dose conversion factors (DCFs) that convert the concentrations of radioactive contaminants in inhaled air and in ingested food and water into 50-year committed effective dose equivalents. These calculations use DCFs that are based on the recent recommendations of the International Commission on Radiological Protection (ICRP 1991a,b).

For ^{14}C, ^{36}Cl and ^{129}I, we include bounding limits, known as groundwater dilution limits, that take into consideration the presence of stable isotopes of these elements in groundwater and the fact that the human body does not distinguish between stable and radioactive isotopes (Davis et al. 1993). That is, in any particular simulation, there is an upper limit to the dose rate from ^{14}C that arises because the human body does not distinguish between radioactive ^{14}C and stable ^{12}C. These carbon isotopes are retained in the body in the same proportion as found in the ingested sources, and the largest ratio of ^{14}C to ^{12}C would be in groundwater that has passed near the disposal vault. We use this largest ratio to determine the (conservative) groundwater dilution limit for ^{14}C (Davis et al. 1993). Similar comments are applicable to ^{36}C and ^{129}I.

Important parameters used in the internal exposure pathways include inhalation rates, food and water consumption rates, composition of diet, factors describing the transfer rates of chemical elements from soils to plants and from plants to animals, hold-up times that describe the delay between the time of contamination and the time of harvesting and ingestion, the number of people in the critical group, the source of their drinking water (a well or a lake) and if they practice irrigation (Davis et al. 1993). Several important parameters pertain to only ^{129}I, ^{36}Cl and ^{14}C. For ^{129}I, they are the amount of iodine retained in the body, the amount of iodine found in the daily diet of the critical group and the concentration of stable iodine (^{127}I) in groundwater (Zach et al. 1996, Davis et al. 1993). For ^{14}C and ^{36}Cl, important parameters are the concentrations of stable carbon and chlorine in groundwater (Zach et al. 1996, Davis et al. 1993, Johnson et al. 1995). Most of these parameters are characterized using probability distributions.

External exposures to the critical group occur from radionuclides in their surroundings (pathways 22 to 26 in Table 3). We assume, for example, that the critical group receives an external dose from standing on the soil of the most contaminated field (Zach et al. 1996, Davis et al. 1993, Zach and Sheppard 1992). Important parameters involving external exposure pathways are the DCFs that convert concentrations of external radioactive contaminants to effective dose equivalents and the duration of exposure to each external source.

The Nonhuman Food-Chain and Dose Submodel

The nonhuman food-chain and dose submodel is similar in function to the human food-chain and dose submodel, except it estimates the radiation dose to nonhuman biota arising from internal and external exposure pathways (Zach et al. 1996, Davis et al. 1993). We consider four generic target organisms: a plant with characteristics similar to a broad range of terrestrial vascular plants, a mammal similar to a herbivore, a bird similar to terrestrial species that eat seeds and fruit, and a fish that represents a range of free-swimming and bottom-feeding species. We assume that each of these target organisms is located in the discharge zones and in this sense they can be regarded as "critical" biota.

Compared with the EIS case study, the calculations in this report include inhalation pathways for the mammal and the bird, groundwater dilution limits for ^{14}C, ^{36}Cl and ^{129}I, a specific activity model for ^{3}H, and a comprehensive list of radionuclides (Zach et al. 1996). In addition, external exposures to the target organisms are calculated from the largest of four potential external pathways involving water immersion, air immersion, soil immersion and vegetation immersion (except for the noble gases that give an external dose only by air immersion). That is, we assume that each target organism continuously inhabits the medium that produces the largest estimated dose rate (Zach et al. 1996). Important parameters for

calculations of dose rates to nonhuman biota calculations are similar to those for the calculation of dose rate to the critical group, with two exceptions:

- there are no hold-up times, so that the biota are affected as soon as they are exposed to radionuclides in their habitat; and

- doses rates are calculated using special DCFs that pertain to the target organisms (Amiro 1992b, 1995) and not to humans. Thus radiation dose to nonhuman biota are reported in units of Gray, the basic unit of absorbed dose of ionizing radiation.

5.5 RADIONUCLIDES CONSIDERED IN THIS REPORT

This report deals with a radiological assessment of used-fuel bundles from CANDU nuclear generating stations and therefore, we require inventories of radionuclides in irradiated UO_2 fuel and the Zircaloy sheaths used to contain the fuel. We assume that all fuel bundles are from the Bruce Nuclear Generating Station, that each bundle has produced thermal energy amounting to 720 GJ/kg of initial uranium, and that they have been stored out of the reactor for at least 10 a. There may be a mix of fuel bundles with somewhat different characteristics in an actual disposal system. However, the differences are expected to be relatively unimportant and would be largely included in the range of values in the probability distributions specified for the inventories.

Used-fuel bundles will contain UO_2 and constituents of Zircaloy, plus

- fission products generated during the fissioning of the UO_2 and neutron activation products of impurities in the UO_2 fuel,

- neutron activation products of the constituents and impurities in the Zircaloy sheaths, and

- members of the actinide decay chains produced by the neutron activation of uranium isotopes.

A comprehensive study by Tait and Theaker (1996) shows that these used-fuel bundles contain about 400 contaminants (we use the collective term "contaminants" to refer to radioactive isotopes and stable isotopes of all elements in the bundles). However, many contaminants are not hazardous. Some are not radioactive and have negligible chemical toxicities. A large number of radioactive isotopes would have negligible radiotoxicity impacts because they exist in very small quantities or because they have short half-lives and would not persist in significant quantities after transport through the vault and geosphere.

In this scoping assessment, we focus on the radionuclides (radioactive isotopes) that are expected to be the dominant contributors to the total radiation dose over times scales up to 10^5 a following closure of the disposal vault. To identify these radionuclides, we used

- a study similar to that described by Goodwin and Mehta (1994) for the EIS case study, but adapted for the disposal system evaluated herein;

- an evaluation of the properties of the radionuclides that would most influence estimates of dose rate (notably radionuclide half-life, mobility in the engineered and natural barriers, initial inventory and release mechanism from the UO_2 and Zircaloy matrices); and

- an examination of the radionuclides that have been evaluated in long-term assessments by other national organizations.

Tables 4 and 5 list the 41 radionuclides evaluated in this report. (We have identified approximately 140 other radionuclides that are tentative candidates for evaluation in a full postclosure assessment, although we expect that they would have small or insignificant contributions to the total dose rate.) The tables also identify the decay chains evaluated in this report. If a radionuclide is not shown in a decay chain, we assume it decays directly to a stable isotope.

- The decay chains in Table 4 are simple and can be represented by a pair of precursor (parent) and progeny (daughter) radionuclides: ^{93m}Nb (progeny) from the radioactive decay of ^{93}Zr (precursor), ^{126}Sb from ^{126}Sn, and ^{90}Y from ^{90}Sr.

- The actinide decay series are more complex because each typically includes 15 or more member radionuclides. However, they can be simplified for this assessment, following the analysis described by Goodwin and Mehta (1994), to the following chains with appropriate adjustments to inventories and dose conversion factors.

  4n+1 chain: ^{241}Am → ^{237}Np (^{233}Pa) → ^{233}U → ^{229}Th (^{225}Ra) (^{225}Ac)
  4n+2 chain: ^{238}U (^{234}Th) → ^{234}U → ^{230}Th → ^{226}Ra (^{222}Rn) (^{210}Pb) (^{210}Bi) (^{210}Po)
  4n+3 chain: ^{243}Am (^{239}Np) → ^{239}Pu → ^{235}U (^{231}Th) → ^{231}Pa (^{227}Ac) (^{227}Th) (^{223}Ra).

  For calculation of releases through natural and engineered barriers, the symbol "→" indicates the connected radionuclides are modelled explicitly as members of a chain, whereas "( )" implies that the enclosed progeny radionuclide can be treated using the secular equilibrium approximation. For example, ^{241}Am and ^{237}Np are modelled explicitly, whereas releases of ^{233}Pa can be estimated from releases of its precursor, ^{237}Np.

To improve computer usage, we make use of the secular equilibrium approximation in calculations of radionuclide transport through natural and engineered barriers. This approximation is applicable when the half-life of a precursor is about 4 or more times larger than the half-life of its progeny and when both the precursor and progeny reside within the barrier for times longer than about 4 times the half-life of the progeny. When these conditions are met, we need only calculate the release from a barrier of a precursor and use that result to estimate the release of its progeny (Goodwin and Mehta 1994). Secular equilibrium is used mostly in the calculations performed in the vault and geosphere models.

6. QUANTITATIVE ANALYSIS OF RESULTS

6.1 OVERVIEW OF THE ANALYSIS

We discuss in the following sections the quantitative results obtained from PR4, a probabilistic systems assessment computer code that uses the models and data described in the previous section to simulate the expected long-term performance of the disposal system. We perform a probabilistic analysis because it provides a systematic approach to account for the effects of parameter uncertainties, and we have shown in the EIS case study (Goodwin et al. 1994a) that uncertainties have a strong influence on estimated impacts over the long time scales of concern.

The time frame required for quantitative evaluation of impacts is 10^4 a (AECB 1987), and the system model and data are considered to provide acceptable descriptions for times up to the onset of

TABLE 4

FISSION PRODUCTS[1] EVALUATED IN THIS REPORT

Radionuclide[2]	Source[3]	Half-Life [a]	Inventory[4] [mol/kg U]
^{14}C	F	5.73×10^{3}	3.70×10^{-6}
^{14}C	Z	5.73×10^{3}	1.46×10^{-6}
^{36}Cl	F	3.01×10^{5}	9.18×10^{-6}
^{36}Cl	Z	3.01×10^{5}	7.31×10^{-7}
^{135}Cs	F	2.30×10^{6}	1.78×10^{-4}
^{137}Cs	F	3.00×10^{1}	1.86×10^{-3}
^{129}I	F	1.57×10^{7}	3.80×10^{-4}
^{93m}Nb[5]	F	1.36×10^{1}	0.0
^{107}Pd	F	6.50×10^{6}	5.95×10^{-4}
^{126}Sb[5]	F	3.40×10^{-2}	0.0
^{79}Se	F	6.50×10^{4}	1.60×10^{-5}
^{126}Sn	F	1.00×10^{5}	4.55×10^{-5}
^{90}Sr	F	2.91×10^{1}	1.16×10^{-3}
^{99}Tc	F	2.13×10^{5}	2.21×10^{-3}
^{90}Y[5]	F	7.30×10^{-3}	0.0
^{93}Zr	F	1.53×10^{6}	1.26×10^{-3}

1 Most of the radionuclides listed are fission products, except for ^{14}C and ^{36}Cl which are neutron activation products of impurities in UO_2 and in Zircaloy.

2 Radionuclides are abbreviated using their atomic mass number and element symbol; for example ^{14}C identifies the isotope of carbon containing a total of 14 neutrons and protons in its nucleus. The character "m" in ^{93m}Nb indicates it is a metastable radionuclide with different properties from ^{93}Nb. In fact, ^{93m}Nb is radioactive whereas ^{93}Nb is stable.

3 The sources of the radionuclides are fission products of UO_2 fuel or neutron activation products of fuel impurities (F) and neutron activation products of Zircaloy materials (Z).

4 Inventories are uncertain for many radionuclides and thus they are specified as probability distributions for the probabilistic systems assessment described in this report. Values cited in this table are median values from the probability distributions. Inventories for some short-lived radionuclides such as ^{90}Y are reported as zero, indicating that they are of concern only because of ingrowth from a precursor, and not from their initial inventory.

5 Indicates the progeny of one of the following precursor-progeny decay chains:
$^{126}Sn \rightarrow {}^{126}Sb$, $^{90}Sr \rightarrow {}^{90}Y$, and $^{93}Zr \rightarrow {}^{93m}Nb$
where $\rightarrow$ shows the direction of decay. The secular equilibrium approximation is acceptable for these progeny radionuclides in the vault and geosphere models.

TABLE 5

MEMBERS OF THE ACTINIDE DECAY CHAINS
EVALUATED IN THIS REPORT

Radionuclide[1]	Source[2]	Half-Life [a]	Inventory[3] [mol/kg U]
^{225}Ac	4n+1	2.74×10^{-2}	0.0
^{227}Ac	4n+3	2.18×10^{1}	0.0
^{241}Am	4n+1	4.32×10^{2}	4.00×10^{-4}
^{243}Am	4n+3	7.38×10^{3}	1.63×10^{-5}
^{210}Bi	4n+2	1.37×10^{-2}	0.0
^{237}Np	4n+1	2.14×10^{6}	1.34×10^{-4}
^{239}Np	4n+3	6.45×10^{-3}	0.0
^{231}Pa	4n+3	3.28×10^{4}	3.50×10^{-8}
^{233}Pa	4n+1	7.39×10^{-2}	0.0
^{210}Pb	4n+2	2.23×10^{1}	0.0
^{210}Po	4n+2	3.79×10^{-1}	0.0
^{239}Pu	4n+3	2.41×10^{4}	1.12×10^{-2}
^{223}Ra	4n+3	3.13×10^{-2}	0.0
^{225}Ra	4n+1	4.05×10^{-2}	0.0
^{226}Ra	4n+2	1.60×10^{3}	3.11×10^{-13}
^{222}Rn	4n+2	1.05×10^{-2}	0.0
^{227}Th	4n+3	5.12×10^{-2}	0.0
^{229}Th	4n+1	7.34×10^{3}	1.58×10^{-9}
^{230}Th	4n+2	7.70×10^{4}	6.06×10^{-9}
^{231}Th	4n+3	2.91×10^{-3}	0.0
^{234}Th	4n+2	6.60×10^{-2}	0.0
^{233}U	4n+1	1.59×10^{5}	3.55×10^{-5}
^{234}U	4n+2	2.44×10^{5}	1.92×10^{-4}
^{235}U	4n+3	7.04×10^{8}	8.15×10^{-3}
^{238}U	4n+2	4.47×10^{9}	4.14×10^{0}

1 Radionuclides are abbreviated using their atomic mass number and element symbol; for example, ^{225}Ac identifies the isotope of actinium containing 225 neutrons and protons in its nucleus.

2 Members of the actinide decay chains originate from the neutron activation of uranium in the UO_2 fuel. Each member of an actinide decay chain belongs to one of four actinide decay series, which are indicated by the formulae 4n, 4n+1, 4n+2 and 4n+3. When the mass number of a radionuclide is divided by 4, the remainder is 0 for members of the 4n series, 1 for the 4n+1 series, 2 for the 4n+2 series, or 3 for the 4n+3 series. For example, ^{238}U, ^{234}U and ^{230}Th are members of the 4n+2 series. In this report, we consider members of the 4n+1, 4n+2 and 4n+3 actinide decay series; There are no members from the 4n series as these radionuclides are expected to be much less important contributors to total dose.

3 Inventories are uncertain for many radionuclides and thus they are specified as probability distributions for the probabilistic systems assessment described in this report. Values cited in this table are median values from the distributions. Inventories for some short-lived radionuclides are reported as zero, indicating that they are of concern only because of ingrowth from a precursor, and not from their initial inventory.

the next glaciation, about 2 x 10^4 a from now (Johnson et al. 1994b, 1996; Davison et al. 1994b; Stanchell et al. 1996; Davis et al. 1993; Zach et al. 1996). During the period of glaciation and at longer times the characteristics of the geosphere and biosphere would be highly uncertain and the corresponding models may not be appropriate; however, releases from the vault are less uncertain because the containers are designed to withstand glacial loads, so that the only significant container failure mechanism is from fabrication defects which are included in the vault model. Our analysis is therefore focused on quantitative estimates of impacts for the first 10^4 a following closure of the disposal vault.

Nevertheless, we present some results that are extended to 10^7 a after closure, the time limit of the simulations. These results are beyond the acceptable time frame of the system model and data, but they are shown because they provide evidence that the model and data exhibit the expected mathematical behaviour. For example, we expect that doses from all radionuclides must eventually decrease because of radioactive decay and that the time of arrival and duration of dose from a radionuclide will be strongly affected by its half-life and by its rate of movement through the engineered and natural barriers. The results extended to 10^7 a can be examined to confirm that these expectations are met and thereby give confidence in the behaviour of the system model at earlier times. Moreover, the long-term results describe trends in behaviour for a system that remains undisturbed for indefinite periods of time and they can be compared with similar results produced by other national waste management programs.

Our probabilistic systems assessment uses results from thousands of simulations. (We use two sampling strategies: simple random sampling and fractional factorial latin hypercube designs (Andres 1995). We have adopted the latter for sensitivity analysis and are evaluating its potential to provide accurate estimates of means using fewer simulations than the former.) In each simulation, a value for every parameter is sampled randomly from its probability distribution. The sampled values are then used in PR4 to estimate the movement of contaminants from the vault to the biosphere and to estimate an environmental impact such as the maximum dose rate to the critical group. Each of the thousands of simulations produces a different estimate of an impact. Taken together, the thousands of estimates yield an empirical distribution of the impact that directly reflects the underlying uncertainty in the parameters of the system model. Since the system model was developed to represent the disposal system, the distribution also reflects the uncertainty associated with the long-term performance of the disposal system.

We condense the distribution of the impact by examining the "expectation" values. The statistical expectation of an impact is its arithmetic mean value; that is, the integral over the sample space (or uncertainty space) of that impact. The arithmetic mean calculated from a set of randomly sampled simulations is an unbiased representation of the entire set of estimates. We can readily estimate the arithmetic mean from the arithmetic average taken over the thousands of estimates produced by PR4. The mean is also the appropriate statistic for use in the prescribed radiological risk equation: "*Calculations of individual risks should be made by using ... the arithmetic mean value of annual individual dose from the distribution of individual doses in a year calculated as the output from probabilistic analysis* (AECB 1987)."

Section 6.2 discusses the two radiological impacts of concern in this report: the average dose rate to a member of the critical group and the average dose rate to representative nonhuman biota. We provide evidence that enough simulations have been performed to yield robust and relatively precise estimates of mean dose rates.

Probabilistic systems assessment was designed to deal with parameter uncertainty, but some features of the system model are easier to understand through the analyses of individual simulations . We describe in the Appendix a synopsis involving 33 simulations and a detailed analysis of four simulations: two are simulations that produce relatively large estimated dose rates, one produces relatively small estimated

dose rates, and the fourth is akin to the median-value simulation. (The EIS case study (Goodwin et al. 1994a) describes a deterministic analysis of the median-value simulation, in which all parameters are assigned values equal to the median of their probability distributions.)

Section 6.3 describes a probabilistic sensitivity analysis, where we identify the most influential parameters and show how these parameters affect the estimated dose rate to a member of the critical group for times up to 10^5 a. Screening to identify the influential parameters is a challenge because there are several thousands of parameters and they interact in complex ways. Our probabilistic sensitivity analysis is based on iterated fractional factorial latin hypercube designs in which parameters are varied across their probability distributions according to a "supersaturated design" (Andres 1995). We have demonstrated (in Goodwin et al. (1994a) for example), that such designs can efficiently and effectively identify the most influential parameters. The design used in this report has several advantages (Andres 1995).

1. We can systematically examine sets of randomly sampled simulations to identify and to rank the uncertain parameters that most influence an estimated impact, taking into account the effects of uncertainty in all parameters. The design uses 24 equally likely subintervals for each parameter, so that we can examine the influence of each parameter over narrow regions of its domain. These same sets of simulations can also be used to estimate the mean dose rate (Andres 1995).

2. We can estimate independently the *linear effect* (i.e., the average effect of changing from small values of a parameter to large values), the *quadratic effect* (i.e., the departure of the average effect from a linear relationship) and *two-way interaction effects* (i.e., the enhanced influence when any pair of parameters are varied in concert).

3. We can quantify how the uncertainty in an influential parameter affects the estimated impact and uncertainty in the estimated impact. This analysis includes simultaneously the effect of uncertainty in all other parameters.

That is, our sensitivity analysis uses the specified parameter probability distributions to identify influential parameters, to rank them in order of influence, and to show how they affect the estimated impact.

Section 6.4 presents results from selected scenarios. The groundwater transport scenario analyzed in this report can be regarded as a collection of sub-scenarios that differ in one or more important features (Goodwin et al. 1994a). For example, the groundwater transport scenario includes variations in which the lake or a water-supply well provides the domestic water used by the critical group. From the thousands of randomly sampled simulations, we can extract the simulations that involve only water-supply wells, or that belong to other defined sub-scenarios, and display the associated estimated impacts.

Section 6.5 provides a summary description of the behaviour of the disposal system. We discuss the fate of each of the modelled radionuclides, showing how their properties influence their movement through the disposal system and their contributions to the total dose rate.

6.2 ANALYSIS OF MEAN DOSE RATE

6.2.1 Dose Rate to the Critical Group

Our assessment indicates that the mean dose rate to members of the critical group would meet the AECB criterion for the hypothetical disposal system evaluated in this document. This conclusion is based on the curves in Figure 15, which shows average dose rate[†] versus time. Two curves show results for this case study; one is based on 14 000 simulations for the fission products (Table 4) and the second is based on 3500 simulations for the actinide decay chains (Table 5) (The average dose rate curves can be added together to give a total, even though the two curves involve different numbers of simulations. However, the confidence bands, discussed below, cannot be conveniently combined and so we display separate curves We completed more simulations for the fission products because, as shown in the figure, as a group they are more significant contributors to the dose rate over the first 10^4 a.) At every time, both curves, and the sum of the two curves, is less than 5×10^{-5} Sv/a, the dose rate associated with the AECB radiological risk criterion (one chance in a million of a serious health effect per year). The AECB radiological risk criterion applies to the first 10^4 a after closure of the vault, and this figure indicates that the criterion is met for times up to (and well beyond) that time.

The average dose rate curves in Figure 15 are calculated from thousands of individual simulations, and there is some residual uncertainty in the exact value of the mean. The band around each average corresponds to a 90% confidence interval. (The bands take into account only the statistical uncertainty arising from the modelled parameters and not other possible sources of uncertainty such as invalid assumptions.) That is, if we repeated this analysis 100 times with different data sets of the same size, the average dose rate at any point in time would lie within these confidence bands about 90 times out of the 100. The narrowness of the bands in Figure 15 indicates we are quite confident in our estimate of the location of the true mean dose curve.

Figure 15 also shows the average dose rate curve that was obtained in the EIS case study (AECL 1994a, Goodwin et al. 1994a). That curve, and the curves for the disposal system evaluated herein, both rise from zero at early times and start to level out below the dose rate associated with the AECB criterion. There are several significant differences between the curves.

1. Time of peaks - the curve in the EIS case study has not reached a peak value by 10^4 a, nor by 10^5 a after closure of the vault, whereas the average dose curves for the disposal system considered herein exhibit a peak near 10^4 a.

2. Number of peaks - the curve in the EIS case study rises steadily from the start to the end of the simulation times (0 to 10^5 a), whereas the average dose curves for the disposal system considered herein shows several local maxima and shoulders.

Figure 16 provides more information from the present study that explains these differences. The figure shows that several radionuclides are significant contributors to the average dose rate. It is clear that ^{129}I contributes more than any other radionuclide to average dose rate at most times up to 10^5 a, but ^{90}Sr is

[†] The average dose rate is computed from the thousands of randomly sampled simulations and is an estimate of the mean dose rate. The mean dose rate itself is the statistical expectation of dose rate that takes into account the modelled uncertainties in the disposal system.

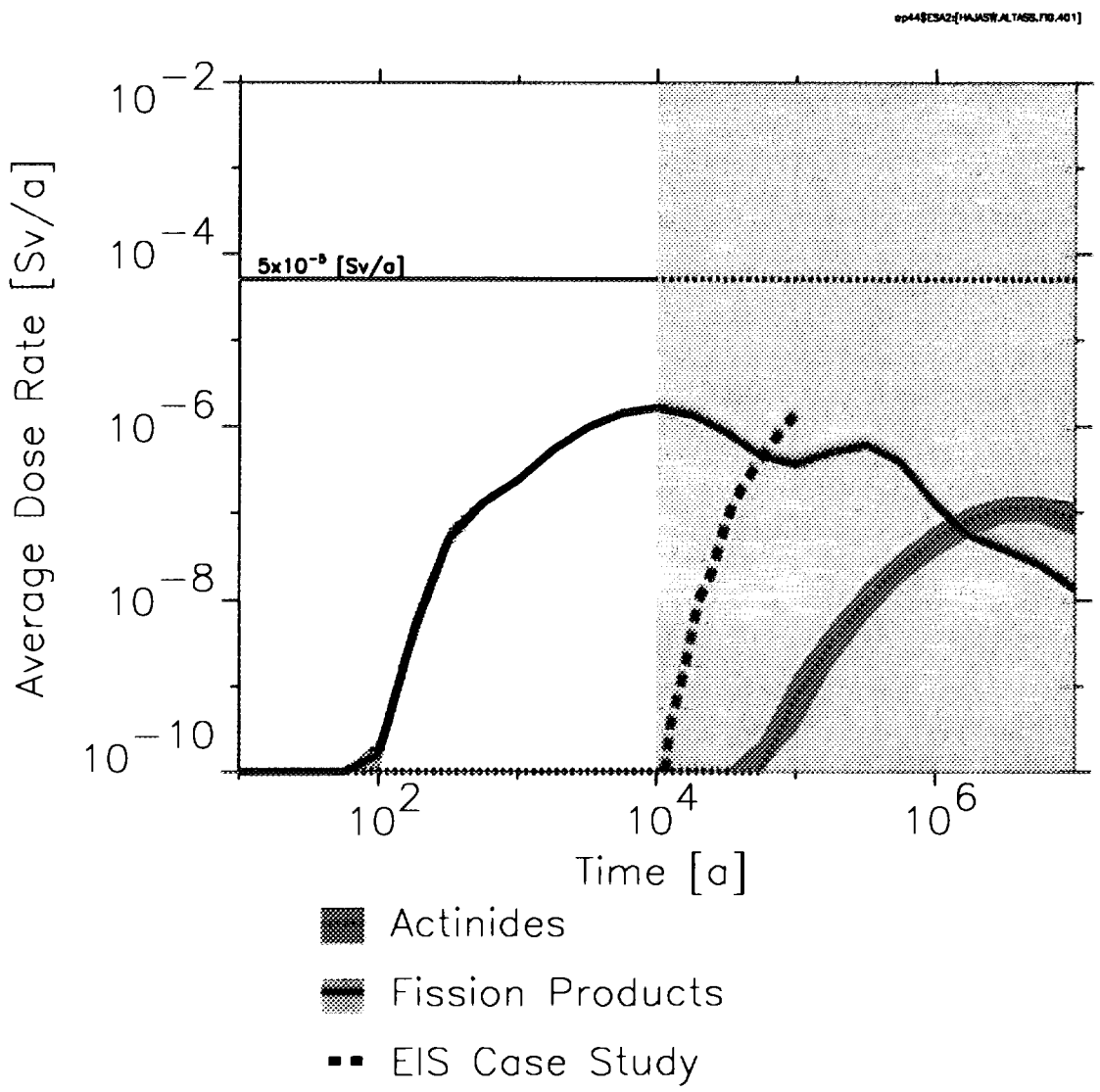

FIGURE 15: Average Dose Rate to the Critical Group. Two curves show the average dose rates to a member of the critical group from the present study, from the 16 fission products in Table 4 and from the 25 members of the actinide decay chains in Table 5. The band around each of the curves shows a 90% confidence interval for the true location of the mean dose rate at each time. The dashed line shows the corresponding average dose rate from the EIS case study. (Goodwin et al. 1994a) The horizontal line, at 5 x 10^{-5} Sv/a, is the dose rate associated with the AECB radiological risk criterion (AECB 1987). The shaded area on the right-hand side of the plot indicates the models and data are less acceptable representations of the disposal system at very long time frames.

the most important contributor at early times and ^{99}Tc and ^{126}Sb become more important at longer times (note that the vertical scale in Figure 16 is logarithmic). In the EIS case study, the average dose rate was dominated at all times up to 10^5 a by ^{129}I, with much smaller (less than 10%) contributions from ^{14}C and ^{36}Cl (Goodwin et al. 1994a, Johnson et al. 1995).

The greater number of contributors shown in Figure 16 for the current disposal system accounts for the number of peaks in the average dose rate curve. These contributors appear because the geosphere

assumed in this study is a less effective barrier (compared with the EIS case study) to the movement of radionuclides once they have been released from the vault. Because their rate of movement in the geosphere is faster, their peak dose rates occur relatively early compared with the peak dose rates in the EIS case study. In this study, for example, the average dose rate curve has a shoulder near 560 a, at a dose rate of about 10^{-7} Sv/a, which is mostly caused by ^{90}Sr. Strontium-90 has a half-life of 29.1 a, but its initial inventory is relatively large (Table 4), and it is relatively mobile in the host rock (Table 1), so that it can contribute to the net dose rate at relatively early times. In the EIS case study, ^{90}Sr was effectively retained by the more effective geosphere barrier and decayed to insignificant levels before it could reach the biosphere.

One might expect that, with a less effective geosphere barrier and with more contributing radionuclides, the curve of total average dose rate for this study would significantly exceed the corresponding curve in the EIS study. This is the case at times before 10^4 a, but not at later times. We attribute these observations to the more robust engineered barriers evaluated in this report, notably the long-lasting containers: we assume that, on average, about 1 in 5000 fabrication-defected containers fail at the time of closure of the disposal vault and that contaminants are then slowly released from the containers by diffusion through small pinhole-sized defects into the surrounding buffer. Some radionuclides such as ^{90}Sr and ^{129}I can move relatively quickly to the biosphere and thus their average dose rates are relatively more important at early times. However, because there are no additional releases (because no other containers fail), their average dose rates show an early peak and then decline. The dose rate maxima obtained in this study support a conclusion that suitable engineered barriers can compensate for a geosphere barrier that is assumed to be relatively ineffective.

Of course if no containers at all fail (as happened in a few of the randomly sampled simulations) then there can be no dose consequences. On the other hand, in a worst-case situation in which every container fails at the time of closure, dose rates for some radionuclides could be expected to rise by more than 10^3 from the estimates shown in Figure 16. For many radionuclides, dose rates would have an approximate linear relationship with the number of failed containers. However, dose rates from some radionuclides would be smaller than that estimated from a linear relationship; for example, dose rates from ^{129}I, ^{36}Cl and ^{14}C would be attenuated because of their groundwater dilution limits, and dose rates from ^{99}Tc and isotopes of uranium, plutonium, thorium and neptunium would be attenuated because their low solubility limits would reduce release rates from the vault.

In Figure 16, the average dose curves appear as narrow peaks for radionuclides such as ^{90}Sr. In contrast, the curve for ^{129}I is broad: it is one of the first and last contributors to the total average dose. The rising and trailing edges of the curves for each radionuclide are controlled by different processes.

1. Release and transport control the rising edge. Radionuclides do not start contributing to dose rates to members of the critical group until they have traversed the engineered and natural barriers and enter the surface environment. In this case study we have assumed that all fabrication-defected containers fail at the time of vault closure; therefore all releases from the failed containers start at the same time. However, some radionuclides are more quickly liberated from the fuel bundles in the containers than others. In addition, different radionuclides have different chemical properties and are delayed to differing degrees by interactions with the successive barriers they must cross. The cumulative effect of these differences determines when dose rates from particular radionuclides start to appear. Releases from ^{129}I appear early because it is instantly released from used fuel when groundwater enters a failed container and because it interacts little with any of the engineered and natural barriers. The dose rate from ^{126}Sn is very small at early times; although it is also instantly released, tin is strongly delayed by sorption on the engineered and natural barriers.

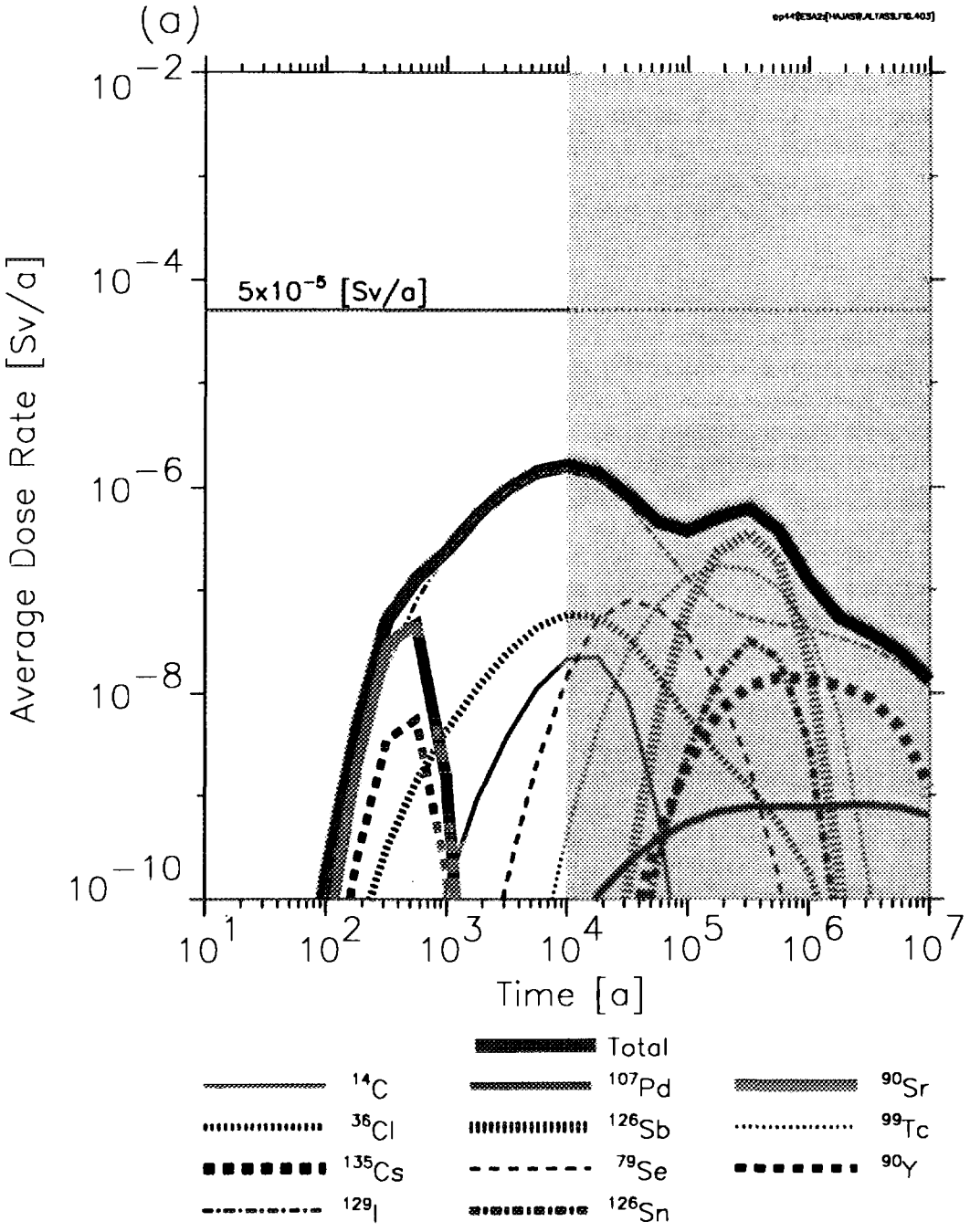

FIGURE 16: Contributions from Different Radionuclides to the Average Dose Rate to the Critical Group (Part a). Parts (a) and (b) of this figure show the average contributions from the fission products in Table 4 (using results from 14 000 simulations) and from the actinide decay chains in Table 5 (3500 simulations). The uppermost curve in both parts shows the total average dose rate (as in Figure 15), and it is the sum of the other curves (although the logarithmic vertical scale makes this assertion difficult to verify by eye). Some radionuclides from Tables 4 and 5 do not appear in the plots because their average dose rates are less that 10^{-10} Sv/a over the entire simulation time frame. Those not shown in part (a) are ^{14}C and ^{36}Cl from the Zircaloy matrix and ^{137}Cs, ^{93m}Nb and ^{93}Zr from the used fuel matrix. Those not shown in part (b) are ^{241}Am, ^{243}Am, ^{210}Bi, ^{239}Np, ^{239}Pu, ^{223}Ra, ^{226}Ra, ^{227}Th, ^{230}Th, ^{231}Th, ^{234}Th, ^{234}U, ^{235}U and ^{238}U. The shaded area on the right-hand side of the plots indicates the models and data are less acceptable representations of the disposal system at very long time frames.

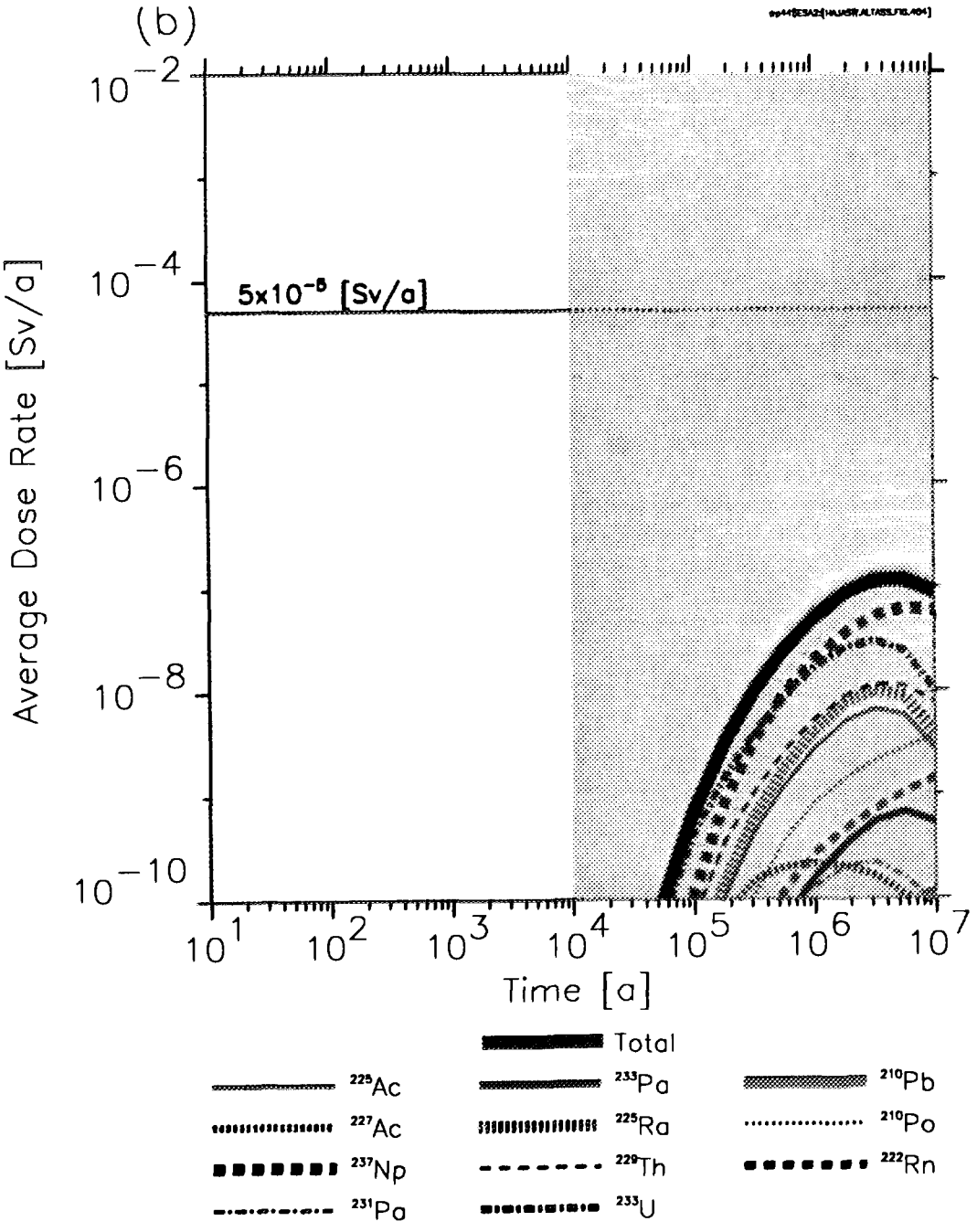

Figure 16 continued. (Part b)

2. Decay and flushing control the trailing edge. All of the dose curves eventually decrease because of radioactive decay or because the bulk of any released inventory has been transported out of (flushed from) the modelled system. Radionuclides such as ^{90}Sr, with a half-life of 29 a, do not persist long in the disposal system. After about 10^3 a, the inventory of ^{90}Sr would have decreased by more than 10 orders of magnitude from its initial inventory; thus its dose rate curve is very small at long times. In contrast, ^{129}I, which has a half-life of almost 16 million years, would lose an insignificant amount of its inventory by 10^3 a and less than half its inventory by 10^7 a. However, the dose rates from ^{129}I start to decline near 10^4 a because much of the released inventory of this mobile radionuclide has passed through the entire disposal system.

The curves in part (b) of Figure 16 show that dose rates attributed to all members of the actinide decay chains are insignificant before 10^4 a. These radionuclides are released slowly as the UO_2 matrix dissolves. In addition, the bulk of the inventory of each chain is found in isotopes of uranium (^{238}U, ^{235}U, ^{234}U and ^{233}U), neptunium (^{237}Np) and plutonium (^{239}Pu) (Table 5), and these elements sorb moderately to strongly on the buffer, the backfill and the rock surrounding the disposal vault and they would precipitate (in all or most of the randomly sampled simulations) in the container, so that their releases to the biosphere are small. Estimated dose rates from the actinide decay chains are small at all times and are associated with most members of the 4n+1 chain and with five radionuclides (^{210}Pa, ^{210}Pb, ^{222}Rn, ^{227}Ac and ^{231}Pa) near the ends of the 4n+2 and 4n+3 chains. In general, the engineered barriers and the permeable geosphere are very effective for members of the actinide decay chains, as well as for many other radionuclides such as ^{126}Sn.

Finally, we note that the Zircaloy matrix is an effective barrier because of its relatively slow rate of dissolution. Part (a) of Figure 16 shows dose rate curves for ^{14}C and ^{36}Cl from the used fuel. The corresponding curves for ^{14}C and ^{36}Cl from the Zircaloy matrix do not appear because their average dose rates are less than 10^{-10} Sv/a at all times. This difference in behaviour is caused only by the rates of release of ^{14}C and ^{36}Cl from UO_2 and Zircaloy; clearly the latter is a very effective barrier to radionuclide release.

6.2.2 Variability of Individual Simulations

The preceding discussion emphasized the average dose rate estimates from a large number of simulations. We examine here the variability from one simulation to another.

Table 6 shows the distribution of total dose rate from 3000 randomly sampled simulations at selected times. The maximum values (the highest observed dose rates) in the last column are not converged; they can vary considerably depending on how many simulations have been done (greater extremes are more likely to appear in larger sets of randomly sampled simulations). The intermediate values have largely converged and would not change much after performing many more simulations.

Figure 17 shows the same data, but with more intervening points to give smooth curves. These percentile bands each contain dose rates from 20% of the simulations; the bottom band corresponds to the 20% of the simulations that had the smallest total dose rate estimates, the next band corresponds to the next 20%, and so on. The upper envelope of the entire set of simulations is marked by the broken line (its position is dependent on sample size, because it represents extremes in behaviour.) The solid line crossing the bands is the total average dose rate curve from Figure 15.

TABLE 6

DISTRIBUTION OF TOTAL DOSE RATES[†] TO THE CRITICAL GROUP AT SELECTED TIMES

Time (a)	*Estimates of Dose Rate Percentiles [Sv/a]*					
	Minimum	20%	40%	60%	80%	Maximum
10	0	0	0	0	0	1.5×10^{-21}
100	0	2.6×10^{-30}	2.8×10^{-23}	1.2×10^{-18}	2.5×10^{-14}	2.4×10^{-7}
1000	0	1.8×10^{-11}	4.9×10^{-10}	1.6×10^{-8}	2.0×10^{-7}	2.2×10^{-5}
10 000	0	3.3×10^{-8}	1.4×10^{-7}	7.3×10^{-7}	2.3×10^{-6}	6.5×10^{-5}
100 000	0	5.5×10^{-9}	1.7×10^{-8}	6.4×10^{-8}	2.5×10^{-7}	4.1×10^{-5}
1 000 000	0	1.3×10^{-9}	6.3×10^{-9}	3.9×10^{-8}	1.4×10^{-7}	3.7×10^{-5}
10 000 000	0	4.2×10^{-10}	2.0×10^{-9}	9.7×10^{-9}	4.2×10^{-8}	3.1×10^{-5}

[†] The minimum and maximum columns give the smallest and largest observed dose rates from a set of 3000 randomly sampled simulations considering all radionuclides in Tables 4 and 5. The other columns give values of dose rate at the stated percentiles. For example, at 10 000 a, the 80th percentile of dose rate is 2.3×10^{-6} Sv/a; 80% of the estimated dose rates in the entire set of simulations are smaller than or equal to this value. The results are shown as-computed, although many values are too small to be physically meaningful. In addition, the results beyond about 10^4 a are shown only for completeness; the models are less acceptable representations of the disposal system at very long time frames.

Table 6 and Figure 17 illustrate a number of features about the randomly sampled simulations.

1. There is significant variation in the results. At any particular time, different simulations have dose rate estimates that could vary by several orders of magnitude. What the figure does not show is that an individual simulation could have a high dose rate estimate at early times and a low dose rate estimate at later times, or vice versa. One reason for carrying out a probabilistic analysis is because no single simulation, nor any small group of simulations, could capture the full range of behaviour that is displayed in a probabilistic analysis of the disposal system.

2. The results are highly skewed. Figure 17 uses a logarithmic scale for dose rate; if a linear scale were used, most of the bands would be indistinguishable from the horizontal axis. That is, the majority of simulations have very small or insignificant environmental impacts at any time, and only a few simulations would have impacts large enough to appear when using a linear scale. The average dose rate estimate is dominated by these latter simulations, and, therefore, it lies mostly in the uppermost band.

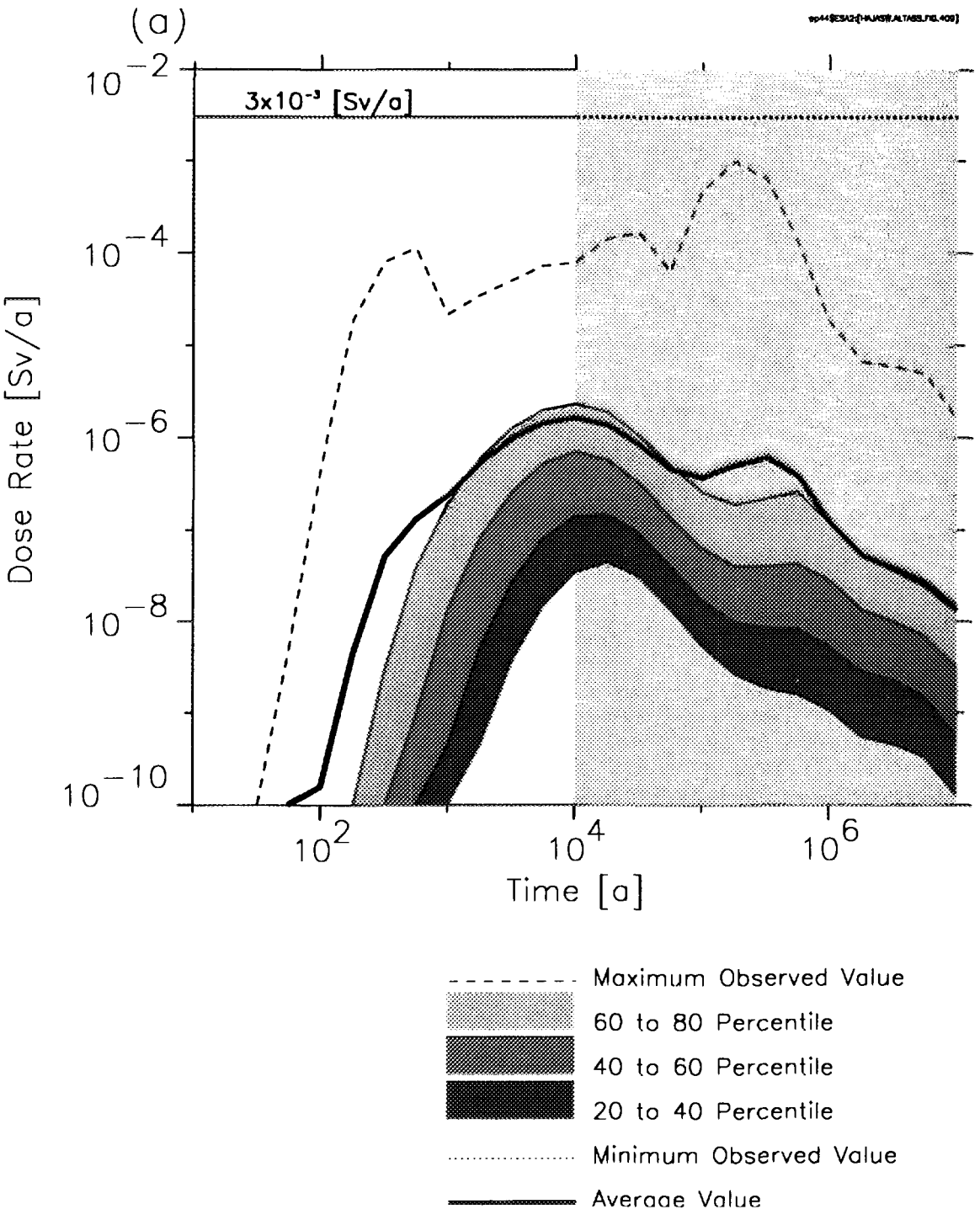

FIGURE 17: Percentile Bands for Dose Rate to the Critical Group (Part a). Parts (a) and (b) of this figure show separately results for the radionuclides in Tables 4 and 5. A set of randomly sampled simulations is partitioned into percentile bands, each containing 20% of the simulations at any point in time. (14 000 are used in part (a) and 3500 in part (b)). The lowest band shows the range of total dose rate for the simulations that have the lowest 20% of dose rate estimates, the next band shows the range for the next 20%, and so on. The solid curve shows the average dose rate. The dotted lines show the lower and upper envelopes of the smallest and largest estimated dose rates at any time for these simulations. The horizontal line at 3×10^{-3} Sv/a is representative of doses rates from natural background. The shaded area on the right-hand side of the plot indicates the models and data are less acceptable representations of the disposal system at very long time frames.

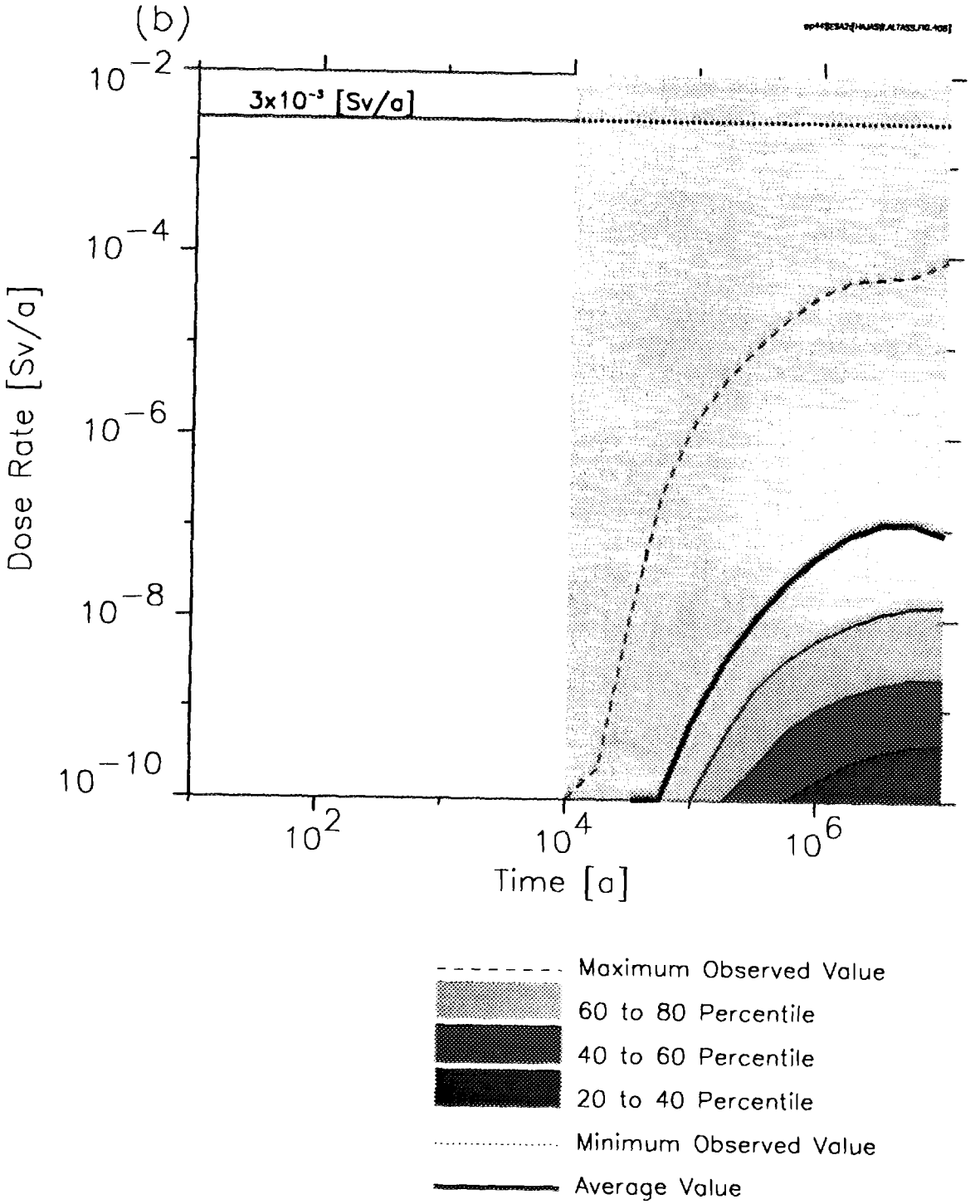

Figure 17 continued. (Part b)

3. The ^{90}Sr peak does not always occur. One of the striking features of Figure 16 is the existence of multiple peaks, including a peak from ^{90}Sr that exceeds the dose rate from ^{129}I near 500 a. However, ^{90}Sr is not a dominant contributor in all simulations. In fact, Figure 17 shows its dose rate is insignificant in at least 80% of the simulations because the shoulder near 500 a is evident only in the upper-envelope curve. Only a few simulations yield dose rates from ^{90}Sr that are large enough to affect the upper envelope of dose rates and the average dose rate curve, but not any of the lower bands.

Part (a) of Figure 18 helps to illustrate this last point. This plot is similar to Figure 17 but it shows dose rates for ^{90}Sr alone. The variability of ^{90}Sr dose rates from one simulation to another is much greater than the variability of total dose rate. In some simulations the engineered and natural barriers are better than in others, and the barriers act to delay the arrival of ^{90}Sr into the surface environment. Delays of a few hundred to a thousand years would provide enough time to allow for substantial decay of ^{90}Sr. The figure suggests that there are only a few simulations in which the combined effect of the barriers is insufficient to prevent appreciable releases of ^{90}Sr to the biosphere, because only the upper-envelope curve is large enough to appear in the plot.

The variability of dose rates for some other radionuclides is also much greater (on a logarithmic scale) than the variability of total dose, which is dominated by dose rates from ^{129}I. Parts (b) and (c) of Figure 18 show the large variability of dose rates from ^{79}Se and ^{99}Tc. Both ^{79}Se and ^{99}Tc occasionally make significant contributions to the total dose rate curve. Part (d) of Figure 18 shows the variability of ^{126}Sn dose rates. Tin-126 and its progeny, ^{126}Sb, contribute to the third peak in the average dose rate curve of Figure 16. Figure 18 (e) and (f) show the variability of ^{129}I and ^{36}Cl dose rates, the two most important contributors to the total dose rate at 10^4 a.

6.2.3 Dose Rate to Nonhuman Biota

Our assessment indicates that there would be no significant radiological effects on nonhuman biota for the hypothetical disposal system evaluated in this document. We base this conclusion on the curves in Figure 19, which shows the average dose rates to four target organisms: a generic plant, mammal, fish and bird.

We have defined the characteristics of these target organisms to be representative of a wide range of organisms found on the Canadian Shield, and we assume they live in, and obtain all their needs from, the vicinity of the discharge zones. These organisms would be exposed to dose rates from natural background, which typically range from 10^{-3} to 10^{-1} Gy/a (Goodwin et al. 1994a). We assume that there would be no significant radiological impacts at the lower limit of natural background dose rates. Figure 19 shows that the average estimated dose rate curves for the four target organisms are well below this lower limit at all simulation times.

The differences in estimated dose rates to the four target organisms are attributed mainly to the ways in which they interact with their environment.

- We assume that the generic plant grows in the vegetable garden, which is located (after the peat bog) on the most contaminated terrestrial discharge zone. Figure 20a shows that the dose rate to the plant is dominated by ^{36}Cl for times up to 10^4 a and beyond. Our analysis shows that the plant is mostly affected by two exposure pathways: external dose rates from ^{36}Cl in soil and internal dose rates from ^{36}Cl taken up by the plant roots and/or deposited on the plant leaves. Iodine-129 has a similar effect, although dose rates are much smaller.

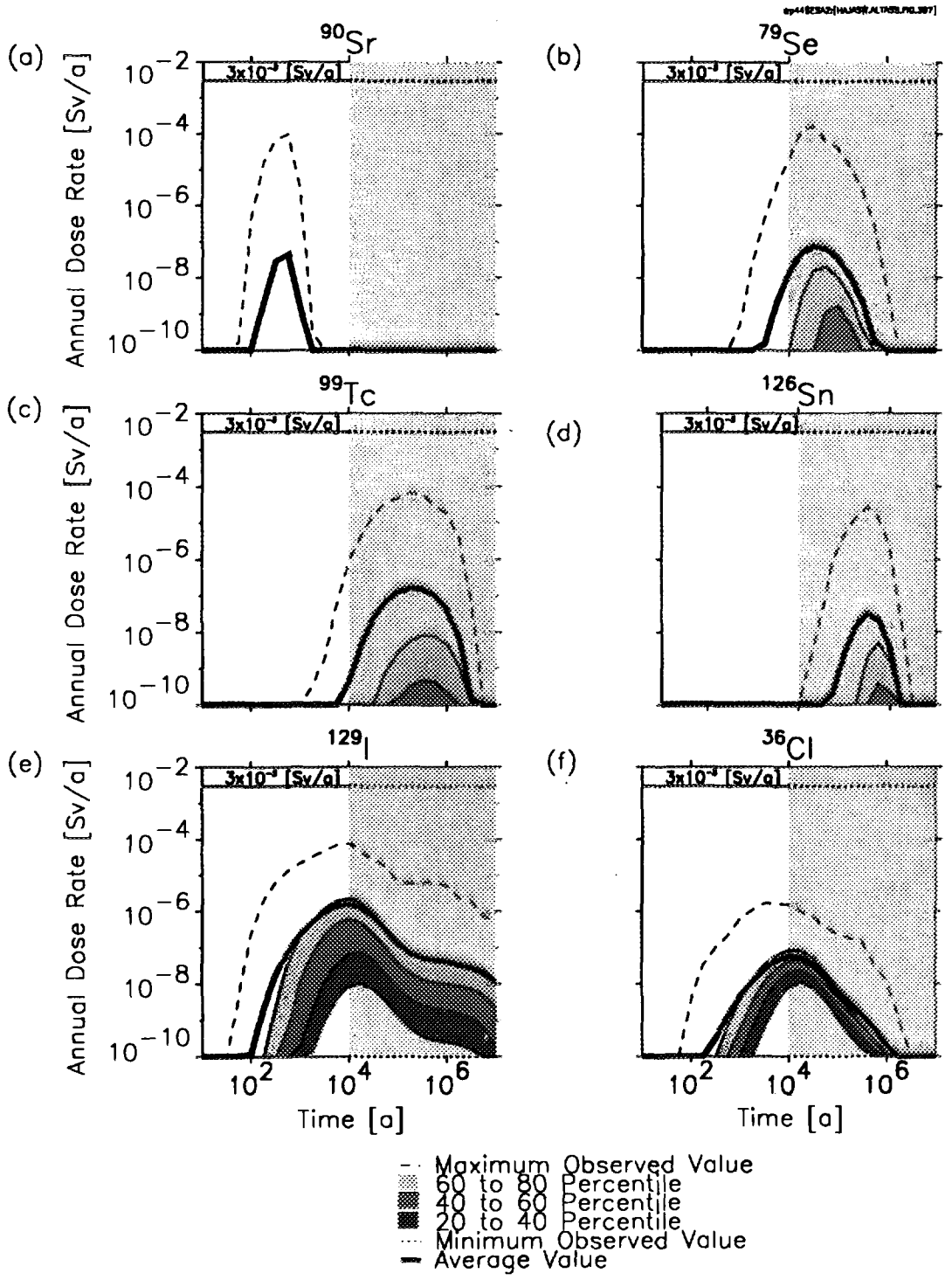

FIGURE 18: Percentile Bands for Dose Rate to the Critical Group from Selected Radionuclides. These plots are similar to Figure 17, except each shows the variability in dose rate estimates from a specific radionuclide. Parts (a) to (f) shows results for ^{90}Sr, ^{79}Se, ^{99}Tc, ^{126}Sn, ^{129}I and ^{36}Cl, respectively. The shaded area on the right-hand side of the plots indicates the models and data are less acceptable representations of the disposal system at very long time frames.

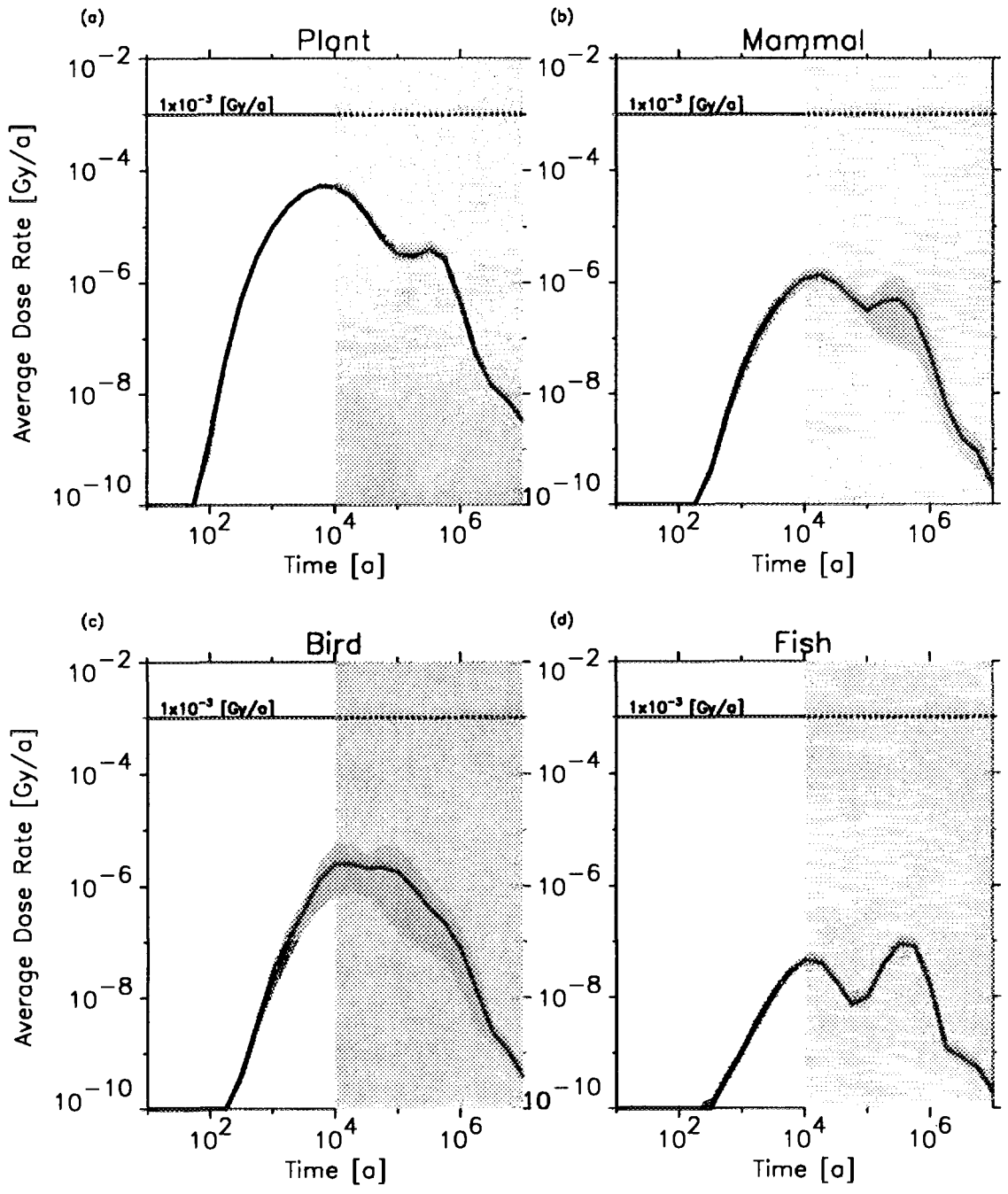

FIGURE 19: Average Dose Rate to the Nonhuman Biota. Parts (a) to (d) show the total average dose rate to a generic plant, mammal, bird and fish respectively. The average is taken from 3500 randomly sampled simulations and sums the contributions from the fission products in Table 4 (dose rates from the actinide decay chains in Table 5 are insignificant for times up to 10^4 a). The bands around each average show a 90% confidence interval for the true location of the mean dose rate. The horizontal line, at 3 x 10^{-3} Gy/a, is the dose rate associated with the lower range of dose rates to these biota from natural background. The shaded areas on the right-hand side of the plots indicate the models and data are less acceptable representations of the disposal system at very long time frames.

- We assume that the generic mammal and the generic bird obtain their food from the forage field, and the analysis described in the Appendix indicates concentrations of contaminants in the forage field can be similar to those in the garden. Chlorine has a large plant/soil concentration ratio (Zach et al. 1996, Johnson et al. 1995) and thus ^{36}Cl is taken up by plant roots, and the major exposure pathway to the mammal and the bird are from ingestion of plants. Thus ^{36}Cl dominates the dose rates to 10^4 a to the mammal and the bird (Figure 20b and 20c). Carbon-14 is also an important contributor for times up to 10^4 a for the generic mammal, and to a lesser extent for the bird, through pathways involving ingestion of drinking water and inhalation of contaminated air. Internal dose conversion factors for ^{14}C are relatively large for generic organisms (Amiro 1992b, 1995), typically about 3 orders of magnitude larger than for humans. Thus dose rates from ^{14}C are expected to be larger for nonhuman biota than for humans.

- We assume that the fish inhabit the lake. Radionuclide concentrations in lake water are generally orders of magnitude smaller than concentrations in contaminated discharge groundwater and thus the dose rates to the generic fish are somewhat smaller than to the generic mammal and bird. Figure 20d indicates that ^{129}I and ^{14}C are the two major contributors to estimated dose rate to the generic fish. At early times, ^{129}I generally has the largest concentration of all contaminants in the biosphere, including the lake and lake sediment, and dose rates to the fish from ^{129}I mainly involve external exposure to lake sediment. Dose rates to the fish from ^{14}C involve internal dose from water and external dose from the lake sediment.

6.3 RESULTS OF THE PROBABILISTIC SENSITIVITY ANALYSIS

In this assessment, we include uncertainty in the parameters of the system model through the use of probability distributions. The probability distribution specified for a parameter defines its feasible values and the likelihood of the values based on current understanding. In every simulation, we randomly sample a value for each parameter for use by the system model to calculate an impact such as dose rate to a member of the critical group. In general, the estimated impact will differ substantially from simulation to simulation because of the variability in parameter values. We investigate here the sensitivity of changes in calculated impacts to variations in the feasible values of individual parameters. We also discuss the implications of these parameter sensitivities.

The main impact of interest in this study is the total dose rate to a member of the critical group. We analyze the logarithm of total dose rate, rather than the total dose rate itself, because at each simulation time the values observed in different simulations vary by several orders of magnitude. Logarithmic transformations are commonly used in the sensitivity analysis of multiplicative models such as that used herein. An analysis of the total dose rate would directly reflect only the variability in the very largest dose rates observed (other values being near zero by comparison), whereas an analysis of the logarithm better reflects the full variability of the data.

Because the causes of these variations can differ from one time to another, the sensitivity analysis is carried out at different simulation times. Table 7 identifies the most influential parameters at 560 a, 10^4 a and 10^5 a. The first two of these times correspond to the time of the shoulder and the time of the maximum in the curve of average dose rate versus time (Figure 15). The third time is included because it was the time of concern for most of the sensitivity analysis in the EIS case study (Goodwin et al. 1994a).

There are more than 5000 parameters in the system model. A standard analysis of variance shows that just the 10 parameters listed at 560 a in Table 7 explain more than 60% of the variability in the logarithm

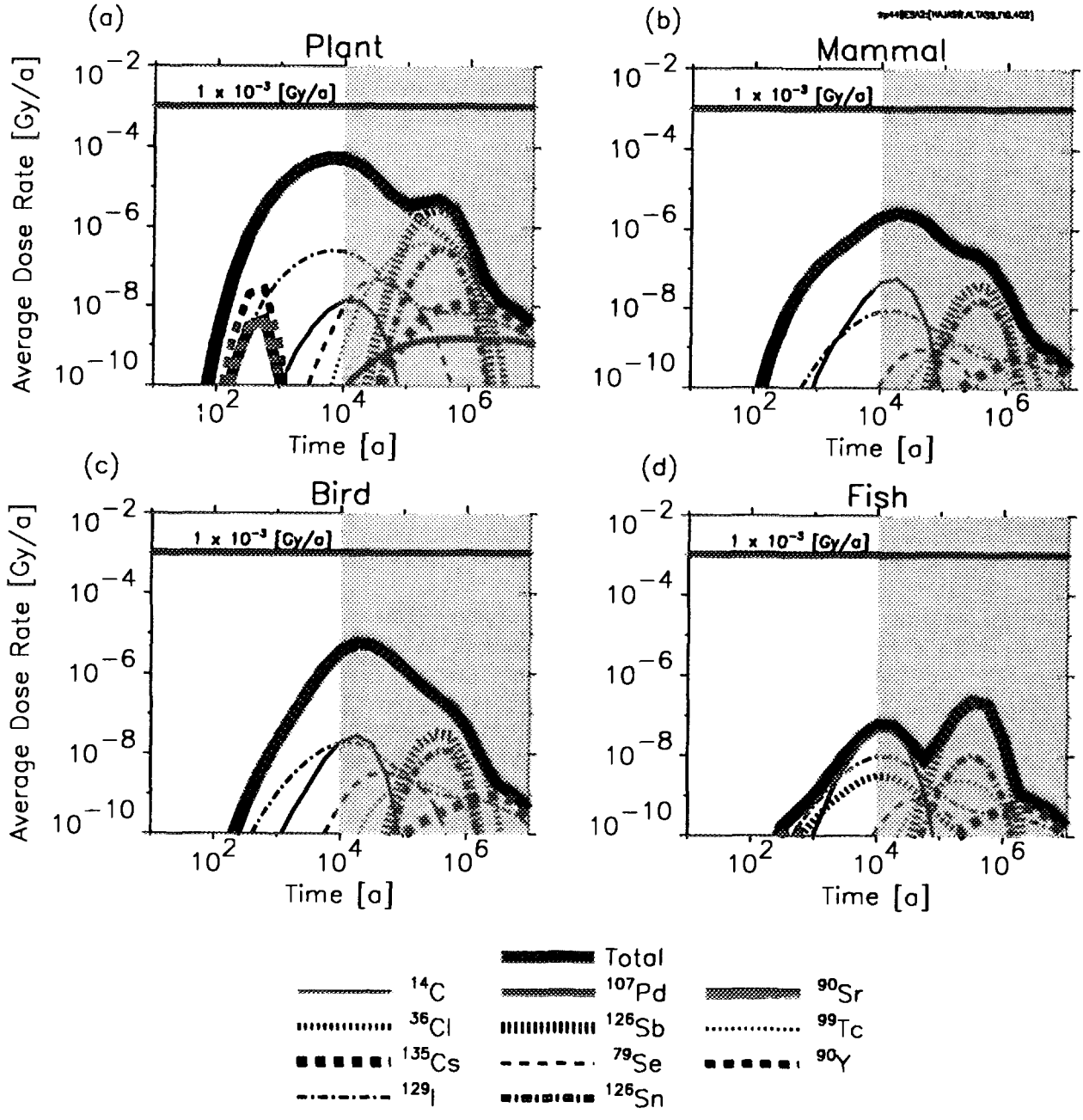

Figure 20: Contributions from Different Radionuclides to the Average Dose Rate to Nonhuman biota. Results are shown for the fission products in Table 4; dose rates from the actinide decay chains are insignificant for times up to 10^4 a. Parts (a) to (d) show dose rates to a generic plant, mammal, fish and bird, respectively. The curves shown are the total average dose rates and the contributions to the total from different radionuclides. Some radionuclides listed in Table 4 do not appear in the plot because their average dose rates are less that 10^{-10} Gy/a over the entire simulation time frame. The shaded area on the right-hand side of the plots indicates the models and data are less acceptable representations of the disposal system at very long time frames.

of total dose rate at 560 a. Similarly, at 10^4 a and at 10^5 a, the listed parameters explain more than 50% of the variability in the logarithm of total dose rate. That is, we have identified parameters that account for most of the variability in the total dose at the three times. The results in Table 7 were determined from analysis of a set of 1920 simulations, randomly selected according to a fractional factorial latin hypercube design.

Table 7 lists values for the *linear effect* of each influential parameter on the total dose rate. In this analysis the linear effect is the average change in the logarithm of total dose rate when the value of a parameter is raised from the bottom one-third of its domain to the top one-third. The *quadratic effect* was also estimated but is not reported in the table since it is small or insignificant for most parameters. The quadratic effect is the difference between the total dose rate in the middle of a parameter's range versus the average of the two extremes: it measures the departure from linearity. We discuss nonlinear effects in the text where they are significant. The table does not show interaction effects among parameters since they have not yet been fully analyzed. An interaction effect indicates if the value for one parameter affects the influence of another on total dose rate.

The three sections of Table 7 have 4 parameters in common.

1. The most influential parameter in all three cases is a switch parameter (PRODMD) that determines in a simulation whether members of the critical group obtain their domestic water from the lake or a well. Variation of this parameter alone accounts for more than one-third of the variation in total dose rates at all three times. A lake is selected if the sampled value of PRODMD is 1, and a well if the sampled value is 2. The linear effect is positive, showing that larger dose rates are generally (but not necessarily always) obtained if a well is selected. Figure 21 shows this effect in a variability partitioning plot. Lake water generally has smaller concentrations of contaminants than well water, because of dilution by the relatively large surface water flows through the lake and because contaminant releases to the lake (but not the well) are delayed by transport through the lake sediment, overburden (except for overburden wells) and part of the bedrock. The linear effects at 10^4 and 10^5 a indicate that these dilution and delay processes can reduce dose rates by between one and two orders of magnitude. At 560 a the effect is much more dramatic. Average dose rates from ^{129}I and ^{90}Sr are rising rapidly at 560 a, and any additional delays in transport (such as transport through the overburden) can reduce dose rates at that time by several orders of magnitude.

2. The iodine aquatic mass-loading coefficient (IMLA) describes the transfer of iodine from surface water into the surrounding atmosphere. Once in the atmosphere, ^{129}I can affect the critical group directly through inhalation, or indirectly through ingestion of plants that are contaminated by deposition. This parameter has a positive linear effect, shown in Figure 21, indicating that greater releases of ^{129}I from the lake to the atmosphere generally cause higher dose rates. It is also consistent with results that show ^{129}I is a major contributor to the average dose rate at all three times, and that ingestion of plants is an important pathway for this radionuclide. The effect of this parameter is nonlinear; variations within the low to moderate range have little impact, but total dose rate is quite sensitive to large values of IMLA. The strong influence of this parameter is perhaps surprising until we examine its probability distribution; this parameter has an unusually broad distribution and very large values are feasible. We conclude, therefore, that uncertainty in the amount of iodine that could escape into the atmosphere is an important factor affecting the uncertainty in total estimated dose rates.

TABLE 7

INFLUENTIAL PARAMETERS AFFECTING DOSE RATE AT THREE DIFFERENT TIMES

Time [a]	*Parameter*[†]	*Description*	*Linear Effect [orders of magnitude]*
560	PRODMD	Source of domestic water used by the critical group (lake or well)	3.8
	SGPROS(LWROC)	Effective transport porosity of the lower rock zone	-2.6
	SGPROS(MIROC)	Effective transport porosity of the middle rock zone	-1.4
	THIKOV(BCSAQ)	Thickness of the overburden at Boggy Creek south (aquatic discharge zone)	-1.4
	IFRACT	Probability of fabrication defects	1.0
	DZPERA	Axial permeability of the excavation damaged zone	0.8
	SGPROS(FZONE)	Effective transport porosity of fracture zones	-0.8
	IMLA	Iodine aquatic mass-loading coefficient	0.7
	IFAILQ(23)	Binomial probability variate for the number of container failures within a sector (sector 23)	0.7
	DPTHWL	Depth of the well	0.7
10^4	PRODMD	Source of domestic water used by the critical group (lake or well)	1.3
	IMLA	Iodine aquatic mass-loading coefficient	0.5
	XCRTIO(I)	Plant/soil concentration factor for iodine	0.4
	IFRACT	Probability of fabrication defects	0.3
	XCRTIO(Cl)	Plant/soil concentration factor for chlorine	0.2
	DPTHWL	Depth of the well	0.2
	NUMMAN	Number of people in the critical group	-0.2
10^5	PRODMD	Source of domestic water used by the critical group (lake or well)	1.1
	IFRACT	Probability of fabrication defects	0.4
	IMLA	Iodine aquatic mass-loading coefficient	0.4
	XCRTIO(I)	Plant/soil concentration factor for iodine	0.4
	STDNOG	Variability in the magnitude of UO_2 corrosion from γ-radiation	0.2
	DPTHWL	Depth of the well	0.2

[†] The name for each parameter (as used in PR4) is listed here to provide an unambiguous cross-reference to the text.

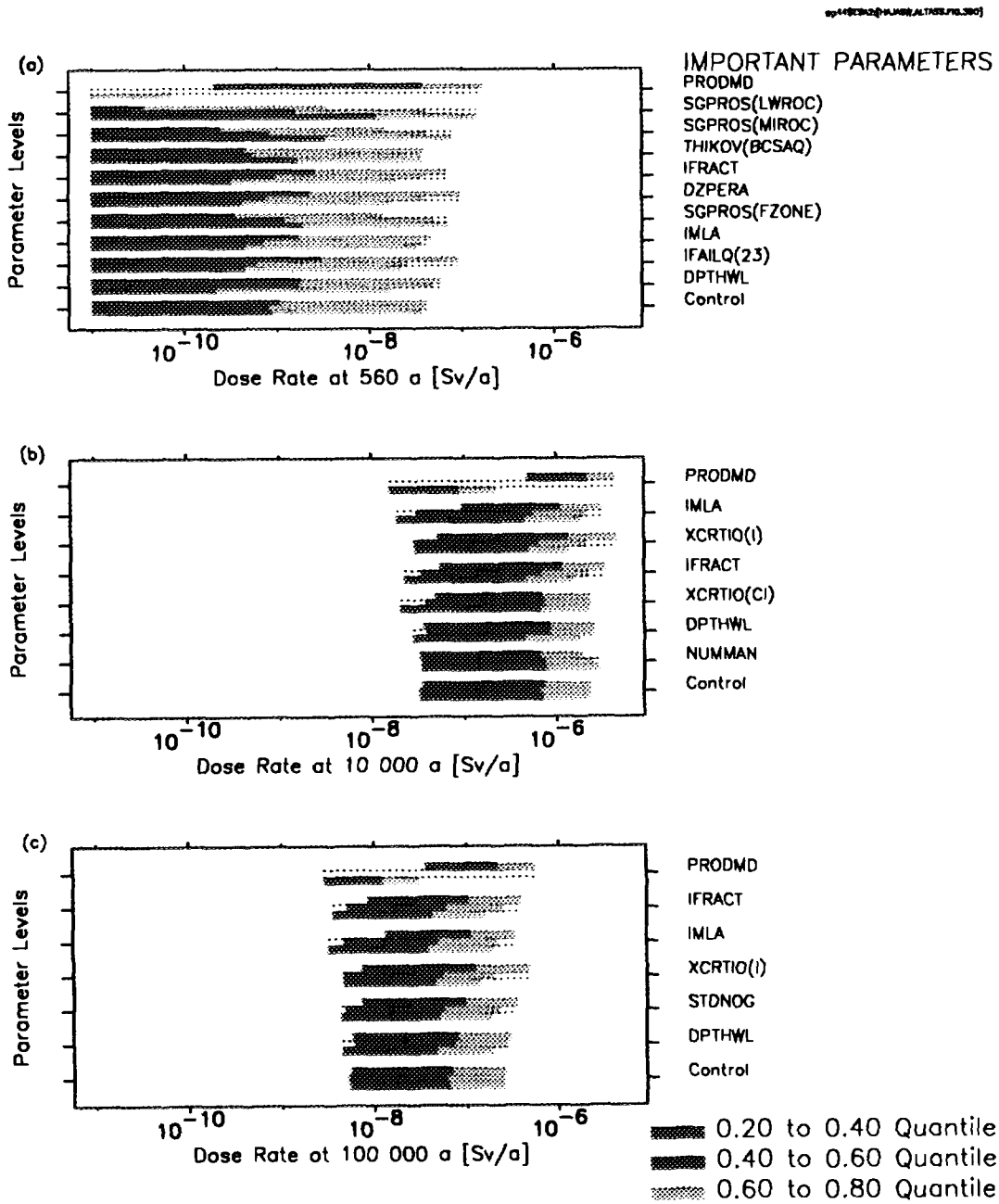

FIGURE 21: Variability Partitioning Plot for Dose Rate and the Most Influential Parameters at Three Points in Time. Parts (a) to (c) show the effect of the most influential parameters in Table 7 on the estimated dose rate at 560 a, at 10^4 a and at 10^5 a respectively, using results from 14 000 randomly sampled simulations (for the radionuclides in Table 4). The horizontal axis shows the dose rate on a logarithmic scale, and the horizontal bars represent the variability in the estimates of dose rate from different simulations. Three horizontal bars are shown for most parameters. The bottom bar corresponds to the lower 1/3 quantile of values of a parameter, and the middle and upper bars correspond to the middle and upper 1/3 quantiles. Only two bars are shown for "source of domestic water" because this switch parameter has only two possible values: the lower bar corresponds to use of a lake and the upper to use of the well. The quantiles of estimated dose are plotted within each bar.

The bottom most plot, labelled "Control", shows the pattern for a parameter that has no influence: given a large number of simulations, the quantiles in the three horizontal bars of the control plot should stack vertically. The other parameters generally show strong trends. For example, the bars for "source of domestic water" clearly indicates dose rates are larger when the well is the source of domestic water. Some parameters show evidence of a quadratic effect.

3. The probability of fabrication defects (IFRACT) specifies the probability that any container in the vault would fail because of fabrication defects. The total number of failures in the entire vault is proportional to the value sampled for this parameter, and it displays the expected positive linear effect: a larger number of failed containers leads to a higher release of all radionuclides and generally to larger estimated dose rates (Figure 21). The exact number of failures within a vault sector also depends on the value of the sector-dependent binomial probability variate (a parameter called IFAILQ(j), where j is the number of the sector). The number of container failures within a sector is discussed further below.

4. Depth of the well (DPTHWL). Wells that are deep enough to reach the bedrock provide a fast contaminant transport pathway through parts of the geosphere, eliminating the overburden and lake sediment and part of the underlying bedrock. At 560 a, deeper wells would be particularly important for short-lived ^{90}Sr and would shorten the time of arrival of doses rates from ^{129}I. As a result, the influence of the well depth is greatest at early times. There is also another effect that occurs at all times. If a well is not deep enough to reach the bedrock, we assume it provides water diluted to the same degree as lake water. The net result is a positive linear effect, meaning that deeper wells generally result in larger dose rates (Figure 21). This parameter has a nonlinear behaviour; the dose rate rises significantly when the well is deep enough to reach bedrock. Its influence is clearly dependent on whether or not a simulation involves the use by the critical group of a water-supply well.

At 560 a, the influential parameters (apart from those already mentioned) pertain to the effectiveness of the different barriers that could delay releases of ^{90}Sr and/or ^{129}I. Delays significantly reduce the dose rate because the curve of average dose rate is rising steeply at this early time (Figure 15). In addition, any barrier that slows down ^{90}Sr by even a few tens of years results in attenuated dose rates because of the decay of this short-lived radionuclide. The most influential parameters at 560 a include the following.

- The effective transport porosities of the lower rock zone, SGPROS(LWROC), the middle rock zone, SGPROS(MIROC), and the fracture zones (including fracture zone LD1), SGPROS(FZONE). In the model representing the geosphere, relatively small porosities correspond to relatively large groundwater velocities which more quickly transport contaminants from the vault to the surface. Hence the linear effects are negative: larger porosities generally lead to smaller estimated dose rates at 560 a (Figure 21a). All these porosities have nonlinear effects, most noticeable for the porosity of the lower rock zone. Low and moderate porosities cause groundwater velocities to be rapid enough to cause some early dose rates at 560 a. High porosities, on the other hand, slow the groundwater velocities so much as to reduce dose rates significantly.

- Thickness of the overburden at the Boggy Creek aquatic discharge zone (THIKOV(BCSAQ)). Thicker layers of overburden result in longer delays in contaminant transport. The influence of this parameter is somewhat reduced because it largely affects dose rate only for simulations in which the critical group obtains their water from a lake or from shallow overburden wells. The linear effect is negative, meaning that small values generally lead to larger estimated dose rates (Figure 21a).

- The axial permeability of the excavation damaged zone (DZPERA). This parameter affects groundwater velocities along the periphery of the vault rooms. Larger velocities tend to draw contaminants from the backfill and buffer by establishing a low-concentration

boundary condition. Thus concentration gradients are larger, enhancing diffusive transport out of the backfill and buffer and enhancing releases into the surrounding rock. The linear effect is positive, meaning that larger values generally result in larger estimated dose rates (Figure 21a). The influence is nonlinear; this parameter must take a relatively large value before it has a significant influence.

- The binomial probability variate for container failures within a sector (sector 23), IFAILQ(23). The vault model uses a binomial distribution to calculate, for each vault sector, the number of containers that have failed because of fabrication defects. This calculation depends on the probability of fabrication defects (IFRACT), the number of containers in a vault sector and a sector-dependent binomial probability variate (LeNeveu 1994). Our analysis indicates that this latter parameter for vault sector 23 is influential at 560 a. It has a positive linear effect since larger values correspond to higher numbers of failed containers (Figure 21a). Typically it must lie in the upper third of its range before any container failures at all occur, and so it has a nonlinear effect. We attribute the importance of this parameter to radionuclide transport times. Sector 23 has the shortest groundwater transit time from the vault to the well and, therefore, the shortest radionuclide transport time. Radionuclides travelling from another sector will take longer to reach the well and will result in lower doses at 560 a. The average dose rate at 560 a is dominated by ^{90}Sr, and as noted earlier, any factors that delay the transport of this radionuclide will have large effects on dose rate at early times.

In summary, the influential parameters at 560 a are those that could reduce the effectiveness of the many barriers, permitting earlier releases of radionuclides into the environment. By 10^4 a, these parameters have lost their influence because there has been sufficient time to permit substantial releases of the mobile radionuclides that are also the major contributors to dose rate, notably ^{129}I and ^{36}Cl. Thus the variable characteristics of the engineered and natural barriers are relatively unimportant in explaining variations in dose rates from one simulation to another at 10^4 a. Parameters that become influential at that time are those that introduce variability in impacts that occur once radionuclides reach the surface environment. We have already seen three parameters in this category, namely the source of domestic water (lake or well), the iodine aquatic mass-loading coefficient and the depth of the well. At 10^4 a, three others appear (Table 7).

- The plant/soil concentration factors for iodine, XCRTIO(I), and for chlorine, XCRTIO(Cl). These parameters describe the transfer of iodine and chlorine from soil to plants, and these plants can affect the critical group by several ingestion pathways. It is reasonable that iodine characteristics are influential, since ^{129}I is by far the largest contributor to mean dose rate at 10^4 a (Figure 15). Similarly chlorine characteristics have an effect because ^{36}Cl is the second largest contributor to mean dose rate at 10^4 a. Our analysis indicates that ^{36}Cl has a higher dose rate contribution than ^{129}I in about 30% of the randomly sampled simulations. The two plant/soil concentration factors have a positive linear effect: larger values lead to higher concentrations in plants and generally to larger estimated dose rates (Figure 21b).

- Number of people in the critical group (NUMMAN). This parameter describes the size of the critical group, with feasible values ranging from 1 to 36 people (Davis et al. 1993). This parameter affects dose rates in many ways. For example, the size of the critical group affects the volume of water they withdraw (from the lake or a well), the size of their garden, the number of domestic animals they raise and the amounts of peat or wood they use for heating. Some associations are complex. For example, two competing processes affect the degree of contamination of well water: larger volumes of well water tend to

capture more contaminants but they also tend to capture more uncontaminated ground water. Our analysis indicates the linear effect is negative and thus smaller critical groups are generally associated with larger mean dose rates to an individual in the group (Figure 21b). A similar result was reported in the EIS case study (Goodwin et al. 1994b). This parameter also has a nonlinear effect: the average dose rate remains about the same until the size of the critical group gets quite large. When the size is sufficiently large, the well cannot supply the demand and we assume that the critical group obtains supplementary water from the lake, resulting in lower dose rates.

Near 10^4 a, there is a broad dose rate peak that lasts for tens of thousands of years, with the major contributors being ^{129}I and ^{36}Cl (Figure 16a). Thus the effects at 10^4 a of the influential parameters can be expected to hold for longer periods of time. By 10^5 a, however, the contributions from ^{129}I and ^{36}Cl are starting to abate, and other radionuclides, such as ^{99}Tc and ^{126}Sb and its precursor, ^{126}Sn, are becoming as important. Even so, the influential parameters at 10^5 a are not much different from those at 10^4 a. The source of domestic water (lake or well), the iodine aquatic mass-loading coefficient, and the container failure fraction have largely the same effects, and for the same reasons, at 10^5 a as they have at 560 a and at 10^4 a. The plant/soil concentration factor for iodine and the depth of the well behave much as they did at 10^4 a. The plant/soil concentration factor for chlorine is no longer important because ^{36}Cl has undergone substantial decay and has largely been flushed out of the disposal system.

At 10^5 a, one additional influential parameter appears: the variability in the magnitude of UO_2 corrosion from γ-radiation fields (STDNOG). The rate of dissolution of the UO_2 matrix in failed containers is affected by radiolysis and STDNOG describes the uncertainty in the magnitude of the UO_2 corrosion rate caused from radiolysis of water by γ-radiation. Large values correspond to more radiolysis, more dissolution of the fuel matrix and greater radionuclide releases by the congruent-release mechanism. Although this parameter affects the release of all radionuclides to some degree, it is particularly important at 10^5 a in slowing the decline of ^{129}I and ^{36}Cl dose rates. Peak dose rates from these radionuclides are mostly associated with the fraction of their inventories that are released by the instant-release mechanism. These releases start at the time of closure of the disposal vault (the assumed time of failure of all fabrication-defected containers) and between 10^4 a and 10^5 a the bulk of the instant-release inventories will have been flushed out of the modelled disposal system. Congruent releases from the dissolution of the UO_2 matrix occur over longer time frames, slowly adding to the inventories of ^{129}I and ^{36}Cl that are moving out of the failed containers. Thus the tails of the dose rate curves for these radionuclides depend on their congruent release from the UO_2 matrix, and the net linear effect is weak but positive (Figure 21c).

6.4 RESULTS FROM SELECTED SUB-SCENARIOS

6.4.1 Introduction

Throughout this document, we assess the groundwater transport scenario. As shown in the discussion below, it can be regarded as a collection of many sub-scenarios that have different features. We describe here results from sets of simulations that are associated with selected features of the disposal system.

It is important, however, to put these results into context. A main objective of our analysis is to compute the radiological risk to the critical group for comparison with the AECB risk criterion. We follow a probabilistic systems assessment approach to quantify the effects of parameter uncertainty. One of many sources of uncertainty pertains to the future behaviour of the critical group. For example, we expect that the critical group that inhabits the disposal site at some time in the future would obtain their domestic water from a well and from the nearby lake, possibly using one or the other or both at different time

periods over the next 10^4 a. To deal with this uncertainty, we analyze two extremes, and assume that either the well or the lake is used in any particular simulation.

- We choose between these two mutually exclusive extremes with a "switch" parameter (Goodwin et al. 1994a) called PRODMD in PR4. PRODMD describes the source of domestic water used by the critical group and has two possible values: 2 means a well will be used and 1 means a lake will be used.

A large set of randomly sampled simulations will contain subsets that correspond to cases where only the well or only the lake serves as the source of domestic water. The sizes of these subsets are determined by the corresponding probability function for PRODMD.

- Based on the current use of water-supply wells on the Canadian Shield (Davis et al. 1993), the critical group would obtain their domestic water from a water-supply well with a probability of 0.5, and from the lake with an equal probability. The probability function for PRODMD is such that its two possible values have an equal chance of occurrence in any randomly sampled simulation. Thus in 1000 randomly sampled simulations, the water-supply well will be selected in (about) 500 simulations, and a lake in the other 500 simulations. (If the probability of use of a well was 0.2, then a water-supply well would be selected in only about 200 simulations, and a lake in the other 800.)

Any set of randomly sampled simulations will contain a mix of simulations as prescribed by the proability function for PRODMD. These simulations will then yield an unbiased average dose rate that reflects the uncertainty in source of domestic water used by the critical group, and this average dose rate can be used to compute the radiological risk.

Of course, we could also perform separate analyses for the two sub-scenarios, each representing one source of domestic water. We would then obtain two estimates of average dose rate, which would be combined in the calculation of radiological risk, using a probability of occurrence of 0.5 for both sub-scenarios. Thus the computed risk would be unchanged.
We have chosen to analyze the more comprehensive "groundwater transport" scenario because this approach has two advantages.

1. There are many possible options that can be described using switch parameters. For example, we use switch parameters to describe whether the critical group has clay, loam, organic or sandy soil types in their garden, whether they use lake sediment as soil, whether they practice irrigation (and whether the water is from the well or the lake), whether they use wood or peat for heating, and whether the group consists of a single person or up to 36 people. Moreover, we can regard almost all uncertain parameters (i.e., those characterized by a probability distribution) as parameters that describe different options or conditions (Goodwin et al. 1994a). For example, the porosity of the lower rock zone (called SGPROS(LWROC) in PR4) ranges from 10^{-5} to 10^{-3}: the smaller values are consistent with a rock having a small occurrence of microfractures and the larger values with a rock having as many as 100 times more microfractures.

   If each possibility were analyzed as a distinct scenario, the number of scenarios would be unmanageable and the computation of risk unnecessarily complex. For example, if there were only 10 different switches or options, there would be 2^{10} or more than 1000 scenarios to be analyzed.

2. Our probabilistic sensitivity analysis treats switch parameters like any other parameter, and we can readily determine if a parameter like PRODMD is influential. Likewise, we can readily determine the influence of large and small porosities of the lower rock zone. (In fact, both PRODMD and SGPROS(LWROC) are identified as influential parameters in Section 6.3). Thus our approach provides a systematic method to examine the influence on average dose rate of different potential sub-scenarios.

From a large set of randomly sampled simulations, we can extract those simulations that have a common feature, such as a value of PRODMD that corresponds to the use of a well. These simulations represent variations contained within the groundwater transport scenario, and can be regarded as sub-scenarios. If enough simulations satisfy the selection criterion, we can analyze them separately, and calculate average dose rate, display the effects of important and influential parameters, and so forth.

Moreover, we can also estimate the probability of occurrence of these sub-scenarios from the fraction of simulations that satisfy the criterion. For example, we would expect the use of a well for domestic water is 0.5. In fact, this is an *a priori* estimate because a well might be sampled in a simulation but subsequently rejected if the capacity of the well is insufficient to meet the demand (see Section 5.3). Our results indicate that the probability of use of a well for domestic water is actually 0.5, because the relatively modest demands for domestic water can always be met. However, this is not the case for irrigation of the garden using well water; the *a priori* probability is 0.45, equal to the probability that the critical group irrigates their garden (0.9) times the probability that they use the well (0.5). We estimate that the actual probability is about 0.41, based on 14 000 randomly sampled simulations. The actual probability is smaller because the well cannot always meet the larger demand for irrigation water, which varies from one simulation to the next depending on parameters such as the size of the garden, the type of soil and the annual meteoric precipitation.

The following section discusses examples of sub-scenarios, showing estimated dose rates versus time. However, the individual curves shown for mutually exclusive sub-scenarios should not be added together to estimate the overall average dose rate; instead the curves should be averaged. In addition, curves shown for different sub-scenarios cannot be combined because they are computed from the same set of simulations.

6.4.2 Sample Results

The following results are calculated from a set of 14 000 randomly sampled simulations. The simulations involve only the fission products and impurity activation products listed in Table 4. No significant effects are expected at times before 10^4 a from the members of the actinide decay chains in Table 5.

Figure 22 shows average dose rate curves from simulations in which the critical group obtains their domestic water from the lake or from a well. It is clear that average dose rates are larger when the critical group uses the well, about 8 times larger at 10^4 a. (This factor of 8 pertains to a ratio of arithmetic means. Table 7 gives a value for PRODMD at 10^4 a that is equal to 1.3 orders of magnitude, or a factor of about 20, for the ratio of geometric means.) Other, more subtle observations can be made. For example, the curve for the well appears at earlier times and has a shoulder near 500 a, consistent with faster transport of contaminants through a well. The shoulder near 500 a is from ^{90}Sr, and dose rates from this radionuclide are much smaller for the lake sub-scenario because of additional delays in transport through overburden, lake sediment and (for bedrock wells) part of the bedrock.

Figure 23 shows average dose rate curves from simulations in which the critical group irrigates their garden using well water, or in which they either do not irrigate or they irrigate with lake water. The

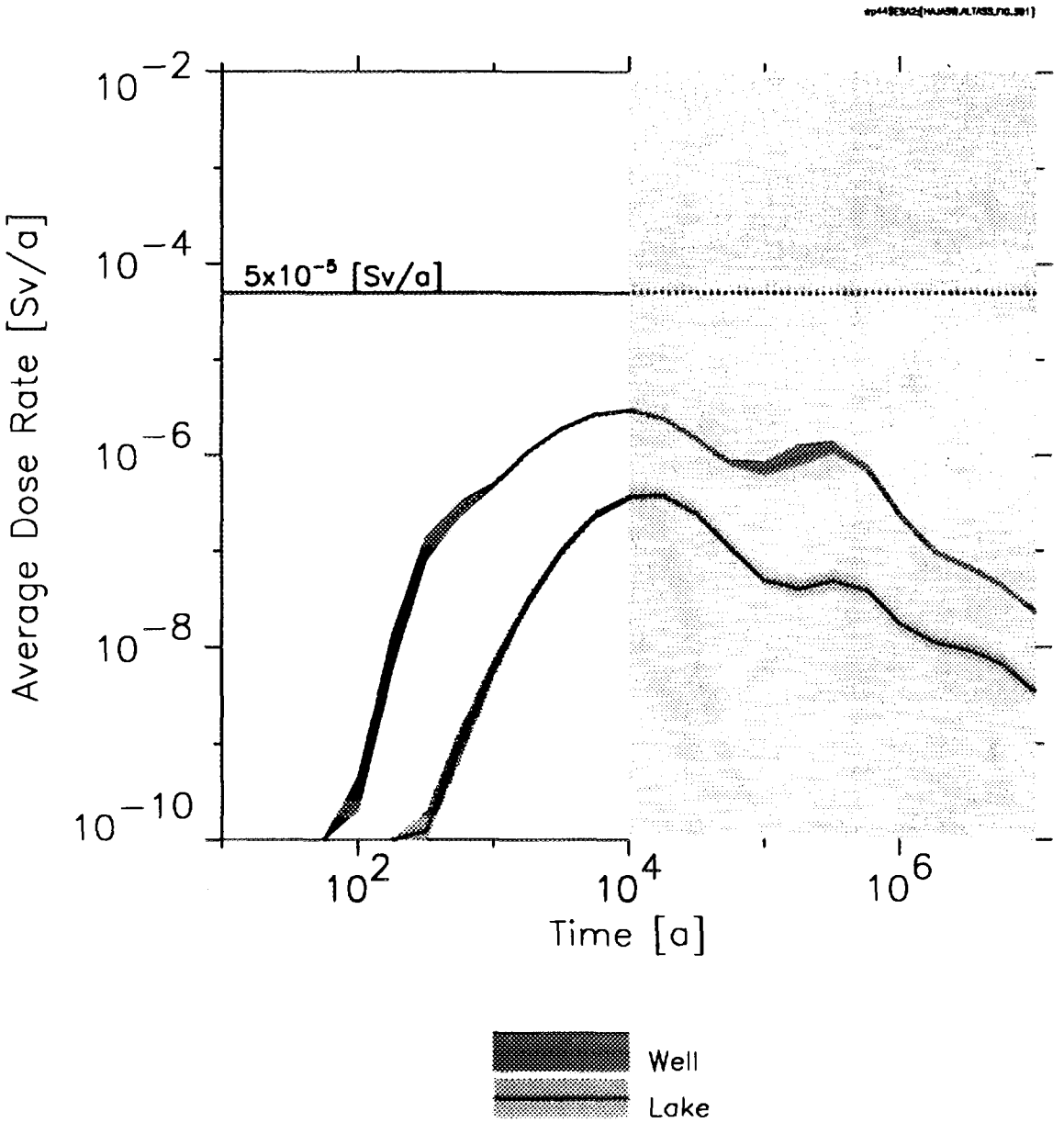

FIGURE 22: Average Dose Rate to the Critical Group from the Simulations Involving the Source of Domestic Water. The two curves show the average dose rate to a member of the critical group when the group obtains its domestic water from a well or from the lake. The bands around the averages are 90% confidence intervals. The horizontal line at 5×10^{-5} Sv/a is the dose rate associated with the AECB radiological risk criterion. The shaded area on the right-hand side of the plot indicates the models and data are less acceptable representations of the disposal system at very long time frames.

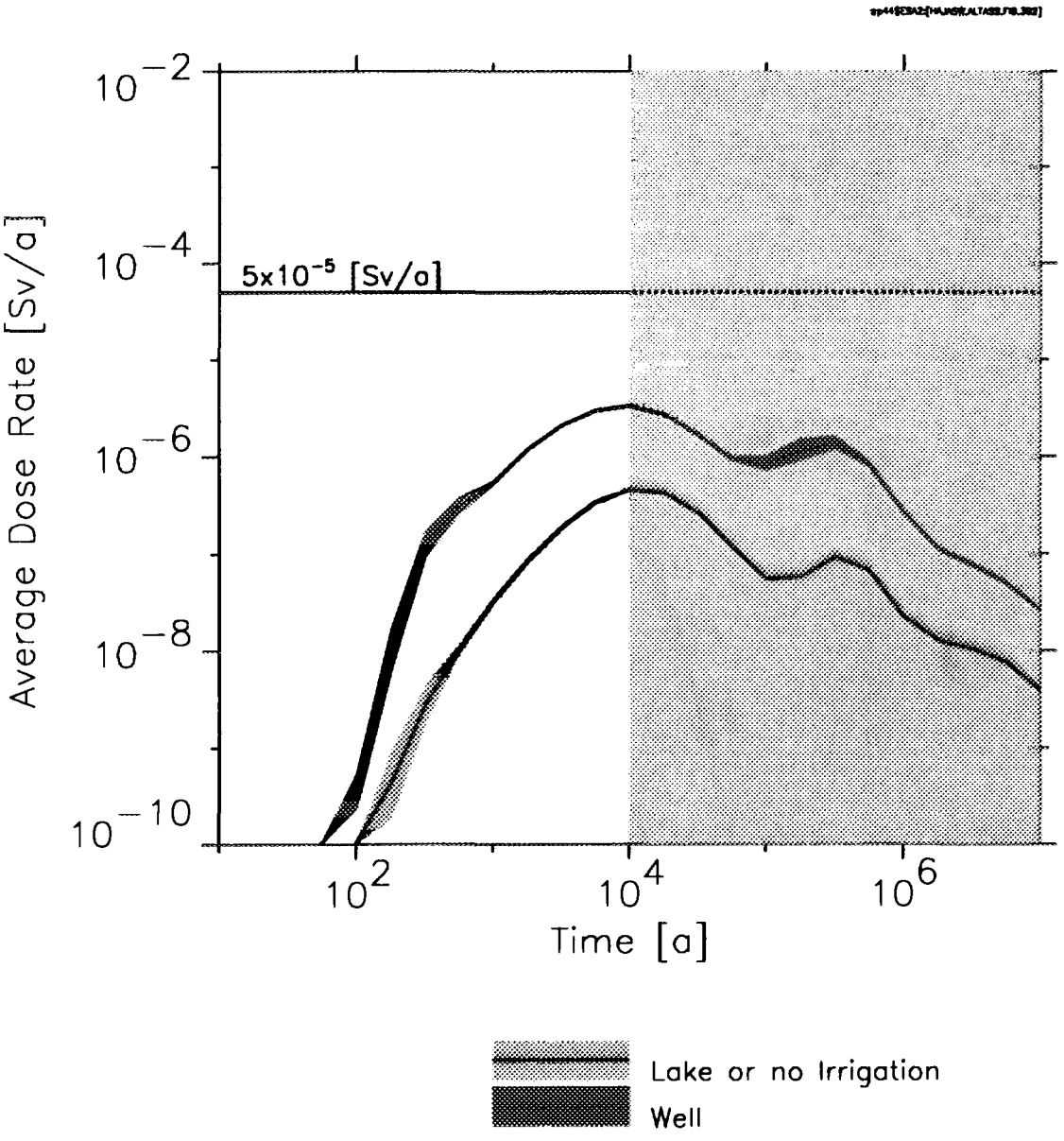

FIGURE 23: Average Dose Rate to the Critical Group from Simulations Involving Irrigation. The two curves show the average dose rate to a member of the critical group when the group irrigates its garden with well water or when they either do not irrigate or they irrigate using lake water. The bands around the averages are 90% confidence intervals. The horizontal line at 5×10^{-5} Sv/a is the dose rate associated with the AECB radiological risk criterion. The shaded area on the right-hand side of the plot indicates the models and data are less acceptable representations of the disposal system at very long time frames.

curves are similar to those in Figure 22, including the shoulder caused by ^{90}Sr for the well-water irrigation curve.

Figure 24 examines the effects of the diet of the critical group. The two curves in part (a) of Figure 24 shows that the average dose rate is not strongly influenced when their diet has high or low ingestion rates of meat. High ingestion rates are defined to be greater than the median value (about 120 kg/a), and low rates are less than the median value. There appears to be a weak effect from ^{90}Sr near 500 a when their diet includes more meat. Similar results and observations occur when their diet has high and low consumption rates of vegetables (Figure 24b), fish (Figure 24c) and birds (Figure 24d). These results indicate that different diet types do not have a large effect on average dose rates.

Figure 25 shows dose rate curves from simulations in which the total number of failed containers in the disposal vault is 10 or less, between 11 and 14 inclusive, or 15 or more, corresponding to the lower, middle and upper third of the calculated values. More failures are associated with larger dose rates; otherwise, however, the curves display the same shapes.

Figure 26 shows dose rate curves from simulations in which the porosities of the lower, intermediate and upper rock zones (SGPROS(LWROC), SGPROS(MIROC) and SGPROS(UPROC)) are greater than or less than their median value. The different behaviour of these rock zones is in accord with the results of the probabilistic sensitivity analysis: for example, the two curves for the lower rock zone (Figure 26a) are quite distinct whereas the two curves for the upper rock zone (Figure 26c) are very similar (Table 7 shows the effective transport porosity of the lower rock zone is an influential parameter, but not the porosity of the upper rock zone). Smaller values of the porosity correspond to larger groundwater velocities and smaller transport delays so that radionuclides arrive earlier in the biosphere. This effect is important near 500 a, associated with the arrival of ^{90}Sr and ^{129}I; it occurs again near 10^5 a associated with the arrival of ^{126}Sn and its progeny, ^{126}Sb. The small-porosity curves show a shoulder near 500 a from ^{90}Sr that is missing from the large-porosity curves. The slower groundwater velocities that occur with larger porosities allow for more significant inventory reductions of ^{90}Sr by decay.

6.5 AVERAGE BEHAVIOUR OF THE DISPOSAL SYSTEM

6.5.1 Introduction

Our probabilistic systems assessment draws results from thousands of randomly sampled simulations to estimate variables such as the mean dose rate to members of the critical group. We can also examine other variables that illustrate the overall behaviour of the disposal system. However, we often cannot focus too closely on intermediate details: because the system model encompasses a wide range of interactions and effects, and because uncertainty in the parameters can greatly change the relative importances of interactions and effects from one simulation to the next, many details are obscured. Thus in an overview of the average behaviour of the disposal system, we are limited to a few of the more important features that are evident in all or most simulations. (On the other hand, we can examine the detailed behaviour of individual simulations, as shown in the Appendix. Nevertheless, no single simulation could cover the full range of possible behaviour in this disposal system.)

We have not yet completed a full analysis of average behaviour for this scoping assessment. The following discussion provides general comments on the performance of the barriers and on the fate of the radionuclides, drawing from an analysis of 240 simulations (randomly sampled using a fractional factorial latin hypercube design (Andres 1995)), from the results of the probabilistic sensitivity analysis, from the deterministic analyses described in the Appendix, and from our understanding of the system model and its data.

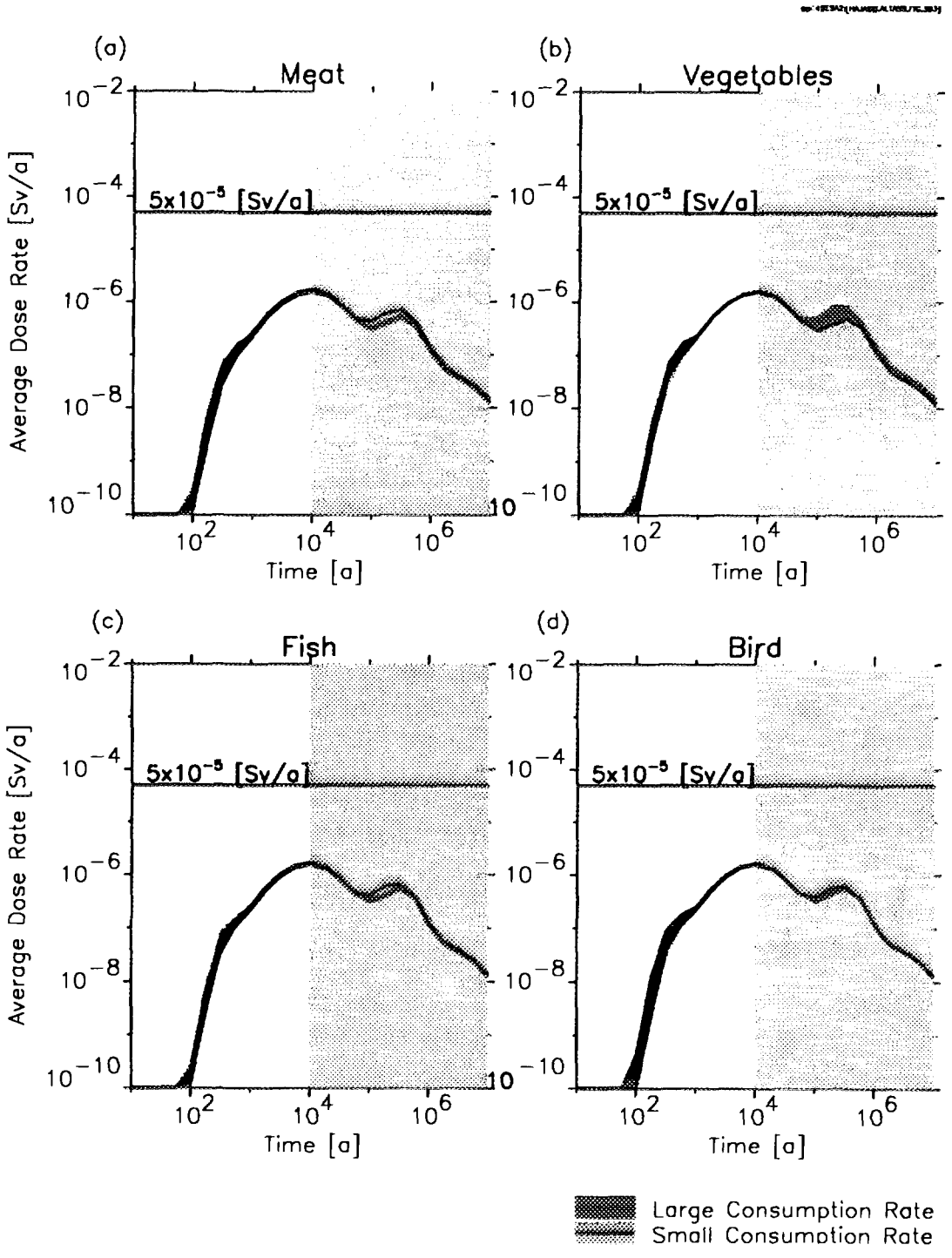

FIGURE 24: Average Dose Rate to the Critical Group from Simulations Involving Diet Options. The two curves in each plot show the average dose rate to a member of the critical group when their diet consists of high or low rates of consumption of different types of food. The bands around the averages are 90% confidence intervals. Part (a) considers meat (greater than or less than about 120 kg/a). (b) is for vegetables (greater than or less than 360 kg/a). (c) is for fish (greater than or less than 9.6 kg/a) and (d) is for birds (greater than or less than 50 kg/a). The horizontal line at 5×10^{-5} Sv/a is the dose rate associated with the AECB radiological risk criterion. The shaded area on the right-hand side of the plot indicates the models and data are less acceptable representations of the disposal system at very long time frames.

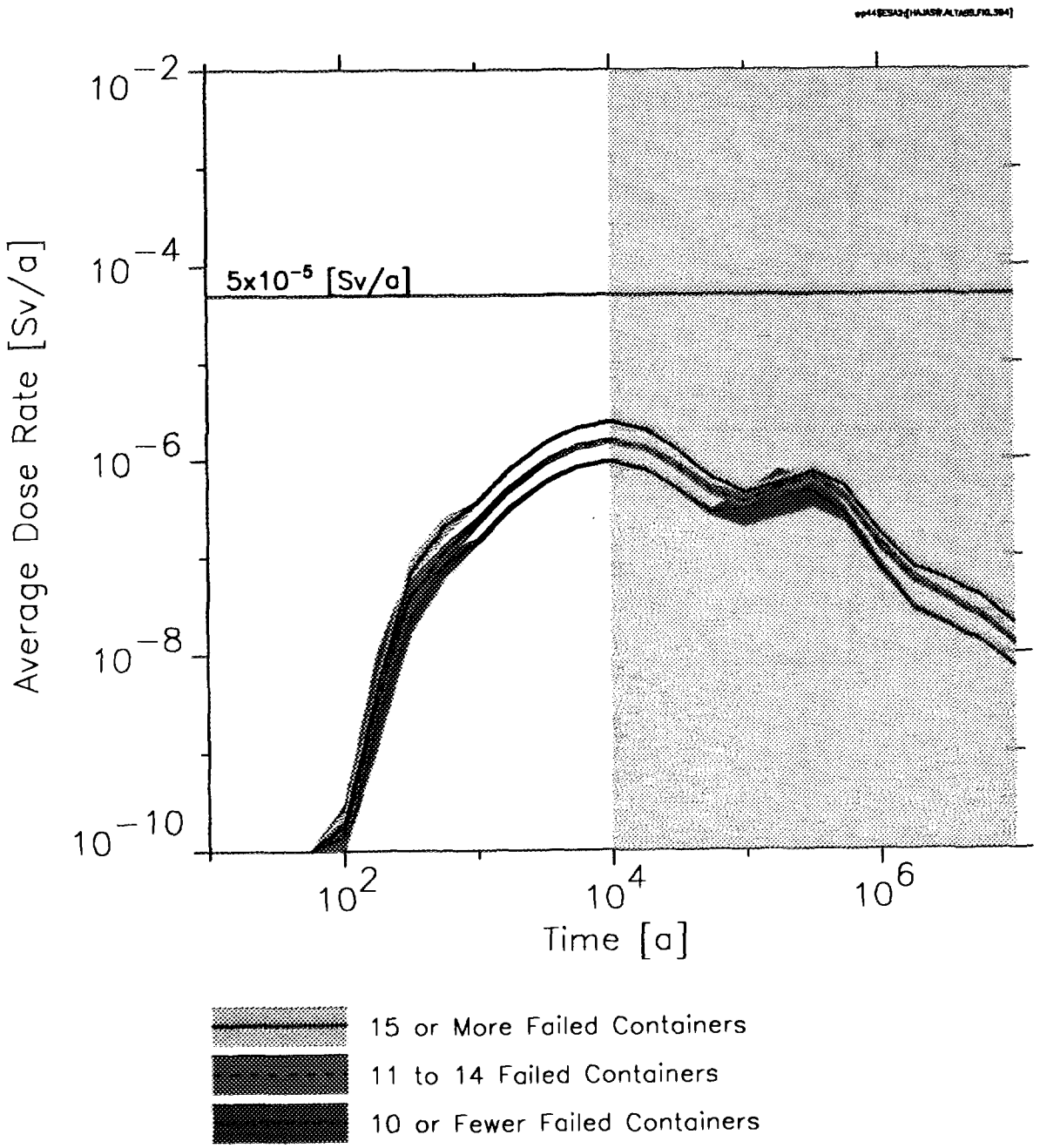

FIGURE 25: *Total Average Dose Rate to the Critical Group from Simulations Involving the Number of Failed Containers.* The curves show the average dose rate to a member of the critical group when the number of failed containers in the disposal vault is 10 or less, between 11 and 14 inclusive, or 15 or more. The bands around the averages are 90% confidence intervals. The horizontal line at 5×10^{-5} Sv/a is the dose rate associated with the AECB radiological risk criterion. The shaded area on the right-hand side of the plot indicates the models and data are less acceptable representations of the disposal system at very long time frames.

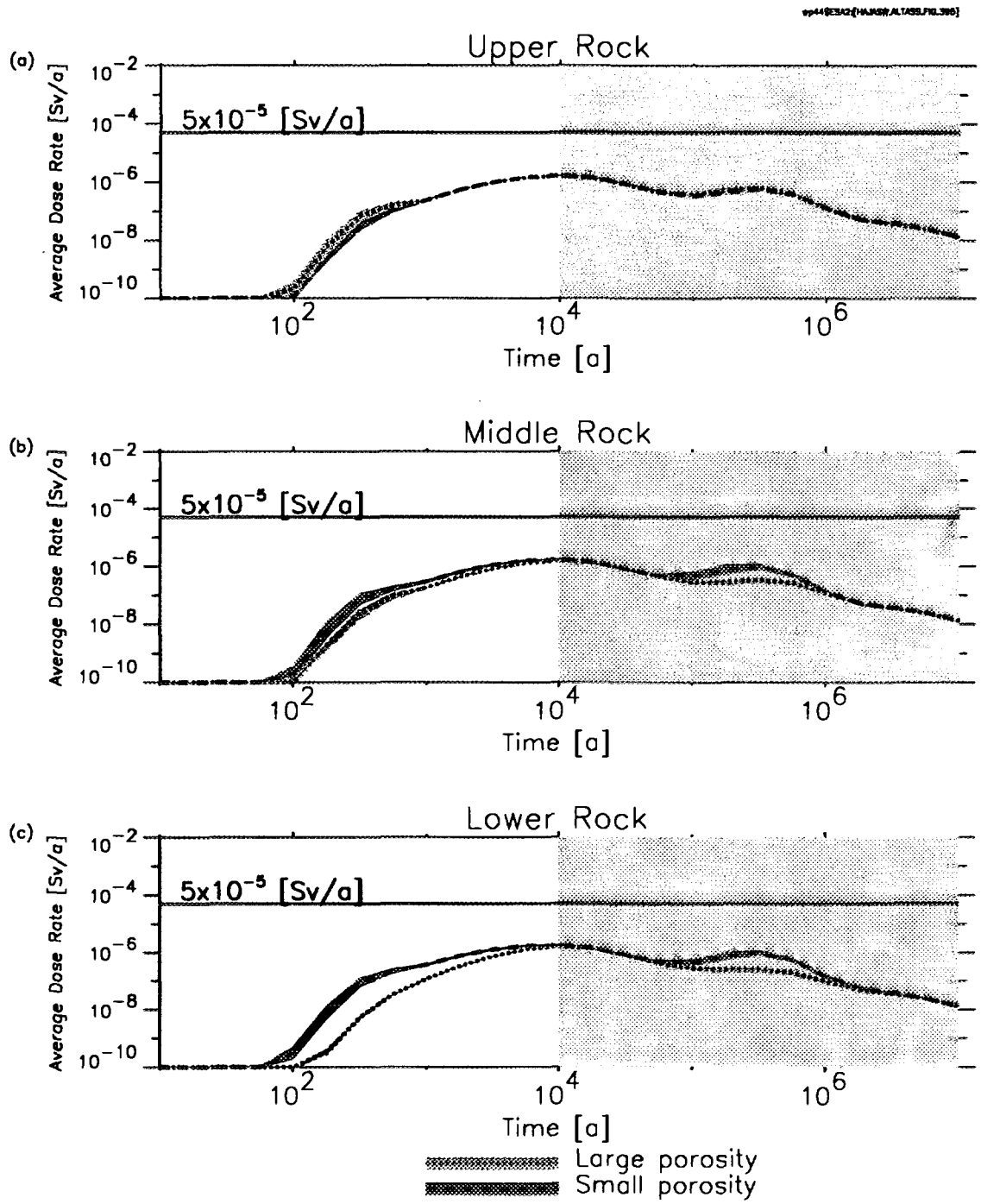

FIGURE 26: Average Dose Rate to the Critical Group from Simulations Involving the Porosity of Three Rock Zones. Parts (a) to (c) are for the upper rock zone, the intermediate rock zone and the lower rock zone respectively. Within each plot, the two curves show the average dose rate to a member of the critical group when the porosity of the rock zone is greater than or less than about 10^{-4}. The bands around the averages are 90% confidence intervals. The horizontal line at 5×10^{-5} Sv/a is the dose rate associated with the AECB radiological risk criterion. The shaded area on the right-hand side of the plot indicates the models and data are less acceptable representations of the disposal system at very long time frames.

6.5.2 Performance of the Engineered and Natural Barriers

The Used Fuel. The vault model simulates congruent-release and instant-release mechanisms from the used fuel, and our analysis shows that both are important in affecting the rate of contaminant releases to the water-filled interior of a failed container.

- The instant-release mechanism is important because we assume that a fraction of the inventory of the instantly released radionuclides is released from the used fuel in the failed containers when the vault is closed.

- The congruent-release mechanism is important because the model assumes dissolution of the UO_2 matrix caused by the early ingress of groundwater, the effects of radiolysis and the use of conservative data that overestimate kinetic dissolution rates (Johnson et al. 1996). From the probabilistic sensitivity analysis, one of the more influential parameters quantifies the magnitude of the UO_2 corrosion from γ-radiation fields: larger fields promote dissolution of the UO_2 matrix. Dissolution is especially enhanced when γ-radiation is strongest and the effect is to maintain relatively high concentrations of contaminants in the water within the container for long times. On average, however, only about 2.6% of the UO_2 matrix dissolves by 10^4 a, and 3.2% by 10^5 a.

Thus used fuel is an affective barrier for all contaminants that are congruently released from the UO_2 matrix.

The Zircaloy Matrix. Contaminants are released from the Zircaloy matrix by the congruent-release mechanism, which is controlled by the low solubility of zirconium (Johnson et al. 1996, 1995). Figure 16a shows that ^{14}C and ^{36}Cl released from the used fuel have significant dose rates, whereas ^{14}C and ^{36}Cl released from the Zircaloy matrix have dose rates that are less than 10^{-10} Sv/a over the entire time frame of the simulations. Thus the Zircaloy matrix is a very effective barrier for radionuclides contained within the matrix.

The Copper Containers. Our analysis shows that the long-lived copper containers are significant engineered barriers, with two important influences on the rate of release of contaminants.

- On average, about 1 in 5000 containers fail (we assume the failures occur at the time of closure of the vault). Conversely, about 4999 in 5000 containers provide absolute containment. Sensitivity analysis shows that estimated dose rates are strongly influenced by the parameters that determine the number of containers that fail because of fabrication defects. Similar conclusions are found in analyses of the EIS case study (Goodwin et al. 1996a).

- Releases from a failed container are controlled by the resistance to diffusive transport through the small, pinhole-sized defect (LeNeveu 1996, SKB 1992). The importance of this process is described further by Johnson et al. (1996), and is a common feature of the example simulations discussed in the Appendix. (In the EIS case study, we conservatively assumed that a container did not influence releases after the container had failed (Johnson et al. 1994a).)

Precipitation. Some chemical elements have a relatively small solubility, even in the aggressive chemical and physical environment within the containers. Precipitation would lower their concentrations inside the failed containers and thus decrease their rates of diffusion from the failed containers. The discussion in the Appendix shows that releases of ^{99}Tc and ^{230}Th are strongly attenuated by this process. Similar

attenuations are expected for other low-solubility radionuclides, notably all isotopes of uranium, neptunium, thorium, plutonium and zirconium. Thus precipitation is an effective natural barrier for low-solubility contaminants.

The Buffer, Backfill and Excavation Damaged Zone. The buffer and backfill act to delay the transport of contaminants from the container to the surrounding rock. Our analysis indicates these media are very effective barriers for contaminants that sorb strongly, such as members of the actinide decay chains and ^{99}Tc. They are less effective for mobile radionuclides, such as ^{129}I and ^{36}Cl. The discussion in the Appendix indicates that the EDZ is an undesirable feature. It generally sustains relatively rapid groundwater velocities and acts as a sink to contaminants in the buffer and backfill for the geosphere modelled herein, where we assume groundwater velocities are large enough that advective transport is more important than diffusive transport. (The EDZ would be a far less significant feature if diffusion dominated contaminant transport in the rock surrounding the disposal vault, as occurred in the EIS case study.) Thus in this report, the EDZ reduces the effectiveness of the buffer and backfill.

A scoping study by Goodwin et al. (1996b) shows that in-room emplacement is generally more robust than borehole emplacement from a long-term performance perspective. The study shows in-room emplacement is particularly effective in delaying releases of ^{99}Tc from the disposal vault.

The Host Geosphere. The hydrogeological properties assumed for the geosphere in this report, and for the lower rock zone in particular, significantly diminishes its role as a barrier compared with the geosphere evaluated in the EIS case study. Groundwater transit times from the vault horizon to the surface environment can be less than 100 a, compared with 10^5 a or more in the EIS case study. Nevertheless, results from the sensitivity analysis show that the geosphere is an important barrier for all radionuclides over short time scales. For example, the dose rates from ^{90}Sr and the time of arrival of early dose rates from ^{129}I are strongly affected by parameters used to describe groundwater transport through the geosphere, notably the effective transport porosity of the lower rock zone (Table 7). The geosphere is also an important barrier over long time scales for contaminants that sorb moderately to strongly on the rock minerals, such as ^{126}Sn, ^{93}Zr, and most members of the actinide decay chains. (The discussion that follows provides more quantitative examples of the effectiveness of the host rock.)

The sensitivity analysis shows that the presence of a water-supply well in the geosphere has a strong influence on estimated dose rates. It is particularly important in the present study because large rates of water withdrawal from the well can have widespread effects throughout the geosphere (Stanchell et al. 1996). Results in Figure 22 (Section 6.4) show that the average dose rate at 10^4 a is about 8 times greater when the critical group obtains its water from a well rather than from the lake. That figure also indicates that the contribution to average dose from ^{90}Sr is important only for simulations involving the well, which we attribute to faster transport of ^{90}Sr because flow paths leading to the well short-circuit parts of the geosphere.

For the disposal system described in the EIS, an important feature is related to the location and orientation of the vault relative to nearby fracture zone LD1. In fact, a derived constraint was adopted in the EIS case study that eliminated the disposal rooms located above LD1 and that had 50 m of rock between LD1 and the closest disposal rooms (Section 6.2 in Goodwin et al. 1994a). For the present study, the assumed properties of the geosphere mean that the region of rock immediately surrounding the disposal vault is a less effective barrier. In fact, the effectiveness of the rock is sufficiently small that the presence of LD1 is far less important in this study than in the EIS case study. Thus our analysis shows that there exists only small differences in dose rate attributed to the different vault sectors, including whether or not those sectors are located in the regions of rock above or below LD1. Moreover, since groundwater transit times through the geosphere are relatively fast in this study, a smaller separation (less

than 50 m) of rock in layer 3 between the disposal rooms and the nearby fracture zone LD1 would not greatly change transit times nor estimated dose rates.

Overall Behaviour of the Engineered and Natural Barriers

We can infer from the data in Tables 8 and 9 the overall behaviour of the engineered barriers in the vault and the natural barriers. These tables present averaged results from 240 simulations, randomly sampled using a fractional factorial latin hypercube design (Andres 1995) for the fission products and actinide decay chains in Tables 4 and 5. The first three columns identify a radionuclide, its half-life and its average initial inventory in the entire vault. The next three parts of the tables show for each radionuclide the following averaged results at 560 a, 10^4 a and 10^5 a:

- total inventory in the system *at* the indicated time, factoring in the effects of radioactive decay and ingrowth;

- total inventory retained within the vault *at* the indicated time, located within the UO_2 and Zircaloy matrices, the containers, the buffer, the backfill and the EDZ;

- total inventory released to the geosphere *up to* the indicated time, calculated as the integral, up to the specified times, of releases from the vault, accounting for decay in the vault but ignoring decay that occurs in the geosphere; and

- total inventory released to the biosphere *up to* the indicated time, calculated as the integral, up to the specified times, of releases from the geosphere, accounting for decay in the vault and geosphere but ignoring decay that occurs in the biosphere.

The results show that the engineered barriers are clearly effective for all radionuclides. The host rock is also very effective at 560 a, and it remains effective at longer times for radionuclides that are short lived or that sorb moderately to strongly. For instance, Tables 8 and 9 display the following results.

- Iodine-129 has a half-life of 1.57×10^7 a and an average initial inventory of 3.1×10^4 mol. Very little inventory is lost because of radioactive decay even after 10^5 a. However, a large fraction of this inventory remains in the vault, still located within the unfailed and the failed containers. During the first 10^4 a, about 0.2 mol in total is released from the vault to the geosphere and 0.09 mol in total reaches the biosphere. That is, only 3×10^{-4}% of the initial inventory of ^{129}I reaches the biosphere within 10^4 a after closure of the vault, rising to 2×10^{-3}% within 10^5 a.

- Strontium-90 has a half-life of 29.1 a and an average initial inventory of 9.5×10^4 mol. Its total inventory decreases to about 0.15 mol at 560 a, and it has virtually disappeared by 10^4 a. Most of its inventory is retained within and decays within the vault: at 560 a only about 2×10^{-6} mol on average survives transport out of the vault to the geosphere and very small quantitities reach the biosphere.

TABLE 8

FATE OF THE FISSION PRODUCTS

Radio-nuclide[2]	Half-Life [a]	Initial Inventory [mol]	Inventory[1] [mol] at 560 a				Inventory[1] [mol] at 10^4 a				Inventory[1] [mol] at 10^5 a			
			Total Inventory	Retained in the vault	Released to the geosphere	Released to the biosphere	Total Inventory	Retained in the vault	Released to the geosphere	Released to the biosphere	Total Inventory	Retained in the vault	Released to the geosphere	Released to the biosphere
$^{14}C(F)$	$5.73x10^3$	$3.0x10^2$	$2.8x10^2$	$2.8x10^2$	$5x10^{-8}$	$2x10^{-12}$	$9.0x10^1$	$9.0x10^1$	$6x10^{-5}$	$8x10^{-6}$	$1.7x10^{-3}$	$1.7x10^{-3}$	$1x10^{-4}$	$4x10^{-5}$
$^{14}C(Z)$	$5.73x10^3$	$1.2x10^2$	$1.1x10^2$	$1.1x10^2$	$3x10^{-13}$	$9x10^{-17}$	$3.6x10^1$	$3.6x10^1$	$2x10^{-10}$	$3x10^{-11}$	$6.6x10^{-4}$	$6.6x10^{-4}$	$5x10^{-10}$	$1x10^{-10}$
$^{36}Cl(F)$	$3.01x10^5$	$7.6x10^2$	$7.6x10^2$	$7.6x10^2$	$9x10^{-5}$	$1x10^{-6}$	$7.5x10^2$	$7.5x10^2$	$5x10^{-3}$	$2x10^{-3}$	$6.1x10^2$	$6.1x10^2$	$2x10^{-2}$	$2x10^{-2}$
$^{36}Cl(Z)$	$3.01x10^5$	$6.0x10^1$	$6.0x10^1$	$6.0x10^1$	$1x10^{-11}$	$6x10^{-13}$	$5.9x10^1$	$5.9x10^1$	$2x10^{-9}$	$7x10^{-10}$	$4.8x10^1$	$4.8x10^1$	$3x10^{-8}$	$2x10^{-8}$
$^{135}Cs(F)$	$2.30x10^6$	$1.5x10^4$	$1.5x10^4$	$1.5x10^4$	$7x10^{-10}$	0	$1.5x10^4$	$1.5x10^4$	$1x10^{-3}$	$3x10^{-11}$	$1.4x10^4$	$1.4x10^4$	$5x10^{-2}$	$2x10^{-4}$
$^{137}Cs(F)$	$3.0x10^1$	$1.5x10^5$	$3.7x10^{-1}$	$3.7x10^{-1}$	$1x10^{-12}$	0	0	0	$2x10^{-12}$	0	0	0	$2x10^{-12}$	0
$^{129}I(F)$	$1.57x10^7$	$3.1x10^4$	$3.1x10^4$	$3.1x10^4$	$4x10^{-3}$	$6x10^{-5}$	$3.1x10^4$	$3.1x10^4$	$2x10^{-1}$	$9x10^{-2}$	$3.1x10^4$	$3.1x10^4$	$7x10^{-1}$	$7x10^{-1}$
$^{107}Pd(F)$	$6.50x10^6$	$4.9x10^4$	$4.9x10^4$	$4.9x10^4$	$2x10^{-6}$	$6x10^{-15}$	$4.9x10^4$	$4.9x10^4$	$5x10^{-4}$	$7x10^{-6}$	$4.8x10^4$	$4.8x10^4$	$2x10^{-2}$	$3x10^{-3}$
$^{79}Se(F)$	$6.50x10^4$	$1.3x10^3$	$1.3x10^3$	$1.3x10^3$	$8x10^{-5}$	$2x10^{-15}$	$1.2x10^3$	$1.2x10^3$	$7x10^{-3}$	$2x10^{-5}$	$4.5x10^2$	$4.5x10^2$	$2x10^{-2}$	$2x10^{-3}$
$^{126}Sn(F)$	$1.0x10^5$	$3.7x10^3$	$3.7x10^3$	$3.7x10^3$	$2x10^{-5}$	0	$3.5x10^3$	$3.5x10^3$	$8x10^{-3}$	0	$1.9x10^3$	$1.9x10^3$	$5x10^{-2}$	$3x10^{-7}$
$^{90}Sr(F)$	$2.91x10^1$	$9.5x10^4$	$1.5x10^{-1}$	$1.5x10^{-1}$	$2x10^{-6}$	$5x10^{-12}$	0	0	$2x10^{-6}$	$6x10^{-12}$	0	0	$2x10^{-6}$	$6x10^{-12}$
$^{99}Tc(F)$	$2.13x10^5$	$1.8x10^5$	$1.8x10^5$	$1.8x10^5$	$6x10^{-11}$	$1x10^{-15}$	$1.8x10^5$	$1.8x10^5$	$1x10^{-6}$	$9x10^{-8}$	$1.3x10^5$	$1.3x10^5$	$2x10^{-3}$	$1x10^{-3}$
$^{93}Zr(F)$	$1.53x10^6$	$1.0x10^5$	$1.0x10^5$	$1.0x10^5$	0	0	$1.0x10^5$	$1.0x10^5$	0	0	$9.9x10^4$	$9.9x10^4$	$3x10^{-11}$	0

[1] Calculated values that are less than 1×10^{-20} mol are reported as zero.

[2] We list here all but three of the radionuclides in Table 4: ^{93m}Nb, ^{126}Sb and ^{90}Y are assumed to be in secular equilibrium with their precursors in the engineered and natural barriers. The sources of the radionuclides are fission products of UO_2 fuel or neutron activation products of fuel impurities (F) and neutron activation products of Zircaloy materials (Z).

TABLE 9

FATE OF THE MEMBERS OF THE ACTINIDE DECAY CHAINS

			Inventory[1] [mol] at 560 a				Inventory[1] [mol] at 10^4 a				Inventory[1] [mol] at 10^5 a			
Radio-nuclide[2]	Half-Life [a]	Initial Inventory [mol]	Total Inventory	Retained in the vault	Released to the geosphere	Released to the biosphere	Total Inventory	Retained in the vault	Released to the geosphere	Released to the biosphere	Total Inventory	Retained in the vault	Released to the geosphere	Released to the biosphere
4n+1 decay chain														
^{241}Am	4.32×10^{2}	3.3×10^{4}	1.3×10^{4}	1.3×10^{4}	0	0	3.5×10^{-3}	3.5×10^{-3}	1×10^{-20}	0	0	0	1×10^{-20}	0
^{237}Np	2.14×10^{6}	1.1×10^{4}	3.0×10^{4}	3.0×10^{4}	0	0	4.3×10^{4}	4.3×10^{4}	9×10^{-15}	8×10^{-20}	4.2×10^{4}	4.2×10^{4}	1×10^{-7}	3×10^{-8}
^{233}U	1.59×10^{5}	2.9×10^{3}	2.9×10^{3}	2.9×10^{3}	0	0	2.9×10^{3}	2.9×10^{3}	6×10^{-11}	3×10^{-15}	3.0×10^{3}	3.0×10^{3}	8×10^{-7}	4×10^{-8}
^{229}Th	7.34×10^{3}	1.3×10^{-1}	6.9	6.9	0	0	8.0×10^{1}	8.0×10^{1}	2×10^{-14}	6×10^{-19}	1.3×10^{2}	1.3×10^{2}	4×10^{-9}	8×10^{-11}
4n+2 decay chain														
^{238}U	4.47×10^{9}	3.4×10^{8}	3.4×10^{8}	3.4×10^{8}	0	0	3.4×10^{8}	3.4×10^{8}	2×10^{-10}	4×10^{-16}	3.4×10^{8}	3.4×10^{8}	8×10^{-6}	1×10^{-6}
^{234}U	2.45×10^{5}	1.6×10^{4}	1.6×10^{4}	1.6×10^{4}	0	0	1.6×10^{4}	1.6×10^{4}	1×10^{-14}	3×10^{-20}	1.7×10^{4}	1.7×10^{4}	4×10^{-10}	5×10^{-11}
^{230}Th	7.70×10^{4}	5.1×10^{-1}	2.5×10^{1}	2.5×10^{1}	0	0	4.3×10^{2}	4.3×10^{2}	9×10^{-18}	0	3.0×10^{3}	3.0×10^{3}	1×10^{-9}	2×10^{-13}
^{226}Ra	1.60×10^{3}	2.6×10^{-5}	5.9×10^{-2}	5.9×10^{-2}	0	0	6.8	6.8	3×10^{-6}	0	6.0×10^{1}	6.0×10^{1}	7×10^{-4}	4×10^{-14}
4n+3 decay chain														
^{243}Am	7.38×10^{3}	1.3×10^{3}	1.2×10^{3}	1.2×10^{3}	0	0	5.1×10^{2}	5.1×10^{2}	3×10^{-16}	0	1.1×10^{-1}	1.1×10^{-1}	3×10^{-10}	0
^{239}Pu	2.41×10^{4}	9.2×10^{5}	9.1×10^{5}	9.1×10^{5}	0	0	6.9×10^{5}	6.9×10^{5}	7×10^{-16}	0	5.2×10^{4}	5.2×10^{4}	1×10^{-7}	1×10^{-12}
^{235}U	7.04×10^{8}	6.7×10^{5}	6.8×10^{5}	6.8×10^{5}	0	0	9.0×10^{5}	9.0×10^{5}	9×10^{-8}	8×10^{-15}	1.5×10^{6}	1.5×10^{6}	7×10^{-4}	3×10^{-6}
^{231}Pa	3.28×10^{4}	2.9	3.2	3.2	0	0	9.3	9.3	9×10^{-16}	0	5.6×10^{1}	5.6×10^{1}	3×10^{-9}	2×10^{-11}

[1] Calculated values that are less than 1×10^{-20} mol are reported as zero.

[2] We list here 12 radionuclides from Table 5, excluding those that are assumed to be in secular equilibrium with their precursors (^{233}Pa, ^{225}Ra, ^{225}Ac, ^{234}Th, ^{222}Rn, ^{210}Pb, ^{210}Bi, ^{210}Po, ^{239}Np, ^{231}Th, ^{227}Ac, ^{227}Th and ^{223}Ra). Members of the actinide decay series originate from the neutron activation of uranium in the UO_2 fuel. Those simulated in this report belong to the simplified 4n+1, 4n+2 or 4n+3 chains.

- Tin-126 has a half-life of 1.0×10^5 a and an average initial inventory of 3.7×10^3 mol; half of its initial inventory remains after 10^5 a. Although most of this inventory is retained in the vault, about 8×10^{-3} mol are released to the geosphere after 10^4 a. However, the strong sorption of tin in the host rock greatly slows down its rate of movement, so that, between 10^4 and 10^5 a, only 3×10^{-7} mol reaches the biosphere.

- Americium-241 has a half-life of 432 a and an average initial inventory of 3.3×10^4 mol. Its total inventory decreases to about 3.5×10^{-3} mol at 10^4 a and it has virtually disappeared by 10^5 a. Most of its inventory is retained within and decays within the vault. Very small quantities are released to the geosphere and none to the biosphere.

- Thorium-230 has a half-life of 7.70×10^4 a and an average initial inventory of 5.1×10^{-1} mol . Its inventory increases with time because of ingrowth from its precursors (^{238}U and ^{238}U), reaching a value of 3.0×10^3 mol at 10^5 a. However, thorium has a low solubility limit and is strongly sorbed by the buffer, the backfill and the host rock. The results in Table 9 show that most of its initial and ingrown inventories are retained within the vault, that the small quantities released to the geosphere are significantly delayed, and that very small quantities reach the biosphere over 10^5 a.

- Plutonium-239 has a half-life of 2.41×10^4 a and an initial inventory of 9.2×10^5 mol. Its inventory increases slightly because of ingrowth from ^{243}Am, but about 95% has decayed by 10^5 a. Plutonium has a low solubility limit and it is strongly sorbed by the engineered and natural barriers. Table 9 indicates most of the ^{239}Pu is retained in the vault, even at 10^5 a, and that only very small quantities reach the biosphere.

6.5.3 Fate of the Radionuclides

The following discussion provide summary information on the radionuclides evaluated in this report.

Carbon-14 exists in both used fuel and in the Zircaloy matrix and arises from neutron activation of impurities (and additives) in the used-fuel bundles. On average, about 3% of its total inventory in the irradiated UO_2 fuel is instantly released. Carbon has a high solubility and is relatively mobile in the engineered barriers and most of the natural barriers, except for the upper rock zone and fracture zone LD1 where there is significant sorption and exchange on calcite ($CaCO_3$) present in these zones. Doses from ^{14}C are limited by dilution with naturally occurring stable ^{12}C in groundwater. There are no significant dose rates from its inventory in Zircaloy over the entire time frame of the simulations. The dose rate from ^{14}C in the used fuel is relatively small for several reasons: its initial inventory is relatively small and it has a relatively short half-life. Moreover, the results in Table 8 suggest that sorption in the geosphere has a strong influence in slowing the rate of transport of carbon. Carbon-14 was a relatively more important contributor in the EIS case study, which used significantly larger values for its initial inventory and its instant release fraction. The smaller values used in the present study are based on more recent experimental data (Johnson et al. 1996).

Chlorine-36 exists in both used fuel and in the Zircaloy matrix and arises mainly from neutron activation of stable ^{35}Cl impurities in the used-fuel bundles. On average, about 8% of its total inventory in the irradiated UO_2 fuel is instantly released. Chlorine has a high solubility and is relatively mobile in the engineered and natural barriers; for example, the results in Table 8 indicate little or no delays occur in the geosphere. Chlorine-36 has small initial inventories, a long half-life, and its dose rates are limited by dilution with naturally occurring stable isotopes of chlorine in groundwater. The inventory of ^{36}Cl in Zircaloy does not produce a significant dose rate over the entire time frame of the simulations.

Chlorine-36 from used fuel is the second largest contributor to the total dose for times near 10^4 a. It was also an important contributor to dose in the EIS case study (Johnson et al. 1995.)

Cesium-135 and Cesium-137 are fission products, and they have similar properties except for their initial inventories and half-lives. On average, about 8% of their total initial inventories are instantly released from the irradiated UO_2 fuel. Cesium has a high solubility and is strongly retained by engineered and natural barriers (Table 8). Cesium-137 has a large initial inventory. However, dose rates from ^{137}Cs are less than 10^{-10} Sv/a over the entire simulation time frame because it has a short half-life: delays in its transport are sufficiently long that no significant quantity is discharged to the biosphere. Cesium-135 also has a large inventory. Dose rates from ^{135}Cs are relatively unimportant for at least 10^4 a (Figure 16a) because it also experiences long transport delays. Neither of these radionuclides was an important contributor to total dose in the EIS case study.

Iodine-129 is a fission product and on average about 8% of its total initial inventory is instantly released from the irradiated UO_2 fuel. It has a high solubility and is one of the most mobile radionuclides, generally exhibiting no sorption or weak sorption on the engineered and natural barriers, except for overburden and lake sediment. The results in Table 8 indicate that iodine is not significantly delayed in the geosphere. It is long-lived and its dose rates are limited by dilution with naturally occurring stable ^{127}I in groundwater. Our analysis shows that ^{129}I is an important contributor to dose rate over the first 10^4 a (and longer) after closure (Figure 16a). Iodine-129 was the dominant contributor to dose rate in the EIS case study.

Palladium-107 is a long-lived fission product with a relatively large initial inventory. It is not instantly released from the irradiated UO_2 fuel. Palladium can be insoluble in a reducing electrochemical environment and it generally sorbs strongly on engineered and natural barriers (Table 8). Our analysis shows that dose rates from ^{107}Pd are relatively small over the entire time frame of the simulations; for example, Figure 16a shows its maximum average dose rate is about 10^{-9} Sv/a. Palladium-107 was not an important contributor to total dose in the EIS case study.

Selenium-79 is a fission product with a moderately long half-life. On average, about 8% of its total initial inventory is instantly released from the irradiated UO_2 fuel. Selenium can be insoluble in a reducing electrochemical environment and it generally displays moderate sorption on engineered and natural barriers, except for the overburden and lake sediment where it is strongly sorbed. Table 8 suggests sorption in the geosphere has a strong effect. The results in Figure 16a show that dose rates from ^{79}Se appear after about 2000 a and it becomes an important contributor to total dose at longer times. Selenium-79 was not an important contributor to total dose in the EIS case study where the geosphere was a much more effective barrier.

Strontium-90 is a fission product with a relatively large inventory, of which an average of about 2.5% is instantly released from the irradiated UO_2 fuel. Strontium has a large solubility and is weakly to moderately sorbed on most barriers; however, the results in Table 8 show that this extent of sorption has a strong influence on releases of short-lived ^{90}Sr from the geosphere. The half-life of ^{90}Sr is 29.1 a, whereas the half-life of its immediate progeny, yttrium-90, is only 2.7 d. Thus we calculate the releases of ^{90}Y to the biosphere from the secular equilibrium approximation. Our analysis shows that ^{90}Sr and ^{90}Y are important contributors to total dose near about 500 a, and that their contributions are insignificant beyond about 10^3 a (Figure 16a). However, our analysis also indicates that their contributions are unimportant in most of the randomly sampled simulations (Figure 18a). We infer that in most simulations one or more barriers are effective in delaying the transport of ^{90}Sr, and that there are only a few rare simulations where all the barriers are ineffective. These radionuclides were not important contributors to total dose in the EIS case study.

Technetium-99 is a long-lived fission product with a relatively large initial inventory. On average, about 6% of its total initial inventory is instantly released from the irradiated UO_2 fuel. Technetium has a low solubility in a reducing electrochemical environment. It is strongly sorbed by the backfill and weakly to moderately sorbed in the geosphere (Table 8). Technetium-99 is not an important contributor to the total dose rate for times up to 10^4 a, although it can be more important at longer times (Figure 16a). This radionuclide was not an important contributor to total dose in the EIS case study, but it did contribute in some sensitivity analyses (see p. 622-625 in Goodwin et al. 1994a).

Tin-126 is a fission product and about 8% of its total initial inventory is instantly released from the irradiated UO_2 fuel. Tin has a low solubility and generally sorbs strongly on engineered and natural barriers (Table 8). The half-life of ^{126}Sn is 1.0×10^5 a, whereas the half-life of its immediate progeny, antimony-126, is only 12 days; thus we do not directly simulate the transport of ^{126}Sb in the vault and geosphere models, but estimate its releases to the biosphere from the secular equilibrium approximation. In using this approximation, ^{126}Sb releases to the biosphere include contributions from the decay of ^{126}Sn in the geosphere segments that touch on the biosphere (as well as contributions from ^{126}Sn releases into the biosphere). These additional contributions are particulary large for the ^{126}Sn - ^{126}Sb chain because tin is strongly sorbed in the geosphere, whereas antimony is very mobile. Thus estimated concentrations and dose rates from ^{126}Sb are generally much larger than the corresponding estimates for ^{126}Sn. Our analysis shows that neither ^{126}Sn nor ^{126}Sb are important contributors to total dose for times up to 10^4 a, although both become significant at longer times (Figure 16a). Tin-126 and ^{126}Sb were not significant contributors to the total dose rate in the EIS case study where the geosphere was a much more effective barrier

Zirconium-93 is a long-lived fission product and has a relatively large initial inventory. It is not instantly released from the irradiated UO_2 fuel. Zirconium is relatively insoluble in the chemical and physical environment within a container, and it sorbs strongly on engineered and natural barriers (Table 8). The half-life of ^{93}Zr is 1.53×10^6 a and the half-life of its immediate progeny, niobium-93m, is 13.6 a. Thus we estimate releases of ^{93m}Nb to the biosphere using the secular equilibrium approximation. Our analysis shows that dose rates from both ^{93}Zr and ^{93m}Nb are insignificant over the entire time frame of the simulations. They were not important contributors to total dose in the EIS case study.

The 4n+1 decay chain involves seven radionuclides, three of which are assumed to be in secular equilibrium with their immediate precursors in the vault and geosphere model:

$$^{241}Am \rightarrow {}^{237}Np\ (\ {}^{233}Pa) \rightarrow {}^{233}U \rightarrow {}^{229}Th\ (\ {}^{225}Ra)\ (\ {}^{225}Ac)$$

where (^{233}Pa) indicates ^{233}Pa is in secular equilibrium with ^{237}Np.

Americium-241 accounts for about 75% of the total mass of the 4n+1 radionuclides. All members of the chain are released congruently with the dissolution of the irradiated UO_2 fuel and all are moderately to strongly sorbed on the engineered and natural barriers (Table 9). Americium, neptunium, protactinium, thorium and uranium are relatively insoluble and would tend to precipitate within the container. The solubility of radium is also small; it may precipitate in the container in some simulations. Our analysis indicates that members of the 4n+1 chain have no significant contributions to the total dose rate for times up to 10^4 a and longer (Figure 16b). Beyond about 10^5 a, there may be contributions from ^{237}Np and progeny further down the chain, but contributions from ^{241}Am are unlikely as its half-life is only 432 a.

The 4n+2 decay chain involves nine radionuclides, five of which are assumed to be in secular equilibrium with their immediate precursors:

$$^{238}U\ (\ {}^{234}Th) \rightarrow {}^{234}U \rightarrow {}^{230}Th \rightarrow {}^{226}Ra\ (\ {}^{222}Rn)\ (\ {}^{210}Pb)\ (\ {}^{210}Bi)\ (\ {}^{210}Po)$$

Uranium-238 contains almost all of the mass of the 4n+2 decay chains and, in fact, its mass is greater than the total mass of all other radionuclides in used fuel. All members of the chain are released congruently with the dissolution of the irradiated UO_2 fuel and all (except ^{222}Rn) are moderately to strongly sorbed on the engineered and natural barriers (Table 9). Thorium and uranium are relatively insoluble and would tend to precipitate within the container. Radium may also precipitate in some simulations. Our analysis indicates that members of the 4n+2 chain have no significant contributions to the total dose rate for times up to 10^4 a and longer (Figure 16b). Dose rates from ^{226}Ra and its progeny would likely be small and delayed for long periods of time. Dose rates from the first four members of this chain would likely be insignificant for very long periods of time.

The 4n+3 decay chain involves nine radionuclides, five of which are assumed to be in secular equilibrium with their immediate precursors:

$$^{243}Am\ (\ ^{239}Np) \rightarrow\ ^{239}Pu \rightarrow\ ^{235}U\ (\ ^{231}Th) \rightarrow\ ^{231}Pa\ (\ ^{227}Ac)\ (\ ^{227}Th)\ (\ ^{223}Ra).$$

Plutonium-239 and ^{235}U account for almost all of the mass of the 4n+3 radionuclides. All members of the chain are released congruently with the dissolution of the irradiated UO_2 fuel, and all are moderately to strongly sorbed on the engineered and natural barriers (Table 9). Americium, neptunium, plutonium, protactinium, thorium and uranium are relatively insoluble and would tend to precipitate within the container. Radium may also precipitate in some simulations. Our analysis indicates that members of the 4n+3 chain have no significant contributions to the total dose rate for times up to 10^4 a and longer (Figure 16b). Actinium-227 and progeny further down the chain may produce small dose rates after a long period of time, but contributions from ^{243}Am through to ^{231}Th are unlikely for very long time frames.

7. CONCLUSIONS

The EIS and supporting documents identify and discuss the environmental criteria, guidelines and standards that would apply to a nuclear fuel waste disposal facility in Canada (AECL 1994a, Goodwin et al. 1994a). The quantitative criterion of most interest is a radiological risk limit for protection of human health from radiotoxic material. Other criteria deal with protection of human health from chemically toxic material, and with "*protection for the general environment from impacts that might arise from either radioactive or non-radioactive contaminants* (AECB 1987)".

In this scoping assessment, we focus on radiological impacts to humans and to nonhuman biota.

Protection of Human Health - Radiological Impacts to Humans

The AECB has specified a quantitative criterion, applicable for times up to 10^4 a, that establishes a radiological risk limit for a group of people that would be exposed to the greatest risk. The calculation of radiological risk uses the following equation (AECB 1987).

$$Risk = \Sigma_i\ p_i\ d_i\ k$$

where the summation is over all significant scenarios. The variables in this equation are as follows.

Risk corresponds to the probability of a serious health effect (defined below) per year that is attributed to the presence of a disposal vault and that might be incurred by an individual in the critical group. The critical group is defined such that their location and lifestyle expose the members of the group to the greatest potential risk.

p_i is the probability of occurrence of the scenario. The analysis in this report deals with the groundwater transport scenario and we conservatively assume (Section 4) that its probability of occurrence is unity. The groundwater transport scenario describes the expected long-term behaviour of the disposal system; other less likely scenarios include deeper water-supply wells used by the critical group and inadvertent human intrusion.

d_i is the arithmetic mean value of the annual effective dose equivalent (called dose rate herein) in units of Sv/a. In this scoping study, we have estimated the mean dose rate from the 41 radionuclides listed in Tables 4 and 5 that are expected to be the major contributors to the total radiation dose over times scales up to 10^5 a following closure of the disposal vault. Figure 15 shows curves of average dose rate versus time.

k is the risk conversion factor which converts dose rate in sieverts per year to serious health effects per year. We report results using two risk conversion factors that differ in their definition of "serious health effects". In 1987, the AECB specified a value of 0.02, where serious health effects are fatal cancers or serious genetic effects occurring to an individual or his or her descendants who would be exposed to the greatest risks (AECB 1987). More recently, the ICRP has recommended a value of 0.073 where serious health effects are fatal and nonfatal cancers or severe hereditary effects (ICRP 1991a).

Figure 27 plots the conditional risk[1] associated with the groundwater transport scenario and the radionuclides expected to be the major contributors to dose rate for the disposal system evaluated in this report. We present two risk curves: the uppermost curve uses the ICRP risk conversion factor and the middle curve uses the AECB factor (the lowermost curve is discussed below). The horizontal line in Figure 27 shows the AECB risk limit: a probability of occurrence of a serious health effect per year equal to 10^{-6} for times up to 10^4 a. Both curves are clearly under the risk limit for times up to 10^4 a and possibly for much longer times.

Figure 27 includes for comparison the corresponding conditional risk curve computed from results described in the EIS case study (Goodwin et al. 1994a). This curve is calculated from the average dose rate curve (Figure 6-18 in Goodwin et al. 1994a) for the equivalent scenario (called the SYVAC scenarios in Goodwin et al. 1994a) and uses the risk conversion factor specified by the AECB (1987). Thus we can make a meaningful comparison between the curve from the EIS case study and the (middle) curve from the present study that uses the same AECB risk conversion factor.

The comparison indicates that the conditional risk at 10^4 a from the EIS case study is about 5 orders of magnitude smaller than the conditional risk from the present study. However, the conditional risk from the EIS case study is rapidly rising at 10^4 a and continues to increase at 10^5 a. The conditional risk from the present study is about 2×10^{-8} a^{-1} at 10^4 a (about 1×10^{-7} a^{-1} using the ICRP risk conversion factor) and it exhibits an overall maximum near this time. Both curves have approximately the same value at 10^5 a. We infer that, compared with the EIS case study, the maximum in the calculated radiological risk in the present study is not necessarily larger, but it is shifted to earlier times.

[1] Our analysis does not include all radionuclides that might be contributors to dose rate, nor all possible scanarios. Therefore, the calculations show the conditional risk and not the total risk.

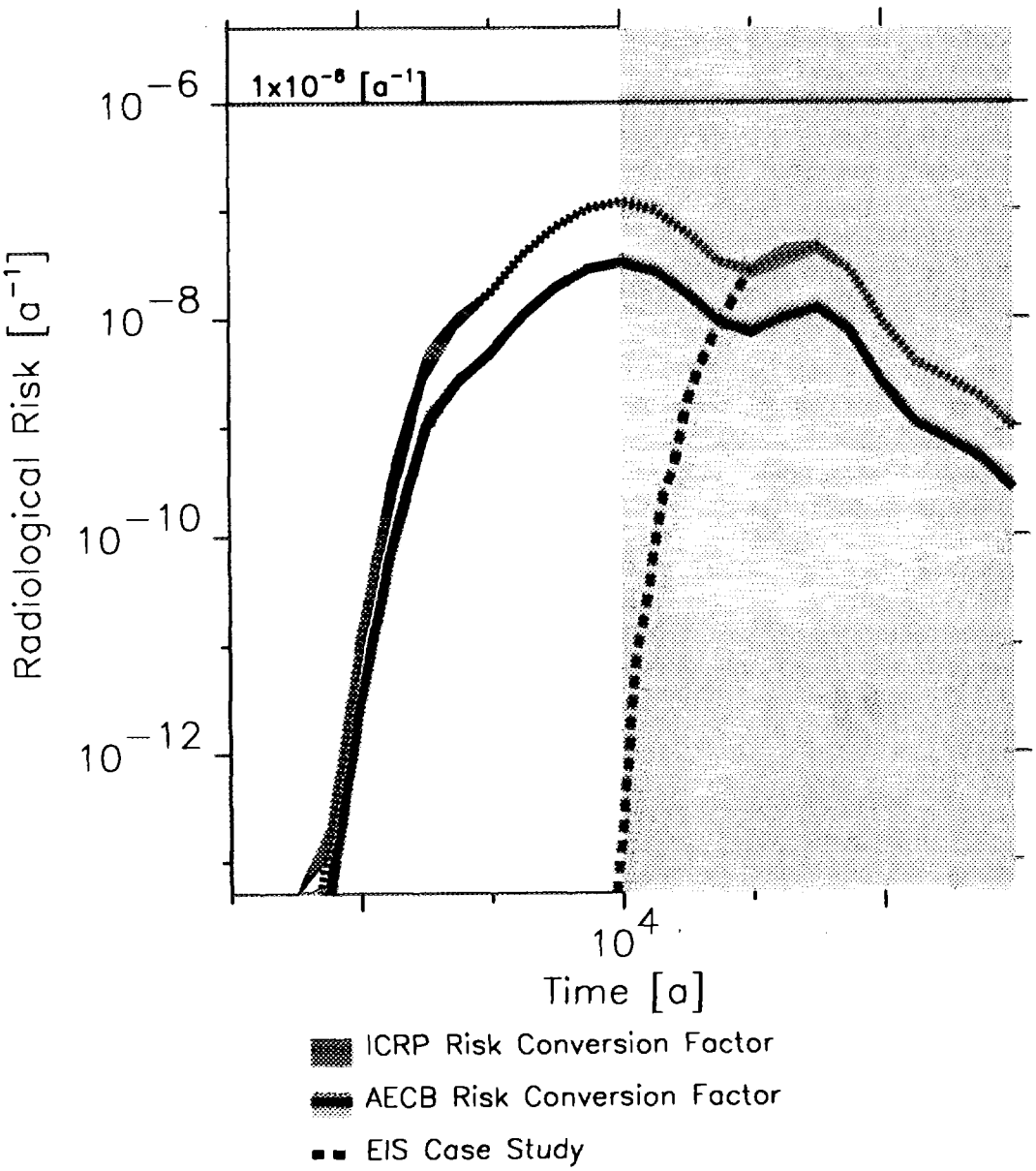

FIGURE 27: Radiological Risk Versus Time. Three risk curves are shown.

- The upper two curves are from the present study. Both plot the conditional radiological risk, or probability of a serious health effect per year, but use different risk conversion factors. The uppermost curve uses a value recommended by the ICRP (1991a), and the lower curve a value specified by the AECB (1987). The results are extended to the time limit of the simulations, which is beyond the time of acceptability of the underlying models and data.
- The lower curve plots a corresponding conditional radiological risk based on results from the EIS case study (Goodwin et al. 1994a) and uses the AECB risk conversion factor.

The horizontal line at a risk of 10^{-6} is the AECB risk limit that applies for times up to 10^4 a (AECB 1987).

Protection of the Environment - Radiological Impacts to Nonhuman Biota

In this scoping assessment, we estimate radiological impacts to four target organisms that are representative of a wide range of nonhuman biota found on the Canadian Shield. We have not identified specific criteria that pertain to protection of such organisms such as an equivalent to the radiological risk criterion for humans.

It is reasonable, however, to expect that there would be no significant impacts to nonhuman biota from exposure to small dose rates. For example, in a 1992 report of the International Atomic Energy Agency (IAEA 1992), an expert committee found no evidence in the scientific literature that dose rates smaller than about 0.4 Gy/a would harm plant or animal populations. Dose rates less than 10^{-3} Gy/a have not been associated with any detectable biological effects and, moveover, plants and animals everywhere are subjected to dose rates in the range of 10^{-3} Gy/a to 10^{-1} Gy/a from natural background.

We assume, therefore, that radiological impacts to nonhuman biota are of no concern if the estimated dose rates are smaller than 10^{-3} Gy/a, the lower range of background dose rates. The results discussed earlier, in Figure 19, show that the average estimated dose rate curves for the four target organisms are well below this lower limit at all simulation times. Thus the disposal system evaluated herein would not have significant impacts on nonhuman biota in the affected regions of the biosphere.

Summary

The objective of this study is to determine whether the disposal system described herein would meet long-term performance and safety criteria. This disposal system differs from that evaluated in the EIS case study mainly in the characteristics of the engineered barriers and the natural barrier of the host geosphere.

- The engineered barriers in the present study include the use of containers fabricated from high-purity copper; most of these containers are expected to provide absolute containment and only about 1 in 5000 would slowly release contaminants that could migrate to the biosphere. The Grade-2 titanium alloy containers as modelled in the EIS case study all failed over a period of a few thousands of years.

- The properties of the host geosphere assumed in the present study are such that it has greatly reduced effectiveness as a barrier to contaminant transport. For example, groundwater transit times from the vault depth to the surface environment are about 1000 times shorter than corresponding transit times in the EIS case study.

For the disposal system described herein, we have quantitatively evaluated the radiological impacts from 41 radionuclides that are expected to be the main contributors to dose rate and for the groundwater transport scenario that describes the expected long-term behaviour of the disposal system. Although not all aspects of the postclosure assessment have been completed, the available results provide strong evidence that the disposal system would meet the radiological risk limit for humans specified by the AECB (1987) and that the disposal system would have no impacts of concern on representative organisms in the affected biosphere. Thus the results support a conclusion that a disposal system with suitably designed engineered barriers can meet long-term performance and safety criteria, even when the disposal vault is located in a geosphere where groundwater transit times from the vault depth to the surface environment are relatively short.

The results also support a conclusion that a high degree of redundancy could be achieved using the engineered barriers that are evaluated in this report, and using the natural barrier of the host geosphere that was evaluated in the EIS case study.

ACKNOWLEDGEMENTS

The authors would like to thank the many people who contributed directly and indirectly to the preparation of this report. Our colleagues made essential contributions to scenario analysis and to the development of models and data required for the analysis. They were also called on to review early drafts, and provided prompt and thoughtful comments and advice. We also gratefully acknowledge the dedicated efforts of M.L. Ryz and E.N. Henschell, who put together the intermediate and final drafts; A. Soonawala, who carried out a very fast but thorough edit; and J. Porcher and K.C. Komosky, who were instrumental in the preparation of many of the figures and plots.

This study was carried out for the Canadian Nuclear Fuel Waste Management Program, which is jointly funded by AECL and Ontario Hydro under the auspices of the CANDU Owners Group.

REFERENCES

AECB (Atomic Energy Control Board). 1987. Regulatory policy statement. Regulatory objectives, requirements and guidelines for the disposal of radioactive wastes - long-term aspects. Atomic Energy Control Board Regulatory Document R-104, 1987 June 5.

AECL (Atomic Energy of Canada Limited). 1994a. Environmental impact statement on the concept for disposal of Canada's nuclear fuel waste. Atomic Energy of Canada Report, AECL-10711, COG-93-1. Available in French and English.

AECL (Atomic Energy of Canada Limited). 1994b. Summary of the environmental impact statement on the concept for disposal of Canada's nuclear fuel waste. Atomic Energy of Canada Limited Report, AECL-10721, COG-93-11. Available in French and English.

Amiro, B.D. 1992a. The atmosphere submodel for the assessment of Canada's nuclear fuel waste management concept. Atomic Energy of Canada Limited Report, AECL-9889, COG-91-199.

Amiro, B.D. 1992b. Radiological dose conversion factors for nonhuman biota for Canada's nuclear waste management concept. Atomic Energy of Canada Limited Technical Record, TR-561*, COG-1-87.

Amiro, B.D. 1995. Radiological dose conversion factors for generic plants and animals. Atomic Energy of Canada Limited Technical Record, TR-658, COG-94-512.*

Andres, T.H. 1995. Sampling methods and sensitivity analysis for large parameter sets. Presented at the SAMO'95 international symposium on Theory and Applications of Sensitivity Analysis of Model Output in computer simulation, Belgirate, Italy, in 1995 September; submitted to the Journal of Computational Statistics and Data Analysis.

Baumgartner, P., D.M. Bilinsky, C. Onofrei, Y. Ates, F. Bilsky, J.L. Crosthwaite and G.W. Kuzyk. 1995. An in-room emplacement method for a used-fuel disposal facility - preliminary design considerations. Atomic Energy of Canada Limited Technical Report, TR-665, COG-94-533*.

Baumgartner, P., D.M. Bilinsky, Y. Ates, R.S. Read, J.L. Crosthwaite, and D.A. Dixon. 1996. Engineering for a disposal facility using the in-room emplacement method. Atomic Energy of Canada Limited Report, AECL-11595, COG-96-223.

Bird, G.A., M. Stephenson and L.J. Corbett. 1992. The surface water submodel for the assessment of Canada's nuclear fuel waste management concept. Atomic Energy of Canada Limited Report, AECL-10290, COG-91-193.

Davis, P.A., R. Zach, M.E. Stephens, B.D. Amiro, G.A. Bird, J.A.K. Reid, M.I. Sheppard, S.C. Sheppard and M. Stephenson. 1993. The disposal of Canada's nuclear fuel waste: The biosphere model, BIOTRAC, for postclosure assessment. Atomic Energy of Canada Limited Report, AECL-10720, COG-93-10.

Davison, C.C., A. Brown, R.A. Everitt, M. Gascoyne, E.T. Kozak, G.S. Lodha, C.D. Martin, N.M. Soonawala, D.R. Stevenson, G.A. Thorne and S.H. Whitaker. 1994a. The disposal of Canada's nuclear fuel waste: Site screening and site evaluation technology. Atomic Energy of Canada Limited AECL Report, AECL-10713, COG-93-3.

Davison, C.C., T. Chan, A. Brown, M. Gascoyne, D.C. Kamineni, G.S. Lodha, T.W. Melnyk, B.W. Nakka, P.A. O'Connor, D.U. Ophori, N.W. Scheier, N.M. Soonawala, F.W. Stanchell, D.R. Stevenson, G.A. Thorne, T.T. Vandergraaf, P. Vilks and S.H. Whitaker. 1994b. The disposal of Canada's nuclear fuel waste: The geosphere model for postclosure assessment. Atomic Energy of Canada Limited Report, AECL-10719, COG-93-9.

EARP (Environmental Assessment Review Panel). 1992. Final guidelines for the preparation of an environmental impact statement on the nuclear fuel waste management and disposal concept. Federal Environmental Assessment Review Office, 13th floor, Fontaine Building, 200 Sacr+ Coeur Blvd., Hull, Quèbec, K1A 0H3.

Goodwin, B.W. and K. K. Mehta. 1994. Identification of contaminants of concern for the postclosure assessment of the concept for disposal of Canada's nuclear fuel waste. Atomic Energy of Canada Limited Report, AECL-10901, COG-93-265.

Goodwin, B.W., D.B. McConnell, T.H. Andres, W.C. Hajas, D.M. LeNeveu, T.W. Melnyk, G.R. Sherman, M.E. Stephens, J.G. Szekely, P.C. Bera, C.M. Cosgrove, K.D. Dougan, S.B. Keeling, C.I. Kitson, B.C. Kummen, S.E. Oliver, K. Witzke, L. Wojciechowski and A.G. Wikjord. 1994a. The disposal of Canada's nuclear fuel waste: Postclosure assessment of a reference system. Atomic Energy of Canada Limited Report, AECL-10717, COG-93-7.

Goodwin, B.W., M.E. Stephens, C.C. Davison, L.H. Johnson and R. Zach. 1994b. Scenario analysis for the postclosure assessment of the Canadian concept for nuclear fuel waste disposal. Atomic Energy of Canada Limited Report, AECL-10969, COG-94-247.

Goodwin, B.W., W.C. Hajas and D.M. LeNeveu. 1996a. Effect of long-lived containers on the postclosure performance of a reference disposal system. Atomic Energy of Canada Limited Report, AECL-11461, COG-95-497.

Goodwin, B.W., W.C. Hajas, D.M. LeNeveu and D.M. Wuschke. 1996b. A scoping comparison of the effect of in-room and borehole emplacement on the long-term performance of a deep geological disposal system. Atomic Energy of Canada Technical Record, TR-736*, COG-96-30.

Greber, M., E.R. Frech and J.A.R. Hiller. 1994. The disposal of Canada's nuclear fuel waste: Public involvement and social aspects. Atomic Energy of Canada Limited Report, AECL-10712, COG-93-9.

Grondin, L., K. Johansen, W.C. Cheng, M. Fearn-Duffy, C.R. Frost, T.F. Kempe, J. Lockhart-Grace, M. Paez-Victor, H.E. Reid, S.B. Russell, C.H. Ulster, J.E. Villagran and M. Zeya. 1994. The disposal of Canada's nuclear fuel waste: Preclosure assessment of a conceptual system. Ontario Hydro Report, N-03784-940010 (UFMED)**, COG-93-6.

Heinrich, W.F. and T.H. Andres. 1985. Response functions of the advection-dispersion equation describing radionuclide migration in a semi-infinite medium; Annals of Nuclear Energy 12 (12), 685-691. Also, Atomic Energy of Canada Limited Report, AECL-8691.

IAEA (International Atomic Energy Agency). 1992. Effects of ionizing radiation on plants and animals at levels implied by current radiation protection standards. International Atomic Energy Agency, Vienna, Austria, Technical Report Series No. 332.

ICRP (International Commission on Radiological Protection). 1991a. 1990 recommendations of the International Commission on Radiological Protection. Annals of the ICRP 21(1-3) (ICRP Publication 60).

ICRP (International Commission on Radiological Protection). 1991b. Annual limits on intake of radionuclides by workers based on the 1990 recommendations. Annals of the ICRP 21(4) (ICRP Publication 61).

Joint Statement. 1978. Joint statement by the Minister of Energy, Mines and Resources Canada and the Ontario Minister of Energy, 1978 June 05. Printing and Publishing, Supply and Services Canada, Ottawa, Canada K1A 0S9.

Joint Statement. 1981. Joint Statement by the Minister of Energy, Mines and Resources Canada and the Ontario Minister of Energy, 1981 August 04. Printing and Publishing, Supply and Services Canada, Ottawa, Canada K1A 0S9.

Johnson, L.H., B.W. Goodwin, S.C. Sheppard, J.C. Tait, D.M. Wuschke, C.C. Davison. 1995 Radiological assessment of ^{36}Cl in the disposal of used CANDU fuel. Atomic Energy of Canada Limited Report AECL-11213, COG-94-527.

Johnson, L.H., J.C. Tait, D.W. Shoesmith, J.L. Crosthwaite and M.N. Gray. 1994a. The disposal of Canada's nuclear fuel waste: Engineered barriers alternatives. Atomic Energy of Canada Limited Report, AECL-10718, COG-93-8.

Johnson, L.H., D.M. LeNeveu, D.W. Shoesmith, D.W. Oscarson, M.N. Gray, R.J. Lemire and N. Garisto. 1994b. The disposal of Canada's nuclear fuel waste: The vault model for postclosure assessment. Atomic Energy of Canada Limited Report, AECL-10714, COG-93-4.

Johnson, L.H., D.M. LeNeveu, F. King, D.W. Shoesmith, M. Kolár, D.W. Oscarson, S. Sunder, C. Onofrei and J.L. Crosthwaite. 1996. The Disposal of Canada's Nuclear Fuel Waste: A study of postclosure safety of in-room emplacement of used CANDU fuel in copper containers in permeable plutonic rock. Volume 2: Vault Model. Atomic Energy of Canada Limited Report, AECL-11494-2, COG-95-552-2.

Kolár , M., D.M. LeNeveu and L.H. Johnson. 1994. Near-field transport of ^{129}I from a point source in an in-room disposal vault. Presented at he XVIII International Symposium for the Scientific Basis for Nuclear Waste Management, Materials Research Society, Kyoto, Japan, 1994.

Kolár, M. and D.M. LeNeveu. 1995. Near-field mass transport from a point source (Instantly failed container) located in a disposal room. Atomic Energy of Canada Limited Report AECL-11172, COG-I-94-444, 1995.

LeNeveu, D.M. and M. Kolár . 1996. Radionuclide response functions to the advection-dispersion equation for a point source along the axis of nested cylindrical media. Atomic Energy of Canada Limited Report AECL-11549, COG-96-90.

LeNeveu, D. 1994. Analysis Specifications for the CC3 Vault Model. Atomic Energy of Canada Limited Report, AECL-10970, COG-94-100.

LeNeveu, D.M. 1996. Radionuclide release rates from a pinhole in a waste container for an inventory-limited and a constant concentration source. Atomic Energy of Canada Limited Report AECL-11540, COG-96-68.

Melnyk, T.W. 1995. Analysis Specifications for the CC3 Geosphere Model. Atomic Energy of Canada Limited Report, AECL-10977, COG-94-101.

Ophori, D.U., D.R. Stevenson, M. Gascoyne, A. Brown, C.C. Davison, T. Chan and F.W. Stanchell. 1995. Revised model of regional groundwater flow of the Whiteshell Research Area: Summary. Atomic Energy of Canada Limited Report, AECL-11286, COG-95-115.

Ophori, D.U., A. Brown, T. Chan, C.C. Davison, M. Gascoyne, N.W. Scheier, F.W. Stanchell and D.R. Stevenson. 1996. Revised model of regional groundwater flow in the Whiteshell Research Area. Atomic Energy of Canada Limited Report, AECL-11435, COG-95-443.

Shoesmith, D.W., F. King and B.M. Ikeda. 1995. An assessment of the feasibility of indefinite containment of Canadian nuclear fuel wastes. Atomic Energy of Canada Limited Report, AECL-10972, COG-94-534.

SKB (Svensk Kärnbränslehantering AB) 1992. SKB 91. Final disposal of spent nuclear fuel. Importance of the bedrock for safety. Swedish Nuclear Fuel and Waste Management Co. Report 92-20.

Sheppard, M.I. 1992. The soil submodel, SCEMR1, for the assessment of Canada's nuclear fuel waste management concept. Atomic Energy of Canada Limited Report, AECL-9577, COG-91-194.

Simmons, G.R. and P. Baumgartner. 1994. The disposal of Canada's nuclear fuel waste: Engineering for a disposal facility. Atomic Energy of Canada Limited Report, AECL-10715, COG-93-5.

Stanchell, F.W., C.C. Davison, T.W. Melnyk, N.W. Scheier and T. Chan. 1996. The Disposal of Canada's Nuclear Fuel Waste: A study of postclosure safety of in-room emplacement of used CANDU fuel in copper containers in permeable plutonic rock. Volume 3: Geosphere Model. Atomic Energy of Canada Limited Report, AECL-11494-3, COG-95-552-3.

Stevenson, D.R., A. Brown, C.C. Davison, M. Gascoyne, R.G. McGregor, D.U. Ophori, N.W. Scheier, F.W. Stanchell, G.A. Thorne and D.K. Tomsons. 1995. A revised conceptual hydrogeologic model of a crystalline rock environment, Whiteshell Research Area, Southeastern Manitoba, Canada. Proceedings of Solutions '95, International Association of Hydrogeologists, Congress XXVI, June 4-10, 1995, Edmonton, Alberta, Canada.

Stevenson, D.R., A. Brown, C.C. Davison, M. Gascoyne, R.G. McGregor, D.U. Ophori, N.W. Scheier, F.W. Stanchell, G.A. Thorne and D.K. Tomsons. 1996. A revised conceptual hydrogeologic model of a crystalline rock environment, Whiteshell Research Area, southeastern Manitoba, Canada. Atomic Energy of Canada Limited Report, AECL-11331, COG-95-271.

Szekely, J.G., L.C. Wojciechowski, M.E. Stephens and H.A. Halliday. 1994. Analysis specifications for the CC3 Biosphere Model BIOTRAC. Atomic Energy of Canada Limited Report, AECL-11078, COG-94-102.

Ticknor, K.V. and T.T. Vandergraaf. 1996. A revised compilation of sorption coefficients for use in geosphere models in performance assessments of used fuel disposal in granitic environments. Atomic Energy of Canada Limited Report, AECL-11343, COG-96-71.

Tait, J.C. and J.R. Theaker. 1996. Light element radionuclides in used CANDU fuel and their potential contribution to postclosure safety assessment. Atomic Energy of Canada Limited Report, AECL-11431, COG-95-440.

Vandergraaf, T.T., K.V. Ticknor and T.W. Melnyk. 1992. The selection and use of a sorption data base for the geosphere model in the Canadian nuclear fuel waste management program. In Radionuclide Sorption from the Safety Evaluation Perspective, proceedings of an NEA Workshop held in Interlaken, Switzerland, 1991 October, Nuclear Energy Agency, Organisation for Economic Cooperation and Development, Paris, 1992.

Wai, R.S.C. and A. Tsai. 1995. Three-dimensional thermal and thermal-mechanical analyses for a used-fuel disposal vault with the in-room emplacement option. Ontario Hydro Report No. N-REP-03780-0083 R00.**

Wikjord, A.G., P. Baumgartner, L.H. Johnson, F.W. Stanchell, R. Zach and B.W. Goodwin. 1996. The Disposal of Canada's Nuclear Fuel Waste: A study of postclosure safety of in-room emplacement of used CANDU fuel in copper containers in permeable plutonic rock. Volume 1: Summary. Atomic Energy of Canada Limited Report, AECL-11494-1, COG-95-552-1.

Zach, R., and S.C. Sheppard. 1992. The food-chain and dose submodel, CALDOS, for the assessment of Canada's nuclear fuel waste management concept. Atomic Energy of Canada Limited Report, AECL-10165, COG-91-195.

Zach, R., B.D. Amiro, G.A. Bird, C.R. Macdonald, M.I. Sheppard, S.C. Sheppard and J.G. Szekely. 1996. The Disposal of Canada's Nuclear Fuel Waste: A study of postclosure safety of in-room emplacement of used CANDU fuel in copper containers in permeable plutonic rock. Volume 4: Biosphere Model. Atomic Energy of Canada Limited Report, AECL-11494-4, COG-95-552-4.

---

* Internal report available from SDDO, AECL Research, Chalk River Laboratories, Chalk River, Ontario K0J 1J0.

** Unrestricted report available from Ontario Hydro, 700 University Avenue, Toronto, Ontario M5G 1X6.

APPENDIX

ANALYSIS OF SELECTED SIMULATIONS

CONTENTS

LIST OF TABLES

LIST OF FIGURES

LIST OF FIGURES (Continued)

APPENDIX

ANALYSIS OF SELECTED SIMULATIONS

A.1 SELECTION OF SIMULATIONS

A.1.1 INTRODUCTION

In this Appendix, we present a detailed analysis of four selected simulations. One is similar to the median-value simulation from the EIS (which we call here the MV Simulation), and the other three are selected from a special set of 32 simulations that were designed to cover the parameter sample space (uncertainty space). The parameter selection strategy used to select these 32 simulations is called a two-level fractional-factorial latin-hypercube design (Andres 1995). Having 32 simulations gives confidence that the set will contain at least one simulation from the top and bottom 5% of estimated dose rates. The latin-hypercube aspect ensures that every part of each parameter's range is examined. The two-level fractional-factorial aspect ensures that all combinations of low and high parameter values for any 3 independent parameters occur the same number of times.

Table A-1 lists dose rates at 10^4 a and the values of several influential and calculated parameters for the 32 simulations and for the MV Simulation. The simulations are sorted in order of decreasing estimated dose rate at 10^4 a.

A.1.2 OVERVIEW OF THE RESULTS FROM THE MV SIMULATION AND THE 32 FRACTIONAL-FACTORIAL SIMULATIONS

In the 32-fractional-factorial simulations and the MV Simulation, ^{129}I is the main contributor to estimated dose rate to 10^4 a in 24 of the simulations and ^{36}Cl from fuel is the main contributor in the other 9 simulations. The most influential parameter, from the probabilistic sensitivity analysis in Section 6.3, is the source of domestic water for the critical group (PRODMD). Of the 17 simulations with the highest dose rate, all but simulation #31 have the well as the source of domestic water.

A cursory look at Table A-1 to identify influential parameters makes it clear that the source of domestic water is important; however, the other influential parameters identified in the probabilistic sensitivity analysis are not so discernible. For example, the iodine aqueous mass loading coefficient (IMLA), which was the second-most influential parameter at 10^4 a, does not show a strong correlation between its values and the dose rates in this set of 32 fractional-factorial simulations. In fact, IMLA takes on its largest value in the ninth lowest dose-rate simulation (#8), and its second highest value is in the fifth highest dose-rate simulation (#29). We observe that one particular parameter does not determine if the dose rate is large or small in this set of simulations with wide ranging parameter values; it is particular combinations of parameters that are important. Moreover, the identification of the most influential parameters cannot be easily (and accurately) done by visual inspection of these results. Instead, statistical measures must be used (as was done in Section 6.3).

Although this set of 32 fractional-factorial simulations is not sufficient to clearly identify the influential parameters in the system model, the set is useful for selecting, from simulations that cover a wide variety of conditions, those simulations that have dose rates near both the high and low ends of the range of dose rate estimates.

TABLE A-1

SUMMARY OF SELECTED INFLUENTIAL PARAMETERS[+] AND RESULTS FROM THE MV SIMULATION AND FROM THE 32 FRACTIONAL-FACTORIAL SIMULATIONS

Simulation #	Maximum Dose Rate up to 10^4 a[*] [Sv/a]	Source of Domestic Water (PRODMD) [-]	Source of Irrigation of Garden [-]	Size of Critical Group (NUMMAN) [-]	Soil Type [-]	Biosphere Performance Factor for ^{129}I[*] (to 10^4 a) [Sv/mol]
27	1.2×10^{-5}	Well	Well	3	Clay	0.28
31	1.2×10^{-5}	Lake	Lake	5	Organic	0.36
21	1.0×10^{-5}	Well	Well	4	Sand	0.17
MV	4.7×10^{-6}	Well	Well	3	Sand	0.15
14	4.6×10^{-6}	Well	Well	3	Sand	0.43
29	4.4×10^{-6}	Well	Lake	6	Clay	0.12
6	4.4×10^{-6}	Well	Well	2	Organic	0.22
26	2.8×10^{-6}	Well	Well	2	Clay	0.20
15	2.6×10^{-6}	Well	Well	2	Sand	0.10
12	2.4×10^{-6}	Well	Well	5	Sand	0.17
18	2.4×10^{-6}	Well	Well	2	Sand	0.21
19	1.9×10^{-6}	Well	Well	2	Sand	0.038
1	1.7×10^{-6}	Well	Well	4	Sand	0.17
7	1.5×10^{-6}	Well	Well	2	Clay	0.069
24	#1.0×10^{-6}	Well	Well	6	Sand	0.00039
4	7.2×10^{-7}	Well	Well	8	Sand	0.038
9	5.9×10^{-7}	Well	None	6	Sand	0.11
32	4.7×10^{-7}	Well	Well	7	Clay	0.028
22	2.3×10^{-7}	Lake	Lake	4	Sand	0.011
30	#1.7×10^{-7}	Lake	None	9	Clay	0.015
10	1.6×10^{-7}	Lake	Lake	4	Sand	0.014
16	#1.4×10^{-7}	Lake	Lake	3	Sand	0.0010
5	1.4×10^{-7}	Lake	None	1	Organic	0.026
11	1.0×10^{-7}	Lake	Lake	11	Sand	0.030
8	7.9×10^{-8}	Lake	Lake	1	Clay	0.010
28	6.2×10^{-8}	Lake	Lake	2	Organic	0.010
20	#5.7×10^{-8}	Lake	Lake	3	Sand	0.0040
25	4.5×10^{-8}	Lake	Lake	3	Clay	0.0017
17	#4.0×10^{-8}	Lake	Lake	3	Sand	0.00074
23	#8.8×10^{-9}	Lake	Lake	5	Sand	0.00022
3	#8.3×10^{-9}	Lake	Lake	4	Loam	0.00063
2	#7.0×10^{-9}	Lake	Lake	5	Loam	0.00028
13	#5.2×10^{-9}	Lake	None	3	Sand	0.0034

[+] The name for influential parameters (as used in PR4) is listed to provide an unambiguous cross-reference to the text.

[*] Calculated parameter. All others are sampled input parameters.

Principal contributor to dose rate is ^{36}Cl. The principal contributor is ^{129}I in all the other simulations.

continued .../

TABLE A-1 (Continued)

	Well Demand* [m^3/a]	Well Depth (DPTHWL) [m]	Fraction of Plume in LD1 Captured by the Well* [-]	Comment	Thickness of Overburden at Boggy Creek South THICKOV(BCSAQ) [m]
27	2800	35	0.43		4.1
31	0	—	0.0	No well	4.9
21	2660	82	0.48		2.1
MV	1330	34	0.29		3.8
14	1190	41	0.28		1.2
29	1320	3	0.0	Overburden well+	2.5
6	1780	22	0.30		2.5
26	1410	18	0.25		4.0
15	938	33	0.23		0.5
12	1830	17	0.28		8.2
18	505	49	0.12		11
19	1090	13	0.19		4.8
1	1150	28	0.26		7.1
7	2100	72	0.41		1.0
24	2160	10	0.0	Overburden well+	0.7
4	4120	55	0.59		9.3
9	1100	100	0.17		7.3
32	11600	43	0.79		2.0
22	0	—	0.0	No well	8.5
30	0	—	0.0	No well	5.3
10	0	—	0.0	No well	0.3
16	0	—	0.0	No well	14
5	0	—	0.0	No well	5.7
11	0	—	0.0	No well	3.5
8	0	—	0.0	No well	4.6
28	0	—	0.0	No well	0.1
20	0	—	0.0	No well	2.9
25	0	—	0.0	No well	3.1
17	0	—	0.0	No well	1.5
23	0	—	0.0	No well	5.9
3	0	—	0.0	No well	3.8
2	0	—	0.0	No well	1.7
13	0	—	0.0	No well	6.5

* Calculated parameter. All others are sampled input parameters.

+ Overburden well that draws water from near surface sources and does not intersect the radionuclide plume in fracture zone LD1. All other wells are bedrock wells that are sited so that they just reach LD1.

continued ..../

TABLE A-1 (continued)

Simulation #	Used Fuel Corrosion Parameter+ (STDNOG) [-]	Fraction of Fuel Dissolved in 10^4 a* [-]	Probability of Fabrication Defects (IFRACT) [-]	Number of Failed Containers*# [-]	Integrated Vault Output for ^{129}I up to 10^4 a* [mol]
27	-0.53	0.013	1 in 2700	22	0.36
31	0.67	0.020	1 in 4300	17	0.34
21	1.53	0.066	1 in 2900	30	1.1
MV	0.0	0.014	1 in 4900	24	0.39
14	-1.07	0.007	1 in 8000	8	0.11
29	0.74	0.027	1 in 3600	17	0.32
6	-0.62	0.010	1 in 5900	11	0.23
26	-1.47	0.004	1 in 3200	18	0.25
15	-0.28	0.019	1 in 6300	10	0.23
12	0.79	0.032	1 in 7400	5	0.13
18	-0.68	0.007	1 in 3800	14	0.14
19	-0.97	0.018	1 in 4100	21	0.50
1	0.32	0.016	1 in 6700	11	0.09
7	-0.23	0.019	1 in 8400	12	0.21
24	0.90	0.046	1 in 2100	35	0.62
4	0.24	0.021	1 in 6800	7	0.18
9	0.43	0.017	1 in 7600	8	0.08
32	1.35	0.055	1 in 4900	14	0.29
22	1.30	0.050	1 in 3900	15	0.42
30	0.03	0.024	1 in 4600	8	0.20
10	0.53	0.029	1 in 5100	9	0.10
16	-1.81	0.006	1 in 5300	14	0.21
5	-0.33	0.014	1 in 6000	8	0.08
11	0.08	0.010	1 in 5400	7	0.12
8	-0.49	0.008	1 in 6500	7	0.15
28	-0.84	0.007	1 in 4400	17	0.13
20	-1.95	0.001	1 in 4600	12	0.08
25	-0.12	0.020	1 in 3400	11	0.22
17	-0.06	0.020	1 in 2500	23	0.35
23	0.22	0.014	1 in 3500	23	0.32
3	1.92	0.077	1 in 9300	6	0.09
2	1.04	0.036	1 in 5000	10	0.12
13	-1.15	0.009	1 in 5500	12	0.12

* Calculated parameter. All others are sampled input parameters

\+ Elsewhere referred to as the variability in the magnitude of UO_2 corrosion from radiolysis of water by γ-radiation.

\# Determined by IFRAC, IFAILQ (the binomial probability variate for the number of container failures within each vault sector) and the number of containers in each sector.

continued .../

TABLE A-1 (continued)

Simulation #	Effective Transport Porosity of Lower Rock Zone (SGPROS LWROC)) [-]	Effective Transport Porosity of Middle Rock Zone (SGPROS (MIROC)) [-]	Effective Transport Porosity of Upper Rock Zone (SGPROS (UPROC)) [-]	Effective Transport Porosity of Fracture Zone (SGPROS (FZONE)) [-]
27	1.0×10^{-5}	1.4×10^{-4}	3.4×10^{-4}	5.4×10^{-2}
31	1.4×10^{-5}	1.2×10^{-4}	1.4×10^{-5}	4.6×10^{-2}
21	3.3×10^{-4}	7.1×10^{-4}	6.4×10^{-5}	1.4×10^{-2}
MV	1.0×10^{-4}	1.0×10^{-4}	1.0×10^{-4}	3.2×10^{-2}
14	3.0×10^{-5}	3.2×10^{-4}	1.8×10^{-5}	7.6×10^{-2}
29	6.5×10^{-5}	1.5×10^{-5}	4.3×10^{-5}	2.3×10^{-2}
6	2.1×10^{-4}	1.9×10^{-5}	1.6×10^{-5}	3.9×10^{-2}
26	8.9×10^{-4}	1.5×10^{-5}	1.3×10^{-5}	1.3×10^{-2}
15	1.2×10^{-4}	4.8×10^{-5}	9.1×10^{-4}	1.8×10^{-2}
12	3.6×10^{-5}	1.1×10^{-5}	4.8×10^{-4}	2.7×10^{-2}
18	6.2×10^{-5}	8.5×10^{-4}	2.2×10^{-5}	1.1×10^{-2}
19	1.5×10^{-4}	1.2×10^{-5}	2.6×10^{-4}	6.7×10^{-2}
1	3.7×10^{-5}	3.4×10^{-5}	3.0×10^{-5}	8.2×10^{-2}
7	1.8×10^{-5}	5.3×10^{-4}	1.6×10^{-4}	1.2×10^{-2}
24	4.9×10^{-5}	5.4×10^{-5}	1.2×10^{-4}	3.6×10^{-2}
4	2.4×10^{-4}	1.0×10^{-4}	6.0×10^{-4}	2.0×10^{-2}
9	4.6×10^{-4}	4.0×10^{-4}	4.2×10^{-5}	4.9×10^{-2}
32	5.0×10^{-4}	1.9×10^{-4}	7.3×10^{-4}	9.6×10^{-2}
22	1.7×10^{-5}	2.6×10^{-4}	7.7×10^{-4}	1.8×10^{-2}
30	1.8×10^{-4}	7.5×10^{-5}	1.8×10^{-4}	2.8×10^{-2}
10	8.0×10^{-5}	1.6×10^{-4}	4.1×10^{-4}	6.3×10^{-2}
16	9.7×10^{-5}	2.5×10^{-5}	9.2×10^{-5}	3.1×10^{-2}
5	2.1×10^{-5}	4.2×10^{-5}	1.4×10^{-4}	8.7×10^{-2}
11	1.7×10^{-4}	2.9×10^{-5}	6.9×10^{-5}	2.4×10^{-2}
8	5.9×10^{-4}	3.0×10^{-4}	2.7×10^{-5}	1.0×10^{-2}
28	1.1×10^{-4}	5.7×10^{-4}	1.1×10^{-5}	4.3×10^{-2}
20	2.7×10^{-5}	5.7×10^{-5}	5.3×10^{-5}	3.4×10^{-2}
25	1.3×10^{-5}	7.3×10^{-5}	1.2×10^{-4}	1.5×10^{-2}
17	8.2×10^{-4}	9.9×10^{-4}	2.3×10^{-4}	2.2×10^{-2}
23	7.3×10^{-4}	2.4×10^{-5}	7.6×10^{-5}	7.0×10^{-2}
3	4.4×10^{-5}	2.3×10^{-4}	3.4×10^{-5}	1.6×10^{-2}
2	2.7×10^{-4}	9.0×10^{-5}	2.9×10^{-4}	5.6×10^{-2}
13	4.1×10^{-4}	4.7×10^{-4}	5.5×10^{-4}	4.1×10^{-2}

continued ..../

TABLE A-1 (concluded)

Simulation #	Axial Permeability of the excavation damaged zone (DZPERA) [m^2]	Iodine Aquatic Mass-Loading Coefficient (IMLA) [-]	Plant/Soil Concentration Factor for Iodine (XCRTIO (I)) [-]	Plant/Soil Concentration Factor for Chlorine (XCRTIO (Cl)) [-]
27	1.1×10^{-16}	8.5×10^{-6}	0.27	48
31	1.4×10^{-17}	5.4×10^{-5}	0.13	5.1
21	4.1×10^{-16}	2.7×10^{-6}	0.024	2.7
MV	1.3×10^{-16}	1.3×10^{-5}	0.038	18
14	3.7×10^{-17}	5.6×10^{-6}	0.75	3.8
29	1.8×10^{-16}	3.6×10^{-4}	1.50	35
6	1.7×10^{-17}	3.8×10^{-5}	0.0036	58
26	1.6×10^{-16}	6.0×10^{-7}	0.035	14
15	1.8×10^{-15}	6.8×10^{-6}	0.00071	370
12	4.2×10^{-15}	1.7×10^{-5}	0.045	0.33
18	6.2×10^{-16}	8.1×10^{-5}	0.17	210
19	6.2×10^{-17}	2.4×10^{-5}	0.0020	0.67
1	2.3×10^{-17}	4.2×10^{-7}	0.060	3.9
7	2.5×10^{-16}	1.8×10^{-5}	0.072	6.3
24	4.5×10^{-17}	1.3×10^{-6}	0.093	140
4	2.2×10^{-16}	2.5×10^{-6}	0.029	500
9	2.0×10^{-17}	1.4×10^{-4}	0.0040	150
32	3.3×10^{-17}	2.0×10^{-4}	0.0016	1.0
22	1.1×10^{-14}	1.7×10^{-6}	1.11	0.18
30	2.9×10^{-15}	4.9×10^{-5}	0.0060	740
10	5.5×10^{-17}	3.3×10^{-5}	0.32	23
16	8.1×10^{-16}	4.1×10^{-6}	0.52	100
5	8.6×10^{-17}	1.4×10^{-5}	0.22	27
11	4.6×10^{-16}	9.8×10^{-5}	0.015	8.4
8	6.2×10^{-15}	4.0×10^{-4}	0.021	9.0
28	1.3×10^{-16}	3.6×10^{-6}	0.00022	71
20	7.0×10^{-17}	2.9×10^{-5}	0.11	18
25	3.1×10^{-16}	1.1×10^{-6}	6.72	11
17	5.9×10^{-14}	2.2×10^{-5}	0.0072	38
23	1.2×10^{-17}	4.7×10^{-6}	0.013	3000
3	1.1×10^{-15}	1.1×10^{-5}	0.051	18
2	1.2×10^{-17}	1.2×10^{-5}	0.011	1.3
13	2.6×10^{-17}	7.9×10^{-6}	0.0092	1.8

A.1.3 SELECTION OF EXAMPLE SIMULATIONS

The MV Simulation was selected as an example since a similar simulation was described in the postclosure document in the EIS (Goodwin et al. 1994). In this simulation, most parameters take on the median values of their probability distributions. The exceptions involve parameters that control mutually exclusive choices (switch parameters) and parameters that control the number of failed containers.

- Values for the switch parameters are either the most probable value (e.g., soil type as sand) or the value that yields the largest estimated dose (e.g., the well is the source of domestic water rather than the lake.)

- Parameters affecting container failures are adjusted to ensure there is precisely one failed container in each of the 24 vault sectors.

We also selected three example simulations from the set of 32 fractional-factorial simulations:

- the two simulations that produced the largest and second largest estimated dose rate at 10^4 a to member of the critical group (Simulations #27 and Simulation #31.)

- one simulation that produced a small estimated dose rate. (Simulation #3). This simulation has the smallest dose rate value up to 10^7 a and the third smallest dose rate value up to the 10^4 a simulation time.

With this choice of simulations we describe in detail a wide variety of differing features and parameter values. However, the combinations of parameter values for the simulations in Table A-1 are not the only combinations that can give high or low estimates of dose rates; other combinations may also produce extreme estimates of dose rates to the critical group.

In the sections that follow we describe the features and processes of these four example simulations. We first describe the behaviour of the vault model in the four simulations followed by a description of the behaviours of the geosphere model and the biosphere model.

A.2 FEATURES OF THE VAULT MODEL

A.2.1 INTRODUCTION

The vault model is outlined in Section 5.2 and described in more detail by Johnson et al. (1996). It simulates the following processes:

- container failure;
- release of contaminants from the used-fuel bundles into the interior of the container;
- precipitation of contaminants inside the container;
- diffusion of contaminants out of the container through a small defect; and
- transport of contaminants through the buffer, backfill and excavation damaged zone (EDZ) into the rock surrounding the disposal vault.

Four vault parameters were determined to be influential in the probabilistic sensitivity analysis (Section 6.3):

- the probability of fabrication defects (IFRACT),
- the binomial probability variate determining the number of container failures within a sector (IFAILQ),
- the variability in the magnitude of the UO_2 corrosion rate caused from radiolysis of water by γ-radiation (STDNOG), and
- the axial permeability of the EDZ (DZPERA).

The first two parameters determine the number of containers that are assumed to fail, the next parameter affects the process of dissolution of used fuel and the last parameter affects the process of mass transport through the buffer, backfill and EDZ. We describe here the main processes in the vault model and the effect of these four influential parameters on these processes.

A.2.2 CONTAINER FAILURE

In the vault model, we assume that the only container failures are initial failures from fabrication defects. The number of failed containers (determined using IFRACT and IFAILQ) is influential in determining the dose rate. In the MV Simulation, we chose values for IFAILQ so that precisely one container fails in each sector of the vault. In the other three example simulations, #27, #31 and #3, the failures are determined by sampling and are more representative of the pattern of random failures expected to occur.

The MV Simulation has 24 failed containers and the total number of failures in Simulations #27, #31 and #3 are 22, 17 and 6 respectively. The pattern of failures by vault sector is shown in Figure A-1. In Simulations #27, #31 and #3, the number of failed containers is correlated with dose rate, with the largest number of failures corresponding to the simulation with the largest dose rate and the smallest number of failures corresponding to the simulation with the lowest dose rate. However, the correlation between the number of failed containers and the dose rate in the simulations in Table A-1 is not very strong.

A.2.3 RELEASE OF CONTAMINANTS FROM USED-FUEL BUNDLES

The used-fuel bundles consist of irradiated UO_2 fuel and Zircaloy sheaths. Contaminants are released from the UO_2 fuel by instant-release and congruent-release mechanisms, and from the Zircaloy by the congruent-release mechanism (Johnson et. al. 1994b). The instant-release fractions are illustrated in Figure A-2 for four radionuclides: ^{129}I, ^{90}Sr, ^{99}Tc, and ^{135}Cs. The figure shows that the variability in instant-release fractions for each radionuclide is quite small between the example simulations. This small variability is consistent with the small standard deviations in the instant-release fractions for these radionuclides (0.008 for ^{90}Sr and 0.01 for the others).

The fraction of the UO_2 matrix dissolved through the effects of radiolysis of the water in the container is given in Table A-2. The models are less acceptable representations of the disposal system at long times and results at 10^7 a are shown only for completeness.

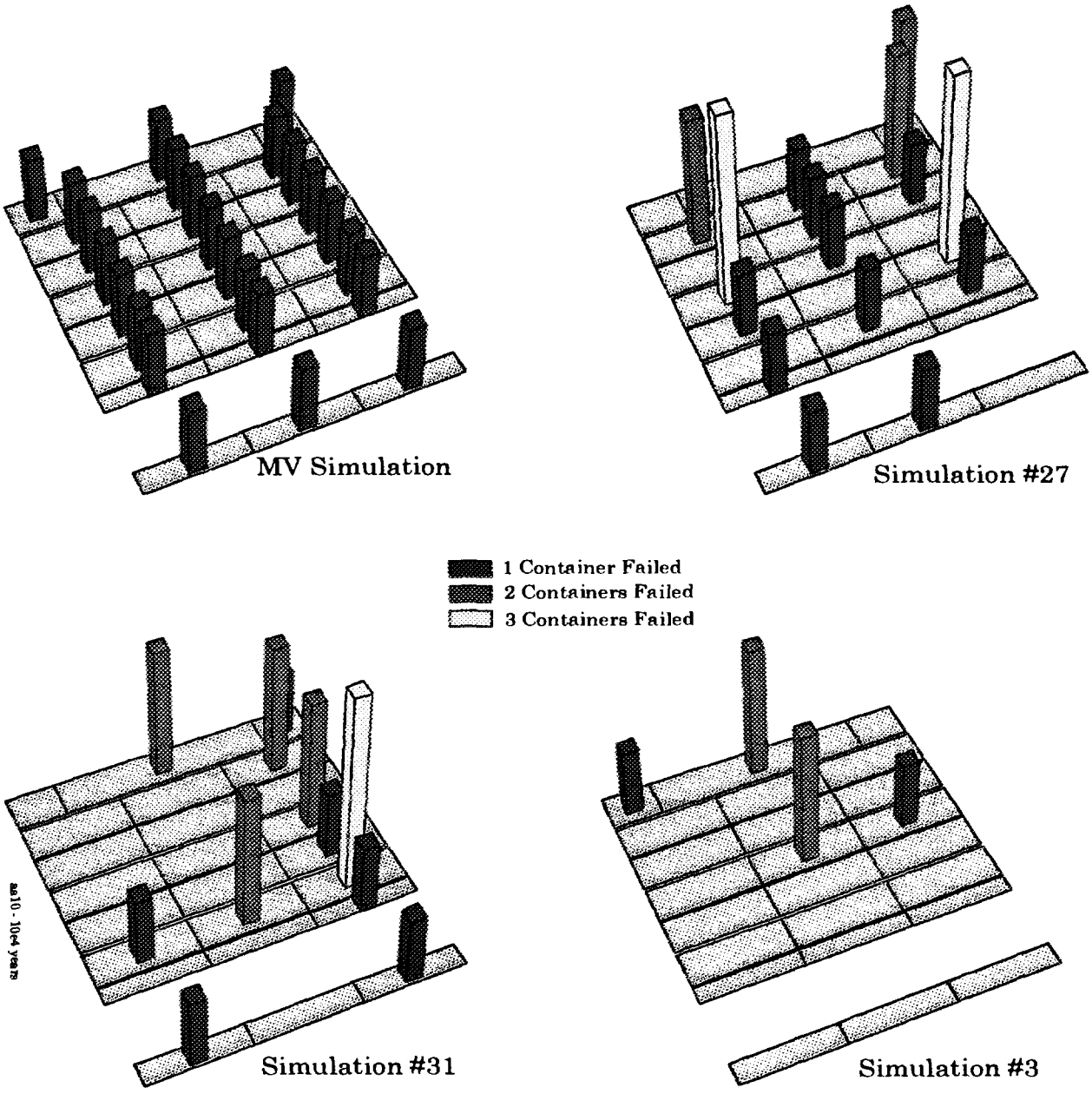

FIGURE A-1: Number of Failed Containers in Each Vault Sector for the Four Example Simulations. The number of failures per sector varies between zero and three in these simulations.

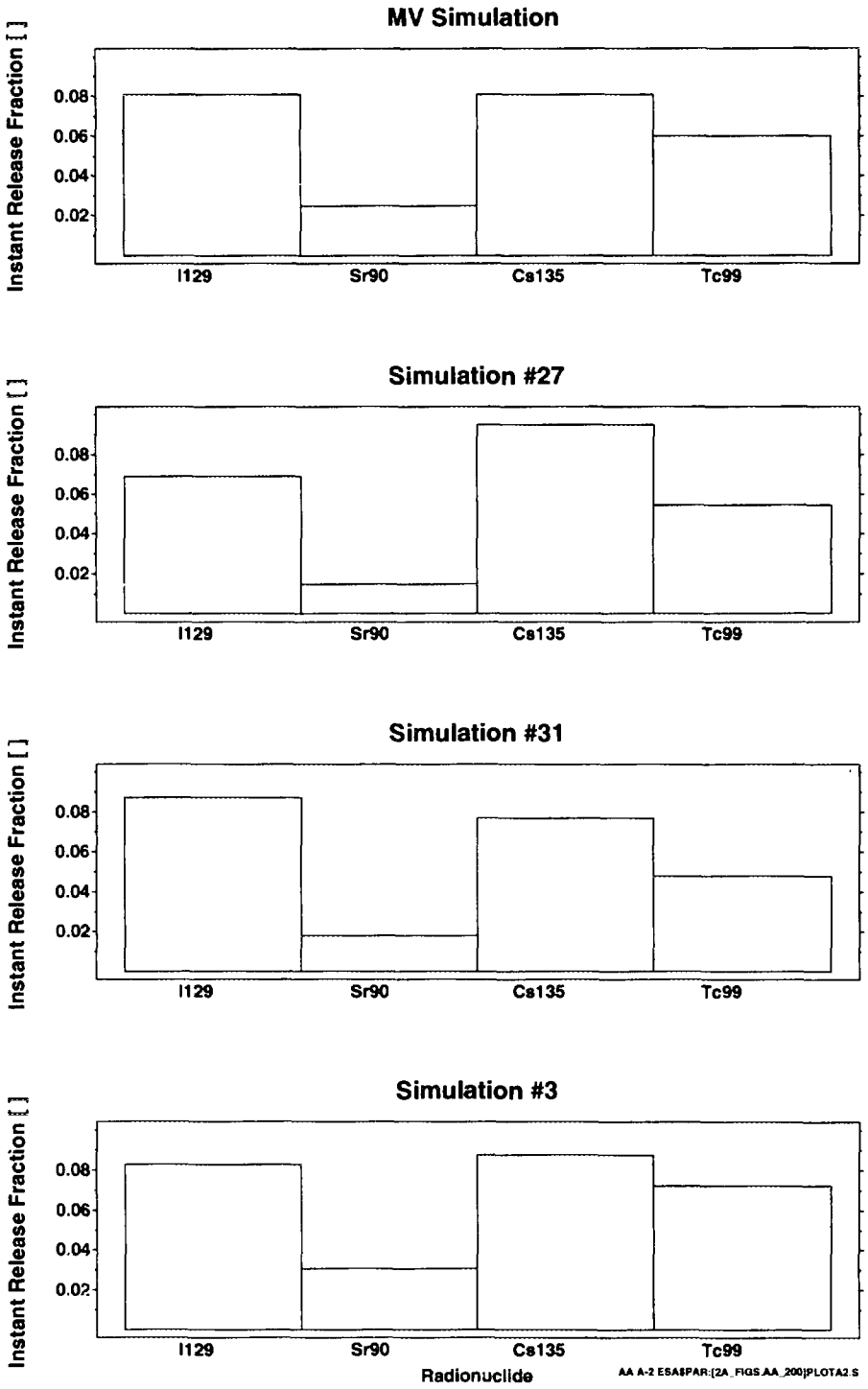

FIGURE A-2: Instant-Release Fractions for ^{129}I, ^{90}Sr, ^{99}Tc, and ^{135}Cs in the Four Example Simulations

TABLE A-2

FRACTION OF FUEL DISSOLVED

Simulation	Fraction Dissolved [-] at 10^4 a	10^7 a
MV Simulation	0.015	0.36
Simulation #27	0.013	0.89
Simulation #31	0.020	0.56
Simulation #3	0.077	1.00

The amount of the used fuel matrix dissolved because of radiolysis effects can be quite large; for example, about 8% dissolves in 10^4 a in Simulation #3. Figure A-3 shows the fraction of used fuel dissolved as a function of time for the four example simulations. Before 10^2 a, there is relatively more rapid dissolution because radiolysis from β- and γ-radiation is relatively high. The plateau between 10^2 a and 10^4 a occurs because the rate of radiolysis becomes about 3 orders of magnitude smaller. The apparent rapid increase on Figure A-3 after 10^5 a is an artifact of the logarithmic scales. It should be noted, however, that these results are very conservative. For example, our model assumes that the used fuel has been out of the reactor for only 10 a and that resaturation of the buffer and backfill is complete at the time of vault closure. Both of these assumptions lead to overestimates of the effects of radiolysis and the dissolution rate of the used-fuel matrix.

The fraction of Zircaloy dissolved is negligible in comparison with the used fuel dissolved. For example, in Simulation #27, the fraction of Zircaloy dissolved within 10^7 a is only 3×10^{-12}.

Since the peak release rate from the vault for most of the major contributors has occurred before 10^5 a, it is the plateau value that is important in determining the dose rate. Since the plateau values of the fraction of fuel dissolved by radiolysis is about the same as the instant-release fraction in some simulations, we might expect that these two parameters would be equally important in determining dose consequence. However, because the fraction of fuel dissolved has much more variability than the instant-release fraction, the sensitivity analysis determines that a parameter controlling fraction of fuel dissolved (STDNOG) is more influential than the instant-release fraction.

The sensitivity analysis (Section 6.3) indicates that the variability in the magnitude of the UO_2 corrosion rate caused by γ-radiation (STDNOG) has a strong influence on dose rates. However, Simulation #3, which has the lowest dose rate of the four example simulations, has the largest fraction of fuel dissolved. These four simulations suggest that the effects attributed to the amount of used fuel matrix dissolved are not overwhelmingly influential.

The release rates from all the engineered layers are shown in Figure A-4 for five example radionuclides, ^{129}I, ^{90}Sr, ^{135}Cs, ^{99}Tc, and ^{230}Th, for Simulation #27. The effects are similar in the other example simulations.

The releases rates from irradiated UO_2 fuel into the interior of the container are the sum of the instant- and congruent-release rates. This total release rate is illustrated in Figure A-4. The instant-release

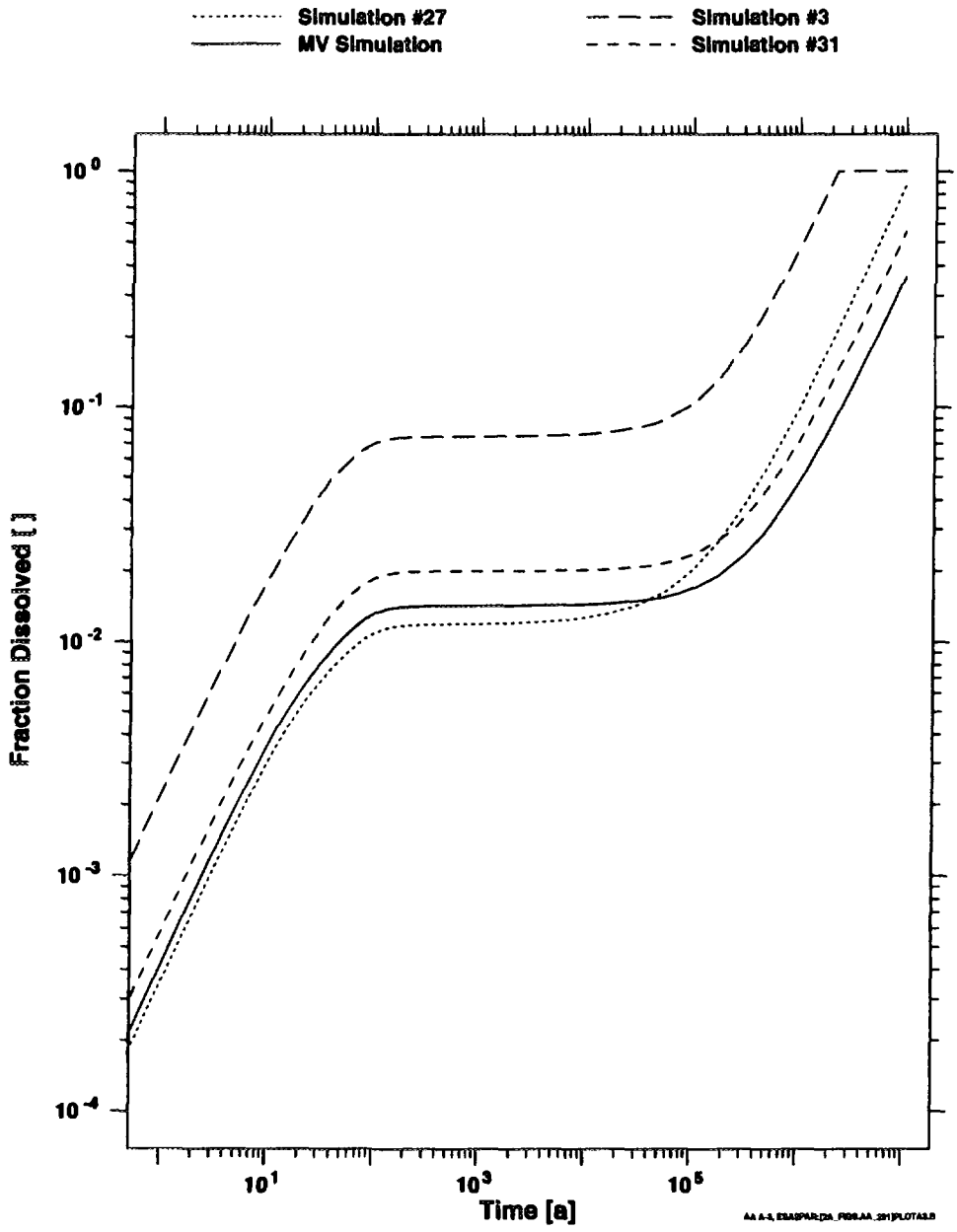

FIGURE A-3: Fraction of Fuel Dissolved as a Function of Time for the Four Example Simulations

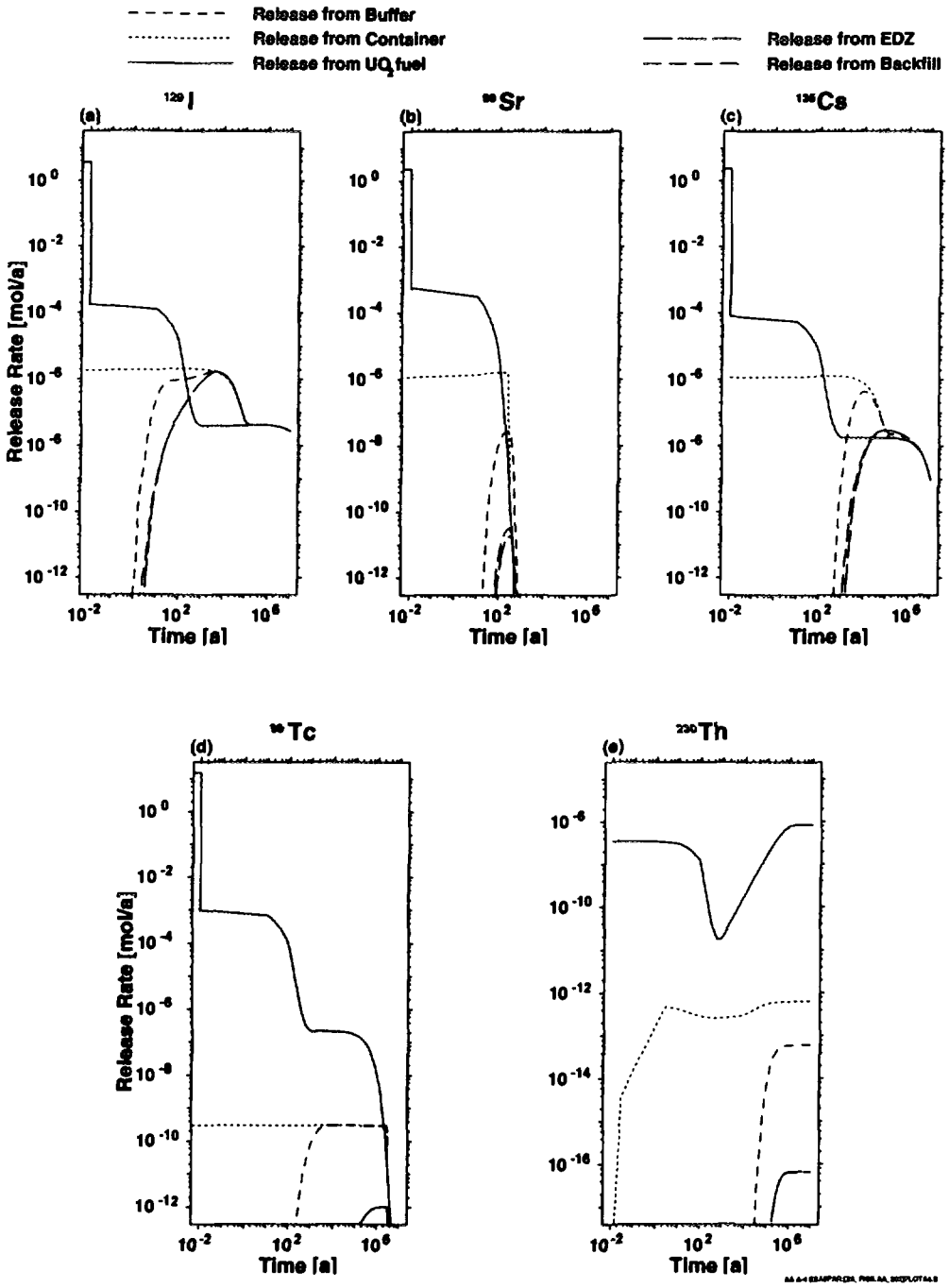

FIGURE A-4: Release Rates of ^{129}I, ^{90}Sr, ^{135}Cs, ^{99}Tc, and ^{230}Th for Simulation #27. The curves show release rates from the used fuel, container, buffer, backfill and EDZ for vault sector 11 in simulation #27. The plot for ^{230}Th is on a different scale than the others. A similar pattern of behaviour is observed for the other vault sectors and in the other example simulations.

appears as narrow pulses occurring before 10^{-2} a. The area under a pulse is equal to the instant inventory of the radionuclide (the product of its instant-release fraction and its initial inventory in UO_2 fuel). Thorium-230 has no instant-release and therefore it has no initial pulse in Figure A-4.

The curves beyond 10^{-2} a show the congruent-release rate, which is governed largely by the rate of radiolysis of the groundwater in contact with the used fuel. The rate of radiolysis from β- and γ-radiation is initially high and diminishes over the next 10^3 a. Subsequently, there is a period of relatively constant release rate caused by radiolysis from α-radiation of the groundwater and a small chemical dissolution rate of the fuel. The congruent-release rate of ^{90}Sr departs from this pattern because it decays rapidly and its release becomes negligible after about 10^3 a. The congruent-release rate of ^{230}Th also departs from this pattern because of ingrowth from its precursors. Ultimately the release rate drops off as a result of radioactive decay. This effect is not observed over the time frame of this simulation time for ^{129}I, which has a long half-life and for ^{230}Th, which ingrows from its long-lived precursors.

A.2.4 RELEASE FROM THE CONTAINER AND PRECIPITATION

The release rate out of the container is determined by diffusive transport through a small, pinhole-sized defect, referred to hereafter as a pinhole. These release rates are shown in Figure A-4 for Simulation #27. The pinhole offers a large resistance to transport and provides a large attenuation in radionuclide release rates. When the release-rate from the used-fuel bundle becomes small at long times, the pinhole no longer attenuates the release; the release from the container comes into steady state with the slow release from the used-fuel bundle. This behaviour is modified for ^{99}Tc and for ^{230}Th, both of which precipitate in the container.

For ^{99}Tc and ^{230}Th the rate of mass transport of dissolved species from the precipitate through the pinhole defect controls the release rate from the container.

- The release from the ^{99}Tc precipitate remains constant until all the precipitate is re-dissolved (reductions in the inventory of ^{99}Tc by decay also has a strong influence in this simulation). Then the release rate drops abruptly to a steady state value determined by the slow rate of release of 99Tc from dissolution of the used-fuel matrix.
- The release rate from the ^{230}Th precipitate varies slowly because of the contribution to its solubility limit from other isotopes of thorium that are ingrowing and decaying. The ^{230}Th precipitate does not completely redissolve within time frame of this simulation.

The release rates from the container in the absence of solubility constraints is contrasted with the release rates with solubility constraints in Figure A-5. Precipitation has a large effect in reducing release rates.

A.2.5 TRANSPORT THROUGH THE BUFFER, BACKFILL AND EDZ

Release rates from the buffer, backfill and EDZ are illustrated in Figure A-4 for the five example radionuclides for Simulation #27. The relative release rates of contaminants through these barriers depends on capacity factors and radionuclide half-lives. The capacity factor increases with increasing sorption and with increasing porosity. Sorption is radionuclide and medium dependent, whereas porosity is only medium dependent. Thus for any given simulation, radionuclides have different capacity factors only because of their different sorption characteristics. The larger the sorption of a radionuclide, the larger the delay and reduction in its release rates during transport through the buffer, backfill and EDZ. The half-lives and the capacity factors for the five example radionuclides in the buffer, backfill, damaged zone and lower rock zone are given for Simulation #27 in Table A-3.

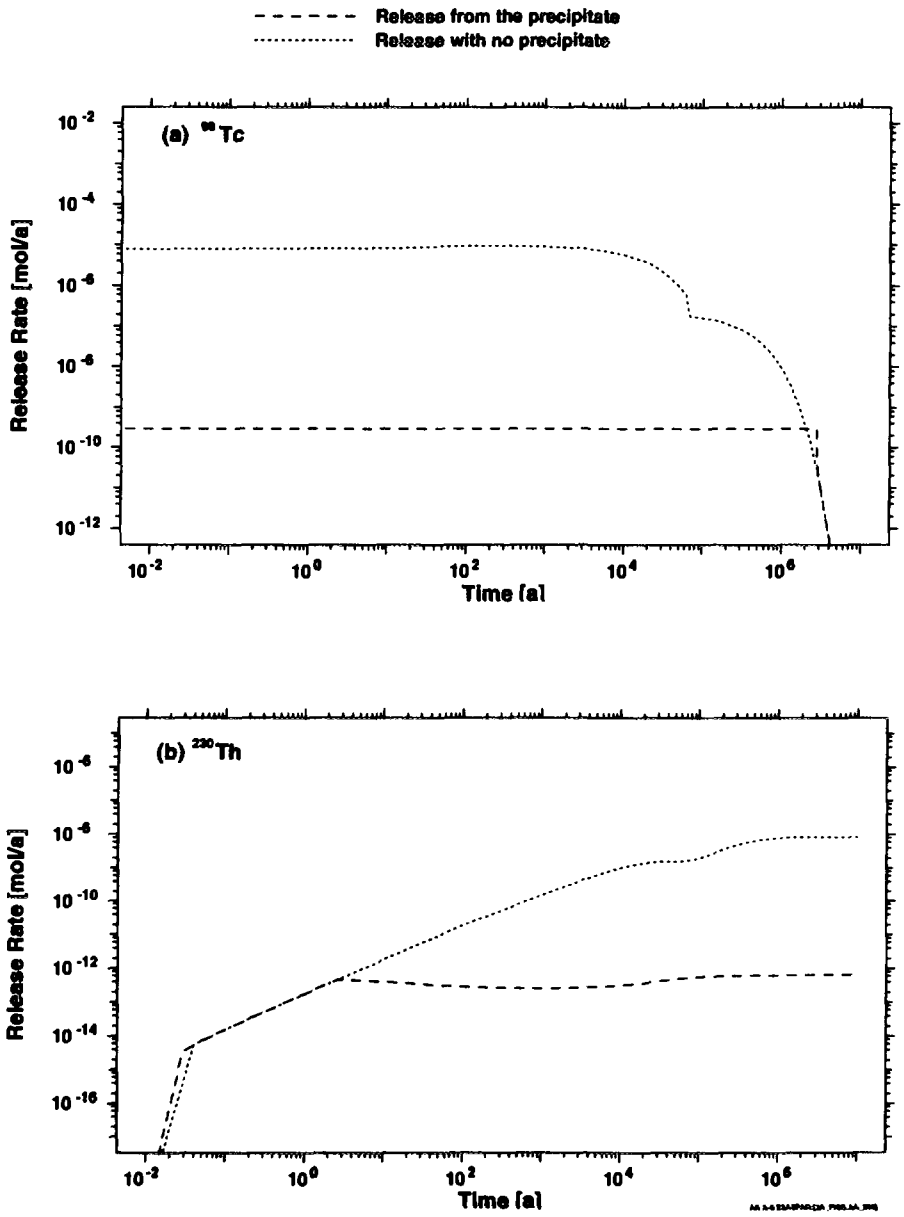

FIGURE A-5: Effect of Precipitation on the Release Rates for Simulation #27. The curves show release rates from the container for (a) ^{99}Tc, and (b) ^{230}Th for vault sector 11 in simulation #27.

For the first member of a decay chain, the smaller the half-life, the larger the reduction in release rates during transport through the buffer, backfill and EDZ, because of the decay that takes place during transport. Other chain members can experience increase in release rates during transport from ingrowth.

TABLE A-3

VAULT CAPACITY FACTORS FOR SIMULATION #27

Radionuclide	Half-Life	Capacity Factors [-]			
	[a]	Buffer	Backfill	EDZ	Lower Rock Zone
^{129}I	1.57×10^{7}	0.2	0.12	8.6×10^{-5}	1.0×10^{-5}
^{90}Sr	2.91×10^{1}	3.0	3.7	3.2×10^{-3}	3.9×10^{-4}
^{135}Cs	2.30×10^{6}	74	58	0.15	1.9×10^{-2}
^{99}Tc	2.13×10^{5}	17	9700	2.1×10^{-4}	2.5×10^{-5}
^{230}Th	7.70×10^{4}	3400	8600	0.30	3.6×10^{-2}

The different behaviours of the five example radionuclides during mass transport through the buffer, backfill and EDZ can be explained in terms of sorption and decay as follows.

- ^{129}I is relatively long-lived and slightly sorbed. As illustrated in Figure A-4, there is no significant attenuation in the maximum release rate for ^{129}I in traversing the buffer, backfill and EDZ, although the backfill delays release rates for about 10^3 a.
- ^{90}Sr is short-lived and is moderately sorbed in the buffer and backfill. Figure A-4 shows sorption of ^{90}Sr delays releases to the extent that substantial decay occurs in both these media.
- ^{135}Cs is strongly sorbed in buffer and backfill causing delays of about 10^4 a and strong attenuation in release rates, as illustrated in Figure A-4.
- ^{99}Tc is very strongly sorbed in the backfill and less strongly sorbed in the buffer. Figure A-4 shows the buffer causes a delay of about 10^2 a to 10^3 a, but the strong sorption in the backfill causes a further delay of more than 10^5 a and a large attenuation in release rates.
- ^{230}Th is very strongly sorbed in both buffer and backfill. As illustrated in Figure A-4, the large sorption causes delays of about 10^5 a and a significant attenuation in release rates.

The probabilistic sensitivity analysis described in Section 6.3 indicates that the axial permeability in the EDZ (DZPERA) is an influential parameter. The EDZ acts like a conduit for groundwater flow. Groundwater velocities are relatively higher in the EDZ because of its higher permeability compared with the other adjacent media, so that radionuclides move through the EDZ relatively quickly. Thus the EDZ acts as a sink, drawing radionuclides out of the buffer and backfill and thereby reducing their effectiveness as barriers. The larger the permeability in the EDZ, the larger the groundwater velocity therein and the more quickly radionuclides are drawn out of the buffer and backfill. In this study, the presence of an EDZ, with relatively large groundwater velocities, is detrimental to the effectiveness of the buffer and backfill barriers.

A.2.6 SECTOR-TO-SECTOR VARIABILITY

Sector-to-sector variability in release rates from buffer, backfill and EDZ is caused by three sector-dependent variables: the effective radius of the defect in the container, the number of failed containers, and the groundwater velocities in the lower rock zone that surrounds the vault sector. Groundwater velocities in the backfill and EDZ are also sector dependent, but their variability is determined by the variability in the groundwater velocity in the lower rock zone so they do not independently influence sector release rates.

The MV Simulation is of particular interest because it uses identical values in all sectors for the effective radius of the pinhole and the number of failed containers. Thus the sector-to-sector variability in release rates for the MV Simulation is determined solely by the variability in the groundwater velocities in the lower rock zone. Indeed, the pattern of variation of groundwater velocity, as illustrated in Figure A-6, matches the pattern of variation in maximum release rates for the MV Simulation for all five example radionuclides. In general, the smaller the half-life and the stronger the sorption, the larger the variation in release rates in response to the variation in groundwater velocities.

In Simulation #27, the effective radius of the pinhole and the number of failed containers varies from sector to sector. The variability in these two parameters largely determines the variability in maximum release, and the effect of the groundwater velocity is no longer apparent. This is illustrated in Figure A-7. In general a larger pinhole radius or a larger number of failed containers yields a larger release rate. When the number of failed containers and the effective radius of the pinhole are both large, they act together to increase the release rate from the vault. Sector 13, illustrated in Figure A-7, has a large number of failed containers (3) combined with a large pinhole radius (1.3 mm), which results in this sector having the highest maximum release rate for all five example radionuclides.

When these two effects are competing, the effect of the radius of the pinhole tends to dominate. A smaller radius provides a greater resistance to transport out of the container and produces smaller release rates. At larger radii, however, the transport resistances of the buffer, backfill and EDZ are larger than the resistance of the pinhole and the model becomes insensitive to changes in pinhole radius. In addition, at long times when most of the inventory has diffused through the pinhole, the releases from a sector become insensitive to pinhole radius.

The importance of the pinhole radius can be seen in Figure A-7 by comparing the release rates for sectors 11 and 12 for the five example radionuclides. The number of containers failing in sector 11 is smaller than in sector 12 (1 versus 3), whereas the effective pinhole radius is larger in sector 11 than in sector 12 (0.69 mm versus 0.21 mm). The release rates from sector 11 are larger than from sector 12, showing the greater importance of the pinhole radius compared with the number of failed containers.

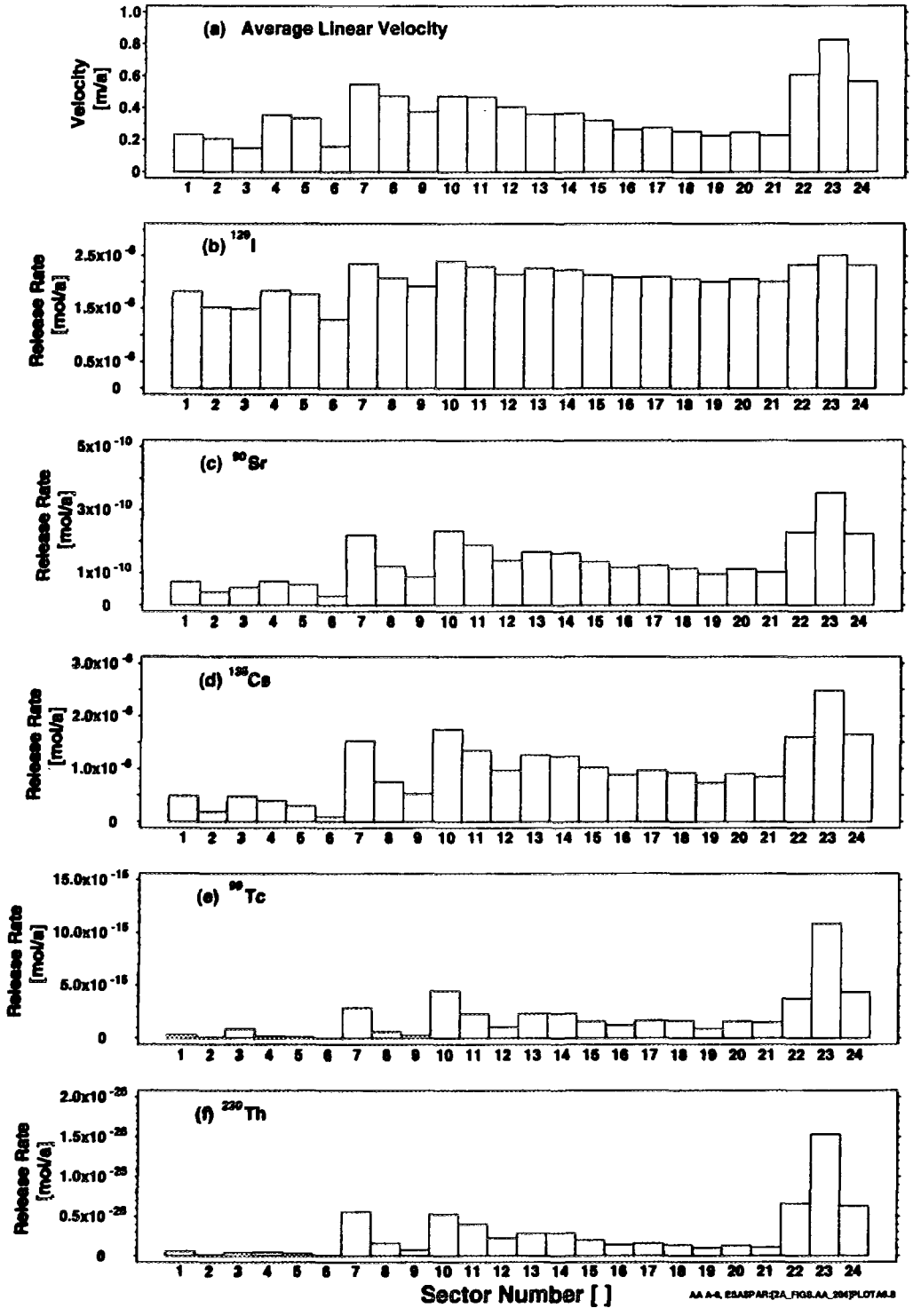

FIGURE A-6: Patterns of Sector-to-Sector Variability in the MV Simulation. The horizontal axes identifies the 24 vault sectors. Part (a) shows the groundwater velocity in the rock surrounding each sector. Parts (b) to (f) show the maximum release rates from the vault for ^{129}I, ^{90}Sr, ^{135}Cs, ^{99}Tc and ^{230}Th respectively.

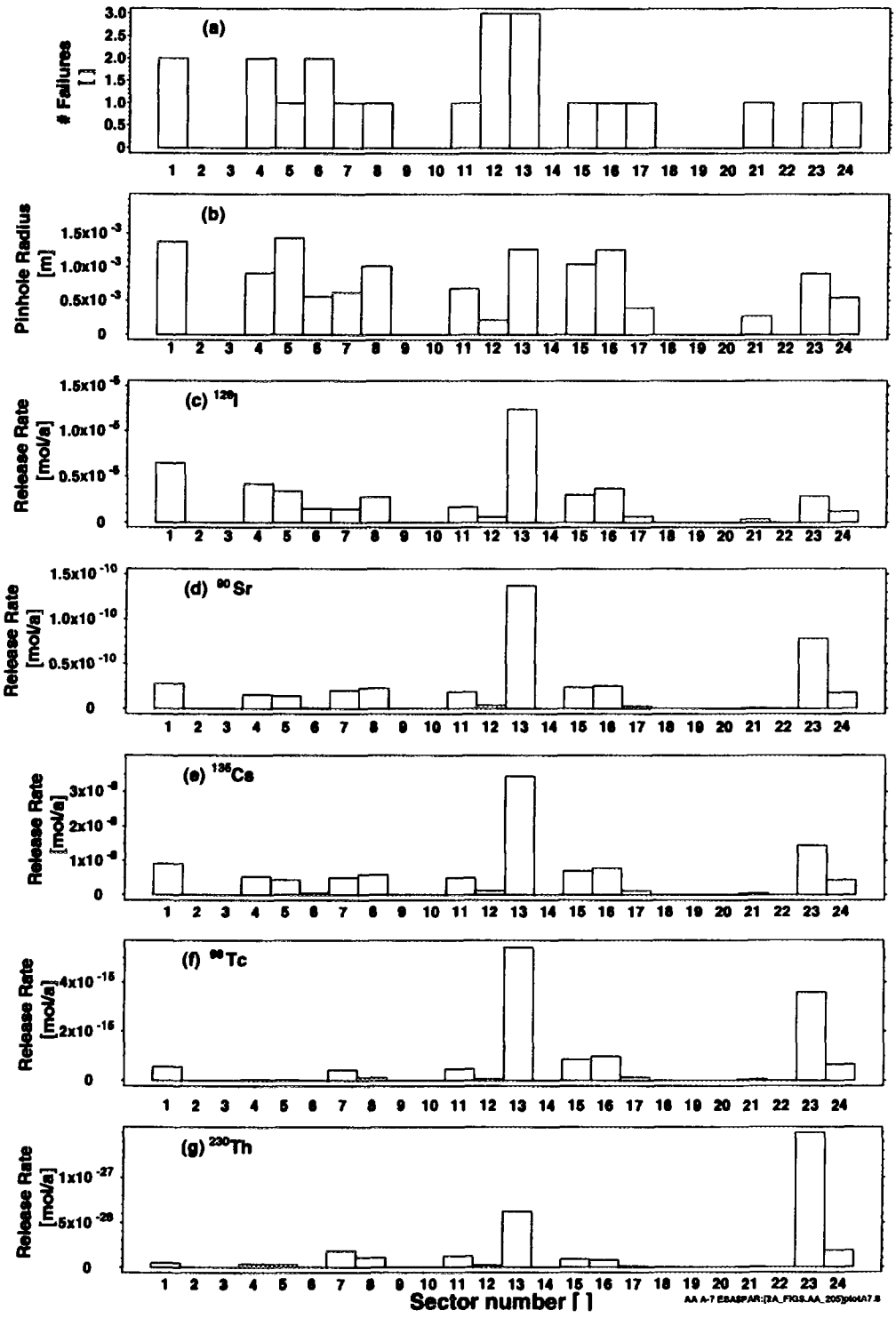

FIGURE A-7: Patterns of Sector-to-Sector Variability in Simulation #27. The horizontal axes identify the 24 vault sectors. Parts (a) and (b) show the number of failed containers and the associated radii of the pinholes (assumed to be identical for all failed containers in a sector). Parts (c) to (g) show the maximum release rates from the vault for ^{129}I, ^{90}Sr, ^{135}Cs, ^{99}Tc and ^{230}Th respectively.

The effect of much larger pinhole radii can be seen in Figure A-7 by comparing the ^{129}I release rates for sectors 4 and 5 with the release rates for sector 11 and 12. In sectors 11 and 12, the effect of the effective pinhole radius (0.69 mm and 0.21 mm) dominates as described in the previous paragraph. In sectors 4 and 5, the number of containers failed dominates because the pinhole radii are relatively large (0.91 mm and 1.4 mm), and the releases have become relatively insensitive to this parameter.

The processes described here, determining sector-to-sector variability in release rates can be applied to explain the variability in the other example simulations. These release rates are further illustrated for the example simulations in Section A.3.3.

A.2.7 TOTAL AMOUNTS RELEASED FROM THE VAULT

We might expect that the dose rate from a radionuclide would increase as more of that radionuclide is released from the vault. Table A-4 gives the total amount of ^{129}I and ^{90}Sr released from the vault in 10^4 a and the maximum dose rate up to 10^4 a for the four example simulations.

TABLE A-4

TOTAL AMOUNTS RELEASED FROM THE VAULT AND DOSE RATE

Radionuclide and Simulation	Integrated Vault Release to 10^4 a [mol]	Dose Rate at 10^4 a [Sv/a]
^{129}I		
MV Simulation	0.39	4.6×10^{-6}
Simulation #27	0.36	1.2×10^{-5}
Simulation #31	0.34	1.1×10^{-5}
Simulation #3	0.09	2.6×10^{-9}
^{90}Sr		
Simulation #31	2.2×10^{-6}	0.0
MV Simulation	8.4×10^{-7}	6.0×10^{-12}
Simulation #3	4.3×10^{-7}	0.0
Simulation #27	1.0×10^{-7}	6.6×10^{-17}

This table indicates that, for the four example simulations, the dose rate from ^{129}I is loosely correlated to amount of ^{129}I released from the vault but the dose rate from ^{90}Sr is not correlated to the amount of ^{90}Sr released from the vault. In addition, the correlation between the amount of ^{129}I released from the vault and the dose rate in the simulations in Table A-1 is not very strong. Similar relationships between amount released from the vault and dose rate also applies for other radionuclides. These relatively poor correlations arise because parameters in the biosphere model have, in most instances, greater influence in determining dose rates than the variation in release rates from the vault.

A.2.8 SUMMARY

Variation in the number of failed containers and in the total amount of ^{129}I released from the vault correlates with dose rate in these four example simulations. This correlation is consistent with the sensitivity analysis described in Section 6.3, where four vault parameters were found to influence dose rates. However, these correlations are not quite so obvious in the simulations in Table A-1. Parameters used in the biosphere model (Section A.4) are generally more influential in determining dose rate than are parameters used in the vault model.

The small size of the defects in a failed container limits transport out of the container for relatively mobile and soluble radionuclides such as ^{129}I. However, the variabilities in the parameters associated with release through a pinhole defect are relatively small, and so these parameters do not strongly influence the variability in dose rate. With larger defect sizes, releases from the vault become limited by transport through the buffer and backfill. Buffer and backfill become important barriers as the importance of the pinhole resistance to mass transport decreases. The presence of the EDZ decreases the effectiveness of the buffer and backfill. Precipitation limits the rates of release from the vault for radionuclides that are relatively insoluble.

All of the processes simulated in the vault model (container failure, slow release from the limited transport through a small defect, precipitation in the container, and transport through the buffer and backfill) can be important, either serving as an effective barrier for a radionuclide or as a redundant barrier.

A.3 FEATURES OF THE GEOSPHERE MODEL

A.3.1 INTRODUCTION

The geosphere model is outlined in Section 5.3 and described in more detail by Stanchell et al. (1996). The assumed properties of the geosphere in this report are such that groundwater transit times from the vault horizon to the surface can be as small as a few tens of years. With transit times this small, the geosphere is not a controlling barrier for mobile nuclides like ^{129}I, except at early times. However, the geosphere is an effective barrier, both at early and longer times, for those nuclides that are moderately or strongly sorbed.

In the MV Simulation, one container fails in each vault sector, and is a radionuclide source for each portion of the contaminant plume travelling through the geosphere. In the other example simulations, not all vault sectors have container failures; hence, the size and shape of the contaminant plume in the geosphere depends on the distribution of container failures in the vault. Figure A-1 shows the distributions of container failures among the 24 vault sectors, for the four example simulations. Figure A-8 illustrates schematically the extents of the contaminant plumes in the geosphere for these example simulations, by showing the segments in the geosphere transport network that connect the vault sectors with failed containers to the discharge zones in the biosphere.

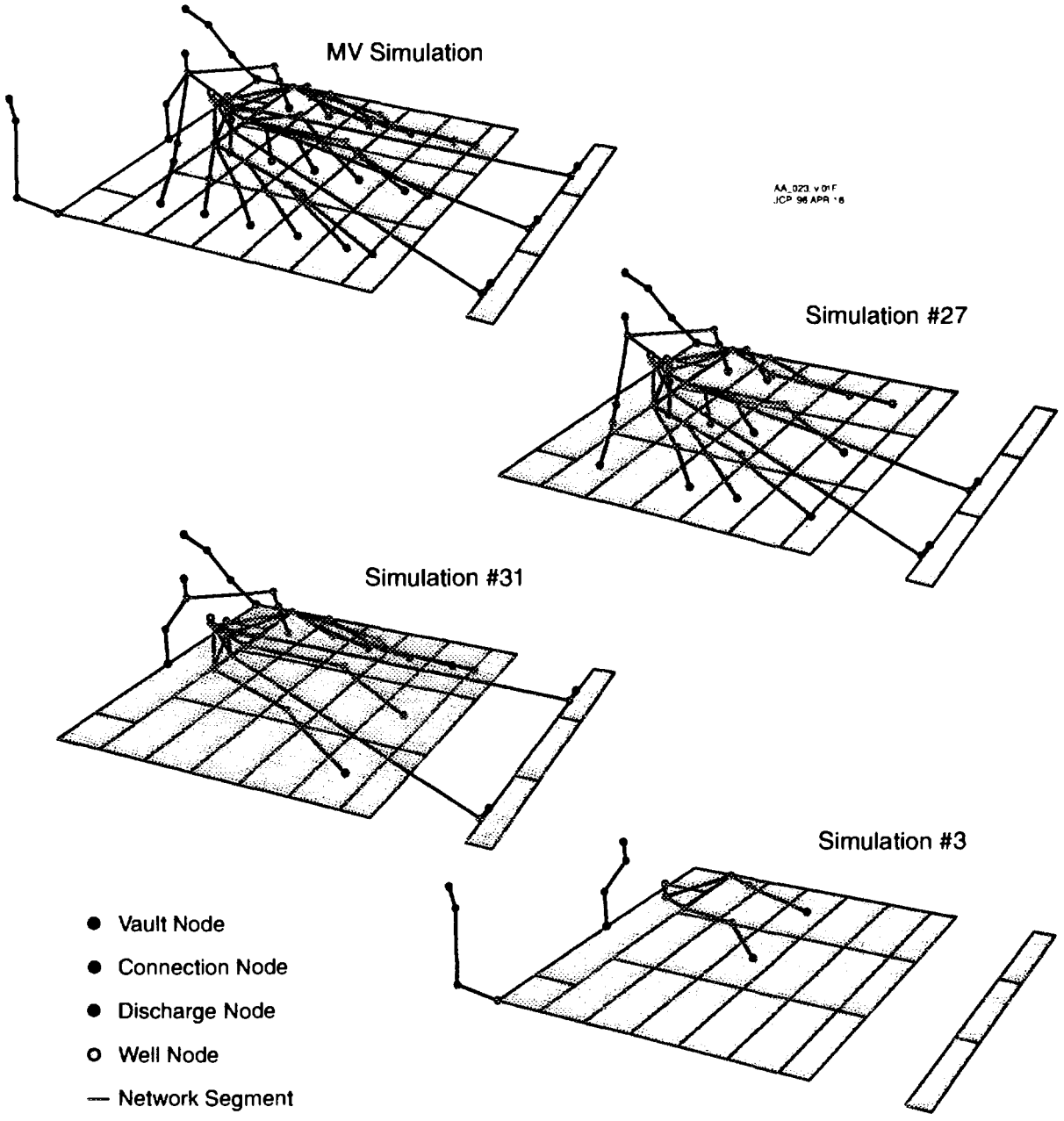

FIGURE A-8: Illustration of Geosphere Transport Networks for the Four Example Simulations. The networks show the contaminant flow pathways from vault sectors with failed containers to discharge zones in the biosphere for the MV Simulation and for Simulations #27, #31 and #3. The figure for the MV Simulation shows the entire network of segments because this simulation has a failed container in every vault sector.

The MV Simulation has one container failure in each of the 24 vault sectors. About 4% of the total vault releases travel to each of the Pinawa Channel North and South discharge zones (aquatic and terrestrial); 7% to the Boggy Creek North discharge zones; and the other 75%, via fracture zone LD1, to either the Boggy Creek South discharge zones or to the well. The well is 34 m deep, captures a portion of the contaminant plume in fracture zone LD1, and reduces the groundwater discharge rate to the Boggy Creek South discharge zones (i.e., if the well were not present, there would be larger discharges to Boggy Creek South).

Simulation #27 has 22 container failures in 15 vault sectors. About 9% of the total vault releases travel to the Pinawa Channel North discharge zones; no releases travel to the Pinawa Channel South discharge zones; 23% travels to the Boggy Creek North discharge zones; and the other 68% travels, via fracture zone LD1, to either the Boggy Creek South discharge zones or to the well. In this simulation, the well is 35 m deep, captures a portion of the contaminant plume in fracture zone LD1, and reduces the groundwater discharge rate to the Boggy Creek South discharge zones.

Simulation #31 has 17 container failures in 11 vault sectors, mostly along one side of the vault. About 6% of the total vault releases travel to the Pinawa Channel North discharge zones, no releases travel to the Pinawa Channel South discharge zones, 24% travels to the Boggy Creek North discharge zones and the other 70% travels via fracture zone LD1 to the Boggy Creek South discharge zones. This simulation does not have a well; all the contaminants travelling in fracture zone LD1 reach the Boggy Creek South discharge zones.

Simulation #3 has 6 container failures in 4 vault sectors. None of the total vault releases travel to the Pinawa Channel North discharge zones; 17% travels to the Pinawa Channel South discharge zones; 33% to the Boggy Creek North discharge zones; and the other 50%, via fracture zone LD1, to the Boggy Creek South discharge zones. This simulation also contains no well; all the contaminants travelling in fracture zone LD1 reach the Boggy Creek South discharge.

A.3.2 EFFECTS OF A WELL

Both the MV Simulation and Simulation #27 include a water-supply well. However, neither Simulation #31, another high dose rate simulation, nor Simulation #3 have a well. Wells capture a portion, based on well depth and demand, of the contaminants from the centre of the plume moving up fracture zone LD1 and reduce the amount of contaminants and groundwater that would otherwise discharge to the Boggy Creek South discharge zones. Wells also capture diluting water from outside of the plume, either lake water infiltrated from the surface or uncontaminated groundwater or both. If contaminants from all vault sectors contribute to the plume, the plume is more concentrated in the centre.

The probabilistic sensitivity analysis (Section 6.3) shows the depth of the well (DPTHWL) is an influential parameter. However, differential effects of well depth are not evident in the MV Simulation and in Simulation #27 since the two wells have almost the same depth. Table A-5 gives a comparison of the properties and effects of the wells in these two example simulations.

The well in Simulation #27 has greater demand, for reasons described in Section A.4.2 and, hence, captures a greater portion of the contaminant plume. However, plume capture is a nonlinear process and the increase in plume capture is not in proportion to the increase in demand. Moreover, the well in Simulation #27 also captures a greater amount of diluting water infiltrated from the lake. For these two reasons, the contaminant concentrations in the well water are smaller in Simulation #27 than in the MV Simulation.

TABLE A-5

PROPERTIES OF THE WELLS IN THE MV SIMULATION AND SIMULATION #27

Property	Value in the MV Simulation	Value in the Simulation #27
Well Depth [m]	34	35
Well Demand [m^3/a]	1330	2800
Rate of Infiltration of Lake Water [m^3/a]	150	950
Reduction of Boggy Creek South Discharge	22%	40%
Fraction of Plume Width Captured	29%	43%
Maximum concentration of ^{129}I in well water [mol/m^3]	1.3×10^{-8}	4.5×10^{-9}

A.3.3 TRANSIT TIMES

Three pathways through the geosphere on the centre line of the vault are used to illustrate transit times through the geosphere. These pathways, illustrated in Figure A-9, pass through a variety of different rock zones and lead to the vicinity of the well.

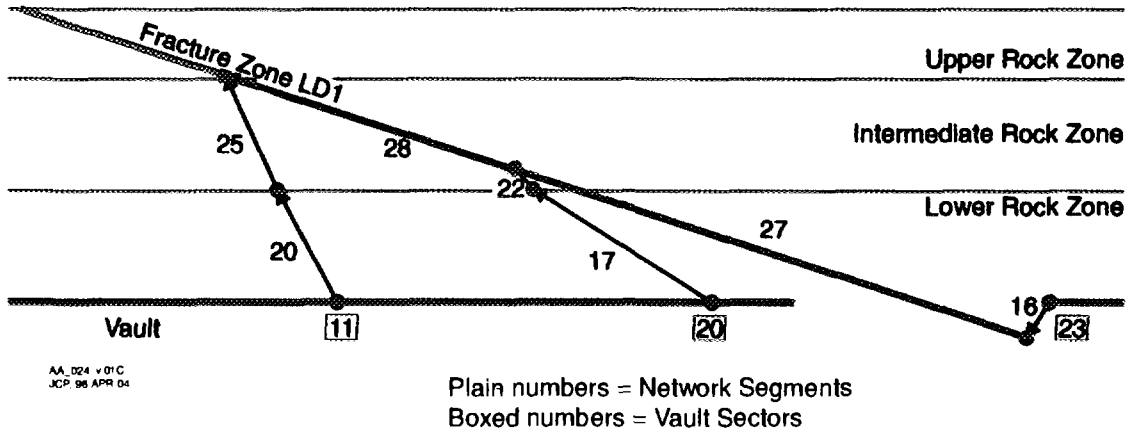

FIGURE A-9: Illustration of Three Geosphere Flow Pathways. The three pathways originate at vault sectors 11, 20 and 23, lying on the centre line of the vault and lead to the vicinity of a well.

1. The pathway from vault sector 23 passes through 64 m of the lower rock zone followed by 1400 m of fracture zone LD1 (segments labelled 16 and 27 in Figure A-9).

2. The pathway from sector 20 passes through 360 m of the lower rock zone, 46 m of the intermediate rock zone, and 550 m of fracture zone LD1 (segments labelled 17, 22, and 28 in Figure A-9).

3. The pathway from sector 11 passes through 210 m of the lower rock zone followed by 380 m of the intermediate rock zone (segments labelled 20 and 25 in Figure A-9).

Figure A-10 illustrates transit times for five example radionuclides, ^{129}I, ^{90}Sr, ^{99}Tc, ^{79}Se, and ^{126}Sn, through these three pathways in the four example simulations. There is not a failed container in each of these associated vault sectors in each example simulation; in such cases the transit times illustrated are those that would be observed if these pathways were in use. The example radionuclides range from nonsorbed (^{129}I) to strongly sorbed (^{126}Sn) and the transit times take into account the retardation caused by sorption.

Figure A-10 shows that overall transit times for a radionuclide in all four simulations are remarkably similar, although the details differ from one simulation to the next. The transit times for ^{129}I lie between 10^2 a and 10^3 a. ^{90}Sr and ^{99}Tc are slightly retarded and generally have transit times in the range 10^3 a to 10^4 a. ^{79}Se is more retarded with transit times in the range 10^4 a to 10^5 a and ^{126}Sn is strongly retarded with transit times of about 10^6 a.

The transit time are strongly influenced by the effective transport porosities in the different zones, and some of these porosities (SGPROS) were identified as influential parameters (Section 6.3). Table A-6 lists transport porosities in the four example simulations.

TABLE A-6

EFFECTIVE TRANSPORT POROSITIES

	Lower rock zone* SGPROS (LWROC) [-]	Middle rock zone* (SGPROS (MIROC) [-]	Upper rock zone* SGPROS (UPROC) [-]	Fracture zones* SGPROS (FZONE) [-]
MV Simulation	1.0×10^{-4}	1.0×10^{-4}	1.0×10^{-4}	3.2×10^{-2}
Simulation #27	1.0×10^{-5}	1.4×10^{-4}	3.4×10^{-4}	5.4×10^{-2}
Simulation #31	1.4×10^{-5}	1.2×10^{-4}	1.4×10^{-5}	4.6×10^{-2}
Simulation #3	4.4×10^{-5}	2.3×10^{-4}	3.4×10^{-5}	1.6×10^{-2}

* The probability distributions specified for the probabilistic analysis are log uniform with a range of 10^{-5} to 10^{-3} for the lower, middle and upper rock zones, and a range of 10^{-2} to 10^{-1} for the fracture zones. The values listed for the MV Simulation are the median values of these distributions.

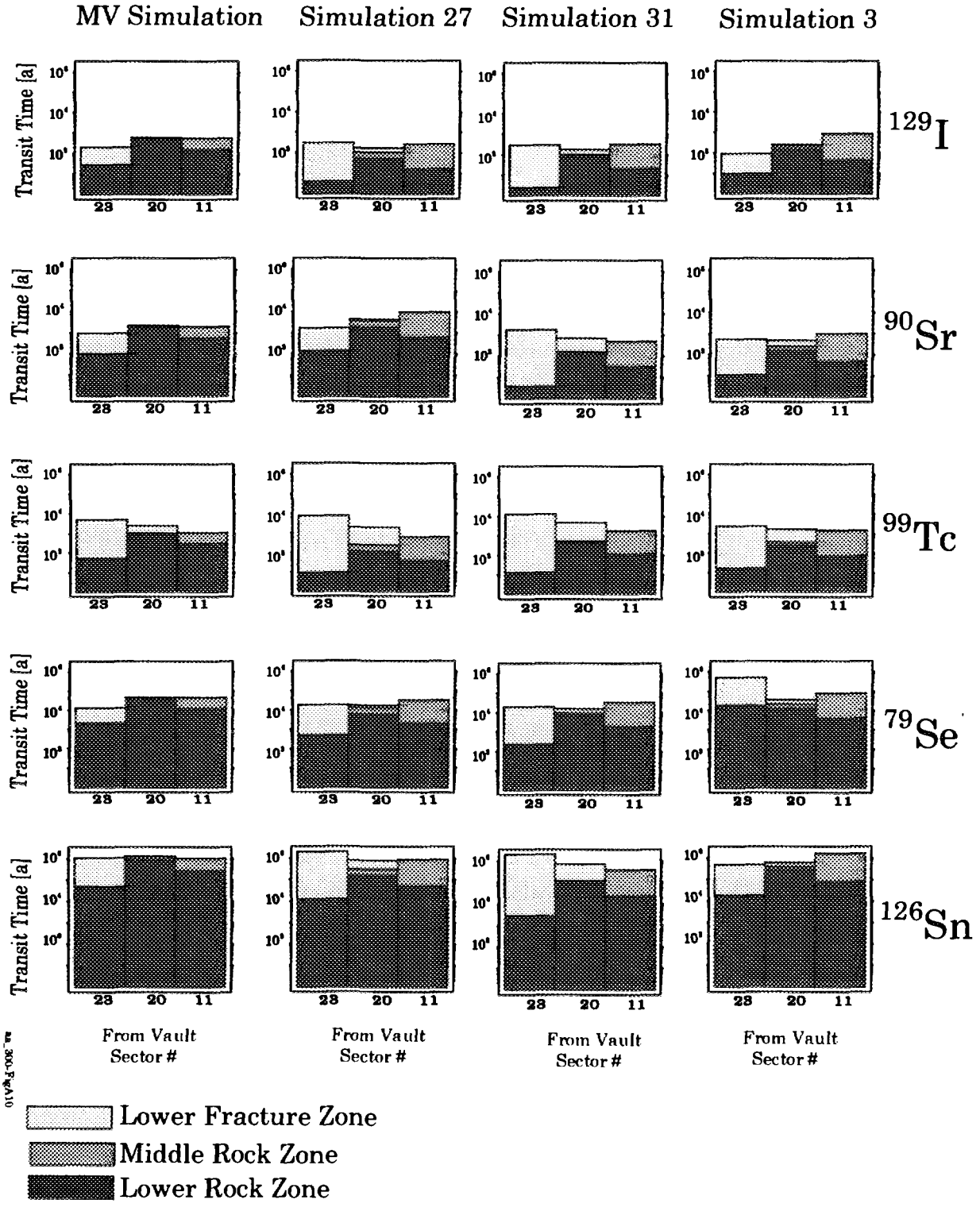

FIGURE A-10: Transit Times for Three Pathways Through the Geosphere. The pathways, illustrated in Figure A-9, are from three vault sectors, 11, 20 and 23, to the vicinity of a well. Transit times, plotted on a logarithmic scale, are shown for ^{129}I, ^{90}Sr, ^{99}Tc, ^{79}Se, and ^{126}Sn for the four example simulations.

Many subtle features can be inferred from Figure A-10. For example, consider the ^{129}I transit times from sector 23 through 64 m of lower rock zone and 1400 m of fracture zone LD1 in the 4 simulations.

- In the MV Simulation, the transit time through the lower rock zone is 25 a and 170 a in fracture zone LD1.

- In Simulation #27, the transit time through the lower rock zone is 4 a. The effective transport porosity is near its minimum value giving near maximum groundwater velocity and near minimum transit time. The effective transport porosity in LD1 is larger than the median value, giving a relatively long transit time of 300 a.

- In Simulation #31, the transit time through the lower rock zone is 2.3 a. The effective transport porosity is small and a high value for dispersivity is also used in this simulation, resulting in a further reduction in transit time. The effective transport porosity in LD1 is also larger than the median value, giving a relatively long transit time of 280 a.

- In Simulation #3, the transit time through the lower rock zone is 9.5 a. The effective transport porosity is smaller than the median and the transit time is small. The effective transport porosity in LD1 is smaller than the median value, giving a rapid velocity and relatively short transit time of 80 a.

Simulation #3 has a low dose rate and the shortest ^{129}I transit times, while Simulations #27 and #31 have high dose rates and the longest transit times. That is, short transit times do not correlate with dose rates in these example simulations, because the geosphere is not effective as a barrier for nonsorbed nuclides and because other model parameters, particularly in the biosphere model (Section A.4), have a greater influence on variations in dose rate. Similar details can be observed from Figure A-10 for the other pathways and the other nuclides.

A.3.4 TRANSPORT THROUGH THE GEOSPHERE

Figures A-11 to A-16 illustrate the total releases of ^{129}I, ^{90}Sr, ^{99}Tc, ^{79}Se, and ^{126}Sn from the vault sectors into the geosphere and the subsequent releases from the geosphere into the biosphere at the discharge zones and the well. Figure A-11 illustrates the spatial geometry of the 24 vault sectors and the approximate locations of the discharge zones that are depicted in subsequent Figures A-12 to A-16 (the discharge zones would have different sizes in the four example simulations but we use the same schematic representation in these figures).

In Figures A-12 to A-16, the vertical separation of the vault and the ground surface is exaggerated and the vertical coordinate is used as a scale for the bar graphs. The heights of the bars indicate the total releases of radionuclides integrated over a 10^4 a time period into the associated aquatic and terrestrial discharge zones. For each radionuclide in these figures, the same linear scaling factor is used for the heights of the bars. Hence the releases of the same radionuclide from the four example simulations can be directly compared.

Table A-7 summarizes the total releases from the vault and the total releases from the geosphere. As previously shown in Figure A-1, the MV Simulation has a single container failure in each of the 24 vault sectors, Simulation #27 has 22 failures occurring in 15 sectors, Simulation #31 has 17 failures occurring in 11 sectors, and Simulation #3 has 6 failures occurring in 4 sectors. The well in the MV Simulation captures contaminants originating in the central row of vault sectors and in the three sectors located above fracture zone LD1. The well in Simulation #27 captures some additional contaminants from the peripheral sectors. There is no well in Simulation #31 or in Simulation #3.

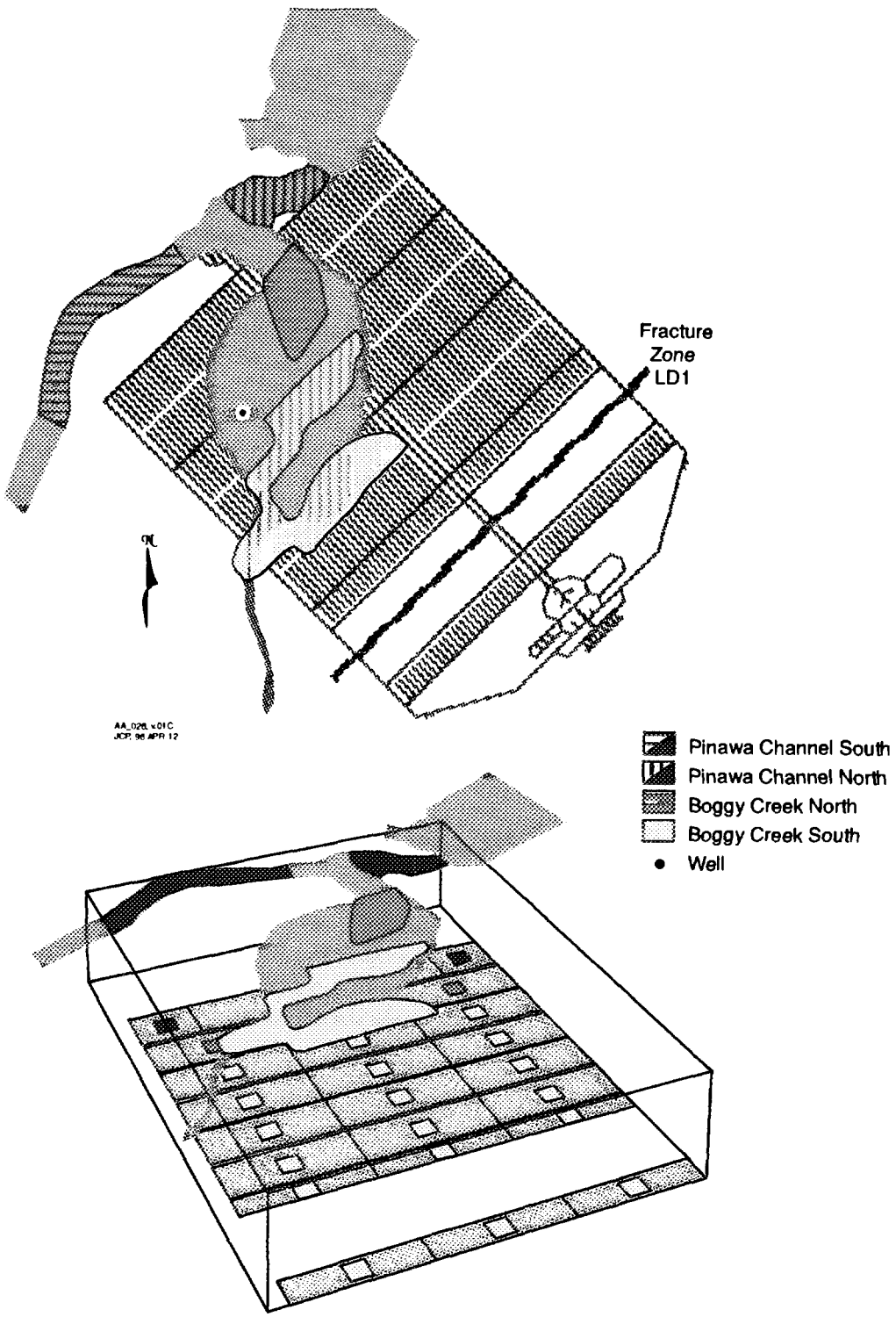

FIGURE A-11: Discharge Zones in the Biosphere. The upper figure is a plan view of the discharge zones in the biosphere, similar to Figure 12. Each discharge zone (combining the associated aquatic and terrestrial zones) is shown with a different colour. The vault sectors that feed the discharge zones (assuming no well is present) use the same colour scheme. The lower figure is a perspective view, showing the correct vertical relationship between the vault and the ground surface. (The views in Figures A-12 to A-16 are vertically exaggerated.)

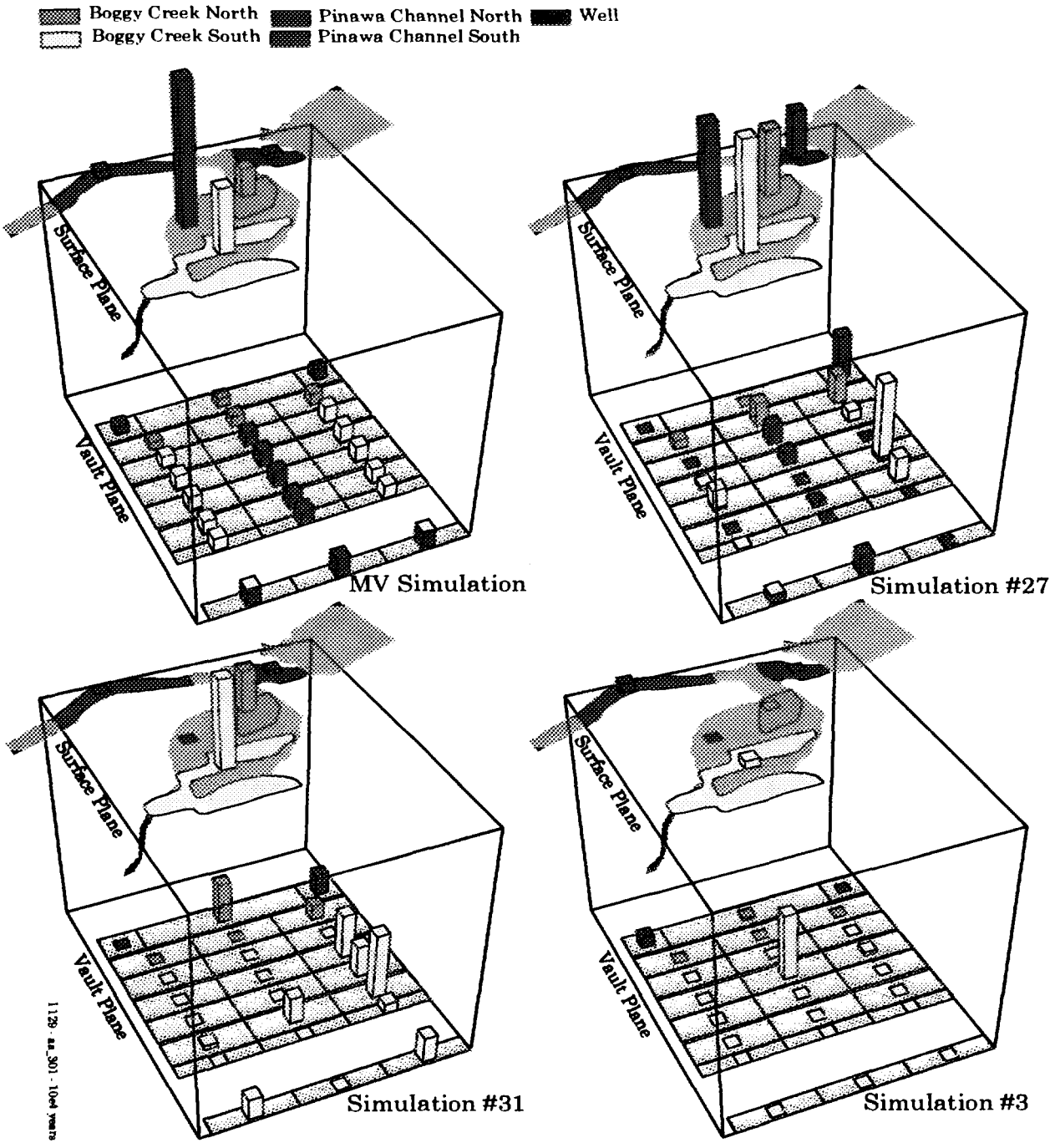

FIGURE A-12: Total Releases of ^{129}I in 10^4 a. Releases are shown from the vault sectors to the geosphere and from the geosphere to the discharge areas in biosphere in the four example simulations. Releases to the associated aquatic and terrestrial zones at each discharge area have been combined. Releases from the vault sectors have been coloured the same colour as the discharge area to which they contribute contaminant releases.

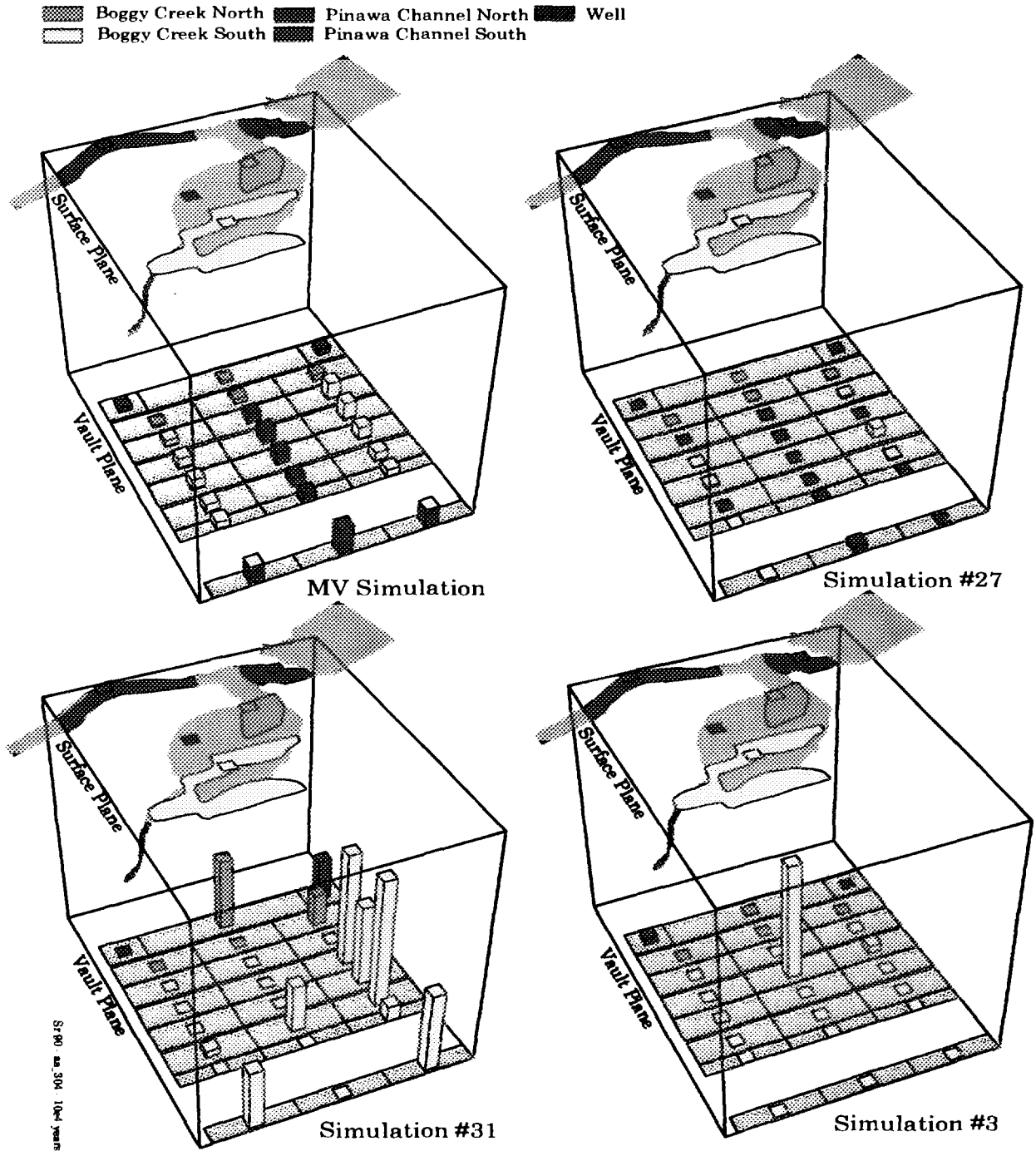

FIGURE A-13: Total Releases of ^{90}Sr in 10^4 a. Releases are shown from the vault sectors to the geosphere and from the geosphere to the discharge areas in biosphere in the four example simulations. Releases to the associated aquatic and terrestrial zones at each discharge area have been combined. Releases from the vault sectors have been coloured the same colour as the discharge area to which they contribute contaminant releases.

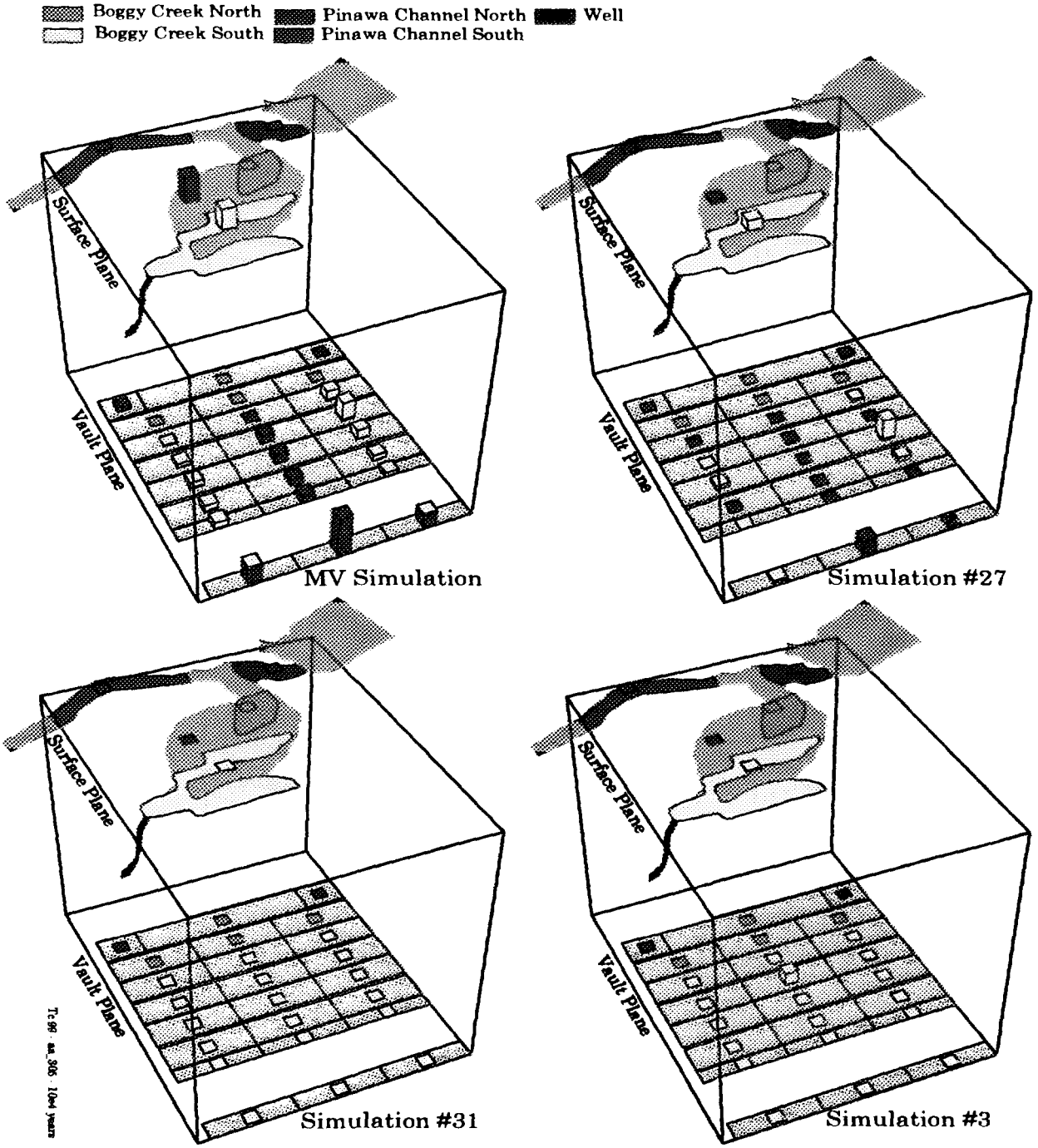

FIGURE A-14: Total Releases of ^{99}Tc in 10^4 a. Releases are shown from the vault sectors to the geosphere and from the geosphere to the discharge areas in biosphere in the four example simulations. Releases to the associated aquatic and terrestrial zones at each discharge area have been combined. Releases from the vault sectors have been coloured the same colour as the discharge area to which they contribute contaminant releases.

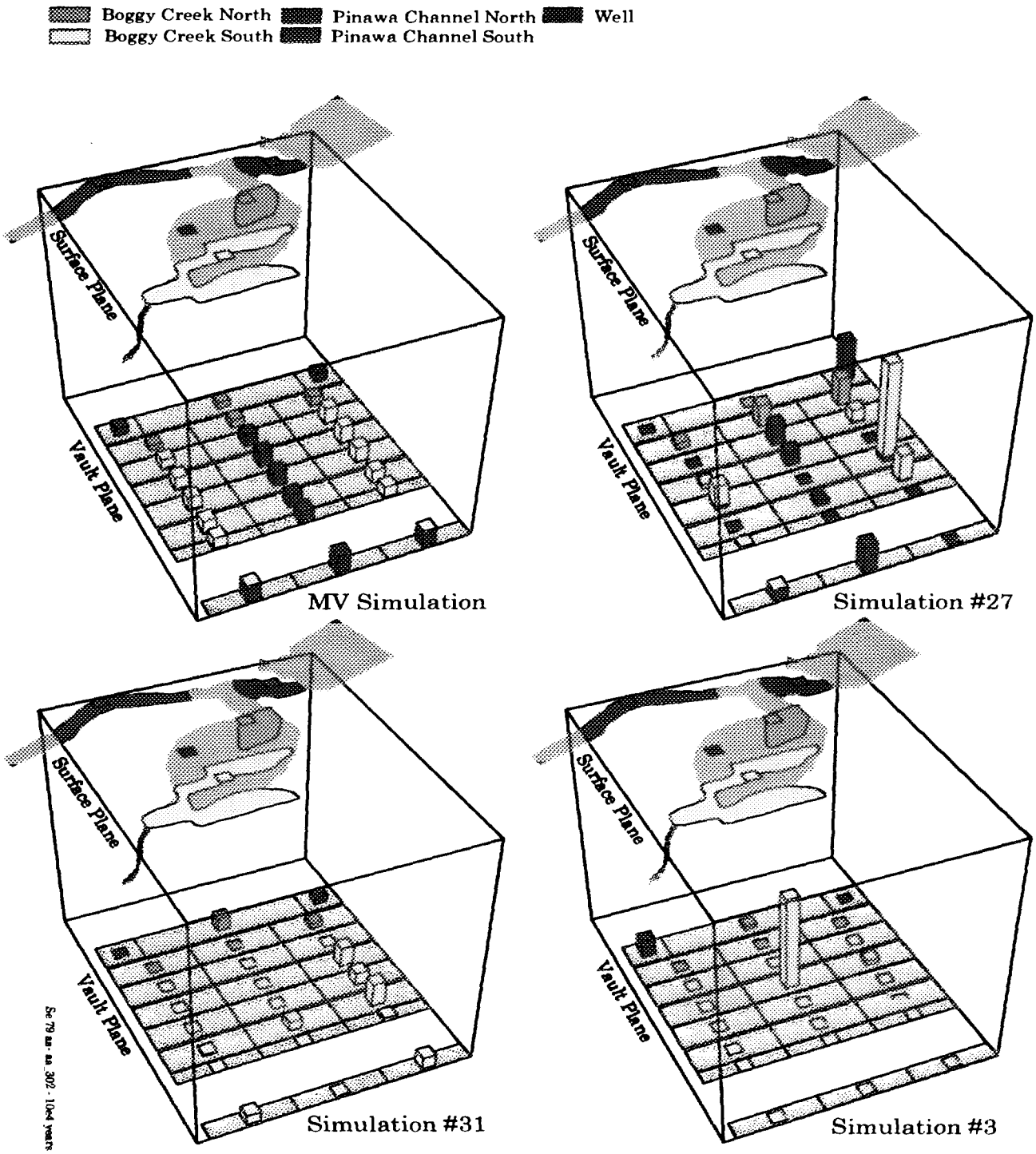

FIGURE A-15: Total Releases of ^{79}Se in 10^4 a. Releases are shown from the vault sectors to the geosphere and from the geosphere to the discharge areas in biosphere in the four example simulations. Releases to the associated aquatic and terrestrial zones at each discharge area have been combined. Releases from the vault sectors have been coloured the same colour as the discharge area to which they contribute contaminant releases.

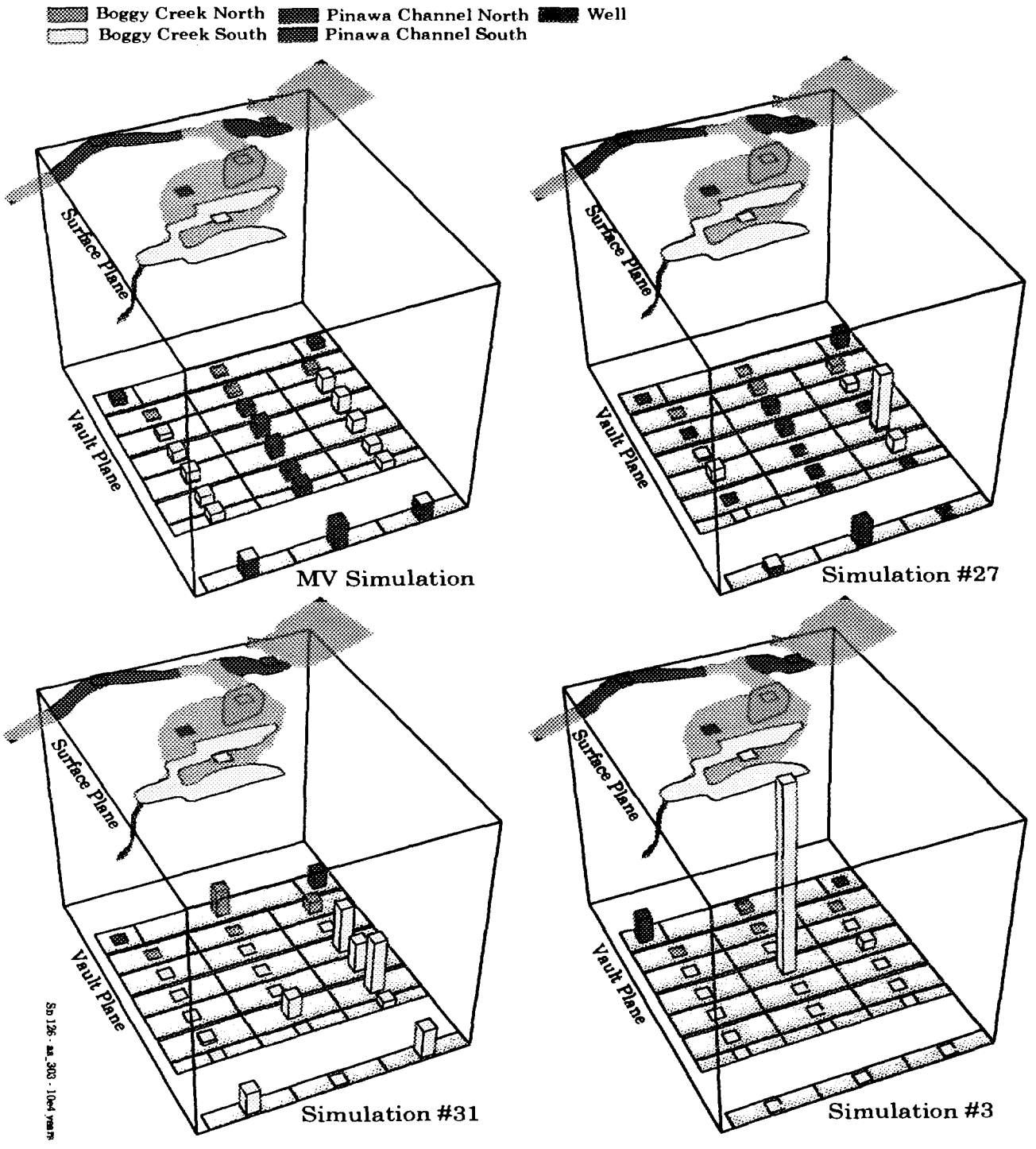

FIGURE A-16: Total Releases of ^{126}Sn in 10^4 a. Releases are shown from the vault sectors to the geosphere and from the geosphere to the discharge areas in biosphere in the four example simulations. Releases to the associated aquatic and terrestrial zones at each discharge area have been combined. Releases from the vault sectors have been coloured the same colour as the discharge area to which they contribute contaminant releases.

Figure A-12 and Table A-7 shows that, for ^{129}I in the MV Simulation and in Simulation #27, the total releases from the geosphere to the biosphere are nearly equal to the total releases from the vault to the geosphere. That is, the geosphere passes on most of the releases from the vault to the biosphere, with some ^{129}I remaining in transit at 10^4 a. Sorption for ^{129}I occurs only in the overburden and sediment layers; retardation factors for iodine in these layers are listed in Table A-8. Simulation #31 has a slightly attenuated geosphere release because the sorption of iodine in the sediment layer is higher than the median value, and, since there is no well, most of the ^{129}I must pass through the lake sediment layers before discharging in the biosphere. Simulation #3 has higher-than-median sorption in both the overburden and sediment, so releases from the geosphere to the biosphere are delayed and attenuated even more. Figure A-17 shows the flow rates as a function of time for the transport of ^{129}I through the upper rock zone, the overburden layer and the sediment layer leading to the Boggy Creek South discharge zone. The upper rock zone has negligible effect on the transport. There is little effect of the overburden and sediment in Simulation #27, but the delay and attenuation provided by the sediment layer in Simulation #31 and both the overburden and sediment layers in Simulation #3 are strong.

Figure A-13 shows that, for ^{90}Sr, the geosphere is an effective barrier and there are essentially no releases to the biosphere in the example simulations. Any releases from the vault decay during transit through the geosphere since ^{90}Sr transit times are of the order of 10^3 a (Figure A-10) and the half-life of ^{90}Sr is only 29.1 a. The attenuation is particularly strong in the simulations without a well since the ^{90}Sr must pass through the overburden and sediment layers and strontium strongly sorbs on the clay minerals and organic deposits in these layers.

Figure A-14 and Table A-7 show that, for ^{99}Tc, releases from the geosphere follow the releases from the vault for the MV Simulation and for Simulation #27. However, releases from the geosphere are attenuated in Simulation #31, where sorption in the overburden layer is relatively large, and in Simulation #3, where median sorption in the sediment layer is relatively large.

Figure A-15 and Table A-7 show that the geosphere is an effective barrier for ^{79}Se, with releases to the biosphere attenuated by about 5 orders of magnitude in the MV Simulation and in Simulation #27. Releases to the biosphere are negligible for Simulation #31 and Simulation #3. Selenium is moderately sorbed in the geosphere.

Figure A-16 shows that the geosphere is a very effective barrier for ^{126}Sn and that there are essentially no releases to the biosphere. Tin is sorbed too strongly to be released from the geosphere in 10^4 a.

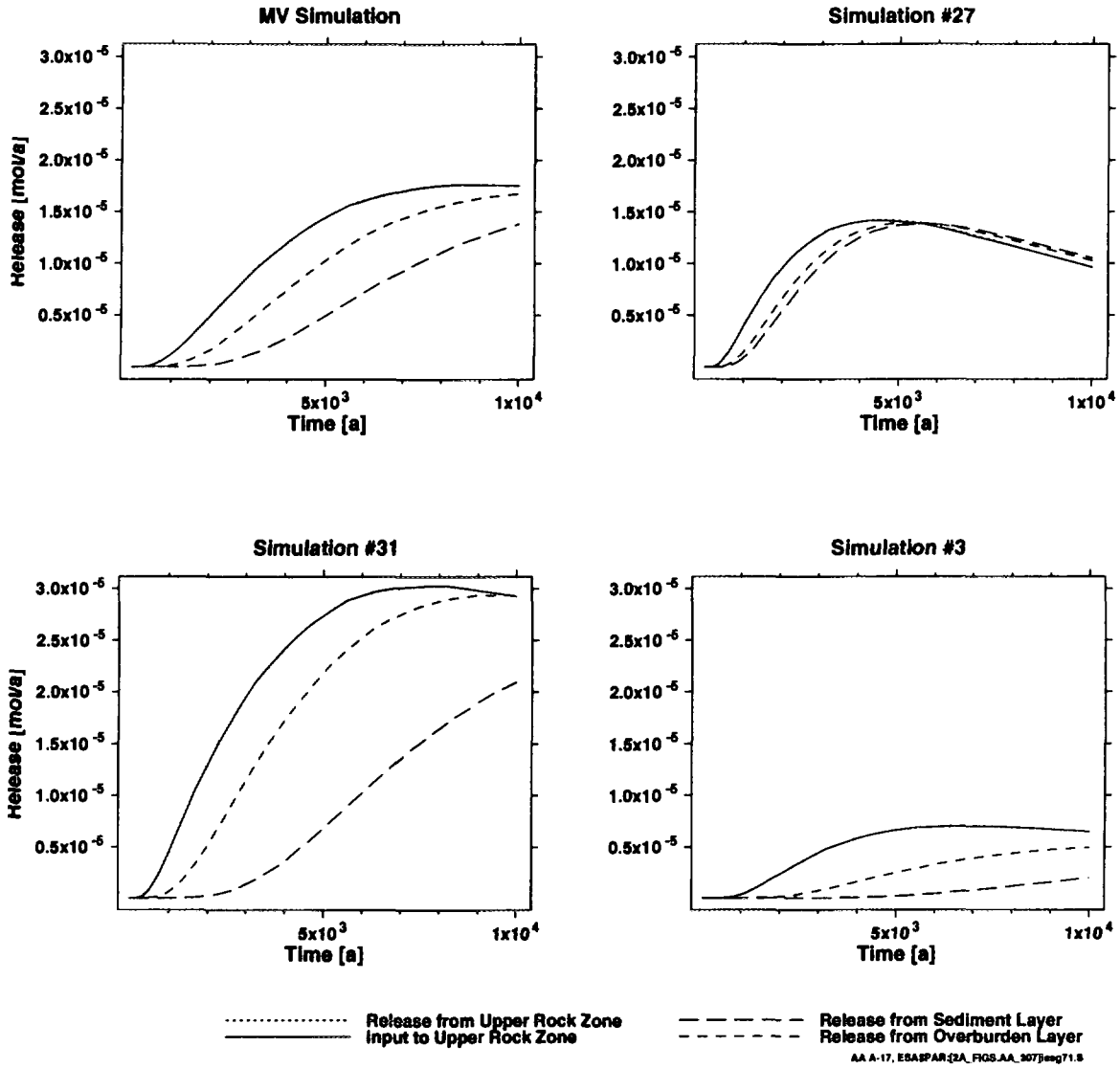

FIGURE A-17: Flow Rates of ^{129}I as a Function of Time. Flow rates are shown into and out of the upper rock zone and out of the overburden layer and the sediment layer leading to the Boggy Creek South aquatic discharge zone for the four example simulations.

TABLE A-7

BARRIER EFFECTIVENESS OF THE GEOSPHERE OVER 10^4 A

Simulation	Total Release of ^{129}I	^{90}Sr	^{99}Tc	^{79}Se	^{126}Sn
MV Simulation					
Vault to geosphere [mol]	0.39	8.3×10^{-7}	1.9×10^{-10}	1.2×10^{-2}	8.6×10^{-3}
Geosphere to biosphere [mol]	0.23	5.5×10^{-15}	4.0×10^{-11}	6.6×10^{-7}	$< 10^{-15}$
Simulation #27					
Vault to geosphere [mol]	0.36	1.0×10^{-7}	5.6×10^{-11}	1.3×10^{-2}	6.0×10^{-3}
Geosphere to biosphere [mol]	0.31	$< 10^{-15}$	1.3×10^{-11}	2.9×10^{-7}	$< 10^{-15}$
Simulation #31					
Vault to geosphere [mol]	0.34	2.2×10^{-6}	1.9×10^{-12}	4.2×10^{-3}	8.9×10^{-3}
Geosphere to biosphere [mol]	0.13	$< 10^{-15}$	1.9×10^{-13}	$< 10^{-15}$	$< 10^{-15}$
Simulation #3					
Vault to geosphere [mol]	0.094	4.3×10^{-7}	1.4×10^{-11}	4.4×10^{-3}	7.6×10^{-3}
Geosphere to biosphere [mol]	0.016	$< 10^{-15}$	1.3×10^{-12}	$< 10^{-15}$	$< 10^{-15}$

TABLE A-8

RETARDATION FACTORS FOR IODINE IN OVERBURDEN AND SEDIMENT

Simulation	Retardation Factors [-] Overburden	Sediment
MV Simulation	6.3	8.6
Simulation #27	2.9	1.1
Simulation #31	4.6	16
Simulation #3	23	23

A.3.5 SUMMARY

Variation in the properties of the geosphere in these four example simulations is not the controlling effect on the estimated dose rates, which mostly arise from ^{129}I and ^{36}Cl at 10^4 a. The geosphere is not an effective barrier to these nonsorbed radionuclides in any of the four simulations. However, the geosphere is an effective barrier for other radionuclides that sorb on the surfaces of rocks and minerals, such as ^{126}Sn, ^{90}Sr, and the members of the actinide decay chains.

A.4 FEATURES OF THE BIOSPHERE MODEL

A.4.1 INTRODUCTION

The biosphere model is outlined in Section 5.4 and described in more detail by Zach et al. (1996). The most influential parameter for total dose rate at 10^4 a is (Section 6.3) the source of domestic water for the critical group (PRODMD). This parameter also has a significant effect on dose rate in the 32 fractional factorial simulations, as shown in Table A-1. Other influential biosphere parameters from the probabilistic sensitivity analysis at 10^4 a (Table 7) are

- the iodine aquatic mass-loading coefficient (IMLA),
- the plant/soil concentration factor for iodine (XCRTIO(I) and for chlorine XCRTIO(Cl), and
- the number of people in the critical group (NUMMAN).

The influence of these latter parameters is weaker than the source of domestic water; their values do not show a strong relationship with dose rate at 10^4 a in Table A-1.

An overall measure of the biosphere model is provided by the biosphere performance factor. This calculated quantity is the integrated dose to humans divided by the integrated geosphere discharge into the biosphere. The biosphere performance factor is a measure of the effectiveness with which the biosphere model transforms geosphere outputs of a radionuclide into radiological dose to humans. Table A-1 shows that large values of the biosphere performance factor for ^{129}I generally correspond to large dose rates from ^{129}I. Of the five highest dose rate simulations, four have the highest biosphere performance factors for ^{129}I. This demonstrates that the biosphere plays an important role in determining total dose rate. (In contrast, there is no similar strong relationship between dose rate and performance factors for the vault or for the geosphere.)

A.4.2 DESCRIPTION OF THE BIOSPHERE IN THE EXAMPLE SIMULATIONS

The MV Simulation has a well used for domestic water and irrigation of the garden. The soil type is sand (the most probable type) and the size of the critical group is three. Use of the well, irrigation of the garden with well water, and a small critical group are generally associated with higher dose rate simulations (Goodwin et al. 1994). The four nuclides contributing the most to the dose rate to humans in the MV Simulation are ^{129}I, ^{36}Cl, ^{14}C and ^{79}Se, in order of importance.

Simulation #27 has a well used for domestic water and irrigation of the garden. The soil type is clay and the size of the critical group is again three. The well demand is more than a factor of two larger than in the MV Simulation because of a larger irrigation requirement for clay soils and a larger value for the annual domestic water requirement per capita. The major contributor to dose rate is ^{129}I, followed by ^{36}Cl, ^{14}C and ^{107}Pd, in order of importance. The biosphere performance factor is large.

Simulation #31 is especially interesting since it is a high-dose simulation that uses the lake for domestic water and irrigation of the garden. The use of lake water is generally associated with lower dose-rate simulations. The size of the critical group is five persons and the soil type is organic. The four radionuclides that produce the highest dose rate to humans up to 10^4 a in this simulation are ^{129}I, ^{36}Cl (from the UO_2 matrix), ^{14}C, and ^{36}Cl (from the Zircaloy matrix), in order of importance. Again, the biosphere performance factor is large.

Simulation #3, in contrast to the simulations described above, has ^{36}Cl (from the UO_2 matrix) as the radionuclide that produces the highest dose rate up to 10^4 a, followed by ^{129}I, ^{36}Cl (from the Zircaloy matrix), and ^{14}C, in order of importance. The size of the critical group is four persons and the soil type is loam. The source of domestic water and irrigation water for the garden is the lake. This simulation is more typical than Simulation #31 in that the use of lake water by the critical group is generally associated with lower dose rates. The biosphere performance factor is small.

A.4.3 CONCENTRATIONS IN BIOSPHERE COMPARTMENTS

The maximum concentrations up to 10^4 a in the garden soil and in the forage field soil for selected radionuclides are listed in Table A-9. The maximum concentrations of ^{14}C, ^{99}Tc and ^{126}Sb in the soils are not shown but are less than 10^{-15} mol/kg.

Figures A-18 to A-21 show plots of ^{129}I concentrations in several biosphere compartments in the four example simulations as a function of time. The figures include the total ^{129}I flow rate into the biosphere. One general feature of this series of plots is that the time dependence of the concentration curves closely parallels the time dependence of the total flow rates of ^{129}I into the biosphere from the geosphere, which in turn mirrors the time dependence of releases from the vault shown in Figure A-4. The near constant releases after 10^5 a are attributed to slow release from dissolution of the used-fuel matrix as described in Section A.2.3.

Figures A-18 to A-21 show the concentrations of ^{129}I in well water (when a well is modelled) are greater than in lake water, since the well draws much of its water from the radionuclide plume moving up fracture zone LD1, and since the larger volume of lake water provides more dilution. In addition, concentrations in the garden soil are typically greater than in the forage field soil, since the garden is located in the more contaminated discharge zones (Davis et al. 1993).

Figure A-18 shows ^{129}I concentrations for the MV Simulation. As expected, the well water has a much higher concentration of ^{129}I than the lake water and the garden soil has a much higher concentration of ^{129}I than the forage field soil.

Figure A-19 shows ^{129}I concentrations for Simulation #27 are similar to those in the MV Simulation, except that the concentration of ^{129}I in the well water is slightly smaller and the concentration of ^{129}I in the garden soil is about three times larger. The concentration in the soil is larger, in spite of the smaller concentration in the well water, because of the different retention characteristics of the clay soil. These curves concur with the observations described in section A.3.1, where it was noted that the well in Simulation #27 supplies more than twice as much water than the well in the MV Simulation and the well water in Simulation #27 is diluted with a greater quantity of the less contaminated water from the surface.

Figure A-20 shows ^{129}I concentrations for Simulation #31. There is a relatively large concentration of ^{129}I in the garden soil, although not as large as in Simulation #27. The concentration of ^{129}I in the forage field soil is also larger and has become almost equal to the concentration in the garden soil. The source of the large concentrations in the soils is caused by atmospheric deposition to the soil surface of ^{129}I from lake water. The soil type is organic, which generally has high sorption coefficients for iodine, and this particular simulation has a very high value (380 L/kg compared with the geometric mean value of 25 L/kg from the associated probability distribution). Although the deposition source is dominant, the ^{129}I concentration in the garden soil is slightly larger than in the forage field soil because of the additional contamination from irrigation with lake water.

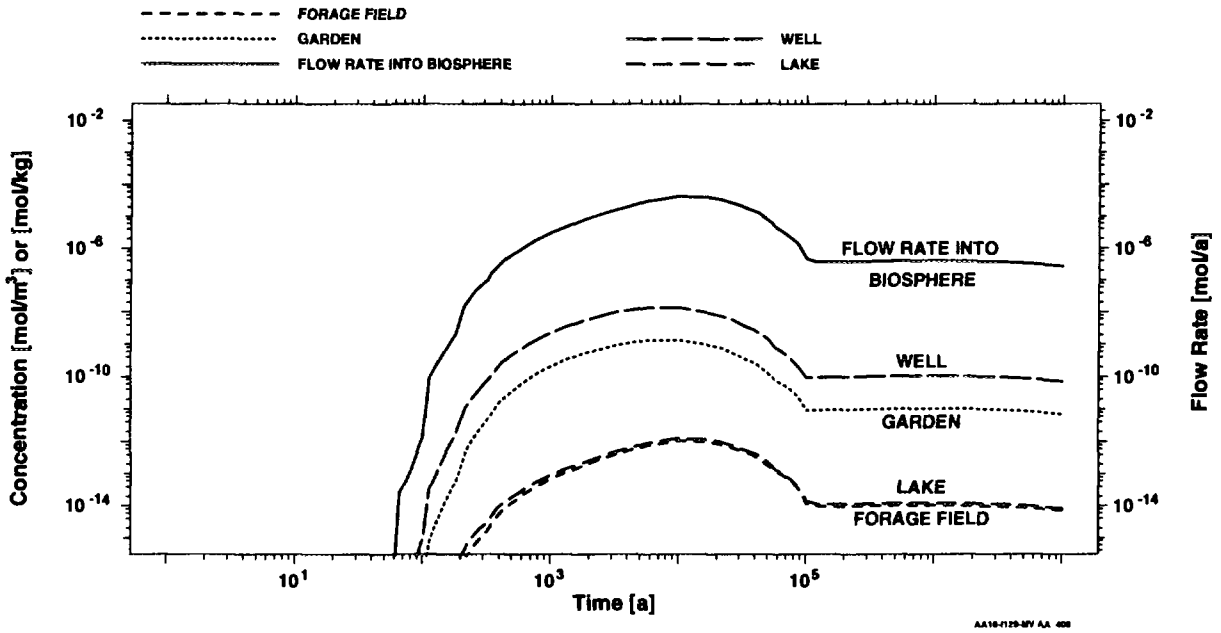

FIGURE A-18: Biosphere Concentrations for the MV Simulation. This figure shows the flow rate [mol/a] of ^{129}I into the 2water [mol/m^3], and in the garden and forage field soils [mol/kg].

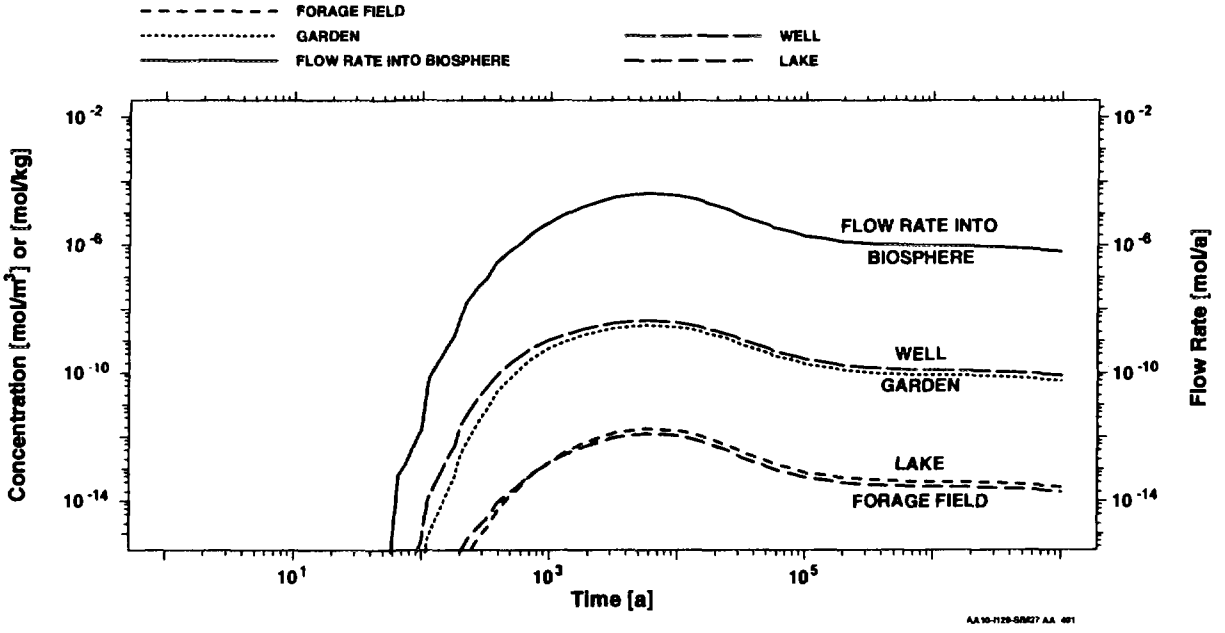

FIGURE A-19: Biosphere Concentrations for Simulation #27. This figure shows the flow rate [mol/a] of ^{129}I into the biosphere, summed over all the discharge zones, and the resulting ^{129}I concentrations in the lake and well water [mol/m^3], and in the garden and forage field soils [mol/kg].

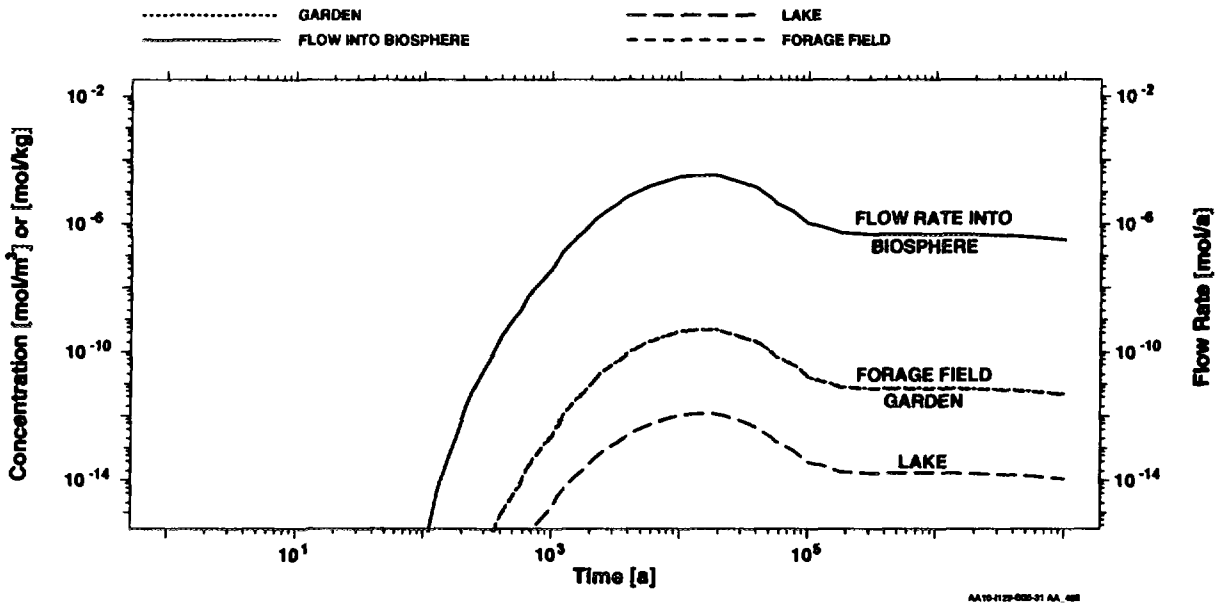

FIGURE A-20: Biosphere Concentrations for Simulation #31. This figure shows the flow rate [mol/a] of ^{129}I into the biosphere, summed over all the discharge zones, and the resulting ^{129}I concentrations in the lake and well water [mol/m^3], and in the garden and forage field soils [mol/kg].

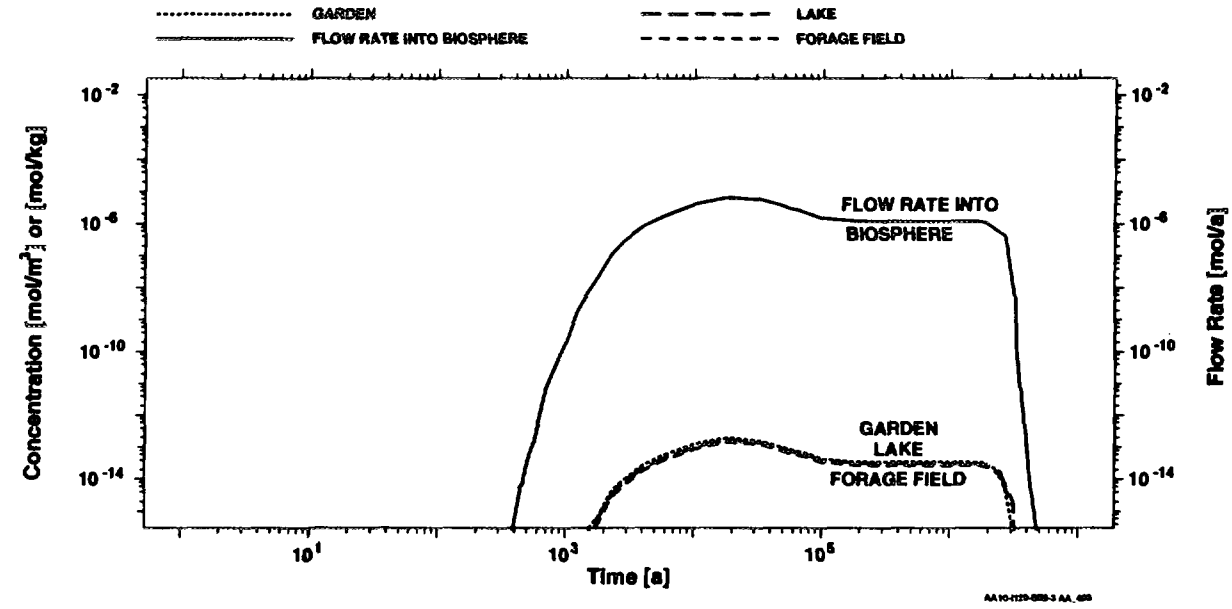

FIGURE A-21: Biosphere Concentrations for Simulation #3. This figure shows the flow rate [mol/a] of ^{129}I into the biosphere, summed over all the discharge zones, and the resulting ^{129}I concentrations in the lake and well water [mol/m^3], and in the garden and forage field soils [mol/kg].

TABLE A-9

CONCENTRATION[+] OF SELECTED RADIONUCLIDES IN THE SOILS OF THE GARDEN AND THE FORAGE FIELD

	^{129}I		^{36}Cl		^{79}Se	
	Garden [mol/kg]	Forage Field [mol/kg]	Garden [mol/kg]	Forage Field [mol/kg]	Garden [mol/kg]	Forage Field [mol/kg]
MV Simulation	1.3×10^{-9}	1.0×10^{-12}	1.0×10^{-10}	5.8×10^{-14}	4.2×10^{-14}	$< 10^{-15}$
Simulation #27	3.1×10^{-9}	1.8×10^{-12}	2.1×10^{-10}	6.5×10^{-15}	2.6×10^{-15}	$< 10^{-15}$
Simulation #31	4.5×10^{-10}	4.3×10^{-10}	1.4×10^{-12}	1.0×10^{-14}	$< 10^{-15}$	$< 10^{-15}$
Simulation #3	1.3×10^{-13}	9.3×10^{-14}	1.9×10^{-14}	3.2×10^{-15}	$< 10^{-15}$	$< 10^{-15}$

[+] Values reported are maximum concentrations up to 10^4 a.

Figure A-21 shows ^{129}I concentrations for Simulation #3. The concentration of ^{129}I in the lake water is smaller than in the other example simulations, reflecting the smaller rate of discharge from the geosphere. The ^{129}I concentrations in the garden soil and forage field soil are also much smaller in this simulation reflecting the smaller concentrations in lake water that is used for irrigation. The forage field soil has an ^{129}I concentration similar to that in the garden soil because atmospheric deposition is the dominant source. However, the ^{129}I concentration in the garden soil is slightly larger because of the additional contamination from irrigation. Concentrations fall towards zero at longer times because, for this simulation, the entire used-fuel matrix has dissolved (Table A-2) and because ^{129}I moves relatively quickly through the disposal system.

A.4.4 PATHWAYS LEADING TO DOSE TO HUMANS

The soil-to-plant-to-human pathways are usually the most important for simulations with the well as the source of domestic water, because of the larger ^{129}I concentrations in soil from irrigation water. The air-to-plant-to-human pathways (pathways 5 to 8 in table 3) are usually the most important for ^{129}I in simulations where the lake is used as the source of domestic water and in some simulations with the well as the water source.

In the MV Simulation (Figure A-22a), the large ^{129}I concentration in the garden soil is reflected in the soil-to-plant-to-human pathways. The large concentration of ^{129}I in well water affects its concentration in the garden soil through irrigation and influences the pathway involving direct ingestion of water (pathway 15 in Table 3). Air deposition of ^{129}I influences the air-to-plant-to-human pathways.

Figure A-22b shows the soil-to-plant-to-human pathways dominate the ^{129}I dose rate to humans in Simulation #27, typical for a simulation using well water for irrigation of the garden. The combinations of large ^{129}I concentrations in the garden soil, domestic water from the well, irrigation of the garden with well water and a relatively large plant/soil concentration factor for iodine (XCARTIO(I)) cause a large contribution to total dose rate from these pathways.

In Simulation #31, the important pathways for ^{129}I are more varied. The soil-to-plant-to-human pathways are the most important pathways, but Figure A-22c shows a number of other pathways are also contributors to human dose rate. The importance of the soil-to-plant-to-human pathway is the result of large concentrations of ^{129}I in the garden soil. The enhanced influence of the animal pathways in Simulation #31 is due to the relatively large concentration of ^{129}I in the forage field soil; the forage field is the food source for the animals. Hence this simulation has large soil-to-plant-to-bird-to-human, soil-to-plant-to-milk-to-human, soil-to-plant-to-meat-to-human and soil-to-animal-to-human pathways. The bird pathways (soil-to-plant-to-bird-to-human and air-to-plant-to-bird-to-human) are unusually large because the parameter that defines the ^{129}I transfer factor from plants to birds is large, coupled with a high plant/soil concentration factor for iodine (XCRTIO(I)) in this simulation. The air-to-plant-to-human and air-to-plant-to-animal-to-human pathways reflect deposition of ^{129}I originating from the lake.

For Simulation #3, Figure A-22d shows that the most important pathways for ^{36}Cl are soil-to-plant-to-human (pathway 4 in Table 3) followed by soil-to-plant-to-meat-to-human (pathway 1 in Table 3). The soil-to-plant-to-human pathway is usually significant for ^{36}Cl because the plant/soil concentration factor for chlorine (XCRTIO(Cl)) is generally large; in this simulation, for example, the value for ^{36}Cl was 18, more than 300 times greater than the corresponding value of 0.051 for the plant/soil concentration factor for iodine (XCRTIO(I)).

A.4.5 GROUND WATER DILUTION LIMITS

For ^{14}C, ^{36}Cl and ^{129}I, we include bounding limits to dose rate, referred to as the groundwater dilution limits, that takes into consideration the presence of stable isotopes of these elements in groundwater and the fact that stable and radioactive isotopes are retained in the body in the same proportion as they occur in their sources (Zach and Sheppard 1992, Davis et al. 1993). If the dose rate predicted for one of these nuclides by all the exposure pathways listed in Table 3 exceeds the associated groundwater dilution limit, the dose rate is set to the limiting value. Table A-10 shows where groundwater dilution limits were reached in these four example simulations.

TABLE A-10

GROUNDWATER DILUTION LIMITS REACHED

	^{129}I	^{36}Cl	^{14}C
MV Simulation	N	Y	N
Simulation #27	Y	Y	Y
Simulation #31	Y	N	N
Simulation #3	N	Y	N

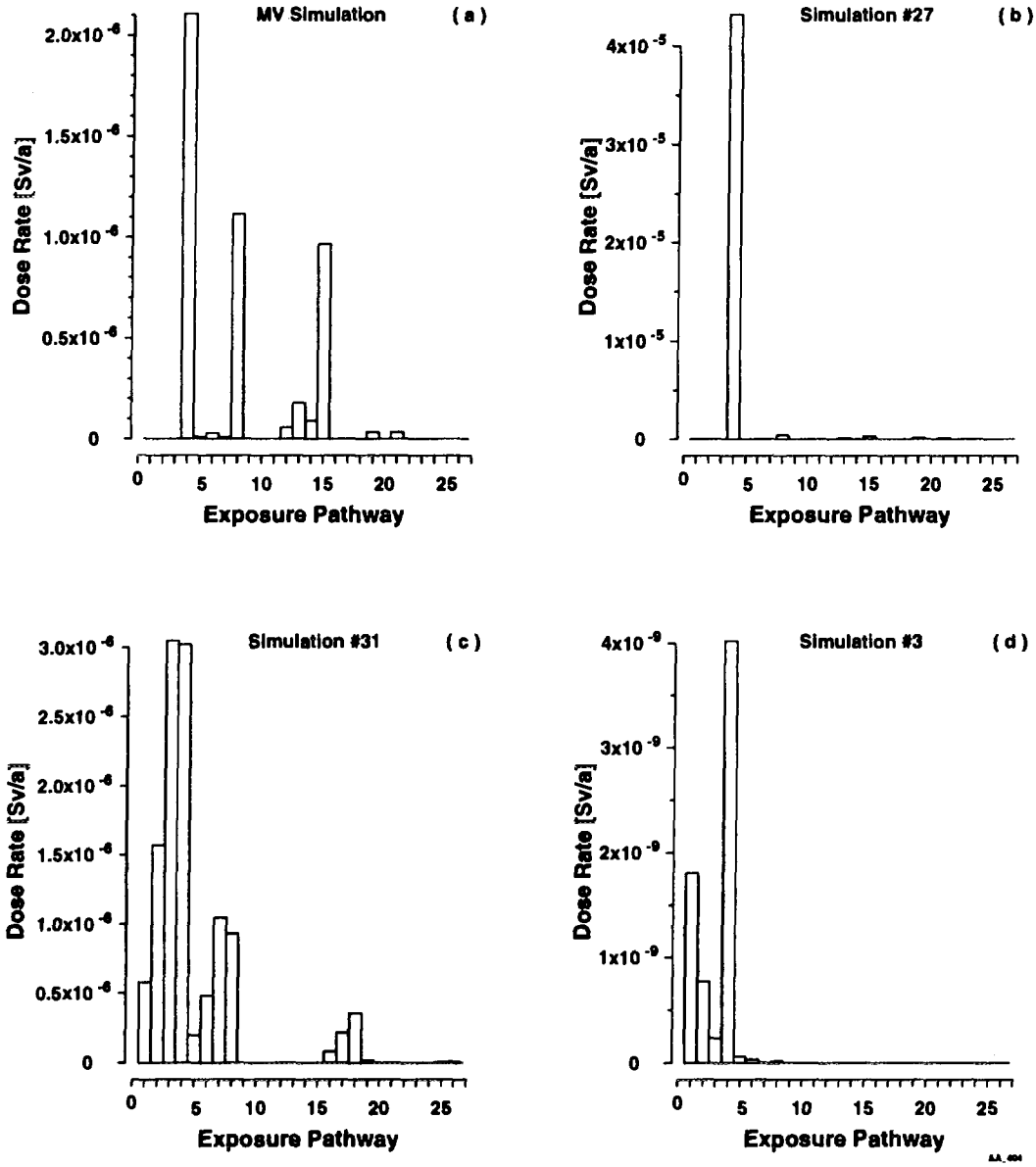

FIGURE A-22: The Exposure Pathways That Contribute to the Total Dose Rate. These results show the contributions from different pathways to the dose rate to a member of the critical group, for the radionuclide that is the most important contributor. Parts (a) to (d) are for the MV Simulation, Simulation #27, Simulation #31 and Simulation #3 respectively. The most important radionuclides are ^{36}Cl for Simulation #3 and ^{129}I for the others. Pathway numbers marked on the x-axis identify the pathway, and correspond to those listed in Table 3. Pathways 1 to 4 involve soil-to-plant-to-human; pathways 5 to 8 involve air-to-plant-to-human; pathways 9 to 11 involve air-to-animal-to-human; pathways 12 to 15 involve water-to-animal-to-human and direct ingestion of water; pathways 16 to 18 involve soil-to-animal-to-human and direct ingestion of soil; and pathways 20 to 26 involve other internal routes and external routes (see Table 3).

A.4.6 SUMMARY

The most important radionuclides at 10^4 a for the example simulations are ^{129}I and ^{36}Cl. The most important biosphere pathways are soil-to-plant-to-human, especially if the garden is irrigated by well water. The source of domestic water is generally the most influential parameter. However, Simulation #31 is an exception; it uses domestic water drawn from the lake but it has a relatively high dose rate. Other parameters can have an influence that can combine to be greater than the influence of the water source. The biosphere performance factor shows a significant correlation with estimated dose rates, indicating that the variability in estimated dose rates is largely determined by variability in the biosphere model parameters.

A.5 CONCLUSIONS

We have used selected simulations from a 32 simulation fractional-factorial Latin-hypercube design and the MV simulation to explore the behaviour of the submodels. In general, the radionuclides are released from used fuel by instant- and congruent-release mechanisms. The releases rates are influenced by rate of radiolysis of the groundwater from γ-radiation. The radionuclides then diffuse through small pinhole-sized defects from a limited number of containers that have failed because of fabrication defects. Subsequently, they diffuse through the buffer and are transported by dispersion and convection through the backfill and EDZ whereupon they enter the lower rock zone. They are transported through various geosphere pathways in the lower rock zone, the fracture zones, the middle rock zones, the upper rock zone and the overburden and sediment to nine discharge zones in the biosphere, including a well. The radionuclides enter the food chain principally through irrigation of a garden with well water or lake water or through atmospheric deposition, and doses are received through consumption of contaminated vegetables and meat.

In these simulations, the estimated dose rates are smaller than the dose rate of 5×10^{-5} Sv/a associated with the AECB radiological risk criterion (AECB 1987). Simulation #27 gives a high dose rate because it has a large number of failed containers (22), a bedrock well is used for domestic water supply, and irrigation of the garden (which was on a clay soil) requires high irrigation rates. The main contributor to dose rate is ^{129}I via soil-to-plant-to-human pathways. Simulation #31 gives a high dose rate because it has a large number of failed containers (17). In spite of having no well, it has high deposition rates onto organic soils that have high sorption coefficients for ^{129}I. The main contributor to dose rate is ^{129}I via the soil-to-plant-to-bird-to-human and soil-to-plant-to-human pathway. Simulation #3 gives a low dose rate because it has a small number of failed containers (6) and no well. The main contributor to dose rate is ^{36}Cl via soil-to-plant-to-human pathways.

The vault provides a significant barrier for all radionuclides because of the long-lived containers, transport limitations through small pinhole-sized defects and delay in transport through the buffer and backfill. The geosphere is an effective barrier for all radionuclides at early times (less than about 10^3 a), but less effective at later times for radionuclides that do not sorb or that sorb weakly. However, it remains an effective barrier at long times for radionuclides that are moderately to strongly sorbed, significantly slowing their rate of transport.

Parameters used in the biosphere model cause most of the variability in the estimates of dose rate. However, apart from the source of domestic water, it is difficult to discern influential parameters from a visual inspection of results; a more systematic statistical-based approach is required.

REFERENCES

AECB (Atomic Energy Control Board). 1987. Regulatory policy statement. Regulatory objectives, requirements and guidelines for the disposal of radioactive wastes - long-term aspects. Atomic Energy Control Board Regulatory Document R-104, 1987 June 5, Ottawa.

Andres, T.H. 1995. Sampling methods and sensitivity analysis for large parameter sets. Presented at the SAMO'95 international symposium on Theory and Applications of Sensitivity Analysis of Model Output in computer simulation, Belgirate, Italy, in 1995 September; submitted to the Journal of Computational Statistics and Data Analysis.

Davis, P.A., R. Zach, M.E. Stephens, B.D. Amiro, G.A. Bird, J.A.K. Reid, M.I. Sheppard and M. Stephenson. 1993. The disposal of Canada's nuclear fuel waste: The biosphere model, BIOTRAC, for postclosure assessment. Atomic Energy of Canada Limited Report, AECL-10720, COG-93-10.

Goodwin, B.W., D.B. McConnell, T.H. Andres, W.C. Hajas, D.M. LeNeveu, T.W. Melnyk, G.R. Sherman, M.E. Stephens, J.G. Szekely, P.C. Bera, C.M. Cosgrove, K.D. Dougan, S.B. Keeling, C.I. Kitson, B.C. Kummen, S.E. Oliver, K. Witzke, L. Wojciechowski and A.G. Wikjord. 1994. The disposal of Canada's nuclear fuel waste: Postclosure assessment of a reference system. Atomic Energy of Canada Limited Report, AECL-10717, COG-93-7.

Johnson, L.H., D.M. LeNeveu, D.W. Shoesmith, D.W. Oscarson, M.N. Gray, R.J. Lemire and N.C. Garisto. 1994. The disposal of Canada's nuclear fuel waste: The vault model for postclosure assessment. Atomic Energy of Canada Limited Report, AECL-10714, COG-93-4.

Johnson, L.H., D.M. LeNeveu, D.W. Shoesmith, F. King, M. Kol_r, D.W. Oscarson, S. Sunder, C. Onofrei and J.L. Crosthwaite. 1996. The Disposal of Canada's Nuclear Fuel Waste: A study of postclosure safety of in-room emplacement of used CANDU fuel in copper containers in permeable plutonic rock. Volume 2: Vault Model. Atomic Energy of Canada Limited Report, AECL-11494-2, COG-95-552-2.

Stanchell, F.W., C.C. Davison, T.W. Melnyk, N.W. Scheier and T. Chan. 1996. The Disposal of Canada's Nuclear Fuel Waste: A study of postclosure safety of in-room emplacement of used CANDU fuel in copper containers in permeable plutonic rock. Volume 3: Geosphere Model. Atomic Energy of Canada Limited Report, AECL-11494-3, COG-95-552-3.

Zach, R., and S.C. Sheppard. 1992. The food-chain and dose submodel, CALDOS, for the assessment of Canada's nuclear fuel waste management concept. Atomic Energy of Canada Limited Report, AECL-10165, COG-91-195.

Zach, R., B.D. Amiro, G.A. Bird, C.R. Macdonald, M.I. Sheppard, S.C. Sheppard and J.G. Szekely. 1996. The Disposal of Canada's Nuclear Fuel Waste: A study of postclosure safety of in-room emplacement of used CANDU fuel in copper containers in permeable plutonic rock. Volume 4: Biosphere Model. Atomic Energy of Canada Limited Report, AECL-11494-4, COG-95-552-4.

Cat. No. / Nº de cat.: CC2-11494/5E
ISBN 0-660-16504-X
ISSN 0067-0367

To identify individual documents in the series, we have assigned an AECL- number to each. Please refer to the AECL- number when requesting additional copies of this document from

Scientific Document Distribution Office (SDDO)
AECL
Chalk River, Ontario
Canada K0J 1J0

Fax: (613) 584-1745 Tel.: (613) 584-3311
ext. 4623

Price: D

Pour identifier les rapports individuels faisant partie de cette série, nous avons affecté un numéro AECL- à chacun d'eux. Veuillez indiquer le numéro AECL- lorsque vous demandez d'autres exemplaires de ce rapport au

Service de Distribution des documents officiels (SDDO)
EACL
Chalk River (Ontario)
Canada K0J 1J0

Fax: (613) 584-1745 Tél.: (613) 584-3311
poste 4623

Prix: D